

ENTANGLEMENT AND DYNAMICS IN
MANY-BODY SYSTEMS

ANUSHYA CHANDRAN

A DISSERTATION
PRESENTED TO THE FACULTY
OF PRINCETON UNIVERSITY
IN CANDIDACY FOR THE DEGREE
OF DOCTOR OF PHILOSOPHY

RECOMMENDED FOR ACCEPTANCE
BY THE DEPARTMENT OF
PHYSICS
ADVISER: S. L. SONDHI

SEPTEMBER 2013

© Copyright by Anushya Chandran, 2013.

All rights reserved.

Abstract

In the first part of this dissertation, we study the dynamics of isolated and clean quantum systems out of equilibrium. We initially address the Kibble-Zurek (KZ) problem of determining the dynamical evolution of a system close to its critical point under slow changes of a control parameter. We formulate a scaling limit in which the nonequilibrium behavior is universal and discuss the universal content. We then report computations of some scaling functions in model Gaussian and large- N problems. Next, we apply KZ scaling to topologically ordered systems with no local order parameter. In the examples of the Ising gauge theory and the $SU(2)_k$ phases of the Levin-Wen models, we observe a slow, coarsening dynamics for the string-net that underlies the physics of the topological phase at late times for ramps across transitions that reduce topological order. We conclude by studying quenches in the quantum $O(N)$ model in the infinite N limit in varying spatial dimensions. Despite the failure to equilibrate owing to an infinite number of emergent conservation laws, the qualitative features of late time states following quenches is predicted by the equilibrium phase diagram.

In the second part of this dissertation, we explore the relationship between entanglement and topological order in fractional quantum Hall (FQH) phases. In 2008, Li and Haldane conjectured that the entanglement spectrum (ES), a presentation of the Schmidt values of a real space cut, reflects the energy spectrum of the FQH chiral edge. Specifically, both spectra should have the same quasi-degeneracy of eigenvalues everywhere in the phase. We offer an analytic, microscopic proof of this conjecture in the Read-Rezayi sequence of model states. We further identify a different ES that reflects the bulk quasihole spectrum and prove a bulk-edge correspondence in the ES. Finally, we show that the finite-size corrections of the ES of the Laughlin states reveal the fractionalization of the underlying quasiparticles.

Acknowledgements

I am deeply grateful to my advisor, Shivaji Sondhi. Late in my third year, he took me on as his student with very little hesitation and has been the ideal mentor to me since then. With the perfect combination of thoughtful criticism and constant encouragement, he has patiently led me through the journey from student and apprentice to colleague and collaborator. Shivaji is always brimming with ideas; his keen insight, clear thinking, enthusiasm and sharp wit made every conversation enjoyable and long meetings at the blackboard lively. My late appearance lent some urgency to our research program, but this didn't stop us from taking weeks to delve into random topics that we were curious about or rush the creative process. Most importantly, physics was always fun with Shivaji; I will forever be thankful to him for this.

I have also been very fortunate to closely collaborate with many extraordinary physicists. Working with Andrei Bernevig was as inspiring as it was exciting; his never-say-die attitude and energy still boggles my mind. Ravindra Bhatt was my first mentor at Princeton; he helped me begin the transformation from an electrical engineer to a physicist. It has also been a great pleasure to work with Steve Gubser and watch his speed and creativity in action. Nicolas Regnault taught me the ins and outs of his beautiful DiagHam code and made the fractional quantum Hall effect as real as it could be for me. Finally, I would like to thank David Huse. David's physical insight is truly remarkable. I have left every conversation with a sense of wonder and a deeper understanding of my work.

The last five years would have been a lot more lonely and far less intellectually stimulating without the many intense conversations with Maria Hermanns, Amir Erez, Vedika Khemani, Fiona Burnell and Chris Laumann. Working with each of you was a blast, we should keep doing it. I want to especially thank Vedika and Chris for reading early versions of this dissertation. The fourth floor at Jadwin has also

been a very stimulating environment, thanks to my office mates, Bo Yang and Mike Kolodrubetz, and the rest of the condensed matter crew, Charles Mathy, Arijeet Pal, Siddharth Parameswaran, Bryan Clark, Joseph Maciejko, Rahul Nandkishore, Benjamin Hsu and Akshay Kumar. I would like to thank the other members of my committee, Curtis Callan and Phuan Ong, who have both taken an interest in my work over the years. Bill Bialek and Ed Groth have also been kind to me in this regard. Finally, I am very grateful to Suzanne Staggs for my summer in Chile at the QUIET telescope and for teaching me about observational cosmology.

Modern research is thankfully not a socially isolated affair and I have benefitted from the insights of very many scientists. I would like to particularly thank Parsa Bonderson, Joshua Combes, Fabian Essler, Benoit Estienne, Matthew Fisher, Roderich Moessner, Vadim Oganesyan, Anatoli Polkovnikov, XiaoLiang Qi, Rahul Roy, Steve Simon and Brian Swingle in this regard. I also want to thank the people who made my PhD possible even before it began: Dagomir Kaszlikowski, Howard Wiseman, Balakrishnan and Anantan. A big thanks to all the administrators at Princeton, especially Jessica Hesslin, Toni Sarchi and Laurel Lerner, for making molehills out of hills. A friendly chat with you has turned many a day around.

For their unquestioning love and support, I thank my family, especially my mom and my dad. It was hard living without them for so many years and I really appreciate that they did everything they could to shrink the distance. I also want to particularly thank my aunt, Ramah, and my cousins, Preethi and Sundeep, for their frequent calls.

Finally, I want to thank all the wonderful friends I made here at Princeton. In particular, I am grateful to my roommates, Maika Takita, Oleg Polyakov, Joseph Benoit and Daniil Leiderman, my classmates, Blake Sherwin, David McGady and Michael Mooney, my chai friends Darren Pais, Anand Ashok and Rohit Lamba, and my only girl friend in Jadwin, Vedika Khemani. Last, I want to thank Chris Laumann for being there for me and for never letting me forget the light at the end of the tunnel.

To Amma and Appa.

Contents

Abstract	iii
Acknowledgements	iv
List of Tables	xii
List of Figures	xiii
I Dynamics	1
1 The Kibble-Zurek Problem: Universality and the Scaling Limit	2
1.1 Introduction	2
1.2 Classification of Protocols	6
1.2.1 Equilibrium description of the critical point	6
1.2.2 Protocols in δ	7
1.3 The Kibble-Zurek length and time	10
1.3.1 TCPs/CCPs	10
1.3.2 ECPs	12
1.4 The KZ Scaling limit	12
1.4.1 TCPs and CCPs	14
1.4.2 ECPs	21
1.4.3 Quantum systems	22
1.5 Comments	24

2	KZ scaling functions in model theories	26
2.1	Classical Systems with Model A dynamics	27
2.1.1	Gaussian Limit	28
2.1.2	Large- N limit	32
2.2	Gaussian Quantum Field Theories	37
2.2.1	Second quantization	37
2.2.2	The scaling limit	39
2.2.3	Quasi-particles, heat density and diagonal entropy	41
2.2.4	Linear protocol	42
2.2.5	CCP - Quadratic protocol	45
2.2.6	The Marginal ECP	47
2.3	Concluding Remarks	56
2.A	Scaling form of $f(t; \tau)$ in the Gaussian theory with Model A dynamics	57
3	String-Net Coarsening in Topologically Ordered Systems	59
3.1	Introduction	59
3.2	Review of the phase diagram of the \mathbb{Z}_2 Gauge Theory	62
3.2.1	The perturbed toric code	62
3.2.2	Pure matter theory ($\Gamma = 0$)	65
3.2.3	Pure Gauge Theory ($J = 0$)	66
3.2.4	The full phase diagram	67
3.3	Kibble Zurek I - Ramp across the Higgs transition	67
3.3.1	Coarsening	68
3.4	Kibble Zurek II - Ramp across the confinement transition	71
3.5	Kibble Zurek III - Ramp across a generic transition in the \mathbb{Z}_2 theory .	75
3.6	Extension to generalized Levin-Wen models	77
3.6.1	Levin-Wen Hamiltonians with Ising transitions	77
3.6.2	Away from the pure \mathbb{Z}_2 limit	84

3.7	Concluding remarks	85
3.A	Scattering times in coarsening	86
3.B	Mapping of general $SU(2)_k$ models to the \mathbb{Z}_2 gauge theory	87
3.B.1	Equal weighting of loops in the ground states at the solvable points	88
3.B.2	Away from the solvable points	91
4	The quantum $O(N)$ model at infinite N	95
4.1	Introduction	95
4.2	The model	98
4.2.1	Statics	98
4.2.2	Dynamics	99
4.3	Ergodicity	102
4.4	Quenches to the ordered phase	106
4.4.1	Problem, methods and background	106
4.4.2	Results	108
4.4.3	The step approximation	115
4.5	Scaling and quenches to the critical point	116
4.6	Concluding remarks	121
4.A	Lack of relaxation to the GGE	123
II	Entanglement	125
5	Entanglement in the quantum Hall phases	126
5.1	The Integer Quantum Hall Effect	129
5.2	Exposing the current imprint	132
5.2.1	Physical edge	132
5.2.2	Virtual edge	134

6	Bulk-Edge Correspondence in the Entanglement Spectra	140
6.1	Introduction	140
6.2	Background	144
6.2.1	Geometry	144
6.2.2	From one to many	146
6.2.3	The Read-Rezayi sequence	147
6.2.4	$(k, 2)$ -admissible configurations	148
6.2.5	Jack polynomials	150
6.3	Entanglement Matrices and Spectra	151
6.3.1	The Orbital Entanglement Matrix (OEM)	152
6.3.2	The Particle Entanglement Matrix (PEM)	159
6.4	Result I: Counting of the PES	163
6.5	Clustering Constraints	167
6.5.1	Derivation	168
6.5.2	Properties	169
6.6	Result II: Bulk-edge correspondence in ES	170
6.6.1	Systemizing the constraints	171
6.6.2	The method	172
6.6.3	Illustrative examples	176
6.7	Concluding remarks	181
6.A	Rank of $\tilde{\mathbf{P}}$	182
6.A.1	$(k, 2)$ -clustering states	182
6.B	Two examples of clustering constraints	184
6.C	Proof of step 1 Sec. 6.6.2	188
6.D	Proof of step 2 in Sec. 6.6.2	190
6.D.1	Effect of dominance on the distance from the cut	190
6.D.2	Effect of clustering constraints	192

6.D.3	Relating PEM rows to OEM rows	195
7	Haldane Statistics in the Finite Size Entanglement Spectra of $1/m$	
	FQH States	197
7.1	Introduction	197
7.2	Effects of a finite bulk on the edge excitation spectrum	200
7.3	Effects of a finite bulk on the OES	203
	7.3.1 An example	206
7.4	Away from the model state	209
7.5	Concluding remarks	210
	Bibliography	211

List of Tables

6.1	Clustering constraints, $N = 3, \nu = 1/2$ Laughlin state.	185
6.2	Clustering constraints, $N = 6, \nu = 1$ Moore-Read state.	187
7.1	Finite-size OES counting.	208

List of Figures

1.1	Domain growth in the 2d Ising model.	3
1.2	Phase diagram of an Ising Magnet.	7
1.3	Three topologies of protocols.	8
1.4	Dynamical regimes in the KZ mechanism.	13
2.1	Two-point function, classical Gaussian theory, linear TCP.	31
2.2	Two-point function, classical large- N theory, linear TCP.	35
2.3	Two-point function, quantum Gaussian theory, linear TCP.	44
2.4	Quasiparticles and entropy, quantum Gaussian theory, linear TCP.	44
2.5	Two-point function, quantum Gaussian theory, quadratic CCP.	46
2.6	Quasiparticles and entropy, quantum Gaussian theory, quadratic CCP.	47
2.7	Two-point function, quantum Gaussian theory, marginal ECP.	50
2.8	Two-point function, quantum Gaussian theory, marginal ECP.	51
3.1	Kitaev's toric code.	62
3.2	Zero temperature phase diagram of the \mathbb{Z}_2 theory in two dimensions.	68
3.3	Duality between the pure \mathbb{Z}_2 gauge theory and the TFIM.	72
3.4	Illustration of KZ scaling functions in the pure \mathbb{Z}_2 gauge theory.	74
4.1	Phase diagram of quantum $O(N)$ model at large N , $1 < d \leq 2$	98
4.2	Phase diagram of quantum $O(N)$ model at large N , $d > 2$	98
4.3	Effective mass, quench from disordered to ordered in $d = 1 + \epsilon$	110

4.4	Structure factor, quench from disordered to ordered in $d = 1 + \epsilon$	112
4.5	Effective mass, quench from disordered to ordered in $d = 3$	114
4.6	Structure factor, quench from disordered to ordered in $d = 3$	114
4.7	Scaling collapse, quench from disordered to ordered in $d = 3$	115
4.8	Scaling collapse, quench to critical point in $d = 2$	118
4.9	$\mathcal{M}(\infty)$ vs d in quenches to the critical point.	119
5.1	Transport data showing the quantum Hall effect.	128
5.2	Classical orbits and the current pattern in Landau orbitals.	131
5.3	Energy and entanglement spectrum of decoupled IQH droplets.	135
5.4	Energy and entanglement spectrum of coupled IQH droplets.	136
6.1	OES, $\nu = 1/2$ Laughlin state.	155
6.2	The partition in orbital space.	158
6.3	PES, $\nu = 1/2$ Laughlin state.	162
6.4	Partition in particle space.	164
6.5	Cartoon of entanglement matrices.	166
6.6	Constraints due to clustering.	169
6.7	Characteristics of an occupation configuration.	172
7.1	Particle-hole excitations of IQH and Laughlin droplets.	201
7.2	Configurations counted by OES.	204
7.3	OES at finite size, $\nu = 1/2$ Laughlin state.	207
7.4	OES of Coulomb state.	209

Part I

Dynamics

Chapter 1

The Kibble-Zurek Problem: Universality and the Scaling Limit

1.1 Introduction

The study of critical points and their associated continuum limits or field theories has been a central and enormously productive exercise in statistical mechanics and condensed matter physics.¹ This study began with the problem of equilibrium finite temperature transitions, was then extended to their dynamics and thereafter to the interplay between criticality and finite size effects [72, 82]. This development has since been replayed in the theory of zero temperature quantum phase transitions [172, 164]. Needless to say, the development of powerful field theoretic methods, most notably conformal field theory in (1+1) dimensions [56] and most recently the gauge gravity duality [1], have significantly advanced this line of work. In all these cases, the field theoretic approach not only describes the critical point, but also the regions of the phase diagram adjacent to it.

¹Chapter based on work with Amir Erez, Steven S. Gubser and S. L. Sondhi [39].

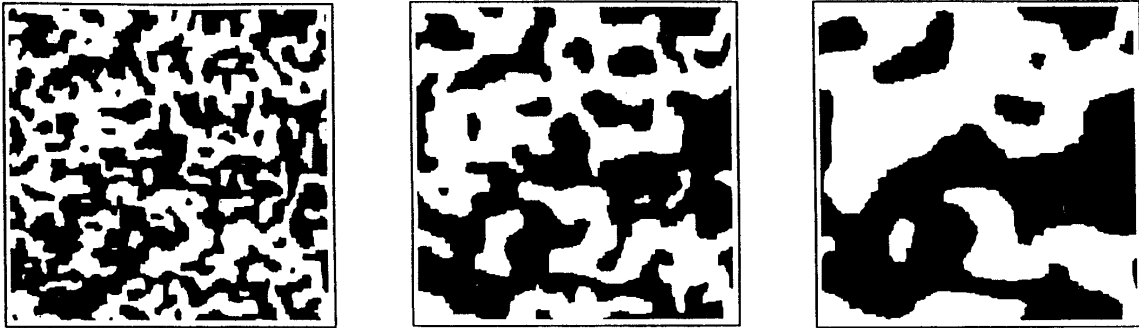


Figure 1.1: Monte Carlo simulation of domain growth in the $d = 2$ Ising model at $T = 0$ after a quench from $T = \infty$. The system size is 256×256 , and the snapshots correspond to 15, 60 and 200 Monte Carlo steps per spin. Reproduced from Ref. [108].

A new dimension to the study of the passage through critical points was introduced by Kibble [106] in the context of the expanding universe, since recast in the language of critical phenomena by Zurek [208]. Their proposal, the “Kibble-Zurek mechanism,” is a theory of the defects generated in a system being cooled through a continuous symmetry-breaking phase transition at a small, but finite rate. Near the transition, the equilibrium relaxation time of the system diverges. It is therefore inevitable that a system being cooled at a finite rate fall out of equilibrium on the approach to the transition. Consequently, the system arrives in the broken symmetry phase with different spatial regions realizing different orientations of the broken symmetry, and topological defects as a result. The mechanism predicts the scaling of the number of these defects with ramp time [208, 209] and has been tested in a variety of systems [43, 95, 162, 6, 129], although quantitative agreement has been established only in zero dimensional annular Josephson junctions [133] and in pattern-forming steady-state transitions [59, 33]. Two reasons for the disagreement between theory and experiment are spatial inhomogeneities and the finite extent of the sample. The Kibble-Zurek mechanism can be extended to account for both effects; recent experiments in ion crystals [153, 192] that test these extensions are very promising².

²Confirmation is still lacking in transitions in thermodynamic systems that are not described within mean field theory.

The Kibble-Zurek mechanism has also been generalized to the setting of quantum phase transitions by Dziarmaga [61, 62], Polkovnikov [143] and Zurek et al. [210], where the role of temperature is played by a non-symmetry breaking control parameter, and to ramps across multi-critical points [58, 57]. The scaling of other physical quantities like excess heat with quench time has also been investigated [51]. Polkovnikov and coworkers have further paid attention to the interplay between finite system size and parameter velocity.

The general problem posed by the work of Kibble and Zurek is that of a slow passage through a critical or multicritical point which we shall term the Kibble-Zurek (KZ) problem (often referred to by the oxymoronic term “slow quench”). This problem is then characterized by a critical point with its equilibrium physics and a “protocol”, which is a particular path in the parameter space of the problem that touches the critical point. In the limit of asymptotically slow motion in parameter space, we expect that the physics is dominated by the critical point and hence is, in an appropriate sense, universal. An important task of theory is then to isolate this universal content and compute it. We should note that the study of universality in the KZ problem, especially in the quantum setting, is a part of a wider current study of non-equilibrium quantum dynamics; for a broader perspective, see the recent colloquia [62, 147].

In previous studies of critical phenomena, two ideas have proven extremely useful. The first is the idea of the scaling limit in which various quantities of interest, such as thermodynamic densities and correlation functions, are postulated to obey certain homogeneity relations. This set of scaling functions along with the critical exponents captures the full universal content associated with a given critical point. The second is the renormalization group which provides an understanding of the origin of this universality and a full computation of its content.

In this chapter and the next, we will make progress on the first front: we will formulate a scaling limit for the KZ problem and report model computations of the resulting scaling functions for a few classical and quantum problems. In appropriate limits, these scaling functions will reduce to those in the equilibrium and the coarsening problems. Except for recent work by Deng et al. [55], Biroli et al. [14] and De-Grandi et al. [52] discussing scaling functions in specific cases, the need for defining full scaling functions has been largely overlooked in the literature. Our contribution is to formalize the idea as a scaling limit for *all* physical quantities for any pairing of a critical point and a protocol.

The second part of the program, beyond our ambition at present, would be the construction of a renormalization group flow. Such a program has been fruitfully pursued in sudden quench studies in classical models with stochastic dynamics (see [31] and references therein). We offer two modest steps in that direction in the next chapter. First, in the classical context, we formulate the path-integral previously written down only for sudden quenches to the KZ problem. This is, in principle, amenable to analysis by standard equilibrium renormalization group techniques. Second, we will prove universality with respect to protocol choice for some model classical and quantum problems. Specifically, we will show that the expectation that only the behavior of the protocols in the vicinity of the critical points is important is, in fact, correct.

In this chapter, we will also offer a tripartite classification of possible protocols based on their “topology”—i.e. whether they cross, turn around at or end at the critical point. The scaling of quantities such as the defect density and the excess heat with quench time has been previously generalized [169, 51] to arbitrary *positive* power-law behavior of the protocol on time near the critical point, that is, the first two kinds of protocols in our classification. Our contribution is the definition of a third class of power-law protocols that asymptotically end at the critical point and the identification of an interesting member—the marginal end critical protocol—that

generates a one parameter family of non-equilibrium deformations of the equilibrium critical state worthy of further study.

Our presentation naturally splits into two chapters. In this chapter, we will introduce the KZ scaling theory. In the next, we will report computations of KZ scaling functions in model theories and prove universality with respect to protocol choice. We begin, in Section 1.2, by defining the protocols of interest and introducing the well known KZ time and length. In Section 1.4, we lay out the scaling formalism for the KZ problem—the definition of the KZ scaling limit and the resulting scaling functions. We also discuss how the KZ scaling functions universally interpolate between the early equilibrium physics and the late time thermalization/coarsening physics. We conclude with a few comments.

1.2 Classification of Protocols

1.2.1 Equilibrium description of the critical point

Consider a multicritical point in d spatial dimensions. Let $\{O_i\}$ denote the set of relevant operators that couple to conjugate fields $\{h_i\}$ and have scaling dimensions $\{\Delta_i\}$. At the critical point, we set $\langle O_i \rangle_{\text{eq}} = 0$. The set of scaling dimensions $\{\Delta_i\}$ and a host of scaling functions constitute the static universal equilibrium content of this critical point. Along with the dynamical exponent z obtained from the time-dynamics, they determine the universality class of the critical point. Let δ parameterize a path in the space of conjugate fields $\{h_i\}$ such that δ is zero at the critical point. For every such path, define the correlation length exponent ν to be $1/(d - \Delta)$, where Δ is the scaling dimension of the most relevant operator that has a projection along the path near $\delta = 0$. Along the path, the correlation length then diverges as $\delta^{-\nu}$ close to the critical point.

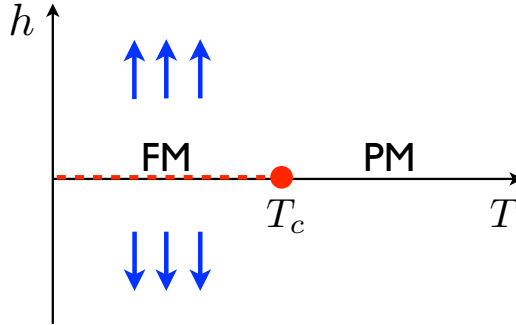


Figure 1.2: Phase diagram of an Ising Magnet ($d > 1$). PM denotes the paramagnetic phase, while FM denotes the ferromagnetic one. The two ordered configurations are shown in blue. The critical point is at $h = 0, T = T_c$. The red dashed line is the line of first order points that terminates at the critical point.

A useful example to keep in mind, particularly for the next section, is the Ising critical point. The phase diagram of an Ising magnet is shown in Fig. 1.2. The relevant operators at the critical point (red dot) are the scalar energy operator and the scalar magnetization, coupling to the conjugate fields of temperature (T) and the longitudinal magnetic field (h) respectively. The first order line in the phase diagram (red dashed line) is of no relevance here.

Unless mentioned otherwise, all length/time-scales are dimensionless and are measured in units of some microscopic length/time.

1.2.2 Protocols in δ

Consider a system prepared in equilibrium at $t = -\infty$ at some fixed distance $\delta_- > 0$ away from the critical coupling $\delta = 0$ being evolved in time along the path $\delta(t)$ in conjugate field space. For simplicity, we restrict ourselves to paths with a unique tangent most relevant operator near $\delta = 0$. The KZ dynamics refines the classification of critical points discussed above using two pieces of data. The first is the symmetry of the path. If the most relevant operator along the path respects all the symmetries of the critical theory, the path is non-symmetry breaking, else it is symmetry-breaking.

In the example in Fig. 1.2, only the paths along the temperature axis at $h = 0$ are non-symmetry breaking. The second is the leading order behavior of $\delta(t)$ near the critical point (strictly speaking, the critical coupling) which we classify below.

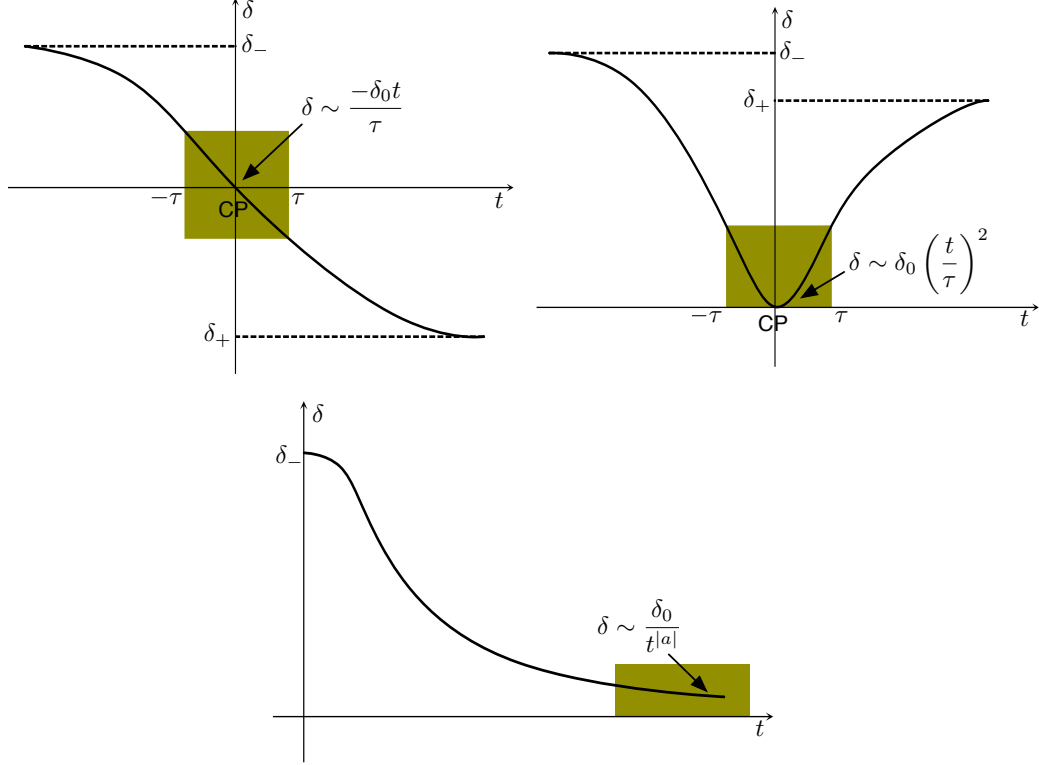


Figure 1.3: Clockwise from top left: examples of Trans-Critical (TCP), Cis-Critical (CCP) and End-Critical (ECP) protocols. The critical point (CP) is at $\delta = 0$. The TCP and CCP pass through the CP at $t = 0$, while the ECP asymptotically approaches the CP as $t \rightarrow \infty$. The leading order expansion of δ is valid in the shaded region.

- Trans-Critical Protocols (TCPs): These protocols take the system across the critical point. They smoothly interpolate δ between $\delta_- > 0$ as $t \rightarrow -\infty$ and $\delta_+ < 0$ as $t \rightarrow \infty$, crossing the critical point at $t = 0$. An example of a TCP is

$$\delta(t; \tau) = -\delta_0 \tanh \frac{t}{\tau}. \quad (1.1)$$

We will shortly show that the dynamic scaling functions are universal with respect to the behavior of the protocol near $t = 0$. In anticipation of this result, we classify the entire family of analytic TCPs by their leading order behavior in a time-scale τ near $t = 0$ as

$$\delta(t; \tau) = \begin{cases} \delta_- & t \rightarrow -\infty \\ \delta_0 \left(-\frac{t}{\tau}\right)^a & t \rightarrow 0 \\ \delta_+ & t \rightarrow \infty \end{cases} \quad (1.2)$$

with a odd. $a = 1$ is the linear protocol, $a = 3$ the cubic and so on.

- **Cis-Critical Protocols (CCPs):** These protocols keep the system in a single phase and touch the critical point at $t = 0$. They smoothly interpolate δ between δ_- as $t \rightarrow -\infty$ and $\delta_+ > 0$ as $t \rightarrow \infty$ through the critical point at $t = 0$. An example of a CCP is

$$\delta(t; \tau) = \delta_0 \tanh^2 \frac{t}{\tau}. \quad (1.3)$$

Eq. (1.2) with a even classifies CCPs. $a = 2$ is the quadratic protocol, $a = 4$ the quartic and so on.

- **End-Critical Protocols (ECPs):** End-Critical-Protocols (ECPs) keep the system in a single phase while asymptotically approaching the critical point. They smoothly interpolate between δ_- as $t \rightarrow -\infty$ and 0 as $t \rightarrow \infty$. The asymptotic approach to the critical point may be with or without a time-scale. Here we restrict ourselves to the family of scale-free protocols:

$$\delta(t) = \begin{cases} \delta_- & t \rightarrow -\infty \\ \delta_0 \left(\frac{t}{\tau}\right)^a = \delta_0 \left(\frac{\tau}{t}\right)^{|a|} & t \gg \tau, \end{cases} \quad (1.4)$$

where $a < 0$ and τ is the time-scale over which the protocol behavior smoothly changes from being a constant to a power law. Unlike in the above two cases, a is not required to be integer valued.

1.3 The Kibble-Zurek length and time

A system evolving from $t = -\infty$ by a TCP, CCP or an ECP with large $|a|$ must fall out of equilibrium near the critical point due to critical slowing down. This is signaled by a diverging relaxation time ξ_t ³. The time at which the system falls out of equilibrium is defined to be the KZ time t_K . The KZ time defines a KZ length $l_K \sim t_K^{1/z}$. l_K manifests in dynamic correlation functions as a crossover scale between equilibrium and non-equilibrium correlations. More intuitively [106, 209], in an ordering transition, order is unable to form on scales larger than l_K due to the finite quench rate, and domains of broken-symmetry phase of size l_K persist in the ordered phase (see Fig. 1.1). We now separately consider the cases of TCP/CCP and ECP.

1.3.1 TCPs/CCPs

The scaling of the KZ length and time with τ follows essentially from considerations in Refs. [210, 143, 169], which we recapitulate here. For pedagogical reasons, we will first present Zurek's original argument for a linear ramp [208] before the general scaling law.

³Near a quantum phase transition, this implies a vanishing many-body gap.

There are two time scales for a slow linear ramp through a critical point. The first is the instantaneous equilibrium correlation time:

$$\begin{aligned}\xi_t(t; \tau) &\sim \delta(t; \tau)^{-\nu z} \\ &\sim \left(\frac{-t}{\tau}\right)^{-\nu z}\end{aligned}$$

If the evolution of the system is adiabatic up to time t , then its correlation time t is $\xi_t(t; \tau)$. The second time scale is the time interval to the critical point, $\chi_t(t)$:

$$\chi_t(t) = -t$$

Initially ($t \approx -\tau$), $\chi_t \gg \xi_t$. The system is far from the critical point, its correlation time is small and the evolution is adiabatic. However, as the ramp proceeds, χ_t decreases while ξ_t increases. At $t = -t_K$, the two are equal and the evolution cannot possibly remain adiabatic as the time that it would take to equilibrate at $t = -t_K$ is the time interval to the critical point!

$$\begin{aligned}\xi_t(t_K; \tau) &= \chi_t(t_K) \\ \Rightarrow t_K &= \tau^{\frac{\nu z}{\nu z + 1}}\end{aligned}$$

The time scale, t_K , is known as the KZ time. We will soon see that it sets the scale for universal non-equilibrium physics near the critical point.

The generalization to other protocols is straightforward. We define $\xi(t; \tau)$ and $\xi_t(t; \tau)$ to be the instantaneous correlation length and time if the system were in equilibrium at $\delta(t; \tau)$. The crucial quantities that determine t_K are the change in the correlation time over a correlation time, $\dot{\xi}_t \xi_t$, and ξ_t itself. When $\dot{\xi}_t \xi_t \ll \xi_t$ or $\dot{\xi}_t \ll 1$, ξ_t is changing slowly enough for the system evolution to be adiabatic. This is the case for $t < -\tau$. As $\dot{\xi}_t$ diverges at the critical point, there must come a time $-t_K > -\tau$

when it is of order one.

$$\begin{aligned}\dot{\xi}_t(t_K; \tau) &= 1 \\ \Rightarrow t_K &\equiv \left(\frac{\tau}{\delta_0^{1/a}} \right)^{\frac{a\nu z}{a\nu z + 1}}.\end{aligned}\tag{1.5}$$

1.3.2 ECPs

The asymptotic behavior of $\dot{\xi}_t$ categorizes the ECPs into three. $|a_c| \equiv 1/(\nu z)$ below.

- Non-adiabatic : When $|a| > |a_c|$, $\dot{\xi}_t$ diverges at the critical point. The system falls out of equilibrium at t_K given by Eq. (1.5) where a is now negative.
- Adiabatic : When $|a| < |a_c|$, $\dot{\xi}_t$ is zero at the critical point. When τ is large, the evolution is adiabatic for all times.
- Marginal : When $|a| = |a_c|$, $\dot{\xi}_t$ is independent of t at the critical point and the only length scale in the problem is $t^{1/z}$. The system is marginally out of equilibrium on this scale in a sense that will become clear soon.

As we are interested in universal behavior *out of equilibrium*, $|a| \geq |a_c|$ henceforth.

1.4 The KZ Scaling limit

The introduction of t_K and l_K is reminiscent of the introduction of finite size cutoffs in the theory of equilibrium critical behavior, and we are led to analogs of the finite size scaling limit and finite size scaling functions. We define the KZ scaling limit to be the limit $\tau \rightarrow \infty$ when time and length scales are measured in units of the diverging KZ scales, t_K and l_K . $\delta(t; \tau) \rightarrow 0$ in this limit, and the system is arbitrarily close to the critical point, evolving non-adiabatically for all t/t_K (the shaded region in Fig. 1.4b). The marginal ECP is special and we discuss it separately at the end of this section.

We now turn to the definition of the scaling functions that arise in the KZ scaling limit. We discuss the scaling functions of various physical quantities and their asymptotic forms in specific cases. We initially consider classical critical points and discuss asymptotic forms when the transition is ordering. We then comment on the special features of quantum critical points.

Our notation is to denote the absolute value of any vector \mathbf{k} by k , and to use \hat{x} and \hat{t} respectively to refer to the scaled length and time, x/l_K and t/t_K . We reserve calligraphic lettering for scaling functions.

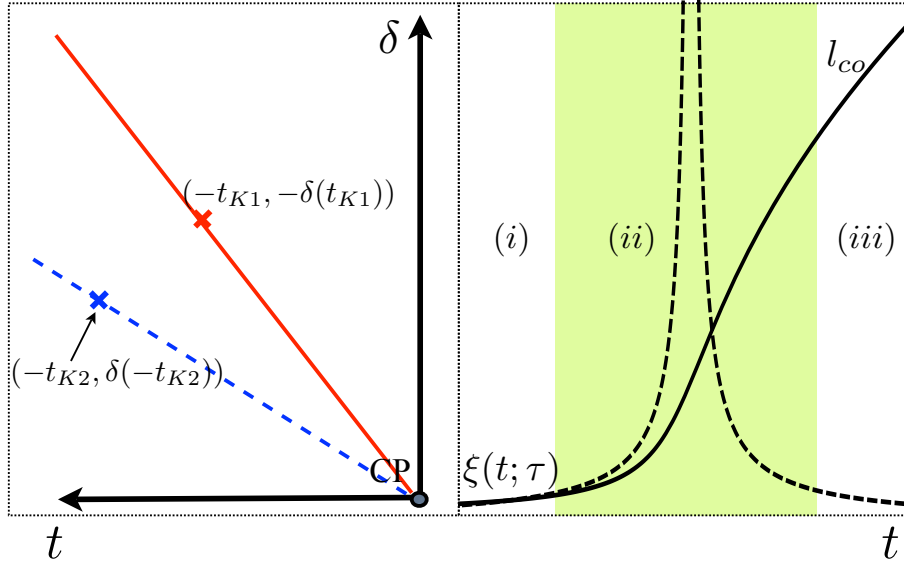


Figure 1.4: Left: δ as a function of t close to $t = 0$ with KZ times shown for a slow (2, dashed) and fast (1, solid) ramp. In the slower ramp, the system falls out of equilibrium earlier ($|t_{K2}| > |t_{K1}|$) but at a smaller distance from the critical point ($\delta(-t_{K2}) < \delta(-t_{K1})$). Right: The correlation length of a system ramped at a finite rate (solid) vs $\xi(t; \tau)$ (dashed). KZ split dynamics into (i) Adiabatic (ii) Sudden and (iii) Post-quench (here coarsening) regimes. The KZ scaling limit describes (ii) with (i) and (iii) as asymptotes.

1.4.1 TCPs and CCPs

Scaling forms of correlation functions

Consider the scalar operator O with scaling dimension Δ . We assume that the theory has translational and rotational invariance⁴. The KZ scaling forms for the one and two-point connected correlation functions are

$$\begin{aligned} \langle O(\mathbf{x}, t) \rangle_\tau &\equiv G_o(t; \tau) \sim \frac{1}{l_K^\Delta} \mathcal{G}_o \left(\frac{t}{t_K} \right) \\ \langle O(\mathbf{x}, t) O(\mathbf{x}', t') \rangle_\tau &\equiv G_{oo}(|\mathbf{x} - \mathbf{x}'|, t, t'; \tau) \\ &\sim \frac{1}{l_K^{2\Delta}} \mathcal{G}_{oo} \left(\frac{|\mathbf{x} - \mathbf{x}'|}{l_K}, \frac{t}{t_K}, \frac{t'}{t_K} \right). \end{aligned} \quad (1.6)$$

When we use \sim to indicate a scaling form of a correlation, as in (1.6), we have a precise limiting statement in mind. For example, in the case of the two-point connected correlator, what we mean is

$$\lim_{\tau \rightarrow^* \infty} l_K^{2\Delta} G_{oo}(x, t, t'; \tau) = \mathcal{G}_{oo} \left(\frac{x}{l_K}, \frac{t}{t_K}, \frac{t'}{t_K} \right), \quad (1.7)$$

where $\tau \rightarrow^* \infty$ means the limit where $\tau \rightarrow \infty$ with $\frac{x}{l_K}$, $\frac{t}{t_K}$ and $\frac{t'}{t_K}$ held fixed.

The scaling forms of all higher order cumulants and cross-correlators with other relevant operators are straightforward extensions of the form in Eq. (1.6). Note that \mathcal{G}_o can be identically zero. This is the case, for instance, in a zero-field temperature quench through the Ising critical point in Fig. 1.2 when O is the spin operator. The finite ramp rate prevents order from forming on scales longer than the KZ length, and $\langle O \rangle_\tau$, the average magnetization, remains zero at all times.

⁴With weak disorder, the KZ scaling forms apply to disorder averaged connected correlation functions. When the disorder distributions are broad, the typical moments satisfy the proposed scaling.

Asymptotic form near equilibrium

By construction of the protocol, we should recover equilibrium scaling forms in certain limits as $\hat{t} \rightarrow \pm\infty$. However, the precise limits are subtle and we derive them below. Recall that the equilibrium scaling limit is the limit of $\delta \rightarrow 0$ holding x/ξ and $(t-t')/\xi^z$ fixed, wherein the two-point correlator has the scaling form,

$$\langle O(\mathbf{x}, t) O(\mathbf{0}, t') \rangle_\delta^{\text{eq}} \sim \xi^{-2\Delta} \mathcal{G}_{OO}^{\text{eq}} \left(\frac{x}{\xi}, \frac{t-t'}{\xi^z} \right). \quad (1.8)$$

The \sim symbol here is distinct from that in the previous subsection.

We consider the limit in which the KZ scaling form Eq. (1.7) reduces to the equilibrium scaling form Eq. (1.8). First, we observe that the relation,

$$\frac{x/l_K}{x/\xi(t; \tau)} = \frac{\xi(t; \tau)}{l_K} = \left| \frac{t}{t_K} \right|^{-a\nu}, \quad (1.9)$$

implies that x/ξ is fixed whenever \hat{x} and \hat{t} are held fixed. Similarly, t/ξ^z and t'/ξ^z are also fixed by \hat{t} and \hat{t}' . Thus, an alternative to the KZ scaling form Eq. (1.7) involving the same two arguments as the equilibrium scaling form may be given:

$$\lim_{\tau \rightarrow^* \infty} \xi^{2\Delta} G_{OO}(x, t, t'; \tau) = \mathcal{G}_{OO}^{(2)} \left(\frac{x}{\xi}, \frac{t-t'}{\xi^z}, \frac{t+t'}{t_K} \right). \quad (1.10)$$

When $|t| \gg t_K$, the system is in instantaneous equilibrium on length and time-scales, ξ and ξ_t respectively. This is the limit in which $\mathcal{G}_{OO}^{(2)}$ must reduce to $\mathcal{G}_{OO}^{\text{eq}}$. Thus, in the limit $(\hat{t} + \hat{t}') \rightarrow \pm\infty$ holding x/ξ and $(t-t')/\xi^z$ fixed:

$$\mathcal{G}_{OO}^{(2)} \left(\frac{x}{\xi}, \frac{t-t'}{\xi^z}, \frac{t+t'}{t_K} \right) \sim \mathcal{G}_{OO}^{\text{eq}} \left(\frac{x}{\xi}, \frac{t-t'}{\xi^z} \right). \quad (1.11)$$

For the original KZ scaling form Eq. (1.7), this translates to the requirement,

$$\mathcal{G}_{OO}(\hat{x}, \hat{t}, \hat{t}') \sim \hat{t}^{2av\Delta} \mathcal{G}_{OO}^{\text{eq}}(\hat{x} \hat{t}^{\nu a}, (\hat{t} - \hat{t}') \hat{t}^{zav}). \quad (1.12)$$

in the same limit. As expected, $\xi(t; \tau)/\xi(t'; \tau) \rightarrow 1$ so that there is a single diverging length in the equilibrium system. Furthermore, time-translation invariance is recovered.

In the example of a temperature ramp through the Ising critical point (Fig. 1.2), the equilibrium equal-time connected spin-spin correlation function decays exponentially on a length scale ξ on either side of the critical point; consequently, Eq. (1.12) when $\hat{t} = \hat{t}'$ must asymptote to

$$\mathcal{G}_{OO}(\hat{x}, \hat{t}, \hat{t}) \sim \hat{t}^{2av\Delta} \exp(-\hat{x} \hat{t}^{\nu a}).$$

Asymptotic form for coarsening dynamics

It is generally believed⁵ that a system quenched to an ordered phase with multiple vacua undergoes coarsening, whereby each local broken-symmetry region grows in time and the system is asymptotically statistically self-similar on a characteristic length scale, $l_{\text{co}}(t) \gg \xi$. Put another way, the two point function heals to its equilibrium value on the scale ξ within each “domain”, and is exponentially suppressed between domains, each of growing length $l_{\text{co}} \gg \xi$. It is very useful to visualize coarsening. In Fig. 1.1, we show snapshots of the evolution of the $2d$ Ising model with Glauber dynamics [81]. The system is in contact with a heat bath, whose temperature is varied linearly: $\frac{T-T_c}{T_c} = \frac{-t}{\tau}$. Domains of up (down) spins are shown in white (black). At late times, both kinds of domains grow as the system attempts to establish long-range order.

⁵For a recent dissent, see Olejarz et al. in Phys. Rev. E **83**, 05144 (2011) who have noted that the 3d Ising Model does not coarsen at zero temperature. More generally, the KZ scaling forms asymptote to the long-time behavior in the sudden quench.

In the late time regime, dynamical scaling is expected to hold when there are no growing scales competing with the characteristic length scale of the domains, l_{co} . For example, as $t, t' \rightarrow \infty$,

$$\langle O(\mathbf{x}, t) O(\mathbf{0}, t') \rangle_{\delta} \sim \xi^{-2\Delta} \mathcal{G}_{OO}^{\text{co}} \left(\frac{x}{l_{\text{co}}(t)}, \frac{x}{l_{\text{co}}(t')} \right), \quad (1.13)$$

where $l_{\text{co}}(t) \equiv t^{\theta} = t^{-a\nu + \frac{a\nu z_d + 1}{z_d}}$.

z_d is a dynamic exponent specific to coarsening. The coarsening scaling forms in various models are reviewed in [22].

When present in the KZ problem, we expect coarsening physics to emerge deep in the ordered phase, i.e. as $\hat{t}, \hat{t}' \rightarrow \infty$, on the length scales $l_{\text{co}}(t), l_{\text{co}}(t')$. Proceeding as in the previous sub-section, we conclude that as $\hat{t}, \hat{t}' \rightarrow \infty$ holding $x/l_{\text{co}}(t)$ and $x/l_{\text{co}}(t')$ fixed, the two-point function must have the limiting form:

$$\mathcal{G}_{OO}(\hat{x}, \hat{t}, \hat{t}') \sim \hat{t}^{2a\nu\Delta} \mathcal{G}_{OO}^{\text{co}} \left(\frac{\hat{x}}{\hat{t}^{\theta}}, \frac{\hat{x}}{\hat{t}'^{\theta}} \right).$$

Note that the limiting equilibrium form requires holding $x/\xi(t)$ fixed and that $l_{\text{co}}(t)/\xi(t)$ diverges as $\hat{t} \rightarrow \infty$.

In the simplest case of Model A dynamics for spins with N -components, $z_d = z = 2$ and $l_{\text{co}}(t) \sim \sqrt{t}$ in the infinite- N limit. Although this phenomenology holds for systems with and without topological defects, the specific form of the equal-time spin-spin correlation function depends on the presence of topological defects [22].

Scaling form of the non-equilibrium correlation length

The non-equilibrium correlation length ξ_{ne} is defined to be the inverse of the decay constant on the longest length scales of the two-point equal-time correlator in real space. In equilibrium, this length is the cross-over scale in correlation functions

between fluctuations dominated by one fixed point and another. A particularly simple definition of ξ_{ne} is,

$$\xi_{\text{ne}}(t; \tau) = \sqrt{\frac{\int dx^d x^2 G_{oo}(x, t, t; \tau)}{\int dx^d G_{oo}(x, t, t; \tau)}}, \quad (1.14)$$

and is useful when G_{oo} is always positive. A more general definition is through the smallest imaginary part of the poles of $G_{oo}(k, t, t; \tau)$ in k -space; we will elaborate on this when the necessity arises. Biroli and coauthors [14] recently discussed the KZ scaling form of ξ_{ne} in non-symmetry breaking TCPs. They observed that ξ_{ne} must asymptote to the equilibrium correlation length, $\xi(t; \tau)$, as $\hat{t} \rightarrow -\infty$; that it must scale according to the critical coarsening form, $t_K^{1/z}$, when $|\hat{t}| \sim O(1)$; and that it must asymptote to the coarsening length l_{co} as $\hat{t} \rightarrow \infty$. Their proposed scaling form can be derived from that of G_{oo} and can be re-written as

$$\xi_{\text{ne}}(t; \tau) \sim l_K \mathcal{L}_{\text{ne}} \left(\frac{t}{t_K} \right). \quad (1.15)$$

The asymptotic behavior of ξ_{ne} for $\hat{t} \rightarrow \pm\infty$ formally translates to the limits

$$\mathcal{L}_{\text{ne}}(x) \sim \begin{cases} |x|^{-a\nu} & x \rightarrow -\infty \\ |x|^\theta & x \rightarrow \infty. \end{cases} \quad (1.16)$$

Absent coarsening physics, the right asymptote reproduces the instantaneous correlation length.

Scaling form of the number of defects

An intuitively appealing picture of the lack of order on length scales greater than the KZ length is through topologically protected point defects of characteristic separation l_K , and/or defects of dimension p with characteristic separation l_K in any hyperplane

of co-dimension p . This picture is really only meaningful if the separation between defects is much larger than the equilibrium correlation length; a constraint met only in the coarsening regime, $t \gg t_K$. In the coarsening regime, the density of a defect of dimension p in the hyperplane of co-dimension p should scale as $1/l_{\text{co}}(t; \tau)^{d-p}$. At fixed positive \hat{t} , this reproduces the celebrated scaling of the defect density with τ ,

$$\text{Density of defects} \sim \left(\frac{1}{l_K} \right)^{d-p} \sim \tau^{\frac{av(d-p)}{avz+1}}. \quad (1.17)$$

The above scaling with τ has been verified in experiments in 0-dimensional annular Josephson junctions [133] and in non-linear optical and hydrodynamical systems undergoing steady-state transitions [59, 33]. It is worth noting that the frequently cited experiments [44, 19] in liquid crystal systems do not test this critical scaling, but instead test the coarsening scaling forms. Although we have presented the above as a natural scaling ansatz, it may be derivable from the known scaling of correlation functions, for example, by the methods of Halperin-Liu-Mazenko for classical transitions [90, 125].

Scaling forms of thermodynamic analogs

The dynamics of classical systems is typically modeled phenomenologically by stochastic differential equations, possibly with conservation laws [99]. It is often useful to reformulate the stochastic dynamics in d -dimensions in terms of a path integral in $(d+1)$ [98, 130]. For Gaussian noise, the generating functional of correlation functions of the fundamental field $O(x, t)$ is

$$Z[J] = \int \mathcal{D}O(x, t) \exp \left(- \int d^d x dt (\mathcal{L} + J(x, t)O(x, t)) \right).$$

Here J is the source for O , and \mathcal{L} is a local Lagrangian density in which parameters of the protocol (like τ) appear as couplings. When hyper-scaling is obeyed, all KZ scaling forms follow from the scaling of the associated free energy.

In this formulation, it is natural to define a time-dependent free energy density. We divide the $(d+1)$ -dimensional space-time into a stack of spatial slices with volume L^d and temporal length Δt . Neglecting boundary effects, we compute the free-energy density of a slice:

$$f(t; \tau) = \lim_{\substack{L \rightarrow \infty \\ \Delta t \rightarrow 0}} \frac{-\log(Z)}{L^d \Delta t} \quad (1.18)$$

where

$$Z(t) = \int \mathcal{D}O \exp \left(- \int_{\mathbf{x} \in [-L, L]^d} d^d x \int_t^{t+\Delta t} dt \mathcal{L} \right).$$

For time-independent δ , f is also time-independent, and its leading non-analytic dependence on δ is $f_{\text{na}} \sim \delta^{\nu d}$. When δ varies with time, we conjecture a scaling form for $f_{\text{na}}(t; \tau)$ in the KZ limit :

$$f_{\text{na}}(t; \tau) \sim \frac{1}{l_K^d} \mathcal{F} \left(\frac{t}{t_K} \right). \quad (1.19)$$

When $t/t_K \ll -1$, the system is asymptotically in equilibrium. Thus,

$$\mathcal{F} \left(\frac{t}{t_K} \right) \sim \left(\frac{t}{t_K} \right)^{a\nu d} \quad \text{when } t/t_K \ll -1. \quad (1.20)$$

This is also the expected asymptotic form of \mathcal{F} if the system does not coarsen for $t/t_K \gg 1$.

1.4.2 ECPs

The definition of the scaling limit, the KZ scaling forms of various observables and their asymptotic behavior when the system is subjected to a non-adiabatic ECP closely follows the TCP discussion. Qualitatively:

- When $\hat{t} \rightarrow 0$, the system evolution is adiabatic and equilibrium scaling forms are recovered on the scale of the instantaneous correlation length and time.
- The long-time behavior of a sudden quench to the critical point is recovered in the limit $\hat{t} \rightarrow \infty$. On a growing length scale $l_{\text{co}}(t) = t^{1/z}$, the system appears self-similar and satisfies dynamical scaling (Eq. (1.13)). On length scales x much smaller than $l_{\text{co}}(t)$, correlations have relaxed to their critical form, while for $x \gg l_{\text{co}}(t)$ the system coarsens.
- Scaled times near 1 probe a universal early-time regime of a sudden quench, i.e. $t \ll \xi_{t,0}$ where $\xi_{t,0}$ is the relaxation time before the quench. In the sudden quench, this regime is tied to boundary criticality [104].

When $|a|\nu z = 1$ in Eq. (1.4), ξ_t is a constant for $t > \tau$. By suitably re-defining constants, Eq. (1.4) can be re-written as :

$$\delta(t) = \begin{cases} \delta_- & t \rightarrow -\infty \\ \left(\frac{\theta}{t}\right)^{1/\nu z} & t \gg \tau. \end{cases} \quad (1.21)$$

The key distinction between the marginal ECP and all the other protocols is that there is only one growing length scale $t^{1/z}$ everywhere in the power-law regime. At late times, we expect the system to appear self-similar on this scale. This leads us to the scaling limit : $x, t \rightarrow \infty$ at fixed θ holding $x/t^{1/z}$ fixed.

$$G_o(t) \sim \frac{1}{t^{\Delta/z}}$$

$$G_{oo}(x, t, t') \sim \frac{1}{t^{2\Delta/z}} \mathcal{G}_{oo} \left(\frac{x}{t^{1/z}}, \frac{t}{t'} \right). \quad (1.22)$$

We emphasize that the scaling functions above do not connect to the adiabatic limit. They are distinct from \mathcal{G}_{oo}^{eq} . Unfortunately, this also implies that they necessarily contain some non-universal data. The source of this non-universality will be clearer in the example of the quantum Gaussian theory in the next chapter (Sec. 2.2.6), where we are nevertheless able to identify interesting non-equilibrium behavior.

1.4.3 Quantum systems

We comment below on the major differences that arise in the treatment of quantum systems.

- The scaling of the correlation functions proceeds as before. However, the analogs of thermodynamic quantities of interest for protocols that begin with the system at $T = 0$ are now the excitation energy density in excess of the energy density in the adiabatic ground state, or “heat” density [51]⁶, and the entropy density for which plausible definitions can be constructed from the diagonal entropy [145, 144] or the entanglement entropy of a macroscopic subregion. These are respectively expected to exhibit the scaling forms

$$q(t; \tau) \sim \frac{1}{l_K^{d+z}} \mathcal{Q} \left(\frac{t}{t_K} \right) \quad (1.23)$$

$$s(t; \tau) \sim \frac{1}{l_K^d} \mathcal{S} \left(\frac{t}{t_K} \right). \quad (1.24)$$

For an isolated quantum system, by construction of the protocol, s and q are constant as $t \rightarrow -\infty$. As $\hat{t} \rightarrow \infty$, s and q also tend to a constant provided the system thermalizes to the Gibbs or the generalized Gibbs ensemble.

⁶See [144] for a discussion of why the total excitation energy is sensibly called heat. For infinite systems where one needs to work with intensive quantities though, a heat density is not a useful concept especially when macroscopic subregions exhibit thermal equilibration.

- For protocols that begin with the system in equilibrium at $T > 0$, a new dimensionless parameter, $k_B T / (\hbar/t_K)$, now enters the quantum problem. Along with the quantities held fixed as the quench time is taken to be arbitrarily large in Sec. 1.4.1, we also hold Tt_K fixed. For example, the scaling form for the 2-point unequal time correlation function is now

$$\langle O(0, t)O(\mathbf{x}', t') \rangle_{\tau, T} \sim \frac{1}{l_K^{2\Delta}} \mathcal{G}_{OO} \left(\frac{x'}{l_K}, \frac{t}{t_K}, \frac{t'}{t_K}, Tt_K \right).$$

The definition of the entropy goes through as before but the excitation energy density is now measured with respect to the energy density that would be obtained in a strictly adiabatic evolution ⁷.

- The excess energy density in the system is vanishingly small in the limit of large τ . Thus, the evolution of the system on the scales t_K, l_K is effectively in the quantum critical region at non-zero temperature T . If the phase transition does not persist at $T \neq 0$, the scaling phenomenology is as presented in the previous section. However, if there is a transition, two diverging KZ time scales, one associated with the classical transition and the other with the quantum, emerge in the $\tau \rightarrow \infty$ limit and a richer scaling limit can be formulated.
- Integrable quantum systems allow the existence of sharply defined quasiparticle excitations; their density resolved by momentum can serve as a uniquely quantum observable for CCPs and ECPs. When the vacuum is not unique, it is not straightforward to define quasiparticles and separate them from domain walls and other topological defects. Currently, we are not aware of an integrable system above one dimension where this question can be properly posed

⁷For an isolated system at finite temperature, the dynamics involves starting with a typical state with the thermodynamic limit energy density. At high temperatures, a typical state must look “classical”; this suggests that the behavior of the entanglement entropy and issues of many-body localization [5] need further examination.

[191] (in one dimension there is no real distinction between quasiparticles and domain walls). Note that the definition of the thermodynamic quantities of heat and entropy do not rely on integrability. For instance, in a cyclic process like a CCP, $q(t; \tau)$ when $t \gg t_K$ is the difference of the system's energy density between symmetric time points.

1.5 Comments

We conclude this chapter with four comments.

- The Kibble-Zurek picture was initially proposed for a linear ramp through a thermal transition. The time-dynamics was decoupled into three regions: the adiabatic regime for $t < -t_K$, the diabatic or sudden or impulse region from $-t_K$ to t_K when the system is frozen, and the post-quench regime for $t > t_K$ when the system is unfrozen and evolves through domain growth [209], defect-anti-defect annihilation etc. Recently [14], this picture was extended to account for evolution in the impulse regime using critical coarsening results. The KZ scaling forms introduced in this article also probe dynamics in the impulse regime with the adiabatic and the post-quench regimes acting as asymptotic limits.
- A finite system dimension L can be readily accommodated in our scaling forms in the combination L/l_K . The results obtained through adiabatic perturbation theory [143, 146] can therefore be fitted within this framework.
- We expect that the KZ scaling forms are unchanged by the inclusion of interaction terms in the dynamics that are irrelevant to the critical theory⁸. In the classical setting, the reformulation of the dynamical problem in d -dimensions as an inhomogenous statistical problem in $(d+1)$ -dimensions allows us to establish

⁸We exclude dangerously irrelevant operators from this discussion as they will modify the asymptotic behavior in the KZ scaling limit.

this by standard power-counting arguments. The quantum case is more subtle and needs to be treated case-by-case.

- As the free Gaussian theory is the stable critical point in $d > 4$, the KZ scaling forms that we calculate below in that theory are universal for $d > 4$. In the classical setting, interaction terms in the Gaussian theory can be treated as perturbations to the action defined in Sec. 1.4.1 and will modify dynamics only on time-scales t_{int} that are parametrically larger than t_K . In the quantum case, these terms induce scattering between the free quasi-particles of the unperturbed theory on time-scales t_{int} that are parametrically larger than t_K . In either case, $t_{int}/t_K \rightarrow \infty$ in the scaling limit and the effects of these terms drop out.

Chapter 2

KZ scaling functions in model theories

Near a critical point, the equilibrium relaxation time of a system diverges and any change of control/thermodynamic parameters leads to non-equilibrium behavior¹. The Kibble-Zurek problem is to determine the dynamical evolution of the system parametrically close to its critical point when the change is parametrically slow. In the previous chapter, we presented an extended and pedagogical discussion of the universal content in the Kibble-Zurek problem. We argued that the non-equilibrium behavior in the limit of an infinitely slow ramp is controlled entirely by the critical point *and* the details of the trajectory of the system in parameter space (the protocol) close to the critical point. Together, they define a universality class consisting of critical exponents—discussed in the seminal work by Kibble and Zurek—and scaling functions for physical quantities, which have not been discussed hitherto. In the previous chapter, we remedied this oversight in the literature by formally defining a scaling limit for physical quantities near classical and quantum transitions for dif-

¹Chapter based on work with Amir Erez, Steven S. Gubser and S. L. Sondhi [39].

ferent sets of protocols and discussing the physics that the scaling functions could capture.

In this chapter, we discuss the physics that the scaling functions *do* capture in a few model theories. We compute and discuss a few scaling functions in three model theories: the classical $O(N)$ vector model endowed with Model A dynamics in the Gaussian and large- N approximations and the quantum $O(N)$ model in the Gaussian approximation. We further prove that the scaling functions are universal with respect to protocol choice. We also show that the end-critical protocol (ECP) in which the critical point is approached asymptotically at late times with the system marginally out of equilibrium leads to logarithmic violations to scaling and anomalous dimensions even in the simple Gaussian problem.

We note that a recent paper by Kolodrubetz et al. reports analogous results for the transverse field Ising model in (1+1) dimensions [117]. This work complements our own results on the quantum Ising universality class above the upper critical dimension $(3 + 1)$ where the critical theory is Gaussian².

2.1 Classical Systems with Model A dynamics

We illustrate the universality of the KZ scaling limit and explicitly compute scaling functions of a vector operator $\vec{\phi}$ in the simplest setting: Model A [99] dynamics with a Landau-Ginzburg-Wilson (LGW) free energy. Model A dynamics is dissipative and obeys no conservation laws. Let $\vec{\phi}$ be an N -component vector field in $d = 3$ dimensions. The dimensionless LGW free-energy and the equation of motion are,

²Anticipating our classification, this statement is strictly true only for the cis- and end-critical protocols. The dangerously irrelevant interaction needs to be included to properly study the trans-critical protocols.

respectively,

$$F = \int d^3x \left[\frac{1}{2} \left(|\nabla \vec{\phi}|^2 + r_0 |\vec{\phi}|^2 + \frac{u}{2N} |\vec{\phi}|^4 \right) - \sqrt{N} h^\alpha \phi_\alpha \right]$$

$$\frac{\partial \phi_\alpha}{\partial t} = -\frac{\partial F}{\partial \phi_\alpha} + \zeta_\alpha. \quad (2.1)$$

x and t are dimensionless and measured in units of the inverse cutoff Λ^{-1} and Λ^{-z} respectively. ζ_α is a zero-mean spatially uncorrelated white-noise stochastic variable for every α . The variance of ζ_α is chosen to be 2 so that the long-time limit of the structure factor computed from the equation of motion when F is time-independent is equal to the equilibrium structure factor:

$$\langle \zeta_\alpha(\mathbf{x}, t) \zeta_\beta(\mathbf{x}', t') \rangle = 2\delta_{\alpha\beta} \delta^3(\mathbf{x} - \mathbf{x}') \delta(t - t'). \quad (2.2)$$

2.1.1 Gaussian Limit

In this limit, we drop the ϕ^4 term in F . The critical point is at $r_0 = 0, h^\alpha = 0$, i.e. at the origin in the (r_0, h^α) parameter space. Let us restrict ourselves to paths in this space that lie along the axes and include the origin. The equilibrium theory is sensible only at the origin and when $r_0 > 0$. We can therefore study CCPs and ECPs along the non-negative r_0 axis ($\delta = r_0$). Luckily, we can also study TCPs along the same axis as the time-dependent fields are finite even when $r_0 < 0$. This physically uninteresting protocol is pedagogically useful. The critical exponents for all such paths are $\nu = 1/2, z = 2$. In the remainder of the discussion, $\delta = r_0$ and $h^\alpha, u = 0$.

Eq. (2.1) is linear in $\vec{\phi}$ and hence diagonal in Fourier space. It can be explicitly solved for any protocol $\delta(t; \tau) = r_0(t; \tau)$ and a fixed noise realization:

$$\phi(\mathbf{k}, t) = \int_{-\infty}^t dt' e^{-\int_{t'}^t dt'' (k^2 + r_0(t''; \tau))} \zeta(\mathbf{k}, t'). \quad (2.3)$$

We have dropped the component label of $\vec{\phi}$ for brevity. Memory of the initial condition at $t = -\infty$ is lost on the time-scale $1/r_0(-\infty; \tau)$ and is therefore absent in the solution above. The equal time structure factor for each component, defined as $\langle \phi(\mathbf{k}, t) \phi(\mathbf{k}', t) \rangle = (2\pi)^3 \delta^3(\mathbf{k} + \mathbf{k}') G_{\phi\phi}(k, t; \tau)$, is

$$G_{\phi\phi}(k, t; \tau) = 2 \int_{-\infty}^t dt' e^{-2 \int_{t'}^t dt'' (k^2 + r_0(t''; \tau))}. \quad (2.4)$$

Scaling limit for tanh TCP

The universality of the scaling limit with respect to details of the the protocol is already apparent when we consider the simple TCP $r_0(t; \tau) = -\tanh(t/\tau)$. This is an example of a protocol that is linear near the critical point, i.e. $a = 1$ in Eq. (1.2). Consequently, the KZ time and length scales are

$$t_K = \sqrt{\tau}, \quad l_K = \tau^{1/4}.$$

Re-writing Eq. (2.4) in units $\hat{k} = kl_K$ and $\hat{t} = t/t_K$,

$$G_{\phi\phi}(k, t; \tau) = 2t_K \int_{-\infty}^{\hat{t}} d\hat{t}' e^{-2 \int_{\hat{t}'}^{\hat{t}} d\hat{t}'' (\hat{k}^2 - t_K \tanh(\hat{t}''/t_K))}.$$

As $\tau \rightarrow \infty$, $t_K \tanh(\hat{t}''/t_K) \rightarrow \hat{t}''$ and the KZ scaling form of the two-point equal time correlation function is

$$\begin{aligned} G_{\phi\phi}(k, t; \tau) &\sim l_K^2 \mathcal{G}_{\phi\phi}(\hat{k}, \hat{t}) \\ &\sim l_K^2 \int_{-\infty}^{\hat{t}} 2d\hat{t}' e^{-2 \int_{\hat{t}'}^{\hat{t}} d\hat{t}'' (\hat{k}^2 - \hat{t}'')}. \end{aligned} \quad (2.5)$$

Observe that the scaling function only depends on the leading behavior of the protocol near the critical point. For all protocols such that $r_0(t; \tau) \sim -t/\tau$ in the vicinity of

zero time, the scaling form of the structure factor is the expression that we have just derived.

Scaling functions for all TCPs and CCPs

Wick's theorem informs us that all higher order cumulants of ϕ only depend on $G_{\phi\phi}$. The details of the protocol enter the expression of $G_{\phi\phi}$ only in the combination $t_K r_0(t; \tau)$. In the scaling limit, for any a in Eq. (1.2), it is easily seen that

$$t_K r_0(t; \tau) \sim \left(\frac{-t}{t_K} \right)^a. \quad (2.6)$$

The scaling function of the equal time correlation function for any protocol with the near-zero behavior in Eq. (1.2) is therefore

$$\mathcal{G}_{\phi\phi}(\hat{k}, \hat{t}) = 2 \int_{-\infty}^{\hat{t}} d\hat{t}' e^{-2 \int_{\hat{t}'}^{\hat{t}} d\hat{t}'' (\hat{k}^2 + (-\hat{t}'')^a)}.$$

As seen from the Fig. 2.1 for the linear TCP, $\mathcal{G}_{\phi\phi}$ and \mathcal{L}_{ne} match equilibrium forms as $\hat{t} \rightarrow -\infty$ and $\hat{k} \gg 1$:

$$\begin{aligned} l_K^2 \mathcal{G}_{\phi\phi}(\hat{k}, \hat{t}) &\sim \xi^2 \mathcal{G}_{\phi\phi}^{\text{eq}}(k\xi(t)) \equiv \frac{\xi(t)^2}{k^2 \xi(t)^2 + 1} \\ \xi_{\text{ne}} &\sim l_K \mathcal{L}_{\text{ne}} \equiv \frac{1}{(-t)^{1/2}}. \end{aligned} \quad (2.7)$$

Observe that $\mathcal{G}_{\phi\phi}(0, 0)$ is finite, indicating the suppression of order on length scales longer than l_K . As $\hat{t} \rightarrow \infty$, the non-equilibrium correlation length grows without bound for TCPs due to the inverted potential. For CCPs, on the other hand, all scaling forms asymptote to the equilibrium forms at large positive times.

In Appendix 2.A, we compute the partition function in (3+1) dimensions and demonstrate the validity of the scaling hypothesis for the free-energy density f_{na} .

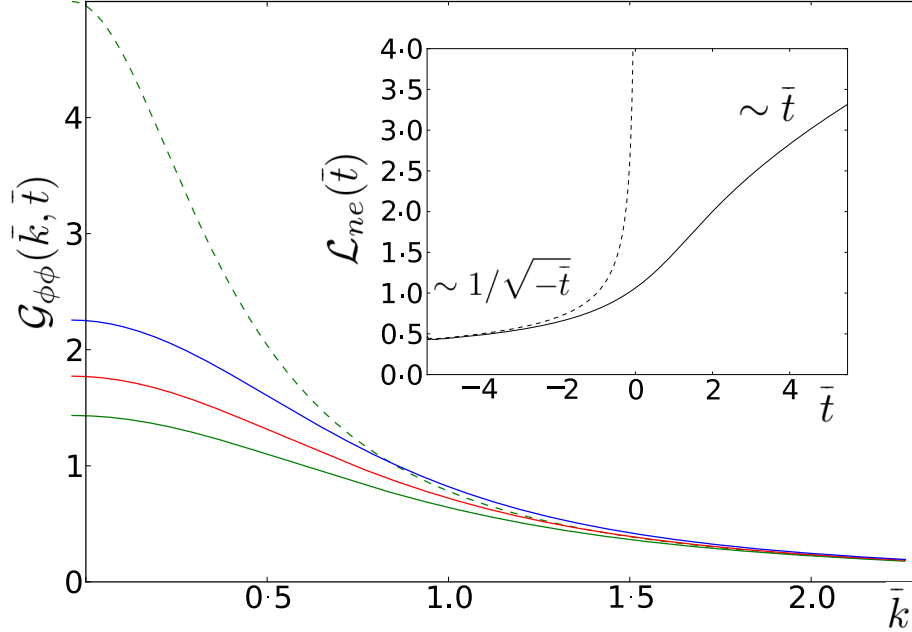


Figure 2.1: $\mathcal{G}_{\phi\phi}(\hat{k}, \hat{t})$ vs \hat{k} at fixed time slices for the linear TCP. The blue, red and green solid lines are respectively at $\hat{t} = 0.2, 0$ and -0.2 . The green dashed line is the correlator if the system were in equilibrium at $\hat{t} = -0.2$. Inset: The scaling form of the non-equilibrium correlation length vs \hat{t} in solid. The dashed line is the instantaneous correlation length in units of l_K , $\xi(t; \tau)/l_K$.

Scaling functions for the ECPs

The scaling functions of the non-adiabatic ECPs is identical to that of the TCPs/CCPs when $a < -1/\nu z$. Their asymptotic behavior may also be verified to be in agreement with Sec. 1.4.2. The more interesting case is the marginal ECP $r_0(t) = \theta/t$. Independent of the early-time regularization on the time-scale τ , $G_{\phi\phi}$ has the asymptotic form in Eq. (1.22):

$$G_{\phi\phi}(k, t) \sim t \mathcal{G}_{\phi\phi}(k\sqrt{t})$$

$$\mathcal{G}_{\phi\phi}(x) \equiv \frac{4e^{-2x^2}}{x^{4\theta+2}} \int_0^x dy e^{2y^2} y^{4\theta+1}.$$

As promised, $\mathcal{G}_{\phi\phi}(x)$ is distinct from $\mathcal{G}_{\phi\phi}^{\text{eq}}(x)$ and the non-equilibrium correlation length is a multiple of the instantaneous one $\xi(t) = \sqrt{t/\theta}$ at late times. The system exhibits critical coarsening and relaxes to the critical point as $t \rightarrow \infty$.

2.1.2 Large- N limit

In the infinite N limit, the LGW theory is exactly solvable in terms of 1 and 2-point correlators. All higher order correlators follow by the application of Wick's theorem. The 1 and 2 point correlators are known exactly in equilibrium and can be reduced to quadrature with Model A dynamics. The theory in $d = 3$ that we discuss here exhibits non-trivial critical behavior and affords us a probe of symmetry-breaking paths and coarsening physics.

Assume in Eq. (2.1) that $h^i \neq 0$ for $i = 1$ and zero otherwise. This specifies all one-point correlators for $i > 1$ to be zero. The two-point connected correlator for every component is the same and is a function of the variable $m^2 = r_0 + u\langle\phi_\alpha^2\rangle$. The well-known self-consistency equations relating $\langle\phi_1\rangle$, $G_{\phi\phi}$ and m^2 are

$$r_0 + u \left(\int^\Lambda \frac{d^3k}{(2\pi)^3} G_{\phi\phi}(k) + \frac{\langle\phi_1\rangle^2}{N} \right) = m^2 \quad (2.8)$$

$$\langle\phi_1\rangle = \frac{\sqrt{N}h^1}{m^2}, \quad (2.9)$$

where Λ is a cutoff on the maximum allowed $|k|$.

The third equation that completes the theory in equilibrium is,

$$G_{\phi\phi}^{\text{eq}}(k) = \frac{1}{k^2 + m^2}. \quad (2.10)$$

The critical point in the equilibrium theory is at $r_0 = r_c = -u\Lambda/2\pi^2$ and $h^\alpha = 0$. The two relevant operators that couple to r_0 and h^α are respectively $|\vec{\phi}|^2$ and ϕ_α , with scaling dimensions 1 and 5/2 in $d = 3$. They are respectively non-symmetry breaking

and symmetry-breaking. Consequently, we can study all three kinds of protocols along the r_0 axis ($\nu = 1, z = 2$) or along any of the h^α axes ($\nu = 2/5, z = 2$).

The equation of motion (2.1) for Model A dynamics is

$$\frac{\partial \phi_\alpha(\mathbf{k}, t)}{\partial t} = -(k^2 + m^2)\phi_\alpha(\mathbf{k}, t) + h^\alpha (2\pi)^3 \delta^3(\mathbf{k}) + \zeta_\alpha. \quad (2.11)$$

This specifies the functional dependence of $G_{\phi\phi}(k, t; \tau)$ on m^2 and completes the dynamical theory.

Scaling limit for TCPs and CCPs along the r_0 axis

Here $h^\alpha = 0$ and $\delta(t; \tau) = r_0(t; \tau) - r_c$. Eq. (2.9) implies that the one-point correlator for all components is zero: $\langle \phi_\alpha \rangle = 0$. We henceforth drop component subscripts. We will make frequent use of the Gaussian result (2.4), which we reproduce here for the reader's convenience:

$$G_{\phi\phi}(k, t; \tau; r_0) = 2 \int_{-\infty}^t dt' e^{-2 \int_{t'}^t dt'' (k^2 + r_0(t''; \tau))}$$

The notation $G_{\phi\phi}(k, t; \tau; r_0)$ emphasizes that $G_{\phi\phi}$ depends on $r_0(t; \tau)$.

Observe that the solution to Eq. (2.11) is exactly that of the free Gaussian case—Eq. (2.3)—with $r_0(t; \tau)$ replaced by $m^2(t; \tau)$. Consequently, the third equation that completes the dynamical theory is

$$G_{\phi\phi}(k, t; \tau) = G_{\phi\phi}(k, t; \tau; m^2), \quad (2.12)$$

where the right hand side refers to the Green's function of (2.12) with $r_0(t; \tau)$ replaced by $m^2(t; \tau)$. The critical value r_c of r_0 in this notation is,

$$r_c = -u \int \frac{d^3 k}{(2\pi)^3} G_{\phi\phi}(k, t; \tau; 0). \quad (2.13)$$

One can now re-express (2.8) as

$$m^2(t; \tau) = \delta(t; \tau) + u \int^{\Lambda} \frac{d^3 k}{(2\pi)^3} \left[G_{\phi\phi}(k, t; \tau; m^2) - G_{\phi\phi}(k, t; \tau; 0) \right]. \quad (2.14)$$

Let us now take the scaling limit. The KZ length and time scales are $t_K = (\tau^a/\delta_0)^{\frac{2}{2a+1}}$ and $l_K = \sqrt{t_K}$. Dimensional considerations imply that the scaling form of $m^2(t; \tau)$ is $m^2(t; \tau) \sim \mathcal{M}^2(\hat{t})/l_K^2$. Using the leading order behavior of the protocol near the critical point, $\delta(t; \tau) \sim (-\hat{t})^a/l_K$, we derive the following scaled form of Eq. (2.14):

$$(-\hat{t})^a + 2u \int_{-\infty}^{\hat{t}} d\hat{t}' \int^{\infty} \frac{d^3 \hat{k}}{(2\pi)^3} \left(e^{-2 \int_{\hat{t}'}^{\hat{t}} d\hat{t}'' (\hat{k}^2 + \mathcal{M}^2)} - e^{-2 \int_{\hat{t}'}^{\hat{t}} d\hat{t}'' \hat{k}^2} \right) = 0 \quad (2.15)$$

We note the following points:

1. The cutoff Λ appears in the unscaled equation only as the upper limit on the momentum integral. In the scaling limit, the upper limit $\sim \Lambda l_K \rightarrow \infty$ and the scaled relation is *cutoff-independent*.
2. The scaled relation, being a limiting form, is *simpler* than the unscaled one.
3. The relation above is unchanged by keeping higher order terms in $r_0(t; \tau)$. This is tantamount to proving the universality of all correlators with respect to details of the protocol away from the critical point in the scaling limit.

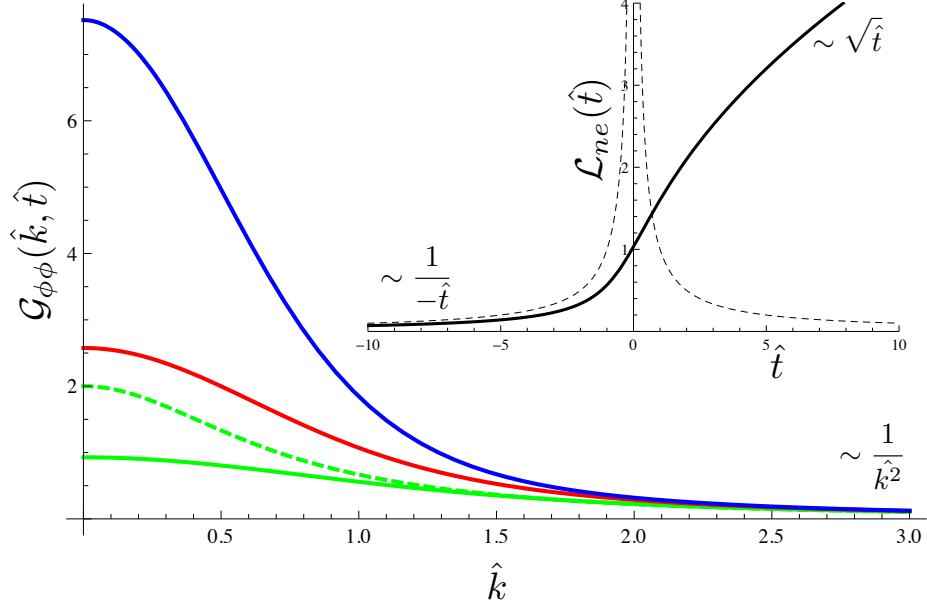


Figure 2.2: $\mathcal{G}_{\phi\phi}(\hat{k}, \hat{t})$ vs \hat{k} at fixed time slices for the linear TCP. The blue, red and green solid lines are respectively at $\hat{t} = 0.5, 0$ and -0.5 . The green dashed line is the correlator if the system were in equilibrium at $\hat{t} = -0.5$. Inset: \mathcal{L}_{ne} vs \hat{t} (solid) and ξ/l_K (dashed).

Scaling forms for the linear TCP

Fortunately, Eq. (2.15) can be solved when $a = 1$. The choice $u = \sqrt{8}\pi$ simplifies pre-factors and makes apparent the form of the solution. Defining

$$f(\hat{t}) \equiv e^{2 \int_0^{\hat{t}} d\hat{t}' \mathcal{M}^2(\hat{t}')} \text{ or } \mathcal{M}^2(\hat{t}) = \frac{f'(\hat{t})}{2f(\hat{t})}, \quad (2.16)$$

the solution is

$$f(\hat{t}) = -3^{1/3} \Gamma(1/3) e^{2\hat{t}^3/3} (\hat{t} \text{Ai}(\hat{t}^2) + \text{Ai}'(\hat{t}^2)).$$

Ai is the Airy function of the first kind and Γ is the gamma function. We may reduce $\mathcal{G}_{\phi\phi}$ to quadrature:

$$\mathcal{G}_{\phi\phi}(\hat{k}, \hat{t}) = 2 \int_{-\infty}^{\hat{t}} d\hat{t}' e^{-2 \int_{\hat{t}'}^{\hat{t}} d\hat{t}'' (\hat{k}^2 + \mathcal{M}^2(\hat{t}''))},$$

and compute all higher cumulants using Wick's theorem.

As $\hat{t} \rightarrow -\infty$, we recover the equilibrium behavior in Eq. (2.7) with $\xi \sim 1/(-t)$. The results from the coarsening literature [22] in this theory are :

$$l_{\text{co}}(t) = \sqrt{t}$$

$$\mathcal{G}_{\phi\phi}^{\text{co}}(kl_{\text{co}}(t)) = \exp(-2(kl_{\text{co}}(t))^2).$$

We should therefore expect that $\mathcal{L}_{\text{ne}} \sim \sqrt{\hat{t}}$ and $\mathcal{G}_{\phi\phi} \sim \hat{t}^{5/2} \exp(-2\hat{k}^2\hat{t})$ as $\hat{t} \rightarrow \infty$. As is seen from Fig. 2.2, both asymptotes are correctly predicted for \mathcal{L}_{ne} . We have checked this for $\mathcal{G}_{\phi\phi}$ as well. This verifies that the asymptotes predicted in Eq. (1.16) and in Eq. (1.14) are correct in this theory.

Scaling limit for TCPs and CCPs along h_1 axis

Setting $r_0 = r_c$, we can explore symmetry-breaking protocols along the h^1 axis. The implicit relation from the self-consistency equations for the linear TCP is

$$\left(\int_{-\infty}^{\hat{t}} d\hat{t}' \hat{t}' \sqrt{f(\hat{t}')} \right)^2 = \int_{-\infty}^{\hat{t}} d\hat{t}' \frac{f(\hat{t}) - f(\hat{t}')}{|\hat{t} - \hat{t}'|^{3/2}}. \quad (2.17)$$

Although scaling is guaranteed, we cannot proceed further as the solution to this equation is not known.

2.2 Gaussian Quantum Field Theories

We now turn to the KZ problem near quantum critical points. Again, it will prove instructive to investigate the class of ferromagnetic critical points with $O(N)$ symmetry. We will consider the simplest non-trivial case, that of Gaussian scalar fields. The Lagrangian we consider is,

$$\mathcal{L} = \frac{1}{2} [\partial_\mu \phi \partial^\mu \phi - m^2 \phi^2] , \quad (2.18)$$

where we permit m^2 to depend on time ($\delta \equiv m^2$). Standard critical exponents include $z = 1$ (owing to relativistic symmetry when m is a constant) and $\nu = 1/2$ (owing to the Yukawa form of the Green's function for static sources when m is a constant).

2.2.1 Second quantization

The second quantized treatment of ϕ is based on the expansion

$$\phi(\mathbf{x}, t) = \int \frac{d^d k}{(2\pi)^d} e^{i\mathbf{k}\cdot\mathbf{x}} \phi_{\mathbf{k}}(t) , \quad (2.19)$$

where we set

$$\phi_{\mathbf{k}}(t) = f_{\mathbf{k}}(t) a_{\mathbf{k}} + f_{-\mathbf{k}}^*(t) a_{-\mathbf{k}}^\dagger \quad (2.20)$$

and impose the commutation relations

$$[a_{\mathbf{k}}, a_{\mathbf{k}'}^\dagger] = (2\pi)^d \delta^d(\mathbf{k} - \mathbf{k}') . \quad (2.21)$$

Owing to rotational symmetry, the mode functions $f_{\mathbf{k}}(t)$ and Green's functions only depend on the magnitude of the momentum k . The mode functions $f_k(t)$ satisfy the mode equation

$$\left[\frac{d^2}{dt^2} + \Omega_k^2(t) \right] f_k(t) = 0 , \quad (2.22)$$

where

$$\Omega_k^2(t) \equiv k^2 + m^2(t). \quad (2.23)$$

One must also impose the Wronskian condition

$$f_k \dot{f}_k^* - \dot{f}_k f_k^* = i \quad (2.24)$$

in order to obtain standard commutation relations between $\phi_{\mathbf{k}}$ and its conjugate $\pi_{\mathbf{k}} = \dot{\phi}_{\mathbf{k}}^\dagger$. Once the mode functions f_k are specified, a Fock space vacuum $|0\rangle$ can be defined through the conditions $a_{\mathbf{k}}|0\rangle = 0$.

In general, Eq. (2.22) is hard to solve exactly. However, the techniques of WKB provide an approximate solution when Ω_k is real, positive and varying “slowly enough”; to this end, let us define the oscillatory, positive frequency WKB solution:

$$\tilde{f}_k(t) = \frac{1}{\sqrt{2\Omega_k(t)}} \exp \left\{ -i \int^t dt' \Omega_k(t') \right\}, \quad (2.25)$$

where the lower limit of integration can be specified at our later convenience. If one defines $\tilde{a}_{\mathbf{k}}(t)$ through the equations $\phi_{\mathbf{k}}(t) = \tilde{f}_k(t)\tilde{a}_{\mathbf{k}}(t) + \tilde{f}_k^*(t)\tilde{a}_{-\mathbf{k}}^\dagger(t)$, and requires $[\tilde{a}_{\mathbf{k}}(t), \tilde{a}_{-\mathbf{k}}^\dagger(t)] = (2\pi)^d \delta^d(\mathbf{k} - \mathbf{k}')$ for all t , then $(\tilde{f}_k(t), \tilde{f}_k^*(t))$ and $(f_k(t), f_k^*(t))$ are related through the standard Bogoliubov transformation.

As m^2 is slowly varying and positive at large negative times, the evolution is adiabatic and we require that the f_k coincide asymptotically with the positive frequency WKB solutions \tilde{f}_k as $t \rightarrow -\infty$. Thus $|0\rangle$ is the “out” vacuum in the parlance of [15, 113], and we assume that our system has been prepared in this vacuum. All expectation values unless otherwise indicated are with respect to this state.

2.2.2 The scaling limit

In the classical context, we first solved the complete dynamical problem for arbitrary initial condition and protocol choice. We then established that all local physical quantities reduced to universal forms *independent of the details of the protocol away from the critical point and the initial conditions* in the KZ scaling limit. We repeat the same exercise here by using WKB methods to solve Eq. (2.22) for a general TCP/CCP in $m^2(t; \tau)$.

Assume that the system is initially prepared in the vacuum state. The solution to Eq. (2.22) is well-approximated by the positive oscillatory WKB solution \tilde{f}_k at early times, and by a linear combination of the WKB solutions, \tilde{f}_k and \tilde{f}_k^* , at late times, as long as the frequency, $1/\Omega_k$, is much larger than the rate at which the frequency changes, $|d \log \Omega_k / dt|$. This yields the condition, $|dm^{-1}/dt| \ll 1$. Within the window $|t| < \tau$, we use the leading order expansion for $m^2(t; \tau)$ in t/τ ,

$$m^2(t; \tau) = m_0^2 \left(\frac{-t}{\tau} \right)^a \left[1 + a_1 \frac{t}{\tau} + \dots \right], \quad (2.26)$$

to conclude that the WKB solutions are valid as long as $|t| \gg t_K$ or $|\hat{t}| \gg 1$. Note that t_K using Eq. (1.5) is,

$$t_K = \tau^{\frac{a}{2+a}} / m_0^{\frac{2}{2+a}}. \quad (2.27)$$

Directly solving the mode equation using the expansion in Eq. (2.26) yields a solution valid in the region $|t| \ll \tau$ or $|\hat{t}| \ll \tau/t_K$. Thus, the overlap in the ranges of the validity of the direct solution and the WKB one is:

$$1 \ll \hat{t} \ll \frac{\tau}{t_K}. \quad (2.28)$$

We are now in a position to take the KZ scaling limit whereby $\tau \rightarrow \infty$ and all quantities are measured in units of the KZ length and time. We first notice that the

region of overlap in Eq. (2.28) diverges. The mode equation near $t = 0$ also simplifies in scaled units. We see from Eq. (2.24) that f_k carries dimensions of \sqrt{t} , so its scaling form is

$$f_k \sim \sqrt{t_K} \hat{f}_{\hat{k}}, \quad (2.29)$$

where $\hat{k} = l_K k$ as usual and $l_K = t_K$. The scaled mode equation in the window $|t| < \tau$ before any limits are taken is

$$\left[\frac{d^2}{d\hat{t}^2} + \hat{\Omega}_k^2(\hat{t}) \right] \hat{f}_{\hat{k}} = 0, \quad (2.30)$$

where $\hat{\Omega}_k^2 = \hat{k}^2 + \hat{m}^2(\hat{t})$ and

$$\hat{m}^2(\hat{t}) = (-\hat{t})^a \left[1 + a_1 \frac{t_K \hat{t}}{\tau} + a_2 \left(\frac{t_K \hat{t}}{\tau} \right)^2 + \dots \right]. \quad (2.31)$$

In the KZ scaling limit, $t_K/\tau \rightarrow 0$ and the corrections in the square bracket vanish, resulting in the simpler scaled mode equation,

$$\left[\frac{d^2}{d\hat{t}^2} + \hat{k}^2 + (-\hat{t})^a \right] \hat{f}_{\hat{k}} = 0. \quad (2.32)$$

The goodness of the approximation is parametrically controlled by the smallness of the parameter t_K/τ . Corrections to the diverging overlap in the ranges of the validity of the solution to the scaled equation above and the WKB one is also controlled by the same small parameter t_K/τ . Thus, the solution to Eq. (2.32) picked out by starting with a positive frequency WKB solution at early times is the same as the one picked out by applying the early-time positive frequency condition directly to the solutions of the limiting equation, Eq. (2.32). This is the sense in which the mode functions in the scaling limit are universal. It is worth noting that these considerations are merely an elaboration of the standard arguments used to justify turning point

formulas in standard WKB treatments of the time-independent Schrödinger equation in the geometric optics limit.

Finally, let us note that the above considerations will not apply to the marginal ECP. For a given non-universal regularization of the protocol at small time ($t < \tau$), the direct solution to the mode equation in the power-law regime ($t \gg \tau$) has no overlap with the positive frequency WKB solution at early times. As we discuss later, this implies that some information about the short time regularization *must* enter the scaling limit.

2.2.3 Quasi-particles, heat density and diagonal entropy

As the Gaussian problem is integrable, quasi-particles are well-defined and infinitely long-lived. The quasi-particle number at momentum \mathbf{k} , \mathcal{N}_k , is defined as the expectation value of the occupation of mode \mathbf{k} and has the scaling form,

$$\begin{aligned} \mathcal{N}_k(\hat{t}) &\equiv \langle \tilde{a}_{\mathbf{k}}^\dagger(\hat{t}) \tilde{a}_{\mathbf{k}}(\hat{t}) \rangle \\ &= \frac{1}{2|\hat{\Omega}_k|} |\partial_{\hat{t}} \hat{f}_k + i\hat{\Omega}_k \hat{f}_k|^2. \end{aligned} \quad (2.33)$$

The excess energy density is given by $q(t; \tau) = \int d^d k / (2\pi)^d \Omega_k \mathcal{N}_k$ and is easily seen to obey the scaling form conjectured in Eq. (1.23). A definition of the entropy density of the system at each instant of time is through the diagonal entropy density. The diagonal entropy density, s , is the entropy density of the diagonal components of the density matrix $\rho(t; \tau)$ in the many-body adiabatic basis. In the Gaussian problem, s is additive in the label \mathbf{k} and this definition simplifies to,

$$s(t; \tau) = - \int \frac{d^d k}{(2\pi)^d} \sum_m \rho_{m\mathbf{k}, m\mathbf{k}} \log(\rho_{m\mathbf{k}, m\mathbf{k}}).$$

Here $\rho_{m\mathbf{k},m\mathbf{k}}$ is the absolute value squared of the overlap between the time-evolved wave-function $|\psi(t)\rangle$, and the m_{th} excited state of the harmonic oscillator labeled by \mathbf{k} . The integral only runs over half the volume in k -space as the modes, \mathbf{k} and $-\mathbf{k}$, are coupled by the Hamiltonian. $\rho_{m\mathbf{k},m\mathbf{k}}$ can be directly computed in the Schrödinger picture because the time-evolved wavefunction is known in terms of the mode functions. In the eigenbasis of the operator $\phi_{\mathbf{k}}$ defined in Eq. (2.20), the wavefunction is a Gaussian [49],

$$\langle \phi_{\mathbf{k}} | \psi \rangle \propto \exp \left[- \int \frac{d^d k}{(2\pi)^d} \left(\frac{1}{|f_{\mathbf{k}}(t)|^2} - i \frac{\dot{f}_{\mathbf{k}}(t)}{f_{\mathbf{k}}(t)} \right) \phi_{\mathbf{k}} \phi_{-\mathbf{k}} \right]$$

up to normalization and time-dependent phases. In the scaling limit, $f_{\mathbf{k}}(t) \sim \sqrt{t_{\kappa}} f_{\hat{\mathbf{k}}}(\hat{t})$ and s has the scaling form predicted in Eq. (1.23). As all that is at issue is the scaling of the mode functions $f_{\mathbf{k}}(t)$, the scaling forms of correlation functions may also be easily verified.

$$G_{\phi\phi}(k, t; \tau) \equiv |f_{\mathbf{k}}(t)|^2 \sim t_{\kappa} |\hat{f}_{\hat{\mathbf{k}}}(\hat{t})|^2 \sim t_{\kappa} \mathcal{G}_{\phi\phi}(\hat{k}, \hat{t}). \quad (2.34)$$

2.2.4 Linear protocol

We now turn to a particular protocol, namely the linear quench, where the KZ time is $t_{\kappa} = (\tau/m_0^2)^{1/3}$. For this case the mode equation can be solved in closed form to give

$$\hat{f}_{\hat{\mathbf{k}}}(\hat{t}) = \sqrt{\frac{\pi}{2}} \left[\text{Bi}(\hat{t} - \hat{k}^2) + i \text{Ai}(\hat{t} - \hat{k}^2) \right], \quad (2.35)$$

where Ai and Bi are Airy functions of the first and second kind. The scaling function of the two-point function from Eq. (2.34) is:

$$\mathcal{G}_{\phi\phi}(\hat{k}, \hat{t}) = \frac{\pi}{2} \left(\text{Ai}^2(\hat{t} - \hat{k}^2) + \text{Bi}^2(\hat{t} - \hat{k}^2) \right). \quad (2.36)$$

As a check we may retrieve the equilibrium result when $\hat{t} \rightarrow -\infty$ holding $k\xi$ or $\hat{k}/\sqrt{-\hat{t}}$ fixed.

$$\mathcal{G}_{\phi\phi}(\hat{k}, \hat{t}) \sim \frac{1}{2\hat{\Omega}_{\hat{k}}}. \quad (2.37)$$

The equilibrium result is not retrieved when $\hat{t} \rightarrow \infty$ because of the pathology of the inverted ϕ^2 term when $\hat{t} > 0$. Instead, $\mathcal{G}_{\phi\phi}$ grows exponentially with \hat{t} . From $G_{\phi\phi}$ we can calculate the non-equilibrium correlation length,

$$\xi_{\text{ne}} \sim t_K \sqrt{\frac{\partial_{\hat{t}}(\text{Ai}(\hat{t})^2 + \text{Bi}(\hat{t})^2)}{\text{Ai}(\hat{t})^2 + \text{Bi}(\hat{t})^2}}. \quad (2.38)$$

whose scaling form \mathcal{L}_{ne} is plotted in Fig. 2.3(a). At large positive t , \mathcal{L}_{ne} grows polynomially instead of exponentially with time, despite the instability of the adiabatic theory with an inverted ϕ^2 term. As the adiabatic problem is pathological for $\hat{t} > 0$, we can only sensibly talk of quasiparticle occupations and thermodynamic quantities as long as $\hat{t} \leq 0$. In Fig. 2.4, we plot $\mathcal{N}_{\hat{k}}(\hat{t})$ and $\mathcal{S}_{\hat{k}}(\hat{t})$ for various values of \hat{k} (the behavior of the excess energy density can be inferred from the number of quasiparticle excitations). The contribution to the total quasi-particle density from the high-wavenumber ($\hat{k} \gg \sqrt{-\hat{t}}$) modes for $\hat{t} \ll -1$ is finite only if $d < 6$:

$$\int_{\sqrt{-\hat{t}}}^{\infty} \frac{d^d \hat{k}}{(2\pi)^d} \mathcal{N}_{\hat{k}}(\hat{t}) \sim \frac{1}{(-\hat{t})^{3-d/2}} \quad \text{if } d < 6.$$

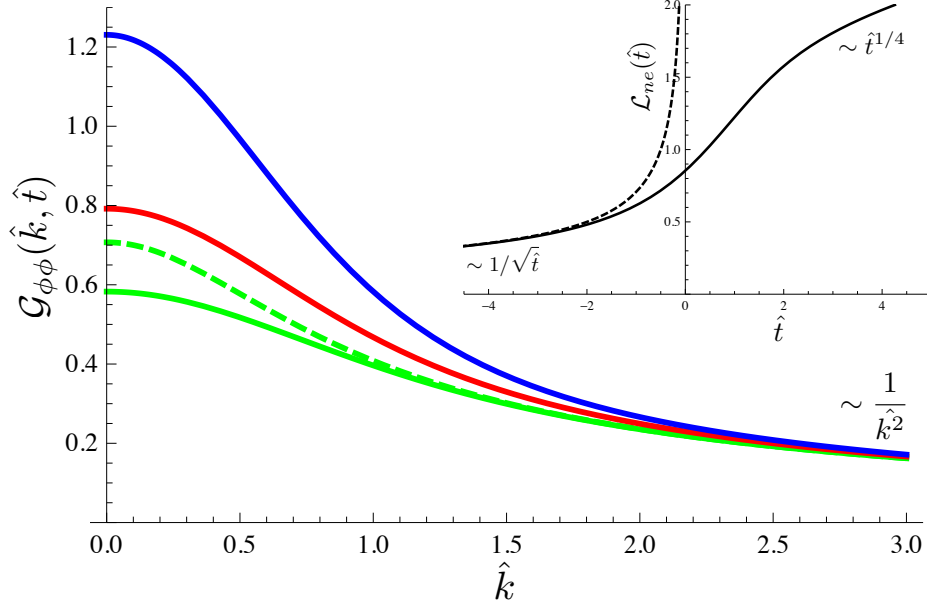


Figure 2.3: $\mathcal{G}_{\phi\phi}$ for the linear TCP. The blue, red and green solid lines are respectively at $\hat{t} = 0.5, 0$ and -0.5 . The green dashed line is the correlator if the system were in equilibrium at $\hat{t} = -0.5$. Inset: \mathcal{L}_{ne} vs \hat{t} (solid) and ξ/l_K (dashed).

The total quasi-particle density, and consequently the energy and entropy density, are ill-defined in the scaling limit within this integrable model when $d \geq 6$. Additionally, observe that $\mathcal{N}_{\hat{0}}$ diverges at $\hat{t} = 0$ because the gap, Ω_0 , between the ground and excited state of the oscillator at $\hat{k} = 0$ closes at $\hat{t} = 0$.

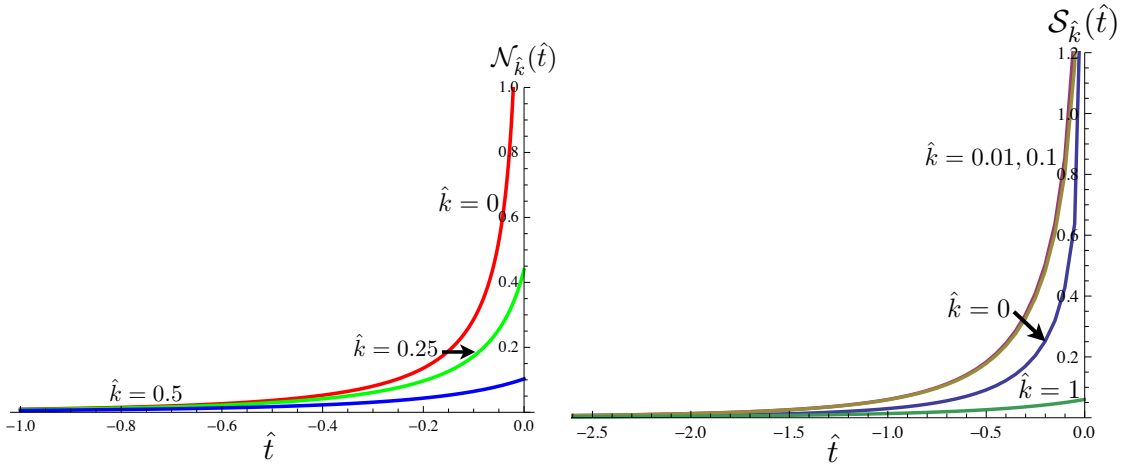


Figure 2.4: Left: Quasiparticle number $\mathcal{N}_{\hat{k}}(\hat{t})$ for $\hat{k} = 0, 0.25, 0.5$. Right: Diagonal entropy $\mathcal{S}_{\hat{k}}$ for $\hat{k} = 0, 0.01, 0.1, 1$ from top to bottom in the linear TCP.

2.2.5 CCP - Quadratic protocol

We now turn to a case where the adiabatic problem is well-defined for all \hat{t} – the quadratic CCP. The KZ time here is $t_K = (\tau/m_0)^{1/2}$. The scaling forms of the mode functions and the equal-time two point function are :

$$\begin{aligned} \hat{f}_{\hat{k}}(\hat{t}) &= 2^{-1/4} e^{-\frac{\pi \hat{k}^2}{8}} D_{\frac{-1+i\hat{k}^2}{2}}(-\sqrt{2}e^{-\frac{i\pi}{4}\hat{t}}\hat{t}) \\ \mathcal{G}_{\phi\phi}(\hat{k}, \hat{t}) &= \frac{e^{-\frac{\pi \hat{k}^2}{4}}}{\sqrt{2}} |D_{\frac{-1+i\hat{k}^2}{2}}(-\sqrt{2}e^{-\frac{i\pi}{4}\hat{t}}\hat{t})|^2. \end{aligned} \quad (2.39)$$

$D_\nu(z)$ is the parabolic cylinder function.

As $\hat{t} \rightarrow \pm\infty$ holding $k\xi$ or \hat{k}/\hat{t} fixed, we recover the equilibrium forms,

$$\mathcal{G}_{\phi\phi}(\hat{k}, \hat{t}) \sim \frac{1}{2\hat{\Omega}_{\hat{k}}}. \quad (2.40)$$

The retrieval of the equilibrium form as $\hat{t} \rightarrow \infty$ is by no means guaranteed. Recent work [117] suggests that this question is intimately tied to the de-phasing of the off-diagonal terms in the time-averaged density matrix in the instantaneous eigenbasis. If the off-diagonal terms do not de-phase, which would be the case for example for the quartic quench, then equilibrium behavior is not expected as $\hat{t} \rightarrow \infty$.

The Gaussian theory imposes further structure on correlators because each momentum mode evolves independently of the others. Consider the time-evolution of the wavefunction of the harmonic oscillator labelled by \hat{k} in the Schrödinger picture. Expanding it in the eigenbasis of the Hamiltonian at time \hat{t} and suppressing the label \hat{k} ,

$$|\psi\rangle \approx A_0|0(\hat{t})\rangle + A_1|1(\hat{t})\rangle \dots$$

The time-evolution is adiabatic when $\hat{t} \gg 1$ and each $|A_i|$ approaches a constant. The relative phase between A_{i+1} and A_i on the other hand grows as : $\int^{\hat{t}} \hat{\Omega}_{\hat{k}}(\hat{t}') dt' \sim \hat{t}^2$.

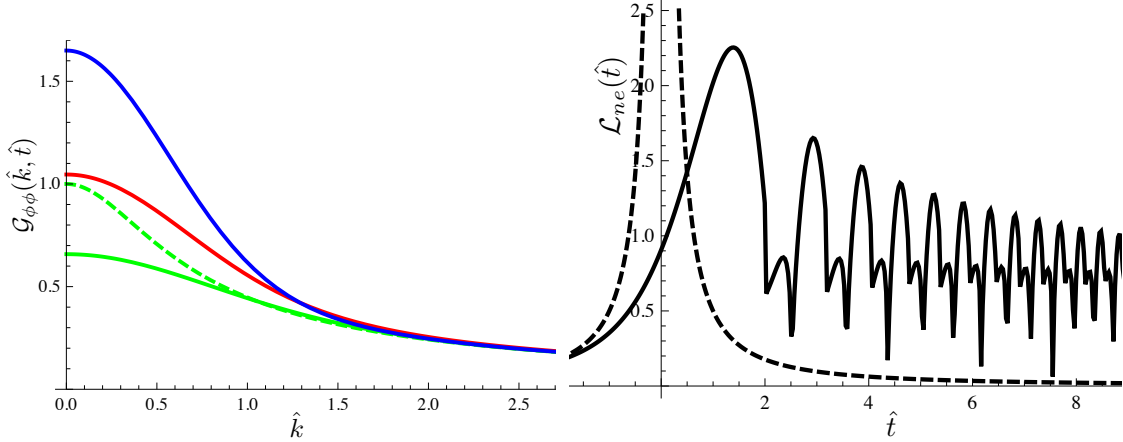


Figure 2.5: Left: $\mathcal{G}_{\phi\phi}$ for the quadratic CCP. The blue, red and green solid lines are respectively at $\hat{t} = 0.5, 0$ and -0.5 . The green dashed line is the correlator if the system were in equilibrium at $\hat{t} = -0.5$. Right: \mathcal{L}_{ne} vs \hat{t} (solid) and ξ/l_K (dashed).

This is the origin of the oscillations of period $1/\hat{t}$ at large positive \hat{t} at each \hat{k} , seen for example in $\mathcal{G}_{\phi\phi}(\hat{k}, \hat{t})$ in Fig. 2.5(a).

The simple definition of ξ_{ne} in Sec. 1.4.1 has to be modified as $\mathcal{G}_{\phi\phi}(\hat{k}, \hat{t})$ has multiple poles in the complex \hat{k} -plane for late times. The pole with the smallest imaginary part determines the decay constant ($1/\xi_{ne}$) over the longest length scales in the two-point function in real-space. The non-equilibrium correlation length is plotted in Fig. 2.5(b). As $\hat{t} \rightarrow \pm\infty$, the envelope of ξ_{ne} behaves as,

$$\xi_{ne}(\hat{t}) \sim \frac{1}{|\hat{t}|}.$$

This confirms the prediction in Eq. (1.16) for CCPs with no coarsening physics. For the reason discussed above, it also exhibits characteristic oscillations of period $1/\hat{t}$ at long times.

Finally, we plot $\mathcal{N}_{\hat{k}}(\hat{t})$ and $\mathcal{S}_{\hat{k}}(\hat{t})$ for various values of \hat{k} in Fig. 2.6. In each oscillator, the quasiparticles and entropy is essentially produced in the time-interval $|\hat{t}| \lesssim 1$. At late times, both quantities settle to a constant dependent on \hat{k} . For

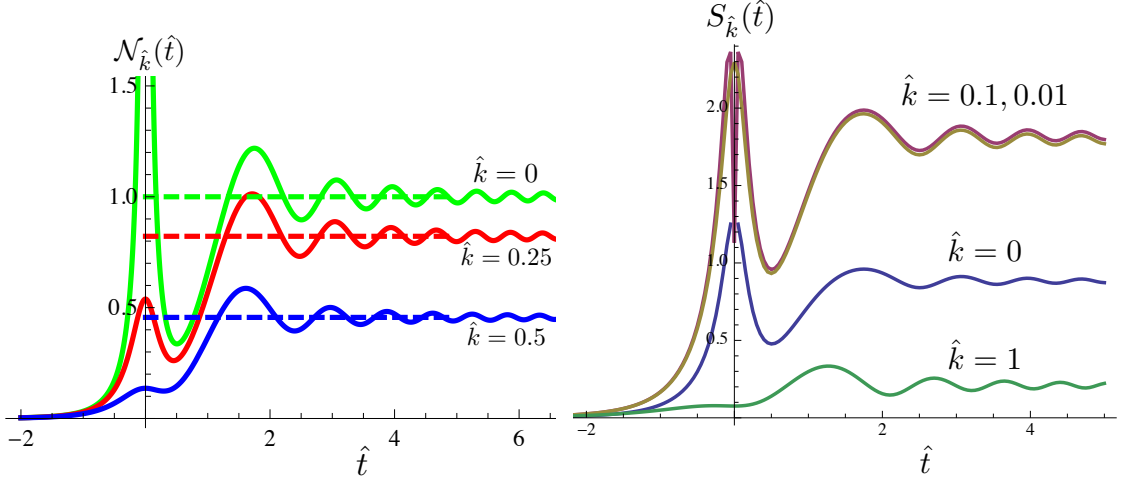


Figure 2.6: Left: Quasiparticle number $\mathcal{N}_{\hat{k}}(\hat{t})$ for $\hat{k} = 0, 0.25, 0.5$. Right: Diagonal entropy $\mathcal{S}_{\hat{k}}$ for $\hat{k} = 0, 0.01, 0.1, 1$ from top to bottom in the quadratic CCP.

example,

$$\mathcal{N}_{\hat{k}}(\hat{t}) \rightarrow e^{-\pi\hat{k}^2} \text{ as } \hat{t} \rightarrow \infty.$$

As was the case for the linear quench, the total quasiparticle and entropy density is finite only if $d < 6$.

2.2.6 The Marginal ECP

The relativistic Gaussian theory provides an ideal setting to study the new non-equilibrium states that arise in the marginal ECP. The protocol is defined by Eq. (1.21) – $m(t)$ smoothly transitions from a constant to θ/t over the time-scale τ and $\dot{\xi}_t$, the parameter that controls adiabaticity, equals $1/\theta$ for $t \gg \tau$. Our naive expectation is that the mode function is of a universal scaling form, $f_k(t) = \sqrt{t}\hat{f}(kt)$, in the scaling limit $t \rightarrow \infty, k \rightarrow 0$ with kt held fixed.

This expectation is violated on two fronts even in the Gaussian problem. The first is that the marginal ECP is by construction unable to entirely “forget” its early time regularization. More precisely, observe that our choice of protocols implies that $|dm^{-1}/dt| \ll 1$ when $t \ll \tau$ while $|dm^{-1}/dt| = 1/\theta$ when $t \gg \tau$. The latter result

shows that for small enough k , it is not possible to reach the power law regime while remaining adiabatic, in contrast to our discussion of the TCP and CCP cases; thus we should expect that *some* non-universal information must make its way into the putative scaling regime. The second and more striking violation is that of scaling. When $\theta > 1/2$ and $|dm^{-1}/dt|$ is closer to obeying the condition of adiabaticity, scaling is violated “mildly” and all physical quantities are periodic functions of $\log(t)$. When $\theta = 1/2$, scaling is violated logarithmically. The most dramatic violation of scaling is when $0 < \theta < 1/2$. Here the adiabaticity condition is strongly broken and the scalar field acquires an anomalous dimension.

Let us now describe how these features emerge in the long time, small momentum form of the mode functions. The mode equation for $t \gg \tau$:

$$\left(\frac{d^2}{dt^2} + k^2 + \frac{\theta^2}{t^2} \right) f_k(t) = 0. \quad (2.41)$$

Define $\lambda \equiv \left| \sqrt{\frac{1}{4} - \theta^2} \right|$ and

$$h(\lambda) = \begin{cases} i\lambda, & \text{if } \theta > 1/2 \\ 0, & \text{if } \theta = 1/2 \\ \lambda, & \text{if } \theta < 1/2. \end{cases} \quad (2.42)$$

Setting $k = 0$, Eq. (2.41) is solved as:

$$f_0(t) = \begin{cases} \sqrt{t} \left(\frac{2^{-\lambda} u}{\Gamma(1+\lambda)} \left(\frac{t}{\tau} \right)^{h(\lambda)} + \frac{-2^\lambda \Gamma(\lambda) v}{\pi} \left(\frac{t}{\tau} \right)^{-h(\lambda)} \right), & \text{if } \theta \neq 1/2 \\ \sqrt{t} (u + v \log \left(\frac{t}{\tau} \right)), & \text{if } \theta = 1/2. \end{cases}$$

The units of t are chosen such that $f_0(\tau) \sim \sqrt{\tau}$. The particular λ -dependent pre-factors are chosen to simplify the solution at all k . v and u are non-universal constants in the equation above. They depend on the detailed pre-asymptotic form of the

protocol and are fixed by the solution to the differential equation with the full time dependence of the mass.

Let us now turn to $k \neq 0$. For times greater than τ , the mode equation is solved by the linear combination,

$$f_k(t) = \sqrt{t} [c_J(k) J_{h(\lambda)}(kt) + c_Y(k) Y_{h(\lambda)}(kt)] . \quad (2.43)$$

$J_\nu(x)$ and $Y_\nu(x)$ are the Bessel functions of order ν of the first and the second kind. The functions $c_J(k)$ and $c_Y(k)$ are presently undetermined except for the requirement of smoothness in k . However, if we examine the region $t \gg \tau$ at small kt , we can obtain their leading order behavior by requiring that they match smoothly to the $k = 0$ forms presented earlier. This localizes the non-universality to the constants u, v discussed already. For $\theta < 1/2$ and k smaller than some non-universal k_0 , this leads to the leading behavior:

$$\begin{aligned} c_Y(k) &= v(k\tau)^\lambda \\ c_J(k) &= u(k\tau)^{-\lambda} - v \frac{(k\tau)^\lambda}{\pi} \cot \pi\lambda . \end{aligned} \quad (2.44)$$

For $\theta > 1/2$, we simply replace λ by $i\lambda$. For $\theta = 1/2$, we find

$$\begin{aligned} c_Y(k) &= \frac{\pi}{2} v \\ c_J(k) &= u - v \log \frac{k\tau e^\gamma}{2} . \end{aligned} \quad (2.45)$$

γ is the Euler-Mascheroni constant. We emphasize that the mode-function and consequently all physical quantities are well-approximated by Eq. (2.43) with the forms of c_J and c_Y above for $t \gg \tau$ and $k \ll k_0$.

We now turn to the physical implications of these solutions for an arbitrary choice of (u, v) that satisfy the constraint imposed by the Wronskian condition Eq. (2.24).

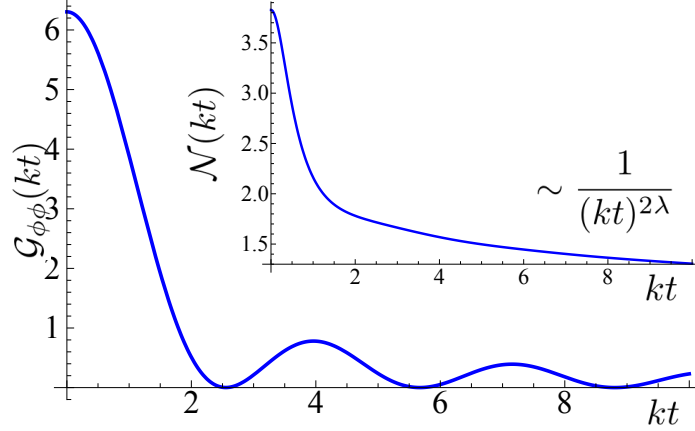


Figure 2.7: $\mathcal{G}_{\phi\phi}(kt)$ and $\mathcal{N}(kt)$ vs kt when $\lambda = 0.1$ and $u/\tau^\lambda = -2.5i$.

First consider the case $0 < \theta < 1/2$, which is strongly non-adiabatic in the sense that $|dm^{-1}/dt| = 1/\theta$ is greater than 2 and may be large. The mode function in Eq. (2.43) can be re-written in the form

$$f_k(t) = t^{1/2} \left(\frac{t}{\tau}\right)^\lambda \left[g_+(kt) + \left(\frac{t}{\tau}\right)^{-2\lambda} g_-(kt) \right]. \quad (2.46)$$

g_+ and g_- are linear combinations of the two Bessel functions and involve the constants u, v . Observe that in the limit of large t ($t \gg \tau$) with kt fixed, the ratio of the second to the first term in the expression above decreases as $(t/\tau)^{-2\lambda}$ ³. Thus, in the scaling limit, $f_k(t)$ simplifies to

$$f_k(t) \sim u't^{1/2+\lambda} \hat{f}(kt) \sim u't^{1/2+\lambda} \frac{J_\lambda(kt)}{(kt)^\lambda}. \quad (2.47)$$

$u' = u/\tau^\lambda$ above. The scaling forms predicted in Sec. 1.4.2 *do not hold*. Instead, the form above is the one expected when the field ϕ has an anomalous dimension λ . The scaling form of $G_{\phi\phi}$ with the modified dimension of ϕ is

$$G_{\phi\phi}(k, t) \sim t^{1+2\lambda} \mathcal{G}_{\phi\phi}(kt). \quad (2.48)$$

³The reader may worry about dropping the second term at the zeros of $g_+(kt)$. Fortunately, the correction to $f_k(t)$ due to $g_-(kt)$ at these points decreases as $t \rightarrow \infty$.

In real-space, this implies that the equal-time two-point correlator decays as $1/x^{d-1-2\lambda}$ at fixed x/t . Analogously, the quasi-particle number $N_k(t)$ has the scaling form $t^{2\lambda}\mathcal{N}(kt)$. The scaling functions are:

$$\mathcal{G}_{\phi\phi}(kt) = |u'|^2 \hat{f}^2$$

$$\mathcal{N}(kt) = |u'|^2 \frac{|(kt)\partial_{kt}\hat{f} + i\sqrt{(kt)^2 + (\theta)^2}\hat{f}|^2}{2\sqrt{(kt)^2 + (\theta)^2}}.$$

They are shown in Fig. 2.7. Three comments are in order. First, in the marginal ECP, $\xi \sim t$ and the time-scale for a change in m is the same as $\xi = \xi_t$. We therefore expect that the non-equilibrium correlation length ξ_{ne} also grow linearly in time. This is indeed the case; the oscillations in $\mathcal{G}_{\phi\phi}(kt) \sim t$ in Fig. 2.7 are of order one period and indicate a peak at $r \sim t$ in the real-space correlator $\mathcal{G}_{\phi\phi}(r/t)$. Second, the excess energy density above the instantaneous vacuum *decreases* as $1/t^{1-2\lambda}$. The marginal ECP thus leads the system to the critical point through a family of new, non-equilibrium states. Finally, all scaling functions are known up to a multiplicative constant (u') in the scaling limit.

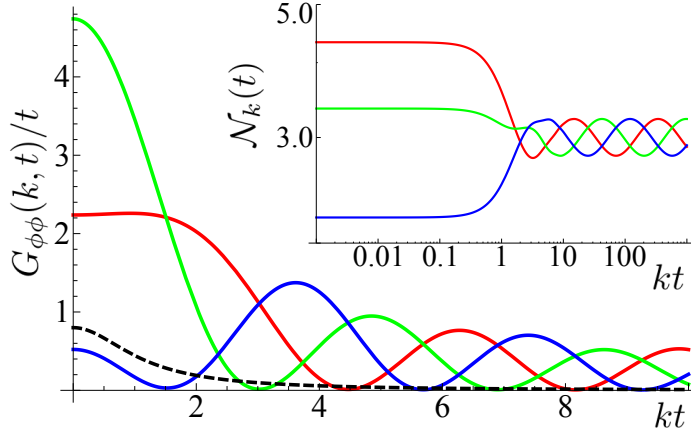


Figure 2.8: $G_{\phi\phi}(k, t)/t$ and $\mathcal{N}_k(t)$ vs kt when $\lambda = i$ plotted at three equally spaced time on the $\log(t)$ scale : $t = 10$ (red), $10 e^{\pi|\lambda|/3}$ (green) and $10 e^{2\pi|\lambda|/3}$ (blue). The dashed line is the adiabatic response. (u, v, τ) are chosen to be $(\sqrt{3}/2, 1, 1)$.

Let us consider the case $\theta > 1/2$, which is weakly non-adiabatic in the sense that $|dm^{-1}/dt| = 1/\theta$ is less than 2 and may be small. A re-writing of the mode function informs us that the scaling is violated only by phases:

$$f_k(t) = \sqrt{t} \left[\left(\frac{t}{\tau} \right)^{i|\lambda|} g_+(kt) + \left(\frac{t}{\tau} \right)^{-i|\lambda|} g_-(kt) \right]. \quad (2.49)$$

These phases affect other physical quantities in the scaling limit, but in relatively mild ways as compared to the previously seen factors of t^λ . For instance, at late times holding kt fixed,

$$G_{\phi\phi}(k, t) \sim t \mathcal{G}_{\phi\phi}(kt, e^{i|\lambda|\log(t/\tau)}), \quad (2.50)$$

where we have expressed $t^{i|\lambda|} = e^{i|\lambda|\log t}$ in order to emphasize that this quantity is periodic in $\log t$. The scaling function \mathcal{N}_k is also periodic in $\log t$. The two “almost-scaling” functions $\mathcal{G}_{\phi\phi}$ and $\mathcal{N}_k(t)$ are plotted in Fig. 2.2.6 for three equally spaced values of $\log t$ within a decade. The late time behavior of $\mathcal{G}_{\phi\phi}$ in the marginal ECP differs markedly from the adiabatic response, show as a dashed line in the plot. The period oscillations in the two-point correlator imply that $\xi_{\text{ne}} \sim t$. The smaller excess energy density proportional to $1/t$ is an indicator that the system is closer to being in equilibrium than for the strongly non-adiabatic case $0 < \theta < 1/2$. In a sense, the factors of $t^{i|\lambda|} = e^{i|\lambda|\log t}$ can be regarded as introducing only “logarithmic” modifications of scaling.

The case $\theta = 1/2$ displays the properties of both the cases discussed above. The relations in Eq. (2.45) imply the form

$$f_k(t) = \sqrt{t} [g_+(kt) + \log(t/\tau)g_-(kt)].$$

At late times with kt fixed, the second term dominates the first and the mode function has the scaling form

$$f_k(t) \sim u \sqrt{t} \log t J_0(kt)$$

All scaling forms are thus modified by pre-factors of powers of $\log t$. The logarithmic violation of scaling is similar to the weakly non-adiabatic case $\theta > 1/2$, while the modification of the dimension of ϕ is similar to the strongly non-adiabatic case. The quasi-particle number here diverges logarithmically in time.

The excess energy density injected into the system decreases as t increases in the strictly Gaussian theory. The marginal ECPs thus define a family of non-equilibrium states that lead to the critical point that are universal when the Gaussian fixed point is stable. The vanishing excess energy density further suggests that the non-equilibrium states generated by the marginal ECP survive even when the fixed point is not Gaussian.

Finally, let us comment on the ECP in the transverse field Ising model in (1+1) dimensions which is famously a model of free fermions. Here $\nu = 1$ and $z = 1$ so the relevant power is now $a = 1$. The explicit solution of the fermionic mode equations exhibits the analogs of our weakly non-adiabatic regime with corrections to scaling that are periodic in $\log t$. Connecting this behavior to our Gaussian results discussed above by continuation in the number of dimensions is an interesting challenge for future work.

Analogies to dS_{d+1}/CFT_d

We showed above that in the long time limit of the solution to the mode-equation in the strongly non-adiabatic case Eq. (2.46), the scalar field acquires an anomalous dimension λ . If we instead took the opposite limit of small time ($t \sim \tau$), the second

term is more important than the first and the anomalous dimension of the scalar field is $-\lambda$. Thus, the effective scaling dimension of ϕ in dimension d is

$$\tilde{\Delta}_{\pm} = \frac{d-1}{2} \pm \lambda. \quad (2.51)$$

at short and long times respectively. Readers familiar with the $(A)dS_{d+1}/(C)FT_d$ literature, in particular [178, 202], will note a similarity between the result Eq. (2.48) and the d -dimensional field theory Green's function obtained in the presence of a double-trace deformation. We can make the analogy closer by noting that the modified scalar field

$$\varphi \equiv t^{\frac{d-1}{2}} \phi$$

obeys an equation of motion which follows from the Lagrangian

$$\mathcal{L} = \frac{1}{2} \sqrt{-\det g_{\alpha\beta}} (-g^{\mu\nu} \partial_{\mu} \varphi \partial_{\nu} \varphi - M^2 \varphi^2), \quad (2.52)$$

where $g_{\mu\nu}$ is the metric of de Sitter space, dS_{d+1} :

$$ds^2 = \frac{L^2}{t^2} (-dt^2 + d\vec{x}^2). \quad (2.53)$$

The length scale L is arbitrary. The de Sitter mass must be given by

$$M^2 L^2 = \theta^2 + \frac{d^2 - 1}{4} \quad (2.54)$$

in order for the equation of motion from Eq. (2.53) to agree with Eq. (2.41). The dimensions Eq. (2.51) are closely related to the usual ones in dS/CFT:

$$\Delta_{\pm} = \frac{d}{2} \pm \sqrt{\frac{d^2}{4} - M^2 L^2} = \tilde{\Delta}_{\pm} + \frac{1}{2}. \quad (2.55)$$

The difference arises due to an important distinction between the late-time Green’s function Eq. (2.48) and the d -dimensional field theory two-point function. Examples of the latter could be computed in dS_{d+1} in terms of early time (that is, small t) properties of mode functions associated to the “out” vacuum: that is, mode functions which are purely positive frequency at late times. Our computation is the reverse of this, in the sense that we investigate late-time properties of mode functions associated with an “in” vacuum. Late time corresponds to the deep interior of dS_{d+1} (more precisely, it is a corner of the global covering space far from the boundary at $t = 0$). Another difference (of lesser consequence) is that in the normal parlance of dS/CFT [178], time flow would be reversed, so that what we call $t = 0$ is the far future while $t \rightarrow \infty$ is the far past.

In the window $kt \ll 1$, $f_k(t)$ is k -independent and equal to $f_0(t)$:

$$t^{\frac{d-1}{2}} f_k(t) \approx a_\varphi t^{\Delta_-} + b_\varphi t^{\Delta_+}, \quad (2.56)$$

where b_φ, a_φ are known in terms of u, v, τ , and in particular have a definite ratio. This setup now bears a strong resemblance to double-trace operator deformations in AdS/CFT [202]. In AdS/CFT, the relativistic conformal symmetry of the boundary theory is broken by the multi-trace deformation. The presence of different powers of x in the real-space Green’s function dependent on the energy scale $1/\tau$ signals a similar breakdown of scaling. The same can be said of the weakly non-adiabatic case, but comparisons with a boundary field theory are harder in this case because the field theory would have to be non-unitary, similar to violations of the Breitenlohner-Freedman bound [23] in AdS/CFT. However, the dS_{d+1} formulation (2.52) does offer some further intuition regarding the weakly non-adiabatic case: Eq. (2.54) shows that large θ implies large $M^2 L^2$. This in turn implies that the Compton wavelength of the

massive scalar is much smaller than the Hubble scale of dS_{d+1} , which is precisely the condition one needs in order to justify a geometric optics approximation.

2.3 Concluding Remarks

Our primary purpose in the previous two chapters has been to systematize the universal content of the KZ problem and to emphasize that all physical quantities give rise to universal scaling functions that span the entire crossover from equilibrium at early times to the late time state. We have presented model computations that bear out this logic. Experiments directed towards observing this broader scaling picture would be highly desirable. We note that the scaling ideas presented here do not rely on the existence of a local order parameter and generalize straightforwardly to the Rajantie-Hindmarsh mechanism [97] as we will discuss in the next chapter.

An obvious challenge is to extend such computations to more physically realizable problems where the field theories are not as simple. Another obvious challenge is to formulate a renormalization group procedure that makes the universality manifest—beyond the case of stochastic classical models with the associated functional integral formalism discussed here.

A byproduct of our analysis has been the identification of an especially interesting ECP which is able to produce anomalous dimensions already at the Gaussian level, through a mechanism similar to the way anomalous dimensions emerge in (A)dS/CFT. A deeper understanding of this phenomenon and its examination in interacting contexts is also a fit subject for further exploration.

2.A Scaling form of $f(t; \tau)$ in the Gaussian theory with Model A dynamics

To determine the generating functional in one higher dimension, we follow the three steps prescribed in [130, 98]:

- Define ϕ_ζ as the solution of the equation of motion in Eq. (2.1) for a given noise history $\zeta : \mathcal{J}\phi_\zeta(\mathbf{k}, t) = \zeta(\mathbf{k}, t)$. \mathcal{J} is a linear operator in the Gaussian theory.
- Rewrite Z as $\int d\zeta P(\zeta) \exp(J\phi_\zeta)$. The noise distribution, $P(\zeta)$, is Gaussian.
- Recognize that the probability distribution for ϕ_ζ is related to the noise distribution as $P_\phi(\phi_\zeta) = P(\mathcal{J}\phi_\zeta) \det(\mathcal{J})$.

The generating functional of correlation functions of ϕ so obtained is

$$Z[J, \tau] = \int \mathcal{D}\phi \det(\mathcal{J}) e^{\int d^3k dt (-2|\mathcal{J}\phi(\mathbf{k}, t)|^2 + J(\mathbf{k}, t)\phi(-\mathbf{k}, t))} \quad (2.57)$$

where

$$\mathcal{J} = \frac{\partial}{\partial t} + k^2 + r_0(t; \tau). \quad (2.58)$$

The functional integral is Gaussian, and the free energy density is expressed in terms of the structure factor in Eq. (2.4) as

$$f(t; \tau) = \int \frac{d^3k}{(2\pi)^3} \log [G_{\phi\phi}^{-1}(k, t; \tau)].$$

The challenge in identifying f_{na} , even in the time-independent setting, lies in subtracting cut-off dependent terms from f that are analytic in δ . Here, it involves subtracting the cut-off dependent equilibrium contribution at the critical point, $f(0, \infty)$, and two terms that are linear and logarithmic in the cut-off. On taking the KZ scaling limit

of the terms remaining, we confirm the scaling form in Eq. (1.19):

$$f_{\text{na}}(t; \tau) \sim \frac{1}{l_K^d} \mathcal{F}(\hat{t})$$

$$\mathcal{F}(\hat{t}) = \frac{1}{6\pi^2} \int_0^\infty d\hat{k} \left(\hat{k}^2 \left(2 + \frac{\hat{k}}{\mathcal{G}_{\phi\phi}} \frac{d\mathcal{G}_{\phi\phi}}{d\hat{k}} \right) + 2 (-\hat{t})^a \right).$$

Chapter 3

String-Net Coarsening in Topologically Ordered Systems

3.1 Introduction

The KZ scaling theory introduced in Chapter 1 provides an elegant framework within which to investigate ramp dynamics of phase transitions beyond those of traditional symmetry breaking.¹ These transitions could involve the destruction of the topological order of states of matter like spin liquids and the fractional quantum Hall phases. Topologically ordered phases are *not* locally distinguished by any order parameter, but are characterized by emergent gauge fields and fractionalized excitations. Their non-local structure makes them particularly robust to local perturbations and well-suited to perform “topological” quantum computation [136]. Despite their robustness, a strong enough perturbation can drive a transition from a topologically ordered phase to a trivial or relatively trivial (i.e. one with a smaller gauge group) phase. For appropriately selected perturbations, this transition will be continuous.

¹Chapter based on work with F. J. Burnell, Vedika Khemani and S. L. Sondhi [38].

This chapter addresses the KZ problem when a system is driven from a topologically ordered phase to a proximate trivial or relatively trivial phase. We do so for a class of topological phases that possess lattice realizations where the gauge degrees of freedom are manifest: these are the toric code/lattice \mathbb{Z}_2 gauge theory [116, 109] and the string-net models of Levin and Wen [122] that realize doubled non-Abelian Chern-Simons theories. By a combination of duality and perturbative arguments, we show that KZ scaling in the generalized sense of Chapter 1 holds for various observables even though the canonical KZ signature of a density of topological defects is not meaningful. We further provide strong arguments that the late time dynamics in the scaling regime exhibits a slow coarsening of the string-net that is condensed in the starting topologically ordered state. To our knowledge, this is the first treatment of a quantum coarsening regime in the dynamics of an isolated quantum system. As the extended string-nets are central to the topological character of the starting phase², their slow decay outside the phase is a (potential) signature of the physics of the parent phase. The restriction to the scaling limit always brings simplification as particular gapped degrees of freedom are, at worst, dangerously irrelevant. That is, they do not affect the scaling regime but do alter the asymptotically long time behavior of the KZ process.

The most relevant precursor to our work is found in the cosmology literature in the papers of Rajantie and Hindmarsh [97, 156]. They studied the non-equilibrium dynamics of ramps through the finite temperature phase transition in the non-compact Abelian Higgs model; their protocol moves between the gapless Coulomb phase with gapped matter to the fully gapped Higgs phase. However, there are three important differences. First, their work involves finite temperature in an essential way. The zero temperature limit of their protocol would involve exciting the system in the gapless phase even before the transition is reached. Second, the non-compactness of

²Sensitivity to the topology of the lattice manifold requires extended degrees of freedom like strings. The strings form nets as the phase is a liquid.

their gauge field makes the physics of their Higgs phase qualitatively different from that of the compact gauge models considered by us. This difference is quite visible in our choice of observables. Third, we work on the lattice in the “electric flux” representation, a natural choice in the condensed matter setting, while they work in the continuum with the vector potential. Thus our discussion of string-net coarsening has no analog in their formulation. In the condensed matter literature, ramps across topological transitions[54] in (1+1)D and sudden quenches in one of our model systems, the perturbed toric code, have been studied before [155, 185]. The sudden quenches are in a completely different limit from the slow ramps we study here as they inject a large amount of energy into the system. Finally, low temperature spin ice exhibits topological order in a classical limit [34] and its dynamics following quenches is dominated by monopoles of the gauge field. However in this case, non-universal lattice effects turn out to dominate the long time behavior [35].

We turn now to the contents of this chapter. We begin in Sec. 3.2 by reviewing the phase diagram of the \mathbb{Z}_2 gauge theory coupled to matter and describing the transitions out of its topologically ordered phase. Readers literate in the canon of topological phases can skim this section for our notation. Section 3.3 summarizes the results of a KZ ramp across the pure matter sector of the \mathbb{Z}_2 theory which has a conventional symmetry-breaking transition. This section also contains a new analysis of coarsening in the (2+1)D transverse field Ising model. In 3.4, we discuss our results on the KZ scaling functions and string-net coarsening for ramps in the pure gauge sector of the theory, which has a confinement transition without a local order parameter. We then generalize the scaling theory to a ramp across an arbitrary point on the critical line in the phase diagram in 3.5. Finally, we turn to generalizations of these results to phases with non-Abelian topological order in Sec. 3.6; specifically, we discuss a particular transition from the $SU(2)_k$ ordered phases. We end with a discussion of generalizations to other theories.

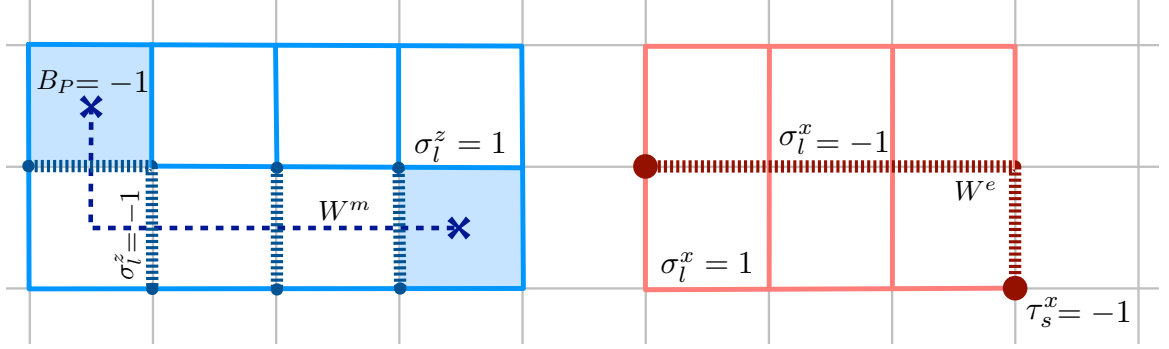


Figure 3.1: A section of the toric-code lattice with operators in the magnetic (left) and electric (right) bases. Matter (τ) and gauge (σ) variables are located on the sites and links respectively. The W^m operator (3.4) flips a string of σ^z variables and creates a pair of magnetic vortices at its endpoints, while the W^e operator flips spins in the x basis to create a pair of electric charges linked by electric flux.

3.2 Review of the phase diagram of the \mathbb{Z}_2 Gauge Theory

The phase diagram of the $(d + 1)$ dimensional \mathbb{Z}_2 gauge theory with matter [73] contains a topologically non-trivial (deconfined) phase and a topologically trivial (confined-Higgs) phase. The topological order in the deconfined phase is described by the BF theory [93]. We work in $d = 2$ for which the \mathbb{Z}_2 theory is precisely (the topologically ordered) Kitaev's toric code with perturbations [109]. We start by reviewing the key features and the excitation spectrum of the toric code. For a good set of lecture notes on the toric code, see [110]. We then discuss two perturbations that drive a continuous transition to a topologically trivial phase.

3.2.1 The perturbed toric code

The toric code [109] is defined in terms of spin-1/2 degrees of freedom that live on the links l of a 2D square lattice:

$$H_{TC} = -K \sum_P B_P - \Gamma_M \sum_s A_s$$

$$\equiv -K \sum_P \prod_{l \in \partial P} \sigma_l^z - \Gamma_M \sum_s \prod_{l: s \in \partial l} \sigma_l^x \quad (3.1)$$

where the A_s and B_P are “star” and “plaquette” operators. s and P denote the sites and elementary plaquettes of the lattice, while ∂P and ∂l are the boundaries of plaquettes and links. H_{TC} can be rewritten as a gauge theory with matter by identifying the σ_l variables as the gauge degrees of freedom, and introducing new spin 1/2 ‘matter’ variables, τ_s , on the sites of the lattice. Upon restricting the expanded Hilbert space to the ‘physical’ subspace of gauge-invariant states

$$G_s |\psi\rangle = |\psi\rangle, \quad G_s = \tau_s^x \prod_{l: s \in \partial l} \sigma_l^x, \quad (3.2)$$

the toric code Hamiltonian (3.1) is equivalent to the gauge-invariant Hamiltonian:

$$H_0 = -K \sum_P \prod_{l \in \partial P} \sigma_l^z - \Gamma_M \sum_s \tau_s^x. \quad (3.3)$$

Note that G_s defines a set of local symmetries at each site since $[H_0, G_s] = 0 \forall s$.

In the x basis of the spin operators, it is useful to think of τ and σ as the electric ‘charges’ and ‘fluxes’ in the theory respectively: $\tau_s^x = -1$ (+1) if an electric charge is present (absent) at site s , while $\sigma_l^x = -1$ denotes the presence of electric flux on link l . In this language, we recognize the gauge-invariant condition (3.2) as the lattice \mathbb{Z}_2 version of Gauss’s law. In the conjugate z basis, the operator $B_P \equiv \prod_{l \in \partial P} \sigma_l^z$ measures the magnetic flux through the plaquette P .

The model is exactly solvable as both terms in H_0 commute with each other and the gauge constraint G_s . The ground state is charge-free and vortex-free: a simultaneous +1 eigenstate of τ_s^x and B_P for all s, P . As the ground state is free of charge, it is a loop gas of electric flux. That is, it is an equal amplitude superposition of configurations where links with $\sigma_l^x = -1$ form closed loops. The degeneracy of the ground state manifold depends on the topology of the lattice; on the torus, it is

four-fold degenerate. The four ground states cannot be distinguished locally. They are labelled by the eigenvalues ± 1 of the non-local Wilson loop operators $W^{nc} \equiv \prod_{l \in C_{nc}} \sigma_l^z$ along the two distinct non-contractible loops C_{nc} on the direct lattice.

The elementary excitations of the model are gapped and are of two types: e and m . e denotes the presence of electric charge on site s , while m is a magnetic vortex on plaquette P characterized by $B_P = -1$. e and m are individually bosonic, but have mutual semionic statistics. The non-local string operators

$$W^e(s, s') = \prod_{\substack{l \in C: \\ s, s' \in \partial C}} \tau_s^z \sigma_l^z \tau_{s'}^z, \quad W^m(\bar{s}, \bar{s}') = \prod_{\substack{l \in \bar{C}: \\ \bar{s}, \bar{s}' \in \partial \bar{C}}} \sigma_l^x \quad (3.4)$$

defined respectively on the curves C and \bar{C} on the direct and the dual lattice, create a pair of electric charges and vortices at their ends as shown in Fig. 3.1.

H_0 is robust to small local perturbations and extends to a topological phase. Nevertheless, a strong enough perturbation will eventually drive a transition into a trivial phase. The toric code Hamiltonian perturbed by transverse fields is $H = H_{TC} - \sum_l \Gamma \sigma_l^x + J \sum_l \sigma_l^z$; both perturbations drive continuous transitions to trivial (spin-polarized) phases when made large. In the gauge-invariant formulation of the \mathbb{Z}_2 gauge theory with matter, the perturbed Hamiltonian takes the form

$$-H = K \sum_P B_P + \Gamma_M \sum_s \tau_s^x + J \sum_l \sigma_l^z \prod_{s \in \partial l} \tau_s^z + \Gamma \sum_l \sigma_l^x. \quad (3.5)$$

The phase diagram of this theory was explained in detail in the seminal paper by Fradkin and Shenker [73] and has more recently been confirmed in several numerical studies [60, 187, 194, 182, 100]. We will now briefly review this model in different parameter regimes.

3.2.2 Pure matter theory ($\Gamma = 0$)

For $\Gamma = 0$, the gauge degrees of freedom are static and frozen into a vortex-free configuration in the ground state sector. It is therefore convenient to diagonalize H in the gauge-variant subspace where $\sigma_l^z = 1$ for all l and project the eigenstates to the gauge-invariant subspace afterwards. The Hamiltonian then maps to the (2+1)D transverse field Ising model (TFIM) for the matter spins:

$$H_{TFIM} = -J \sum_{\langle ss' \rangle} \tau_{s'}^z \tau_s^z - \Gamma_M \sum_s \tau_s^x. \quad (3.6)$$

On tuning J , the TFIM undergoes a conventional ‘Higgs’ phase transition from a paramagnetic phase to a symmetry-broken ferromagnetic phase. In a complementary view, the static electric excitations e defined at the toric code point ($\Gamma = J = 0$) acquire dynamics when $J \neq 0$ and eventually condense at a critical value of J . The transition is in the 3D Ising universality class and is detected by the local order parameter, $\langle \tau^z \rangle$ in the gauge-variant subspace. In the gauge-invariant subspace, τ_z maps on to a non-local string operator.

After projection, the state with $\{\sigma_l^z = 1\}$ is the vortex-free configuration in the topological sector defined by the Wilson loop $W^{nc} = 1$ for both non-contractible loops on the torus. This choice maps to a TFIM with periodic boundary conditions in both directions of the torus; the remaining three topologically inequivalent vortex-free configurations generate TFIMs with different boundary conditions (periodic-antiperiodic etc.). The four-fold degeneracy of the topological phase vanishes in the Higgs/ferromagnetic phase.

3.2.3 Pure Gauge Theory ($J = 0$)

In this case, matter is static. The ground state is in the charge-free sector ($\tau_s^x = 1$), and the Hamiltonian for the gauge variables in this sector is:

$$H_{\mathbb{Z}_2} = -K \sum_P B_P - \Gamma \sum_l \sigma_l^x. \quad (3.7)$$

When Γ/K is small, the gauge variables are weakly fluctuating and the elementary excitations are well-described as vortex pairs. At some critical Γ/K , the vortices condense and the gauge variables strongly fluctuate past this point. This transition cannot be diagnosed by a local order parameter. Instead, the vortex condensate phase is marked by the vortex pair creation operator, $\langle W^m \rangle \neq 0$ for vortices separated by long distances. In the conjugate electric field basis, flux loops become costly as Γ is increased; hence the transition is from a topological loop gas phase at the toric code point to a phase in which flux loops become confined.

In a different language, the transition is understood as a deconfinement-confinement transition for the static electric charge [73] and is diagnosed by the free energy cost of creating a pair of (infinitely separated) charges. The cost is finite in the deconfined phase, but infinite in the confined phase, and is equivalent to the change in behavior of the expectation of the contractible Wilson loop:

$$W(L) \equiv \left\langle \prod_{l \in C} \sigma_l^z \right\rangle \quad (3.8)$$

from a perimeter law ($W(L) \sim \exp(-L)$) to an area-law ($W(L) \sim \exp(-L^2)$). C is a contractible loop and L is its perimeter.

In $d = 2$, the \mathbb{Z}_2 Ising gauge theory is self dual [195, 116]. Thus the pure gauge theory also maps to a (2+1)D TFIM and the confinement-deconfinement transition belongs to the 3D Ising universality class. The details of this duality are explained

in Ref. [116], and have been summarized in Fig. 3.3. We emphasize that despite the duality, the transition is *not* described by a local order parameter, as will be even clearer in Sec. 3.6.

3.2.4 The full phase diagram

The full $T = 0$ phase diagram of the Ising gauge theory in (2+1)D is shown in Fig. 3.2. Fradkin and Shenker [73] have shown that the confinement/Higgs transitions are stable on moving away from the pure gauge/matter axes. Further, the Higgs and confined phases are smoothly connected. However the diagnostics previously discussed, like the Wilson loop, no longer differentiate between the two phases. In a recent paper [84], Gregor et. al. have shown that an appropriately defined line tension, related to the Fredenhagen Marcu [75, 76] order parameter studied by lattice gauge theorists, can be used to diagnose the transition everywhere in the phase diagram. We will use this quantity in combination with the topological ground state degeneracy to study ramps across generic points on the critical line in the phase diagram.

3.3 Kibble Zurek I - Ramp across the Higgs transition

The KZ formalism that we developed in Chapter 1 applies straightforwardly to the linear ramp (a TCP) across the conventional 3D Ising transition along the pure matter line ($\Gamma = 0$) if we identify the control parameter δ with $\frac{\Gamma_M - \Gamma_{Mc}}{\Gamma_{Mc}}$. The two exponents that determine the KZ length and time are ν and z . Near the 3D Ising transition, $\nu = 0.627$ and $z = 1$ [68]. To avoid repetition, we only discuss the new analysis of the scaling content at late times below. All the KZ notation below was introduced in Chapter 1.

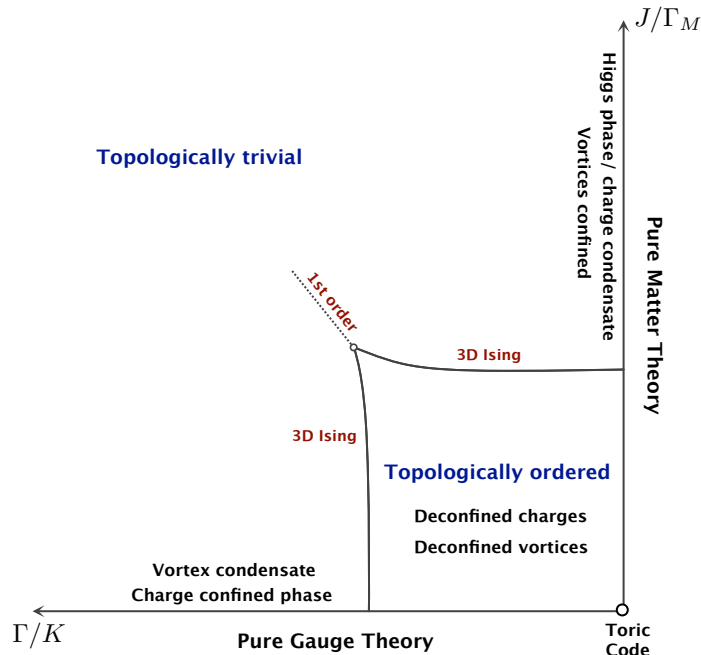


Figure 3.2: $T = 0$ phase diagram of the \mathbb{Z}_2 theory in $d = 2$ dimensions. The matter and gauge axes are dual, and the Higgs and charge confined phases are smoothly connected.

3.3.1 Coarsening

We now address the late time dynamics of the KZ ramp. Recall that in Sec. 1.4.1, we stated that a *classical* system quenched to an ordered phase with multiple vacua undergoes coarsening. In Sec. 2.1.2, we checked this in the example of the classical $O(N)$ vector model in the large- N approximation. We now generalize this idea to the KZ ramp in the *quantum* TFIM.

For simplicity, let us stop the ramp in the ordered phase at some $t/t_K = \hat{t}^s \gg 1$, while continuing to measure time and length on the scales set by t_K, l_K . The superscript s denotes stopping. The system initially appears disordered. At infinitely long times however, we expect that the system is thermal and ordered, as the (2+1)D TFIM is not known to be integrable. Further, we expect the approach to equilibrium to be through domain growth or coarsening, driven by the lack of long range order at late times. The system then locally breaks the symmetry but is globally disordered,

with long domain walls past the growing length scale, $l_{co}^s(t) \gg l_K$. Assuming local equilibration, the physics of coarsening can be captured in a hydrodynamic theory with two slow modes: the non-conserved, scalar order parameter and the conserved energy density.³ We shall call this Model C in a slight abuse of language (properly it refers to the theory with thermal noise included [99]). As $\hat{t} \rightarrow \infty$, we therefore predict that the system obeys the dynamic scaling hypothesis, that is, it looks self-similar on the scale of a growing length $l_{co}^s(t; \tau)$. Define the two-point function as:

$$\langle \tau_s^z(t) \tau_{s'}^z(t) \rangle_\tau \equiv G_{\tau\tau}^s(|\mathbf{s} - \mathbf{s}'|, t; \tau), \quad (3.9)$$

and denote its scaling function by $\mathcal{G}_{\tau\tau}^s$. At late times, the dynamical scaling hypothesis predicts that:

$$\mathcal{G}_{\tau\tau}^s(\hat{x}, \hat{t}) \sim (\hat{t}^s)^{2\nu\Delta} \mathcal{G}_{\tau\tau}^{co}(\hat{x}l_K/l_{co}^s), \quad (3.10)$$

where $l_{co}^s(t; \tau) = l_K \left(\frac{t}{t_K} \right)^{1/z_d}$ and $z_d = 2$.

The value of the dynamic exponent, z_d , quoted above is only known numerically[115, 114]. $\mathcal{G}_{\tau\tau}^{co}$ is a scaling function that can also be computed within Model C [115, 114, 205, 131].

The above discussion hinges on two key assumptions. First, the infinite time state of the system should have long-range order, that is, the late time evolution should be in the ordered phase. More precisely, we require the excess energy density at the stopping time $q(\hat{t}^s; \tau)$ to be smaller than critical energy density $q_c(\hat{t}^s; \tau)$, below which the system will be ordered in equilibrium. The dominant contribution to q (at \hat{t}^s) is from the defect density on the scale l_K frozen in at $t \approx t_K$. Assuming that these defects evolve adiabatically for $t > t_K$, we may conservatively estimate q to scale as

³The momentum density appears as an additional conserved quantity in this field theory. It is our current belief that this does not change the relevant power in the coarsening regime, but we are investigating this.

the single-particle gap $1/\xi(\hat{t}^s; \tau)^z$. As promised, this density is much smaller than the instantaneous critical density, $q_c \sim 1/\xi^{d+z}$:

$$\frac{q}{q_c} \sim \xi^d \sim \left(\frac{1}{\hat{t}^s}\right)^{\nu d} \ll 1. \quad (3.11)$$

For all $\hat{t} > \hat{t}^s$, the energy of the system is conserved and q and q_c do not change in time. Thus, the system evolves in the ordered phase at late times.

The second assumption is that of local equilibration over hydrodynamical time-scales. In Model C, the latter is the time-scale for domain growth by l_K . It can be inferred from Eq. (3.10) to be $\delta t_{co} \sim t_K \hat{t}^{1-1/z_d}$. On the other hand, the time-scale for local equilibration processes on the scale l_K is set by t_K . The validity of Model C as the late-time dynamical description relies on the equilibration time being much smaller than δt_{co} . As the inequality $t_K \ll \delta t_{co}$ is parametrically controlled by \hat{t} , the coarsening behavior in Model C is a better and better approximation to the quantum dynamics as $\hat{t} \rightarrow \infty$.

Finally, in the original KZ problem (where we don't stop the ramp), the late time evolution is also in the finite-temperature ordered phase as the relation $q/q_c \ll 1$ holds for every $t/t_K \gg 1$. However, the continuously changing parameter in the Hamiltonian affects the local equilibration argument in two important ways. First, the characteristic size of the domains grows at a slower rate:

$$l_{co}(t; \tau) = l_K \left(\frac{t}{t_K}\right)^\theta \quad \text{where } \theta = \nu \left(\frac{z}{z_d} - 1\right) + \frac{1}{z_d}. \quad (3.12)$$

In the (2+1)D TFIM, $\theta = (1 - \nu)/2$ and is smaller than $1/z_d$. This slowing down can only help in the argument given above. The second effect is that the single particle gap Δ grows as $1/t_K(t/t_K)^{\nu z}$ at late times. This, however, increases various scattering times (and consequently various equilibration times) in the problem and the applicability of hydrodynamics here becomes a delicate affair. In Appendix 3.A,

we argue that the process that drives coarsening and increases entropy involves the interaction of the long domain walls with the bulk quasiparticles within each domain. As the bulk quasi-particles scatter off the walls parametrically many times before the system parameters are changed, coarsening can at least self-consistently be justified. We therefore conjecture that the two point function as $\hat{t} \rightarrow \infty$ holding $x/l_{co}(t)$ fixed obeys dynamic scaling:

$$\mathcal{G}_{\tau\tau}(\hat{x}, \hat{t}) \sim \hat{t}^{2\nu\Delta} \mathcal{G}_{\tau\tau}^{co}(\hat{x}l_K/l_{co}). \quad (3.13)$$

In this process, the entropy density increases weakly in time. The late time asymptotes for the excess energy density and the entropy density reflect this:

$$\begin{aligned} \mathcal{Q}(\hat{t}) &\sim q_0 \hat{t}^{\nu z} + q_1 \hat{t}^{\nu z - \theta} \\ \mathcal{S}(\hat{t}) &\sim s_0 - s_1 \hat{t}^{-\theta}. \end{aligned} \quad (3.14)$$

The leading terms in \mathcal{S} would be present even if the evolution were adiabatic. The sub-leading term is the thermodynamic signature of coarsening. From this point, every time we invoke results from coarsening, the reader should keep in mind the subtleties presented in this section.

3.4 Kibble Zurek II - Ramp across the confinement transition

We now ramp across the pure gauge theory Eq. (3.7) by tuning Γ . In this case, the transition is from a topologically ordered deconfined phase to a confined one, and there is no description in terms of a local order parameter. Nevertheless, we will now show that the KZ mechanism for Landau transitions discussed in the previous

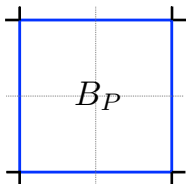
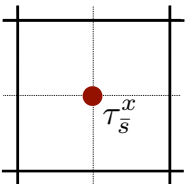
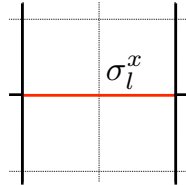
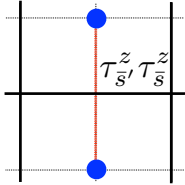
Pure \mathbb{Z}_2 gauge theory	\longleftrightarrow	Transverse field Ising Model
	\longleftrightarrow	
Magnetic Flux		Transverse field
	\longleftrightarrow	
Electric Flux		Domain wall
Confined/ Deconfined phase	\longleftrightarrow	Ferromagnetic/ Paramagnetic phase

Figure 3.3: Table summarizing the duality between the pure \mathbb{Z}_2 gauge theory (3.7) and the TFIM in $d = 2$. Dark and light lines denote the direct and dual lattice respectively.

section can be generalized to these transitions. Additionally, the loops and strings characterizing the topological phase (string-nets) will coarsen.

Our main tool is the duality in $(2 + 1)$ D between the pure gauge theory and the TFIM summarized in Fig. 3.3. Importantly for us, the presence of electric flux on a link (of the direct lattice) maps to a domain wall between the TFIM spins (on the dual lattice), while the vortex operator B_P maps to the dual transverse field. The duality also ensures that a finite temperature confined phase exists, and that coarsening is described by the hydrodynamics of Model C.

For specificity, we begin the ramp at the deconfined toric code point in one of the ground state sectors. The ground state is a loop gas of the electric flux lines in the σ^x basis. By duality, these are the domain walls of the paramagnetic phase of the TFIM. The system falls out of equilibrium in the deconfined phase before it is taken

through the transition, with a network of loops of minimum size l_K . In the confined phase, flux loops map to the costly domain walls of the dual ferromagnetic phase. Post the diabatic regime in the confined phase, this network of loops (string-nets) is diluted (average size increases as l_{co}) as the system coarsens. More generally, we can imagine string-nets being diluted in a generic topological theory and we will show some examples of this in Section 3.6.

As before, energy conservation requires the decreasing electric flux density to be compensated for by an increasing bulk energy density. Essentially, the system arrives in the confined phase (which is a vortex condensate) with a greater electric field density and a smaller magnetic vortex density as compared to the instantaneous ground state. The subsequent evolution through coarsening increases the typical size of the electric flux loops to $l_{co}(t)$, thereby decreasing the electric field density and increasing the bulk energy density of the vortex condensate.

Next, the two-point correlator that detects long-range order in the dual TFIM, $\langle \tau_{\bar{s}}^z \tau_{\bar{s}'}^z \rangle$, maps to the vortex pair creation operator (3.4), $\langle W^m(\bar{s}, \bar{s}') \rangle$ that detects vortex condensation. As the condensed phase is also a confining phase for charge, a non-zero value of $\langle W^m \rangle$ for long strings detects charge confinement. The asymptotic behavior of the scaling form for $\langle W^m \rangle$ is given by Eq. (3.13), identical to that of the two-point function discussed in the pure-matter theory. In particular, in the coarsening regime, the dual TFIM is ordered on length scales less than $l_{co}(t)$. Correspondingly, $\langle W^m \rangle$ is also non-zero on scales shorter than $l_{co}(t)$ but decays exponentially on longer length scales. Thus, the non-local string operator $\langle W^m \rangle$ probes the crossover scale from confinement to deconfinement as a function of time. Fig. 3.4(a) shows the scaling for $\langle W^m \rangle$.

Finally, we can consider an interesting observable that we did not discuss in the TFIM. This is the Wilson loop (3.8), $W(R, t; \tau)$ on a curve of radius R . Were the evolution to be adiabatic, $W(R, t; \tau)$ for large R would obey a perimeter law when

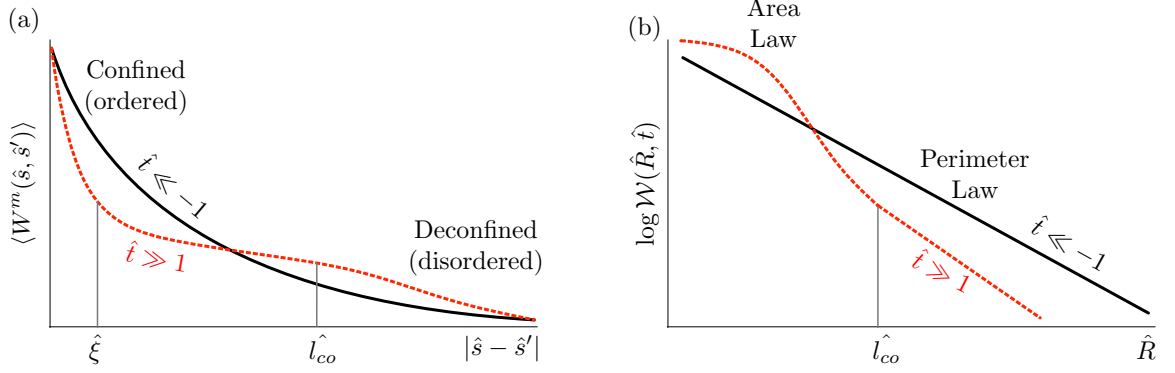


Figure 3.4: An illustration of two scaling functions showing adiabatic behavior in the deconfined phase at early scaled times (black) and coarsening behavior in the confined phase at late scaled times (red). The crossover on the scale $\hat{l}_{co} \equiv l_{co}/l_K$ in the red curves is a signature of string-net coarsening. The hat superscript denotes scaled variables like $\hat{t} = t/t_K$ etc. (a) The scaling function of the string operator that creates a pair of vortices at \hat{s} and \hat{s}' ($\langle W^m \rangle$ defined in Eq. (3.4)) as a function of the scaled vortex separation $|\hat{s} - \hat{s}'|$. This operator is dual to the two-point correlator $\langle \tau_s^z \tau_{\hat{s}'}^z \rangle$ in the TFIM. (b) The logarithm of the scaling function of the Wilson loop as a function of the scaled radius illustrating Eq. (3.15). The time dependence of $\hat{\xi}$ and \hat{l}_{co} is respectively $\hat{t}^{-\nu}$ and \hat{t}^θ .

$t < 0$ and an area law when $t > 0$. In the KZ scaling limit, the scaling of the Wilson loop takes the form $W(R, t; \tau) \sim \mathcal{W}(\hat{R}, \hat{t})$, where $R/l_K = \hat{R}$. Its asymptotic behavior is:

$$\mathcal{W}(\hat{R}, \hat{t}) \sim \begin{cases} \exp(-\hat{R} \hat{t}^\nu), & \text{if } \hat{t} \ll -1 \\ \exp(-(\hat{R} \hat{t}^\nu)^2), & \text{if } \hat{t} \gg 1 \text{ and } \hat{R} \ll \hat{t}^\theta \\ \exp(-(\hat{R}/\hat{t}^\theta)), & \text{if } \hat{t} \gg 1 \text{ and } \hat{R} \gg \hat{t}^\theta. \end{cases} \quad (3.15)$$

These scaling forms follow simply from the picture of adiabatic evolution when $\hat{t} \ll -1$ and a growing length $l_{co}(t)$ separating confinement from deconfinement when $\hat{t} \gg 1$. The Wilson loop therefore also probes the crossover scale from confinement to deconfinement as a function of time. Fig. 3.4(b) shows the scaling of the Wilson loop.

3.5 Kibble Zurek III - Ramp across a generic transition in the \mathbb{Z}_2 theory

We will now see how the discussions of the previous two sections can be generalized to ramps crossing any critical point in the full \mathbb{Z}_2 phase diagram. First, consider moving off the pure gauge line by introducing a small, but non-zero J . The coupling to matter is irrelevant to the $T = 0$ transition; hence, the confinement-deconfinement transition in Fig. 3.2 persists for non-zero J and remains in the same universality class. Since the gap to charge excitations does not close on making J non-zero, we can re-write the Hamiltonian as one with no gauge-matter coupling (to any fixed order in J) through a canonical unitary transformation. The transformation defines “dressed” charge and gauge operators – in the dressed variables, the ground state is charge-free and Δ_c is the non-zero gap to charge excitations.

As we heat the system in the process of the ramp, we also need to consider the finite temperature phase diagram and the excited spectrum when $J \neq 0$. Although the ground state is (dressed) charge-free, the excited states have an exponentially small density of charge, $e^{-\Delta_c/T_{eff}}$, at any effective temperature T_{eff} corresponding to an excess energy density q . The presence of charge at finite temperatures is extremely significant for the late-time coarsening picture for two reasons. First, it destroys the finite temperature confined phase at any non-zero J , without which a coarsening description is not meaningful. Synergistically, a finite density of charge implies that the electric field lines naturally end somewhere. Thus, the pictures of flux-loops/domain walls coarsening are no longer sensible at the longest length scales.

Fortunately, the Kibble-Zurek scaling limit saves us from the problems raised above. This is because the ratio q/q_c goes to zero as $t/t_K \rightarrow \infty$ (Eq. (3.11)) or equivalently, the effective local temperature, T_{eff} , computed from q goes to zero in the scaling limit (T_{eff} is well-defined as the system is locally in equilibrium. See

Sec. 3.3.1). Δ_c , on the other hand, remains finite. This implies that the ratio of the average distance between charges to the KZ length, $e^{\Delta_c/T_{eff}}/l_K$, is formally infinite in the scaling limit. Thus, while the dressed charges modify the *true* long-time behavior by ending coarsening, the scales on which they do so lie outside the KZ scaling regime: in this way, the coupling to matter is a dangerously irrelevant variable in the KZ problem (in the scaling limit).

While we can write scaling functions for dressed observables, the results are not very elegant since the Hamiltonian dependent dressed operators are different at different points in time. A crisper solution is to use the line tension[84]/ Fredenhagen-Marcu (FM) order parameter[75, 76] alluded to previously. This is defined as

$$R(L) = \frac{W_{1/2}(L)}{\sqrt{W(L)}} = \frac{\langle \tau_s^z (\prod_{l \in C_{1/2}} \sigma_l^z) \tau_{s'}^z \rangle}{\sqrt{\langle \prod_{l \in C} \sigma_l^z \rangle}}, \quad (3.16)$$

where C is a square loop of side L and $C_{1/2}$ is the open rectangle of sides L and $L/2$ obtained by cutting C in half, s, s' are the endpoints of $C_{1/2}$ and W is the contractible Wilson loop.

As $L \rightarrow \infty$, $R(L)$ is zero in the deconfined phase and non-zero otherwise. In this way, $R(L)$ acts as a test of long range “order”, and appropriately generalizes the two-point spin correlator $G_{\tau\tau}$ from the pure matter theory (3.9), and the vortex pair creation operator W^m (3.4) from the pure gauge theory. In fact, in the gauge-variant subspace $\{\sigma_l^z = 1\}$ on the pure matter line, $R(L)$ exactly reduces to $G_{\tau\tau}$. The scaling form and asymptotes of $R(L)$ therefore follows from that of $\mathcal{G}_{\tau\tau}$. Of course, by duality, an identical analysis can be carried out by perturbing away from the pure-matter line as long as we interchange the gauge and matter degrees of freedom.

3.6 Extension to generalized Levin-Wen models

In this section, we generalize the Kibble-Zurek problem to transitions in which topological order is reduced as opposed to destroyed. Specifically, we consider transitions out of a broader, non-Abelian, class of topological phases in lattice spin models of the Levin-Wen [122] type. Along special lines in the phase diagram, we show that the dynamics and scaling properties are exactly equivalent to those of the \mathbb{Z}_2 gauge theory. We identify analogous observables and the coarsening degrees of freedom of the string net that is condensed in the starting topological phase. However, we will see that the mapping of the dynamics is not an equivalence. We then consider perturbations away from this line, finding that as for the \mathbb{Z}_2 gauge theory, in the scaling limit these other perturbations do not alter the coarsening dynamics, but can be either irrelevant or dangerously irrelevant perturbations.

We restrict our discussion to the subset of $SU(2)_k$ models whose topological order is that of a doubled, achiral, Chern-Simons theory with gauge group $SU(2)$ and a coupling constant of k in appropriate units, though the construction of Ref. [122] is more general. We also restrict to particular transitions that change the topological order by condensing bosonic vortex defects; the transitions we consider here were shown [25] to be dual (in a certain limit) to the TFIM.

3.6.1 Levin-Wen Hamiltonians with Ising transitions

The $SU(2)_k$ models we study live in a Hilbert space built from tensoring a finite set of spin variables on each link of a honeycomb lattice, $\sigma_l \in \{0, \frac{1}{2}, 1, \dots, \frac{k}{2}\}$. These are analogous to the set of possible electric fluxes ($\sigma_l^x = \pm 1$) in the \mathbb{Z}_2 gauge theory. The idealized Levin-Wen Hamiltonians are similar in spirit to the toric code, and are

constructed from a set of commuting projectors

$$H_{LW} = -K \sum_P \mathcal{P}_P - \Gamma_M \sum_s \mathcal{P}_s \quad (3.17)$$

where P represents a plaquette, and s a site. These models can be viewed as deformations of lattice gauge theories with a continuous gauge group. They are ‘deformed’ in the sense that their representation theory is truncated, even though the gauge group is not discrete. In our context, a lattice $SU(2)$ theory would have electric fluxes corresponding to all allowed spin values $0, 1/2, 1, \dots$, while the models in question have a maximum spin $k/2$. (We refer to the link spins as ‘electric flux’ though, more accurately, they are the representations of the lattice gauge/quantum group). Instead of describing our analysis for general values of k , we will now specialize to $k = 2$ in the interests of pedagogical simplicity and return to comment on the generalization subsequently.

We now discuss the detailed form of the Hamiltonian (3.17) for $SU(2)_2$. The vertex projector \mathcal{P}_s penalizes violations of angular momentum conservation, analogous to the Gauss’s law constraint $G_s = 1$ in the \mathbb{Z}_2 theory. If the three links entering a vertex have spins i, j and l , angular momentum conservation requires $l \in i \times j$. The rules for adding angular momentum have to be modified to be consistent with the truncation, however. For the $SU(2)_2$ model, the result is [17]:

$$\mathcal{P}_s \left| \begin{array}{c} k \\ i \quad j \end{array} \right\rangle = \begin{cases} 1 & \begin{array}{c} \text{---} \\ \diagup \quad \diagdown \\ (0, 0, 0) \end{array} \quad \begin{array}{c} \text{---} \\ \diagup \quad \diagdown \\ (0, 1, 1) \end{array} \quad \begin{array}{c} \text{---} \\ \diagup \quad \diagdown \\ (\frac{1}{2}, \frac{1}{2}, 1) \end{array} \quad \begin{array}{c} \text{---} \\ \diagup \quad \diagdown \\ (\frac{1}{2}, \frac{1}{2}, 0) \end{array} \\ 0 & \text{otherwise} \end{cases} \quad (3.18)$$

where it is understood that the eigenvalue of \mathcal{P}_s is independent of interchanging the spins on the three links entering the vertex.

The plaquette term \mathcal{P}_P projects onto states in which P has no magnetic flux, and is written as a superposition of “raising operators”: $\mathcal{P}_P = \frac{1}{\mathcal{D}}(\mathbf{1} + \sum_{\sigma=1/2}^{k/2} a_\sigma B_P^\sigma)$, where B_P^σ raises all spins on the plaquette P by σ in the truncated spin space. By “raising”, we mean a combination of raising and lowering angular momenta in the truncated spin space. \mathcal{D} is the total quantum dimension, equal to 2 here, while the coefficients a_σ depend on the quantum dimension [122] of the spin representation σ . In $SU(2)_2$, they are $a_0 = 1$, $a_{1/2} = -\sqrt{2}$, $a_1 = 1$. B_P^σ raises all spins in P by raising the spin on each link $l \in \partial P$. The action of B_l^σ on a link l with spin $i \in \{0, 1/2, 1\}$ is:

$$\begin{aligned} B_l^i |0\rangle &= |i\rangle \\ B_l^{1/2} |1/2\rangle &\propto |0\rangle \pm |1\rangle & B_l^{1/2} |1\rangle &\propto |1/2\rangle \\ B_l^1 |1/2\rangle &\propto |1/2\rangle & B_l^1 |1\rangle &\propto |0\rangle \end{aligned}$$

The numerical coefficients are chosen such that the amplitude for creating any configuration with a 0-eigenvalue under \mathcal{P}_s is 0, ensuring that the vertex and plaquette projectors commute. Their precise value is related to the $6j$ symbols of the quantum group $SU(2)_2$, but we will not require their detailed form here. Interested readers can consult Ref. [122] for more details.

As \mathcal{P}_P and \mathcal{P}_s commute, the spectrum of the Hamiltonian can be determined exactly. The ground state is a generalization (a string-net) of the loop gas ground state of the toric code, though there can be relative sign differences between terms in the Levin-Wen ground state wavefunction. As in the toric code, the excited eigenstates of (3.17) consist of “matter” excitations of energy Γ_M , and “vortex” excitations, of energy K . In the $SU(2)_2$ model there are anyonic spin-1/2 charges, fermionic spin-1 charges, and spin-1/2 or spin-1 vortices, both of which have bosonic statistics. The spectrum can be made to correspond exactly to that of the doubled $SU(2)_2$ Chern-

Simons theory. Accordingly the topological ground state degeneracy is known [100] to be 9, as in the doubled Chern-Simons theory.

We can drive a phase transition in our system by perturbing the model (3.17) with transverse fields which create pairs of charges or vortices, as we did for the toric code by adding σ_l^x and σ_l^z . The vortex excitations have bosonic statistics and hence transverse fields which create vortex pairs can drive a transition to a vortex condensed phase in which string-nets are confined. On the other hand, the analogue of the Higgs transition is not evident for our problem as both charges are non-bosonic.

To drive the Ising transition that we are interested in, we add a transverse field which will condense spin-1 vortices. The Hamiltonian that we will tune through this transition is

$$H_{\text{SU}(2)_2} = -K \sum_P \frac{1}{2} (\mathbf{1} + B_P^1) - \Gamma_M \sum_s \mathcal{P}_s - K \sum_P \frac{1}{\sqrt{2}} B_P^{1/2} - \Gamma \sum_l (-1)^{2\sigma_l} \quad (3.19)$$

where we have separated \mathcal{P}_P into operators that “raise” spins by integer and half-integer amounts, and added a transverse field perturbation, $\Gamma(-1)^{2\sigma_l}$. The transverse field creates a pair of spin-1 vortices on the plaquettes adjacent to l , and has eigenvalue 1 on integer spin links, and -1 on half-integer spin links. Because the transverse field term squares to the identity (and all vortex creation operators commute), the vortices are Ising like.

On every plaquette P and site s , the eigenvalues of B_P^1 and \mathcal{P}_s are conserved, since these operators commute with $H_{\text{SU}(2)_2}$. Thus, we can consider the transition engendered by varying the ratio K/Γ in the subspace of the Hilbert space where the conditions

$$\mathcal{P}_s |\Psi\rangle = |\Psi\rangle, \quad B_P^1 |\Psi\rangle = |\Psi\rangle \quad (3.20)$$

are always satisfied. In this subspace, the transition can be mapped onto the transition in the pure \mathbb{Z}_2 gauge theory discussed in Sect. 3.2.3, and is therefore in the 3D Ising universality class as discussed in Ref. [25]. Here we give a different derivation of this result which focuses on the ground state wavefunctions and is better adapted to our purposes in this chapter.

To understand the mapping between $H_{\text{SU}(2)_2}$ and $H_{\mathbb{Z}_2}$ (3.7), notice first that the condition $\mathcal{P}_s|\psi\rangle = |\psi\rangle$ ensures that we are always working in the “charge-free” sector where the (deformed) angular momentum is conserved at each vertex. This, together with Eq. (3.18), stipulates that we only need to consider configurations where the number of half-integer spins entering each vertex is even - or equivalently, configurations in which half-integer spins form closed loops. Similarly, in the absence of charge in the pure \mathbb{Z}_2 theory (3.7), the gauge constraint G_s in Eq. (3.2) ensures that links with electric flux ($\sigma^x = -1$) form closed loops. The Levin-Wen transverse-field operator $(-1)^{2\sigma_l}$ assigns an energy penalty to the spin 1/2 edges that form these loops, similar to the action of the transverse-field term σ_l^x on links with electric flux in the \mathbb{Z}_2 theory. *Thus both models describe a transition in which loops (of half-integer spin variables in the Levin-Wen case or $\sigma^x = -1$ variables in the \mathbb{Z}_2 gauge theory case) become confined, and vortices become condensed as Γ/K increases.*

There is, however, a qualitative difference between the operators $\prod_{l \in \partial P} \sigma_l^z$ and $B_P^{1/2}$, both of which change the number of loops in a given configuration. While σ_l^z simply flips the spin on the link l , the operator $B_P^{1/2}$ maps a spin 0 or 1 link to a spin 1/2 link, but a spin 1/2 link to a superposition of a link in the state 0 and a link in the state 1. Thus one might worry that the two operators generate the same set of configurations (after identifying $s = 0, 1$ with $\sigma^x = 1$, and $s = 1/2$ with $\sigma_x = -1$), but with different statistical weights.

We show in Appendix 3.B that this is in fact not the case. Specifically, we prove that for any Γ , the ground state wave-function of either model can be expressed in

the form

$$|\Psi\rangle = \sum_{\{l\}} \beta_{\{l\}}^\Gamma |\Psi_{\{l\}}\rangle \quad (3.21)$$

where $\{l\}$ denotes a set of links on which $\sigma_l = 1/2$ in the Levin-Wen model restricted to (3.20), or $\sigma_l^x = -1$ in the pure \mathbb{Z}_2 gauge theory. Crucially, we find that $\beta_{\{l\}}$ is the same for each set $\{l\}$ in both models. Operators in the Levin-Wen model which commute with the conditions (3.20) are either diagonal in the vortex basis, or diagonal in the spin basis and sensitive only to the spin on each edge modulo 1. The expectation value of any such operator is therefore identical to that of its \mathbb{Z}_2 analogue, cementing the equivalence of the two models.

We conclude that within the sub-sector (3.20), the transition is equivalent to that of the pure \mathbb{Z}_2 gauge theory, and dual to that of the TFIM. It follows that our previous discussion of string net coarsening, and the scaling of vortex creation operators, applies *mutatis mutandis* to the model at hand.

Note, however, that the topological order of the initial and final phases of Eq. (3.19) is not the same as in the \mathbb{Z}_2 gauge theory; there are additional deconfined excitations on both sides of the transition. (In fact, the confined phase of $H_{\text{SU}(2)_2}$ is a \mathbb{Z}_2 gauge theory [26]). There must therefore be some operators in the Levin-Wen model whose behavior through the ramp is not captured by the mapping to the Ising gauge theory.

To make this more explicit, we consider the fate of Wilson loop operators. In the Levin-Wen model there are two of these:

$$\begin{aligned} W_{1/2}(R, t; \tau) &= \left\langle \prod_{l \in C} B_l^{1/2}(t) \right\rangle \\ W_1(R, t; \tau) &= \left\langle \prod_{l \in C} B_l^1(t) \right\rangle. \end{aligned} \quad (3.22)$$

In order not to create vortices along the curve C , these raising operators must act with appropriate configuration-dependent complex coefficients, as discussed in Refs. [122, 24]. $W_{1/2}(R, t; \tau)$ is clearly the analogue of the Wilson loop operator in the \mathbb{Z}_2 gauge theory; its expectation value obeys a perimeter law in the small Γ/K phase, and an area law in the large Γ/K phase, and its universal scaling in a linear ramp is given by Eq. (3.15). However, as the spin-1 variable remains deconfined throughout the phase diagram, $W_1(R, t; \tau)$ always obeys a perimeter law. Its expectation remains constant in the scaling limit as the system passes through the critical point.

Though we have primarily discussed the $SU(2)_2$ Levin-Wen model, the main results apply to a large family of models in which there is an excitation that behaves like the Ising vortex [25]. Specifically, all the $SU(2)_k$ models exhibit Ising transitions in which the half-integer spins (integer spins) can be mapped onto \mathbb{Z}_2 gauge configurations with $\sigma^x = -1$ ($\sigma^x = 1$). They have two families of Wilson-line operators: the half-integral Wilson line operators, which obey an area law in the confined phase, and scaling relations analogous to those of Eq. (3.15); and the integral Wilson line operators, whose expectation values do not depend on t, τ and which remain perimeter law throughout the ramp.⁴

It is worth mentioning that the Ising transition we have discussed here is but one of a variety of confining transitions that can be realized in Levin-Wen models [25, 78]. In the $SU(2)_2$ model discussed above, for example, we could also add a transverse field term of the form $\cos \pi s_l$ (which has eigenvalues $(1, 0, -1)$ for $s_l = (0, 1/2, 1)$, respectively). This confines both spin-1/2 and spin 1 labels, engendering a transition to a completely confined phase where both Wilson loop operators in Eq. (3.22) obey an area law. In this case the vortices that proliferate are not Ising-like, however, since the operator $\cos \pi s_l$ does not square to 1. Very little is known about the critical theory in this case, and we expect that the transition is not in the 3D Ising universality class,

⁴The Higgs transition may survive when k is a multiple of 4 as some of the charges are bosons. Little is known about these transitions.

so that the scaling functions and coarsening behavior will be fundamentally different from those of the \mathbb{Z}_2 gauge theory.

3.6.2 Away from the pure \mathbb{Z}_2 limit

Thus far, we did not concern ourselves with the other excitations in the $SU(2)_2$ Levin-Wen model as their number was conserved in the ramp and we remained in the subspace (25) at all times. However, the other excitations, charges of spin 1 and 1/2, and vortices of spin 1/2, will be created in a ramp if we perturb away from the limit of Eq. (3.19) by adding terms to the Hamiltonian which break the local conservation laws. In particular, the spin 1/2 charge has anyonic statistics relative to the condensing vortices, so that a finite density of these destroys confinement (these are analogous to the matter sources of the Ising gauge theory). Once again, the KZ scaling limit saves the day. These spin 1/2 charges remain gapped throughout the transition. Thus, as for the Ising gauge theory with matter, in the scaling limit we expect that the density of all of these excitations is vanishingly small throughout the coarsening regime; terms violating the conservation of the spin-1/2 charge at each vertex then act as dangerously irrelevant variables in the manner described in Section 3.5.

Spin 1 charges and spin-1/2 vortices, however, have bosonic statistics relative to the spin 1 vortex, and do not have analogues in the \mathbb{Z}_2 theory. Once again, for small perturbations which violate the exact local conservation of these excitations, they remain gapped throughout the transition and hence do not affect coarsening in the KZ scaling limit. Since a dilute density of such charges does not destroy confinement, however, we expect that they will not destroy coarsening even outside of the scaling limit.

3.7 Concluding remarks

In this chapter, we have initiated the study of the Kibble-Zurek problem for topologically ordered phases by studying the linear ramp across a transition that reduces/breaks topological order and written down a scaling theory for it. Interestingly, unlike broken symmetry cases where it is natural to ramp from less to more order, here it is more natural to ramp from more to less order. The latter leads to our identification of the slow dynamics of string net coarsening much as the former leads to defect coarsening *à la* Kibble and Zurek. Of course, one *can* study the reverse protocol and the associated scaling although we have not done so here in the interests of not taxing the reader’s patience unduly.

The basic framework here can be easily generalized to other transitions out of topological phases; although for string-net coarsening to be visible, the gauge degrees of freedom must have a ready identification. Examples are transitions out of \mathbb{Z}_n phases with $n \geq 3$ in $d = 2 + 1$ and with $n \geq 2$ in $d = 3 + 1$. The Levin-Wen models also offer a “target rich” domain, although the analysis is likely to prove more complicated for more general condensation transitions. It will also be interesting to move to contexts with conserved currents where one can study the temporal and spatial evolution of transport coefficients, such as the Hall conductance.

Finally, for the statistical mechanically inclined, we would like to draw attention to our identification of gapped matter as a dangerously irrelevant variable in the dynamical KZ context. This is clearly a more general idea—e.g. irrelevant departures from integrability will be similarly dangerous—and it suggests that in the KZ problem, more couplings will be classified as such than in the standard equilibrium analysis.

3.A Scattering times in coarsening

Here, we identify the dynamical process enabling coarsening at late times alluded to in Sec. 3.3.1, and justify that it remains in equilibrium during the KZ ramp. The criterion to remain in equilibrium is that the time-scale for such a process, t_{co} , is parametrically smaller than the time-scale for the change in the transverse-field t_Γ . Using $(\Gamma_M - \Gamma_{Mc}) = -t/\tau$, we estimate t_Γ to be:

$$t_\Gamma \equiv \frac{\Gamma_M - \Gamma_{Mc}}{d\Gamma_M/dt} = t.$$

The system at late times has two kinds of excitations that are remnants of the paramagnetism at early times: 1) The long domain walls of average size l_{co} and 2) The bulk gapped quasi-particle excitations about each ferromagnetically ordered state. As $t/t_K \rightarrow \infty$, the latter can be treated as classical particles. The average density of these particles and their momentum is essentially determined at $t \sim t_K$ and is fixed to be $\sim 1/l_K^2$ and $1/l_K$ respectively. Their mass is determined by the gap $\Delta(t)$. The growing mass and the long inter-particle distances as compared to the instantaneous correlation length ξ justify the classical particle approximation. An average velocity of these particles can be determined as

$$v_p \sim \frac{p}{m} \sim \frac{1/l_K}{\Delta},$$

where p is the average momentum and m the mass. The mechanism of coarsening proceeds through the transfer of energy between the long domain walls and these particles. To wit, the relevant time-scale t_{co} is the scattering time between these particles and the wall:

$$t_{co} \equiv \frac{l_{co}}{v_p}.$$

Recall that the growth law when ξ is a function of time is (Eq. (3.12)):

$$l_{co}(t; \tau) \sim \xi(t; \tau) \left(\frac{t}{\xi(t; \tau)^z} \right)^{1/z_d} \sim l_K \left(\frac{t}{t_K} \right)^{\frac{1-\nu}{2}},$$

where in the last step, we have substituted the critical exponents of the (2+1)D TFIM, $z = 1$, $z_d = 2$. Putting the pieces together, we see that $t_{co} \ll t_\Gamma \Rightarrow \nu < 1$. This certainly holds at the 3D Ising critical point where $\nu \approx 0.6$. Thus, we conclude that coarsening described by Model C is indeed the correct long time asymptote for the KZ scaling functions in a linear ramp.

Finally, we observe that all dynamical processes in the (2+1)D TFIM do not remain in equilibrium in the KZ ramp at late times. The scattering time between quasi-particles, t_{pp} , grows as Δ^2 in this limit and is parametrically larger than t_Γ . A hydrodynamical description, if it exists, is therefore more delicate than the case when the ramp is stopped at some $t/t_K = \hat{t}^s$.

3.B Mapping of general $SU(2)_k$ models to the \mathbb{Z}_2 gauge theory

In this Appendix, we will discuss in more detail the mapping from the confining transition in the $SU(2)_2$ Levin-Wen model to the pure \mathbb{Z}_2 gauge theory (3.7). As discussed earlier, the transition in question involves varying K/Γ in Eq. (3.19), while restricting the Hilbert space to states with eigenvalue 1 under the vertex projector, and the integer part of the plaquette projector. In this subspace, links with half-integer spins form closed loops. The mapping to the pure gauge \mathbb{Z}_2 theory involves mapping half-integer (integer) spins to the presence (absence) of \mathbb{Z}_2 electric flux $\sigma^x = -1$ (+1). The transverse field operator $(-1)^{2\sigma_l}$ maps to σ_l^x , and $B_P^{1/2}$ to $B_P =$

$\prod_{l \in \partial P} \sigma_l^z$. We will now show that the probability to be in any loop configuration is the same in both theories for every choice of K/Γ .

We will begin with some notation. Let C denote the collection of links on the lattice that form closed loops, and $\langle \alpha_{1/2}(C) \rangle$ the probability for a configuration in C . We will work here in the restricted Hilbert space of states for which

$$\mathcal{P}_s |\Psi\rangle = |\Psi\rangle \quad B_P^1 |\Psi\rangle = |\Psi\rangle \quad (3.23)$$

and assume that our lattice has no boundary. To make the analogy to the \mathbb{Z}_2 gauge theory, we also define the analogous operator, $\alpha_x(C)$, whose expectation value gives the probability for a closed loop configuration of links with $\sigma_l^x = -1$.

Our objective is to prove that, for every Γ and K , $\langle \alpha_{1/2}(C) \rangle = \langle \alpha_x(C) \rangle$. Since operators that commute with the conditions (3.23) are either diagonal in the spin basis and sensitive only to $s_l \bmod 1$, or diagonal in the vortex basis (dual to the basis of spin-1/2 loops), this is sufficient to prove that their critical behavior is identical.

We will carry out the proof in two steps. First, we will show the equality for the two solvable points $\Gamma = 0, K > 0$ and $K = 0, \Gamma > 0$, where we can construct exactly the ground-states in both models. We will then use perturbation theory to argue that the result holds throughout the phase diagram.

3.B.1 Equal weighting of loops in the ground states at the solvable points

For $K = 0, \Gamma > 0$, the ground state has $\sigma_l^x \equiv 1$ in the \mathbb{Z}_2 gauge theory, and $\sigma_l \in \{0, 1\}$ for the Levin-Wen model. In this limit, for any C we have trivially that $\langle \alpha_{1/2}(C) \rangle = \langle \alpha_x(C) \rangle = 0$ and the result holds.

Focusing on the opposite limit ($\Gamma = 0, K > 0$), let us construct the exact ground states in the two models. We begin with the \mathbb{Z}_2 gauge theory. Let $|0\rangle$ denote the

state with $\sigma^x = 1, \tau_s^x = 1$ on all links and sites. This satisfies the Gauss law, but is not an eigenstate of the plaquette projector. To construct such an eigenstate, we take

$$|\Psi_{TC}\rangle = \frac{1}{\sqrt{N}} \sum_{n=1}^{N_P} \sum_{*\mathbb{P}_n} \prod_{P \in *\mathbb{P}_n} B_P |0\rangle = \frac{2}{\sqrt{N}} \sum_{\{C\}} |\Psi_C\rangle \quad (3.24)$$

where $*\mathbb{P}_n$ runs over all possible distinct choices of n plaquettes on the lattice, and N is a normalization. This sum generates all possible configurations C of loops with $\sigma^x = -1$, weighted equally (each configuration is in fact generated twice, since $\prod_P B_P = 1$). Since $B_P^2 = 1$, $B_{P_i} \prod_{P \in *\mathbb{P}_n} B_P = \prod_{P \in *\mathbb{P}'_n} B_P$, where $*\mathbb{P}'_n$ is $*\mathbb{P}_n$ with P_i either added (if it was not originally in the set) or deleted (if it was). It follows that

$$\frac{1}{\sqrt{N}} \sum_{n=1}^{N_P} \sum_{*\mathbb{P}_n} B_{P_i} \prod_{P \in *\mathbb{P}_n} B_P |0\rangle = \frac{1}{\sqrt{N}} \sum_{n=1}^{N_P} \sum_{*\mathbb{P}_n} \prod_{P \in *\mathbb{P}_n} B_P |0\rangle$$

and $|\Psi_{TC}\rangle$ is a ground state.

A similar construction can be used in the Levin-Wen models. Let $|\Psi^e\rangle$ be a state satisfying (3.23), with σ_l an integer for every link l (careful inspection of these two conditions reveals that $|\Psi^e\rangle$ is a superposition of configurations of closed spin-1 loops).

Now consider:

$$|\Psi_{LW}\rangle = \frac{1}{\sqrt{N}} \sum_{n=1}^{N_P} \sum_{*\mathbb{P}_n} \prod_{P \in *\mathbb{P}_n} \frac{1}{\sqrt{2}} B_P^{1/2} |\Psi^e\rangle \quad (3.25)$$

We will show presently that

$$\left(B_P^{1/2}\right)^2 = 1 + B_P^1 \quad B_P^{1/2} B_P^1 = B_P^1 B_P^{1/2} = B_P^{1/2} \quad (3.26)$$

Using this fact, we have

$$B_{P_i}^{1/2} \prod_{P \in *\mathbb{P}_n} B_P^{1/2} = \begin{cases} \prod_{P \in *\mathbb{P}_n \setminus P_i} B_P^{1/2} (1 + B_{P_i}^1) & P_i \in *\mathbb{P}_n \\ \prod_{P \in *\mathbb{P}_n \cup P_i} B_P^{1/2} & P_i \notin *\mathbb{P}_n \end{cases}$$

It follows that

$$\frac{1}{\sqrt{2}} B_{P_i}^{1/2} |\Psi_{LW}\rangle = |\Psi_{LW}\rangle \quad (3.27)$$

and $|\Psi_{LW}\rangle$ is a ground state.

Now, for any closed loop L , we can generate a configuration with $\sigma_l = 1/2$ on all links in L , and no other links, by acting on $|\Psi^e\rangle$ with the product of $B_P^{1/2}$ on all plaquettes inside the loop or all plaquettes outside the loop (these are the only such configurations on the right-hand side of Eq. (3.25)). In the \mathbb{Z}_2 gauge theory the same holds for closed loops of $\sigma^x = -1$. Hence given C , we have

$$\begin{aligned} \langle \alpha_{1/2}(C) \rangle &= \frac{1}{N} \langle \Psi^e | \left(\prod_{P \in * \mathbb{P}(C)} \frac{1}{\sqrt{2}} B_P^{1/2} \right)^2 | \Psi^e \rangle \\ &= \frac{1}{N} \langle \Psi^e | \prod_{P \in * \mathbb{P}(C)} \frac{1}{2} (\mathbf{1} + B_P^1) | \Psi^e \rangle \\ &= \frac{1}{N} \end{aligned} \quad (3.28)$$

where $*\mathbb{P}(C)$ contains either all plaquettes inside, or all plaquettes outside, the closed loops in configuration C , and the last equality is a result of imposing (3.23). Thus for $\Gamma = 0$ all possible configurations of spin-1/2 loops occur with equal probability in the ground state of the $SU(2)_2$ Levin-Wen model.

We note that these results carry over directly to the more general case of an $SU(2)_k$ Levin-Wen model, upon replacing spin-1/2 (spin-1) with the set of all half-integer (integer) spins, and $B_P^{1/2}$ (B_P^1) with the sum of all half-integer (integer) spin-raising terms in the plaquette operator (weighted by their respective quantum dimensions).

It remains to show that Eq. (3.26) holds, which we will do for general k . We let $\mathcal{P}_P^{1/2} = \frac{1}{\mathcal{D}} \sum_{\sigma=1/2, 3/2, \dots} a_\sigma B_P^\sigma$ denote all half-integer raising terms in the plaquette operator, and $\mathcal{P}_P^1 = \frac{1}{\mathcal{D}} \left(\mathbf{1} + \sum_{\sigma=1, 2, \dots} a_\sigma B_P^\sigma \right)$ denote all integer terms. Following Levin and Wen, we choose the constant \mathcal{D} such that $\mathcal{P}_P \equiv \frac{1}{2} \left(\mathcal{P}_P^1 + \mathcal{P}_P^{1/2} \right)$ is a projector.

We then have

$$\begin{aligned} (\mathcal{P}_P^1 + \mathcal{P}_P^{1/2})^2 &= (\mathcal{P}_P^1)^2 + (\mathcal{P}_P^{1/2})^2 + \mathcal{P}_P^{1/2}\mathcal{P}_P^1 + \mathcal{P}_P^1\mathcal{P}_P^{1/2} \\ &= 2(\mathcal{P}_P^1 + \mathcal{P}_P^{1/2}) \end{aligned}$$

Now, $(\mathcal{P}_P^{1/2})^2$ and $(\mathcal{P}_P^1)^2$ both contain only terms that raise the spins in P by an integer amount, while $\mathcal{P}_P^1\mathcal{P}_P^{1/2} = \mathcal{P}_P^{1/2}\mathcal{P}_P^1$ contains only half-integral raising operators.

It follows that

$$(\mathcal{P}_P^1)^2 + (\mathcal{P}_P^{1/2})^2 = 2\mathcal{P}_P^1, \quad \mathcal{P}_P^1\mathcal{P}_P^{1/2} = \mathcal{P}_P^{1/2}. \quad (3.29)$$

We also have

$$(\mathcal{P}_P^1 + \mathcal{P}_P^{1/2})(\mathcal{P}_P^1 - \mathcal{P}_P^{1/2}) = 0 \quad (3.30)$$

since it can be shown[25] that $(\mathcal{P}_P^1 + \mathcal{P}_P^{1/2})$ projects onto flux-free states, while $(\mathcal{P}_P^1 - \mathcal{P}_P^{1/2})$ projects onto states with an Ising vortex. It follows that

$$(\mathcal{P}_P^{1/2})^2 = (\mathcal{P}_P^1)^2 = \mathcal{P}_P^1 \quad (3.31)$$

This also implies that \mathcal{P}_P^1 is a projector, and thus that the eigenvalues of \mathcal{P}_P^1 are 0 and 1. (From Eq (3.31) and the fact that \mathcal{P}_P is a projector, it follows that the eigenvalues of $\mathcal{P}_P^{1/2}$ are 0, ± 1 ; when restricted to configurations where $\mathcal{P}_P^1|\Psi\rangle = |\Psi\rangle$, they are ± 1 , as one expects from the correspondence of $\mathcal{P}_P^{1/2}$ to the plaquette term of the toric code.)

3.B.2 Away from the solvable points

Next, we wish to show that the result of the previous section holds true throughout the phase diagram. One way to do this is to invoke the result of Ref. [25], where it was shown that within the subspace of states satisfying (3.23), the $SU(2)_k$ Levin-Wen models are exactly dual to the transverse-field Ising model. We can identify all

states in this Hilbert space by the configuration of dual Ising spins (together with their topological ground-state sector, in periodic boundary conditions). The duality relation— which also holds for the \mathbb{Z}_2 gauge theory — ensures that the probability amplitude to be in a given vortex configuration is identical in both models. The physical operators in this Ising subspace are either diagonal in the vortex (or dual Ising spin) basis, or diagonal in the basis of spin-1/2 loops. (These are precisely the operators that do not cause violations of (3.23), and cannot distinguish between edges of spin 0 and spin 1). It follows that all expectation values of such operators — including $\langle \alpha_{1/2}(C) \rangle$ — must also be identical to their \mathbb{Z}_2 analogues (such as $\langle \alpha_x(C) \rangle$).

Here we will take an alternative, perturbative approach to prove the desired result. We will begin at an arbitrary point in the deconfined phase, and consider constructing the wave-functions in both theories to some finite order in perturbation theory. These wave functions are linear combinations of the unperturbed (Levin-Wen or toric code) ground state, together with excited states of the form

$$|\Psi_{\{l\}}\rangle = \prod_{l \in \{l\}} h_l |\Psi_0\rangle \quad (3.32)$$

where we have defined the transverse field operator $h_l \equiv \sigma_l^x$ for the toric code, and $(-1)^{2s_l}$ for the Levin-Wen model, and $|\Psi_0\rangle$ denotes the unperturbed ground state. If l_1 and l_2 are two links bordering plaquette P , we have

$$\begin{aligned} \sigma_{l_{1,2}}^x B_P &= -B_P \sigma_{l_{1,2}}^x \\ (-1)^{2s_{l_{1,2}}} B_P^{1/2} &= -B_P^{1/2} (-1)^{2s_{l_{1,2}}} \\ [\sigma_{l_1}^x \sigma_{l_2}^x, B_P] &= [(-1)^{2s_{l_1}} (-1)^{2s_{l_2}}, B_P^{1/2}] = 0 \end{aligned}$$

Thus $|\Psi_{\{l\}}\rangle$ is a state with vortices on each plaquette with an odd number of edges in the set of links $\{l\}$. It also follows that choices of $\{l\}$ which differ by a product

$\prod_{l \in C^*} h_l$, where C^* is a set of closed curves on the dual lattice, create identical excited states, as $\prod_{l \in C^*} h_l |\Psi_0\rangle = |\Psi_0\rangle$. Finally, we have

$$\langle \Psi_{\{l\}} | \Psi_{\{l'\}} \rangle = \delta_{\{l\} \cup \{l'\}, C^*} \quad (3.33)$$

In other words, the inner product is 1 if the combination of the two sets $\{l\}$ and $\{l'\}$ of links forms a set of closed curves on the dual lattice, so that $|\Psi_{\{l\}}\rangle$ and $|\Psi_{\{l'\}}\rangle$ have vortices on the same plaquettes. Similarly, we may compute matrix elements of the Hamiltonian within these excited states via:

$$\langle \Psi_{\{l\}} | \prod_{l \in \{l''\}} h_l | \Psi_{\{l'\}} \rangle = \delta_{\{l\} \cup \{l'\} \cup \{l''\}, C^*} \quad (3.34)$$

The crucial point is that for any choice of $\{l\}, \{l'\}, \{l''\}$, these matrix elements are identical in both models. Since the weight of each unperturbed excited state in the exact ground state can be constructed perturbatively using only matrix elements of this form, it follows that

$$|\Psi\rangle = \sum_{\{l\}} \beta_{\{l\}}^\Gamma |\Psi_{\{l\}}\rangle \quad (3.35)$$

with $\beta_{\{l\}}$ the same for each set $\{l\}$ in both models.

Finally, we observe that $\alpha_{1/2}(C)$ and $\alpha_x(C)$ both have the form

$$\alpha_\nu = \prod_{l \in C} \frac{1}{2} (1 - h_l) \quad (3.36)$$

and, in particular, commute with h_l on every link. (Here $\alpha_\nu = \alpha_{1/2}(C), \alpha_x(C)$ as appropriate). This, together with the relation (3.34), implies that

$$\langle \alpha_\nu \rangle_\Gamma = \sum_{\{l\}, \{l'\}} \bar{\beta}_{\{l\}}^\Gamma \beta_{\{l'\}}^\Gamma \langle \Psi_0 | \prod_{l \in \{l\}} h_l \alpha_\nu \prod_{l \in \{l'\}} h_l | \Psi_0 \rangle$$

in both models. We have already shown that the coefficients $\beta_{\{l\}}^\Gamma$ are the same, and the possible choices of $\{l\}, \{l'\}$ on which the δ function has support are a geometric property of the lattice. Invoking the result of the previous subsection, we can thus conclude that for all Γ in the deconfined phase,

$$\langle \alpha_{1/2}(C) \rangle_\Gamma = \langle \alpha_x(C) \rangle_\Gamma \quad (3.37)$$

Our derivation has implicitly relied on the fact that we can construct the exact ground state perturbatively, starting from the ground state of the toric code or Levin-Wen solvable point. Thus the above argument fails at the critical point, and in the phase where Γ/K is large. In this regime, however, we may make essentially the same argument, by replacing h_l with the plaquette operator, and $|\Psi_{LW}\rangle, |\Psi_{TC}\rangle$ (denoted by $|\Psi_0\rangle$ in the derivation above) with $|\Psi^e\rangle$ and $|0\rangle$ respectively. In this case, the basis of excited states generated will be an eigenstate of σ^x (toric code) or $(-1)^{2s}$ (Levin-Wen). There is no need to define an analogue of C^* , since if two distinct products of plaquette projectors produce the same loop configuration state, then their product is the identity operator.

In each phase, we can thus argue that Eq. (3.37) holds to arbitrary order in perturbation theory. It follows that as the phase transition is second order, it must also hold at the critical point, proving the result.

Chapter 4

The quantum $O(N)$ model at infinite N

4.1 Introduction

The study of the out of equilibrium dynamics of closed quantum systems has intensified greatly in recent years inspired in considerable measure by advances in the experimental study of cold atomic systems [85, 86, 165, 183, 163, 16].¹ We have explored one important theme in this work through the study of the Kibble-Zurek problem: the interplay between non-equilibrium dynamics and phase structure. A second theme that we have not touched upon so far is the presence and nature of equilibration starting from a non-equilibrium state and its relationship to integrability. An interesting stream of work has postulated and examined the notion of a generalized Gibbs ensemble (GGE) in which an integrable system relaxes to a maximum entropy state consistent with *all* of its constants of motion [161, 107].

A large fraction of this work has concerned itself, for natural reasons of tractability, to systems in spatial dimension $d = 1$ where analytic [27, 36, 47, 51, 132, 30] and

¹Chapter based on work with Arun Nanduri, Steven S. Gubser and S. L. Sondhi [41].

computational power [160, 117] can be readily brought to bear. This restriction to $d = 1$ however does not allow the study of the impact of dimensionality, known to be important for equilibrium behavior. In this chapter, we study a model where one *can* move between dimensions while retaining tractability—the quantum $O(N)$ vector model in the infinite N limit (see Ref. [135] for a comprehensive introduction). This model has much to commend it. It yields an equilibrium phase diagram in the Gibbs ensemble in various dimensions whose topology is correct for $N \geq 3$. It also yields critical exponents which incorporate corrections beyond Gaussian critical behavior in $d < 3$ and correctly locates the lower and upper critical dimension at $d = 1$ and $d = 3$ respectively.

The above results *assume* that the Gibbs ensemble is reached. In this chapter, we study the late time states of the model starting out of equilibrium and ask to what extent the equilibrium phase diagram is a guide to the late time behavior. We note that the model has certainly been the object of prior study, in the first instance from a cosmology inspired interest in non-equilibrium field theory [21, 46, 13, 20] and more recently from the condensed matter/statistical mechanical viewpoint [173, 50, 168]. We build on this work but find that there are still new things to say on this problem, largely due to asking some fresh questions from the condensed matter/statistical mechanical perspective.

Our results organize themselves naturally into the two themes we noted at the outset. First, we revisit the question of equilibration in the infinite N vector model. If the model were to exhibit equilibration, the late time state could be inferred from the finite temperature phase diagram. In the infinite N limit, we show that not only does the model not lead to equilibration on account of an infinite number of conserved quantities, it also does *not* relax to a generalized Gibbs ensemble (GGE) consistent with these conserved quantities. Instead, an infinite number of new conservation laws emerge at late times and the system relaxes to an *emergent* GGE consistent with

these. The emergent GGE has the same conserved quantities as a non-interacting, purely Gaussian, vector model [28, 4, 48]. Second, we examine spatially homogenous quenches starting from ground states in the disordered phase to the critical coupling and into the couplings in the ordered phase. For the latter, we show that the late time state exhibits coarsening in the sense of a diverging equal time correlation length in $d > 2$ for sufficiently gentle quenches. Our numerics further suggest that the system coarsens towards a non-equilibrium critical state as $t \rightarrow \infty$. For larger quenches in $d > 2$ or for any quenches in $d \leq 2$, we find that no coarsening is possible. Instead, the late time state is disordered. For quenches to the critical point, we find no coarsening for all d but coarsening in the scaling limit for $d \geq 3$ consistent with the lack of scattering at the Gaussian fixed point and previous results on the Gaussian theory [28]. Interestingly, the results on quenches are qualitatively what one would predict assuming equilibration following an injection of energy density and yet they hold for a system that does not equilibrate.

In the following, we document these claims. We begin with a review of the infinite N vector model and the equations that must be solved to determine its dynamics in Section 4.2. In Section 4.3, we discuss the issue of ergodicity or equilibration. In Section 4.4, we describe our results on global quenches into the ordered phase. In Section 4.5, we discuss global quenches to the critical point and show that the stability of the Gaussian fixed point for $d \geq 4$ when it comes to equilibrium behavior also shows up in the behavior of non-equilibrium quenches provided one takes a scaling limit similar to the KZ scaling limit. We finish with some concluding remarks in Section 4.6 and relegate some technical material to an appendix.

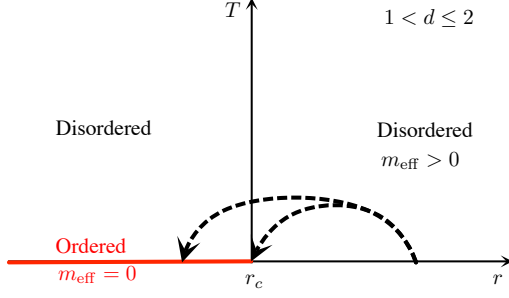


Figure 4.1: Topology of the equilibrium phase diagram of the $O(N)$ model in the infinite N limit in spatial dimensions $1 < d \leq 2$. The dashed lines indicate the different quenches that we study.

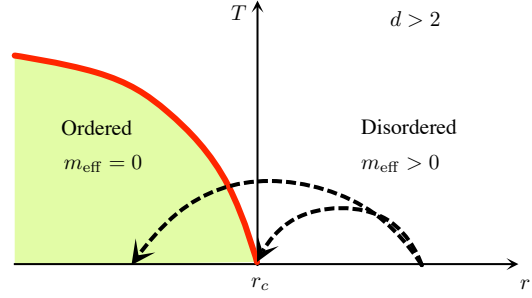


Figure 4.2:] Topology of the equilibrium phase diagram of the $O(N)$ model in the infinite N limit in spatial dimensions $d > 2$. The dashed lines indicate the different quenches that we study.

4.2 The model

4.2.1 Statics

The Hamiltonian of the quantum $O(N)$ model in d spatial dimensions is

$$H = \frac{1}{2} \int d^d x \left(|\vec{\Pi}|^2 + |\vec{\nabla} \vec{\Phi}|^2 + r |\vec{\Phi}|^2 + \frac{\lambda}{2N} |\vec{\Phi}|^4 \right), \quad (4.1)$$

where $\vec{\Phi}$ and $\vec{\Pi}$ are canonically conjugate N -component fields,

$$[\Phi_i(\vec{x}), \Pi_j(\vec{x}')] = i \delta^d(\vec{x} - \vec{x}') \delta_{ij}. \quad (4.2)$$

In the limit $N \rightarrow \infty$, the equilibrium physics is soluble. In the disordered phase, $\langle \vec{\Phi} \rangle = 0$, the ground state of H is well-approximated by the ground state of a free field theory with mass m_{eff} that is determined self-consistently:

$$m_{\text{eff}}^2 = r + \lambda \left\langle \frac{|\vec{\Phi}|^2}{N} \right\rangle \quad (4.3)$$

$$\left\langle \frac{|\vec{\Phi}|^2}{N} \right\rangle = \int^\Lambda \frac{d^d k}{(2\pi)^d} \frac{1}{2\sqrt{|\vec{k}|^2 + m_{\text{eff}}^2}}, \quad (4.4)$$

where Λ is the cutoff. The effective mass m_{eff} is proportional to the single-particle gap and controls the phase diagram (Figs. 4.1, 4.2). In the disordered phase, $m_{\text{eff}} > 0$, while in the ordered phase, when suitably re-defined, m_{eff} is the mass of the Goldstone bosons and equals zero. We describe the phase diagram in greater detail in Sec. 4.4. The solubility in equilibrium can be traced to two related sources: 1) The ground state is a (Gaussian) symmetric product state over component indices, and 2) the expectation value:

$$\left\langle \frac{|\vec{\Phi}|^2}{N} \Phi_i \right\rangle = \left\langle \frac{|\vec{\Phi}|^2}{N} \right\rangle \langle \Phi_i \rangle + O\left(\frac{1}{N}\right) \quad (4.5)$$

factorizes to leading order in $1/N$. These two features of the infinite N model in equilibrium make the dynamical problem tractable as well.

4.2.2 Dynamics

Now consider preparing the system at $t = 0$ in a product state symmetric in the component indices:²

$$|\psi(0)\rangle = \prod_{i=1}^N |\beta\rangle_i. \quad (4.6)$$

The wavefunction of each component, $|\beta\rangle$, can be freely chosen. In particular, $|\psi(0)\rangle$ need not be Gaussian or be a ground state of the infinite N model anywhere in the disordered phase. In general, it does not satisfy Wick's theorem. The evolution of the state $|\psi(0)\rangle$ for $t > 0$ is generated by H . The Heisenberg equations of motion are:

$$\frac{d\Phi_i}{dt} = \Pi_i$$

²More generally any state, such as the ground state for some value of the bare parameters, which is well approximated by such a product state for *finite* point correlation functions. The dynamics is also tractable for the class of density matrices that have product structure in the component index.

$$\frac{d\Pi_i}{dt} = \nabla^2\Phi_i - r\Phi_i - \frac{\lambda}{N}|\vec{\Phi}|^2\Phi_i. \quad (4.7)$$

For the rest of this article, we work in the Heisenberg picture. Remarkably, the factorization in equilibrium in Eq. (4.5) holds out-of-equilibrium as well:

$$\left\langle \frac{|\vec{\Phi}(t)|^2}{N}\Phi_i(t) \right\rangle = \left\langle \frac{|\vec{\Phi}(t)|^2}{N} \right\rangle \langle \Phi_i(t) \rangle + O\left(\frac{1}{N}\right). \quad (4.8)$$

As in equilibrium, this factorization leads to an effective mass in a free field theory that is determined self-consistently. However, the effective mass is now time-dependent. More formally, consider the Hamiltonian for a free field theory with the time-dependent mass $m_{\text{eff}}(t)$ determined self-consistently at each t :

$$H_{\text{eff}}(t) = \frac{1}{2} \int^\Lambda \frac{d^d k}{(2\pi)^d} \left[|\vec{\Pi}_{\vec{k}}|^2 + (|\vec{k}|^2 + m_{\text{eff}}^2(t)) |\vec{\Phi}_{\vec{k}}|^2 \right] \quad (4.9)$$

$$m_{\text{eff}}^2(t) \equiv r + \lambda \left\langle \frac{|\vec{\Phi}(t)|^2}{N} \right\rangle. \quad (4.10)$$

Above, $\Phi_{j\vec{k}} = \int d^d x \Phi_j(\vec{x}) e^{-i\vec{k}\cdot\vec{x}}$ and $\Pi_{j\vec{k}} = \int d^d x \Pi_j(\vec{x}) e^{i\vec{k}\cdot\vec{x}}$ so that $[\Phi_{i\vec{k}}, \Pi_{j\vec{k}'}] = i(2\pi)^d \delta^d(\vec{k} - \vec{k}') \delta_{ij}$. We evolve the state $|\psi(0)\rangle$ with H_{eff} . We also evolve $|\psi(0)\rangle$ with H in the limit $N \rightarrow \infty$. The formal statement is that all correlation functions involving a finite number of components are identical in the two cases at any fixed t . Thus, to determine observables and correlation functions, we need only solve for the dynamics in a free field theory with mass $m_{\text{eff}}(t)$. As in equilibrium, the infinite N model out-of-equilibrium goes beyond the free field theory through the single self-consistency condition on $m_{\text{eff}}(t)$ (Eq. (4.10)). Henceforth, we suppress the component index when an expectation value is independent of it. Specifically, we replace $\langle |\vec{\Phi}(t)|^2 \rangle / N$ by the expectation $\langle \Phi^2(t) \rangle$ of a single component. When not indicated, all operators in a correlation function are assumed to have the same component label.

A convenient way to determine correlation functions from $H_{\text{eff}}(t)$ is to expand $\Phi_{\vec{k}}(t)$ and $\Pi_{\vec{k}}(t)$ in a fixed basis at $t = 0$:

$$\begin{aligned}\Phi_{\vec{k}}(t) &= \frac{f_{\vec{k}}(t)}{\sqrt{2}} a_{\vec{k}} + \frac{f_{-\vec{k}}^*(t)}{\sqrt{2}} a_{-\vec{k}}^\dagger \\ \Pi_{\vec{k}}(t) &= \frac{d\Phi_{\vec{k}}^\dagger(t)}{dt}.\end{aligned}\tag{4.11}$$

Above, the $(a_{\vec{k}}, a_{\vec{k}}^\dagger)$ and $(a_{-\vec{k}}, a_{-\vec{k}}^\dagger)$ are two independent sets of fixed ladder operators with the usual commutation relations. The $f_{\vec{k}}(t)$ are complex-valued coefficients known as mode functions. The commutation relations stipulate that:

$$\begin{aligned}f_{\vec{k}}(t) &= f_{-\vec{k}}(t) \\ \text{Im}[f_{\vec{k}}(t) \dot{f}_{\vec{k}}^*(t)] &= 1.\end{aligned}\tag{4.12}$$

Given an initial state, we may choose any fixed basis to decompose the field operators in. This is a coordinate choice; in this article, we pick the particular fixed basis in which:

$$\langle a_{\vec{k}} a_{\vec{k}'} \rangle = 0, \quad f_{\vec{k}}(0) = f_{\vec{k}}^*(0).\tag{4.13}$$

It is then easy to see that $f_{\vec{k}}(0)$ and $|\dot{f}_{\vec{k}}(0)|$ fix all the coefficients in Eq. (4.11) at $t = 0$. For example, Eq. (4.12) determines the phase of $\dot{f}_{\vec{k}}(0)$ etc. Both functions follow from the two-point functions in the initial state:

$$\begin{aligned}\langle \Phi_{\vec{k}}(0) \Phi_{\vec{k}'}^\dagger(0) \rangle &= \frac{f_{\vec{k}}(0)^2 \mathcal{N}_{\vec{k}}}{2} (2\pi)^d \delta^d(\vec{k} - \vec{k}') \\ \langle \Pi_{\vec{k}}(0) \Pi_{\vec{k}'}^\dagger(0) \rangle &= \frac{|\dot{f}_{\vec{k}}(0)|^2 \mathcal{N}_{\vec{k}}}{2} (2\pi)^d \delta^d(\vec{k} - \vec{k}') \\ \text{Re}[\langle \Phi_{\vec{k}}(0) \Pi_{\vec{k}'}(0) \rangle] &= \text{Re}[\dot{f}_{\vec{k}}(0)] f_{\vec{k}}(0) \mathcal{N}_{\vec{k}} (2\pi)^d \delta^d(\vec{k} - \vec{k}').\end{aligned}\tag{4.14}$$

if we substitute for the phase of $\dot{f}_{\vec{k}}(0)$ from Eq. (4.12). $\mathcal{N}_{\vec{k}}$ above is related to the sum of the occupations of the $\pm\vec{k}$ modes in the initial state:

$$\mathcal{N}_{\vec{k}} \equiv 1 + n_{\vec{k}} + n_{-\vec{k}}, \quad \langle a_{\vec{k}}^\dagger a_{\vec{k}'} \rangle = n_{\vec{k}} (2\pi)^d \delta^d(\vec{k} - \vec{k}').$$

Finally, from $H_{\text{eff}}(t)$, the definition of m_{eff}^2 in Eq. (4.10), and Eq. (4.11), we obtain the equations of motion for the mode functions:

$$\left(\frac{d^2}{dt^2} + |\vec{k}|^2 + m_{\text{eff}}^2(t) \right) f_{\vec{k}}(t) = 0 \quad (4.15)$$

$$m_{\text{eff}}^2(t) = r + \frac{\lambda}{2} \int \frac{d^d k}{(2\pi)^d} |f_{\vec{k}}|^2 \mathcal{N}_{\vec{k}}. \quad (4.16)$$

Given the correlation functions in Eq. (4.14) and the condition in Eq. (4.12), we can propagate this system of coupled second-order differential equations forward in time to solve for $f_{\vec{k}}(t)$. We may then compute any correlation function of interest by means of Eq. (4.11) and the solutions for the mode functions.

4.3 Ergodicity

To determine the nature of the late time state, we need to identify all the quantities that are conserved in the dynamics (Eq. (4.15,4.16)). First, as the evolution is generated by a Hamiltonian, the total energy is conserved. This would be true for any isolated quantum system. Additionally at infinite N , the operators $L_{\vec{k}}^z$ defined below also commute with H in the class of states in Eq. (4.6).

$$L_{\vec{k}}^z \equiv \frac{\Phi_{\vec{k}}^\dagger \Pi_{\vec{k}}^\dagger - \Phi_{\vec{k}} \Pi_{\vec{k}}}{i}. \quad (4.17)$$

Thus,

$$\frac{d\langle L_{\vec{k}}^z \rangle}{dt} = 0. \quad (4.18)$$

We use $\vec{k} > 0$ to denote half the momenta; each \vec{k} in the set labels the pair $(\vec{k}, -\vec{k})$. Note that the component label has been suppressed in the definition of $L_{\vec{k}}^z$; there is actually one conserved quantity for every $\vec{k} > 0$ and component label. However, for our class of initial states (Eq. (4.6)), $\langle L_{\vec{k}}^z \rangle$ is the same for every component and we can safely drop the label. The conserved quantity $\langle L_{\vec{k}}^z \rangle$ has two interpretations. One is the angular momentum of the 2d harmonic oscillator at $\vec{k} > 0$ in $H_{\text{eff}}(t)$. The second is in the fixed basis in which $\langle L_{\vec{k}}^z \rangle = n_{\vec{k}} - n_{-\vec{k}}$. This difference is conserved as the scattering processes that lead to exchange of momenta between pairs of bosons is suppressed at infinite N . Finally, observe that $L_{\vec{k}}^z$ is not a local operator in real space. However, a suitable linear combination of the $L_{\vec{k}}^z$ at different \vec{k} is. Defining $I^-(\vec{n}) = \int \frac{d^d k}{(2\pi)^d} L_{\vec{k}}^z \sin(\vec{k} \cdot \vec{n})$ and using Eq. (4.17), we see that $I^-(\vec{n}) = \int d^d x (\Phi(\vec{x})\Pi(\vec{x} - \vec{n}) - \Phi(\vec{x})\Pi(\vec{x} + \vec{n}))$. As promised, $I^-(\vec{n})$ is a sum of local conserved densities. It is non-zero only if the system is not inversion symmetric. It is worth noting that there is a similar conserved quantity in the free Majorana field theory/ transverse field Ising model [83, 152, 66].

There are therefore half as many conserved quantities as the number of degrees of freedom. This is reminiscent of an integrable system in which the number of conserved quantities equals the number of degrees of freedom. For example, the free field theory ($\lambda = 0$) is integrable and has two conserved quantities for each $(\vec{k}, -\vec{k})$ pair: the energy in the 2d oscillator and the angular momentum $L_{\vec{k}}^z$. In such systems, the correlations in the late time state are conjectured to be reproduced by the generalized Gibbs

ensemble (GGE) [161, 62] :

$$\rho_{GGE} = \exp\left(-\sum_{i=1}^M \mu_i O_i\right),$$

where the O_i commute with the Hamiltonian and the μ_i are fixed by $\langle O_i \rangle$ in the initial state. In the free field theory, for some classes of initial states (including the ground states of the free theory at any $r > 0$), this conjecture can be directly checked.

The collection of conserved quantities in the $O(N)$ model at infinite N suggests that the late time state should thermalize to the following GGE:

$$\rho_{GGE} = \exp\left(-\beta H - \int_{\vec{k}>0} \mu_{\vec{k}} L_{\vec{k}}^z\right). \quad (4.19)$$

We argue in two (possibly related) ways below that the dynamics *fails* to relax to this GGE.

First, note that Eq. (4.16) depends on a c-number associated with the initial state. A reasonable expectation would be that correlation functions at late times also depend on this c-number. However, correlation functions derived from the GGE do not. This suggests that the GGE is not the correct description of the late-time dynamics. In Appendix 4.A, we sharpen this intuition by showing that the structure factor at late times depends on $\mathcal{N}_{\vec{k}}$. It follows that two-point function in real-space is also a function of the $\mathcal{N}_{\vec{k}}$, thus proving the claim that the system does not relax to the GGE for all local observables. We note that Ref. [13] arrived at the same conclusion by constructing a particular non-linear combination of equal-time correlation functions that were independent of time and involved $\mathcal{N}_{\vec{k}}$.

The second argument hinges on the numerical observation that $m_{\text{eff}}^2(t)$ generically approaches a non-negative constant, m_f^2 , as $t \rightarrow \infty$. This implies that the different \vec{k} modes decouple and the theory is effectively free at late times. Thus, an extensive set of conserved quantities (equal to the number of angular momenta) *emerges* at late

times:

$$E_{\vec{k}} = |\vec{\Pi}_{\vec{k}}|^2 + (|\vec{k}|^2 + m_f^2)|\vec{\Phi}_{\vec{k}}|^2, \quad \vec{k} > 0 \quad (4.20)$$

and the system appears integrable. As these extra conserved quantities are independent of $\langle L_{\vec{k}}^z \rangle$, it is clear that the system does not relax to the strict GGE in Eq. (4.19). However, the system does relax to an *emergent* GGE with the $E_{\vec{k}}$ and $L_{\vec{k}}^z$ as conserved quantities. The argument for the emergent GGE hinges on the theory being free once $m_{\text{eff}}^2 \approx m_f^2$. Define t_f so that $m_{\text{eff}}^2 \approx m_f^2$ for $t > t_f$. If the state of the system at $t = t_f$ lies within the class of initial states that relaxes to a GGE under the evolution of the free theory, then we are guaranteed that the emergent GGE is the correct description for $t \gg t_f$. It is known that all initial states that are physically relevant (exponentially decaying spatial correlations, well-defined conserved densities in the thermodynamic limit etc.) relax to a GGE under the evolution of a free bosonic theory. The state of the $O(N)$ model at $t = t_f$ is physical; thus the system *always* relaxes to the emergent GGE. In particular, in the sudden quenches that we discuss in the following section, the late time state is described by an emergent GGE whenever it is disordered. By default, whenever we say GGE, we mean Eq. (4.19). The other GGE will always be referred to as emergent GGE.

This leaves open the possibility that there is a more restrictive GGE that includes some unknown additional conserved quantities that *will* describe the late time states. While we cannot rule this out, we (and previous workers on this problem) have not been able to find such quantities.

4.4 Quenches to the ordered phase

4.4.1 Problem, methods and background

We now turn to the late time behavior of protocols starting from ground states in the disordered phase wherein the coupling is changed to a value in which the ground state is ordered (see Figs. 4.1 and 4.2). For specificity and because our interest here is primarily in the late time behavior, we will take these protocols to be sudden quenches, i.e. the coupling will be changed instantly to its new value. Our conclusions will generalize *mutatis mutandis* to more elaborate protocols such as those of interest in the Kibble-Zurek problem. Right after the quench, the system is in an excited state for the new Hamiltonian, i.e. one with a non-zero energy density. For a system which thermalizes, the late time state can be read off from the equilibrium phase diagram by converting the energy density into an equivalent temperature. Interestingly, despite the lack of relaxation in the quantum $O(N)$ model at infinite N , we will find that the phase diagram is *still* a good heuristic for the late time behavior when the system is quenched, in a sense we will shortly make precise.

But first, let us describe the setup of the problem more precisely. Recall that the mode functions are constrained by Eqs. (4.12) and (4.13). Polar coordinates make these constraints more transparent. Define $f_{\vec{k}} \equiv |f_{\vec{k}}| \exp(i\theta_{\vec{k}})$. Eq. (4.12) then provides a relation between the amplitude and the phase of the mode function:

$$\dot{\theta}_{\vec{k}} = \frac{-1}{|f_{\vec{k}}|^2}. \quad (4.21)$$

Together with the initial condition $\theta_{\vec{k}}(0) = 0$, this allows us to reconstruct the mode function at all t from $|f_{\vec{k}}(t)|$ alone. The equation of motion for $|f_{\vec{k}}(t)|$ follows from

Eq. (4.15,4.16):

$$\left(\frac{d^2}{dt^2} + |\vec{k}|^2 + m_{\text{eff}}^2(t) \right) |f_{\vec{k}}| - \frac{1}{|f_{\vec{k}}|^3} = 0 \quad (4.22)$$

$$m_{\text{eff}}^2(t) = r + \frac{\lambda}{2} \int \frac{d^d k}{(2\pi)^d} |f_{\vec{k}}|^2 \mathcal{N}_{\vec{k}}. \quad (4.23)$$

It suffices to solve these equations subject to the initial conditions discussed below to determine $f_{\vec{k}}(t)$.

We pick the initial state of the system for $t < 0$ to be the ground state in the disordered phase. That is, we prepare the system in the ground state of H (Eq. (4.1)) with bare coupling $r = r_0$ greater than the critical coupling r_c . This state is the ground state of a free field theory with the effective mass m_0 . The relation between m_0 and r_0 is given by Eq. (4.4). In this state:

$$\begin{aligned} \mathcal{N}_{\vec{k}} &= 1, & \Omega_{k0} &= \sqrt{|\vec{k}|^2 + m_0^2} \\ f_{\vec{k}}(t < 0) &= \frac{1}{\sqrt{\Omega_{k0}}}, & \dot{f}_{\vec{k}}(t < 0) &= -i\sqrt{\Omega_{k0}}. \end{aligned} \quad (4.24)$$

Ω_{k0} above is the frequency of the harmonic oscillator at \vec{k} . At $t = 0$, we suddenly quench to the ordered phase ($r < r_c$). We note that in terms of our discussion earlier, the conserved angular momenta are all zero so that the associated chemical potentials $\mu_{\vec{k}}$ in the GGE are all also zero.

For the most part we will rely on numerical solutions of the dynamical equations. Specifically, we numerically solve Eqs. (4.22,4.23) subject to the initial conditions in Eq. (4.24). We sample $|f_{\vec{k}}|$ on a grid of points in momentum space with the infrared spacing $1/L$ and the ultra-violet cut-off Λ ; we present data only for the largest system sizes L in which the finite-size effects are minimal.³ We have also ascertained that the average energy is conserved at least to one part in 10^4 . The dimensional

³Some of the data involved sampling the interval with quadratic spacing.

dependence of the late time physics is easily accessible as the spatial dimension d can be varied continuously in these simulations. As we employ a lattice in momentum space, we drop the delta function factors in the continuum theory from this point on. Correlation functions that appear in the rest of the article should rightly be thought of as structure factors.

As advertised, we are looking to use the equilibrium phase diagram to rationalize the behavior of our solutions. To this end, we quickly review the properties of the finite T equilibrium phases (see Figs. 4.1 and 4.2). First, in $d < 2$, the system is always disordered for all $T > 0$. Correlations decay to zero exponentially with distance and the inverse of the effective mass, $1/m_{\text{eff}}$ plays the role of the correlation length. $m_{\text{eff}} > 0$ in this phase. In $d > 2$, there are two phases for $r < r_c$ (r_c is the zero temperature quantum critical point). For $T > T_c(r)$, the system is disordered. As we just discussed, $m_{\text{eff}} > 0$ in this phase. For $T < T_c(r)$, the system is ordered. The magnetization $\langle \vec{\Phi} \rangle$ is non-zero and the two-point function $\langle \vec{\Phi}(\vec{x}) \cdot \vec{\Phi}(0) \rangle$ decays as a power law $1/|\vec{x}|^{d-2}$ to the positive constant $|\langle \vec{\Phi} \rangle|^2$. A numerically useful property of such a two-point function is that the volume under the curve on long length scales $|\vec{r}|$ scales as $\sim |\langle \vec{\Phi} \rangle|^2 |\vec{r}|^d$. The effective mass squared is zero in this phase and is, physically, the mass of the $(N - 1)$ Goldstone modes. At the critical temperature T_c , $m_{\text{eff}}^2 = 0$ and the two-point function decays to zero as $1/|\vec{x}|^{d-2}$.

4.4.2 Results

Our first result is the one that we alluded to in Sec. 4.3: the late time effective mass squared tends to a non-negative constant, $m_f^2 \geq 0$. This is observed in all our numerical solutions. Certainly, $m_f^2 < 0$ is ruled out on grounds of stability. Heuristically, the result follows from the averaging over many momentum modes which oscillate at different frequencies. Once the effective mass settles, the density matrix in the eigenbasis of H dephases and is effectively diagonal.

The limiting behavior of the effective mass divides into two classes with very different physical content.

In the first case, the effective mass squared tends to a positive constant ($m_f^2 > 0$). It is easily checked that this implies a finite correlation length at late times. The late time behavior is then qualitatively the same as that of the equilibrium disordered state. We emphasize that we are not implying thermalization: m_f^2 is not a function of the excess energy density and the angular momenta $\langle L_k^z \rangle = 0$ alone. It depends on many properties of the initial state. Similarly, the form of the late time correlations are not given by the appropriate GGE.

In the second case, m_{eff}^2 tends to zero as $t \rightarrow \infty$ and the correlation length diverges in the same limit. We shall refer to this behavior as coarsening. This case subsumes two cases—that of strict coarsening and that of coarsening to a critical state. By strict coarsening, we mean the analog in our system of the process in an ergodic system in which the system is quenched from the disordered to the ordered phase and the symmetry is only broken locally [22]. The domains of broken symmetry grow with time; their characteristic size at late times, $l_{co}(t)$, grows as t^{1/z_d} , where z_d is a dynamic exponent. Within each bubble, the two point function heals to its equilibrium value $|\langle \vec{\Phi} \rangle|^2$ on a length scale $\xi \ll l_{co}(t)$. On the longer length scale $l_{co}(t)$, it decays to zero. In contrast, by coarsening to a critical state, we mean the analog of the the system approaching a critical state with no length scale except $l_{co}(t)$ and hence no domains exhibiting equilibrium magnetization. In either case, the system is self-similar on the scale $l_{co}(t)$ and a dynamical scaling theory emerges in the limit $t \rightarrow \infty, |\vec{k}| \rightarrow 0$ holding $|\vec{k}|^{z_d} t$ fixed. In this limit, the equal time structure factor has the scaling form:

$$\langle \Phi_{\vec{k}}(t) \Phi_{\vec{k}}^\dagger(t) \rangle \sim \frac{1}{|\vec{k}|^\delta} \mathcal{G}(|\vec{k}|^{z_d} t), \quad (4.25)$$

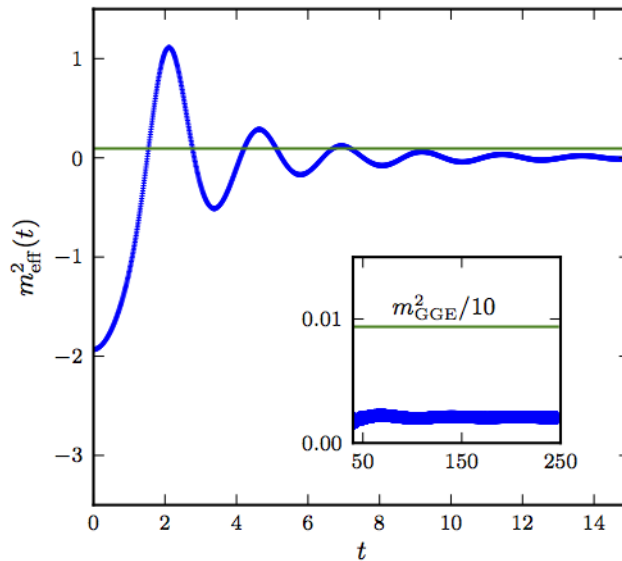


Figure 4.3: Plot of $m_{\text{eff}}^2(t)$ vs t for a sudden quench from the disordered phase to the ordered phase in $d = 1 + \epsilon$. The green line shows m_{GGE}^2 , the effective mass squared predicted by the GGE. Inset shows late time. System parameters: $\epsilon = 0.1$, $L = 1200$, $\Lambda = \pi$, $r_0 = r_c + 2$, $r = r_c - 1$, $\lambda = 1$.

where \mathcal{G} is the scaling function. When the system is strictly coarsening, the volume under the two-point function should grow as $l_{co}(t)^d$. That is, the structure factor at zero momentum should as $l_{co}(t)^d$. Thus, $\delta = d$ for strict coarsening. On the other hand, when the system is coarsening to a critical state, the growth of the volume under the two-point function with time is slower. Thus, $\delta < d$.

To numerically confirm that the system is coarsening, we will ask that the structure factor at late times have the scaling form predicted by Eq. (4.25). We will then use the value of δ to differentiate between the two possibilities. Let us now turn to the amplitude and spatial dimension dependence of the late time behavior of our sudden quenches.

Consider first sudden quenches in $d \leq 2$. Relatively small system sizes are sufficient to determine the late-time behavior near $d = 1$ rather than at $d = 2$. We therefore work at $d = 1 + \epsilon$. Fig. 4.3 shows $m_{\text{eff}}^2(t)$ for $d = 1.1$; the inset contains

the longest time behavior. Observe that m_{eff}^2 can be negative in the course of the evolution. This is not alarming because it is not the steady state behavior and does not imply instantaneous imaginary correlation lengths. The negative values of m_{eff}^2 merely indicates that $\langle \Phi^2(t) \rangle < (-r)$. The mode functions then grow exponentially, causing m_{eff}^2 to become positive. This explains the initial oscillatory behavior of m_{eff}^2 . However, at late times, m_{eff}^2 settles to the positive value m_f^2 (see inset). The green line in both plots is the effective mass squared predicted by the GGE, m_{GGE}^2 . The system definitely does not relax to the GGE as m_{GGE}^2 is almost two orders of magnitude larger than m_f^2 . The equal time structure factor is plotted in Fig. 4.4 at different times. By the Riemann-Lebesgue lemma, only the time-averaged structure factor contributes to the two-point function in real-space. Thus, the green curve is sufficient to understand the behavior of correlations in real-space. All three structure factors lead to exponential correlations in real-space.

The positivity of m_f^2 is not specific to our choice of initial conditions. Recall that stability arguments dictate that $m_f^2 \geq 0$ if the effective mass goes to a constant as $t \rightarrow \infty$. We now show analytically that $m_f^2 = 0$ is physically impossible in $d \leq 2$. To this end, suppose $m_f^2 = 0$. Then, the solution for $f_{\vec{k}}(t)$:

$$f_{\vec{k}} = A_{\vec{k}} \cos(|\vec{k}|t) + \frac{B_{\vec{k}}}{|\vec{k}|} \sin(|\vec{k}|t), \quad (4.26)$$

where $A_{\vec{k}}$ and $B_{\vec{k}}$ are complex valued functions that depend on the initial conditions. Whatever the detailed form, their amplitude must be finite and non-zero and $\text{Im}[A_{\vec{k}}B_{\vec{k}}^*] = 1$ (from Eq. (4.12)). The above solution has to be consistent with m_f^2 determined through Eq. (4.16) (or Eq. (4.23)). For $d < 2$, this is impossible as the RHS is different from zero by an amount divergent in the long time limit:

$$r + \frac{\lambda}{2} \int \frac{d^d k}{(2\pi)^d} |f_{\vec{k}}|^2 \mathcal{N}_{\vec{k}} \sim t^{2-d}. \quad (4.27)$$

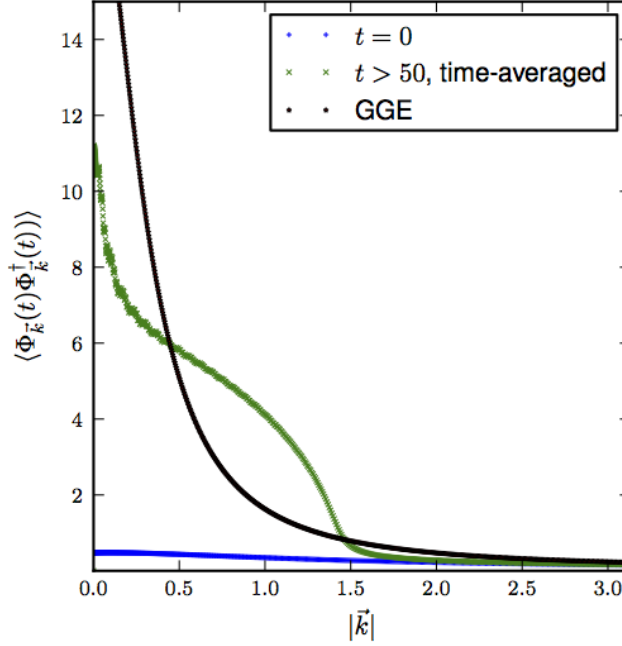


Figure 4.4: Plots of $\langle \Phi_{\vec{k}}(t) \Phi_{\vec{k}}^\dagger(t) \rangle$ vs $|\vec{k}|$ at different times for a sudden quench from the disordered phase to the ordered phase in $d = 1 + \epsilon$. System parameters: $\epsilon = 0.1$, $L = 1200$, $\Lambda = \pi$, $r_0 = r_c + 2$, $r = r_c - 1$, $\lambda = 1$.

Therefore, $m_f^2 > 0$ for $d < 2$ and the late time state is disordered. The argument at $d = 2$ is more delicate; it involves showing that the RHS is different from zero by a finite quantity.

The above proof suggests that for $d > 2$ different quenches *can* lead to a vanishing m_f^2 and hence coarsening. Indeed, our numerical results for $d > 2$ confirm this expectation and show two kinds of late time behaviors. Shown in Fig. 4.5 is the plot of $m_{\text{eff}}^2(t)$ at late times for a sudden quench of “small amplitude” to the ordered phase in $d = 3$. We define a “small amplitude” quench to be a sudden quench in which the injected energy density is smaller than that in the critical ensemble at r . At late times, the effective mass is seen to oscillate about zero with a decaying amplitude. Thus, m_f^2 is indeed zero.

In Fig. 4.6, we plot various structure factors: 1) at $t = 0$, 2) the averaged structure factor at late times and 3) the connected structure factor predicted by the GGE. We compute the averaged structure factor only for the wave numbers $|\vec{k}| \gtrsim 0.1$. For $t > 25$, their amplitudes, $|f_{\vec{k}}|$, oscillate about the green curve. Again, by the Riemann-Lebesgue lemma, the green curve is sufficient to compute the late time two-point function in real-space at distances $\lesssim 2\pi/0.1$ in lattice units. Observe that despite the lack of relaxation to the GGE, the tail of the green curve falls off as $1/|\vec{k}|^2$, just like the curve computed from the GGE (black). In the inset in Fig. 4.6, we plot $|f_0(t)|$ as a function of t . At early times, $|f_0(t)|$ is order one as in the initial state. At late times, it grows linearly with t . This implies that the volume under the two point function $|f_0|^2$ grows as t^2 . This is consistent with the scenario of coarsening to a non-equilibrium critical state, as we will show now.

We now check if the structure factor has the scaling form predicted in Eq. (4.25). Shown in Fig. 4.7 is the plot of the scaling function \mathcal{G} vs $|\vec{k}|t$. The curves at different $|\vec{k}|$ collapse when $z_d = 1, \delta = 2$. As $\delta < d$, the system is coarsening to a non-equilibrium critical state, as opposed to strict coarsening (in agreement with Ref. [168]). Physically, when $z_d = 1$, the size of a correlated region at time t is set by the horizon. This is the fastest possible growth and is possibly too fast to establish long-range order. An interesting avenue for future work is to investigate the nature of the coarsening process in the $O(N)$ model at infinite N limit in different spatial dimensions. Preliminary results show that the system always coarsens to a non-equilibrium critical state. However, the critical state itself varies with dimension.

On injecting an energy density greater than that in the critical ensemble at r , the late time behavior is qualitatively the same in Figs. 4.3,4.4. Again, as was the case for $d \leq 2$, the GGE does not reproduce the late time behavior.

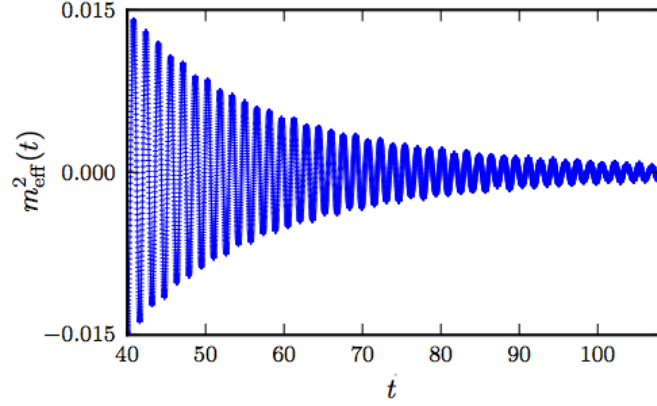


Figure 4.5: Plot of $m_{\text{eff}}^2(t)$ vs t for a sudden quench of small amplitude (see text for definition) from the disordered phase to the ordered phase in $d = 3$. The ratio of the injected excess energy density to the critical energy density is approximately 0.7. System parameters: $L = 700$, $\Lambda = \pi$, $r_0 = r_c + 2$, $r = r_c - 4$, $\lambda = 1/2$.

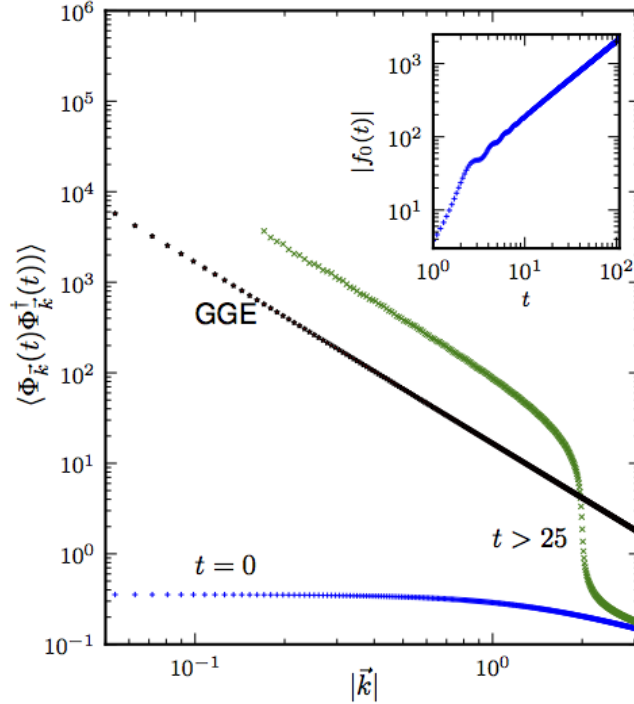


Figure 4.6: Plots of $\langle \Phi_{\vec{k}}(t) \Phi_{\vec{k}}^\dagger(t) \rangle$ vs $|\vec{k}|$ at different times for a quench of small amplitude from the disordered phase to the ordered phase in $d = 3$. The green curve is the averaged structure factor for $t > 25$ (see text). Inset: The amplitude of the mode function at $|\vec{k}| = 0$, $|f_0(t)|$, vs t . See the label of Fig. 4.5 for system parameters.

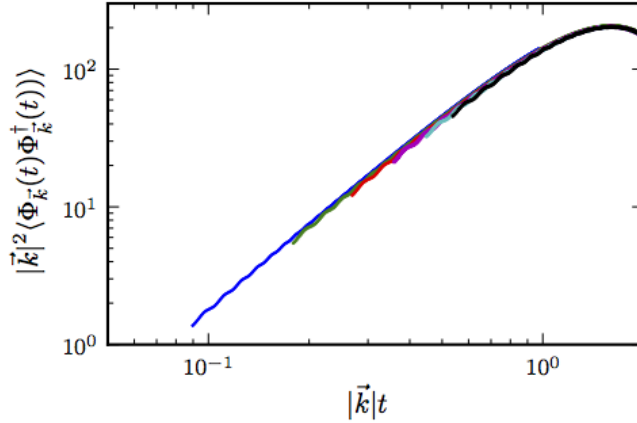


Figure 4.7: The structure factor multiplied by $|\vec{k}|^2$ vs $|\vec{k}|t$ for the quench of small amplitude from the disordered phase to the ordered phase in $d = 3$. The six curves that exhibit the scaling collapse predicted by Eq. (4.25) are at the six smallest values of $|\vec{k}|$, $|\vec{k}| = 2\pi m/L$, where $m = 1, \dots, 6$ and $L = 700$. We conclude that $z_d = 1, \delta = 2$.

4.4.3 The step approximation

The dimensional dependence of the late time physics is well captured by the step approximation, first introduced in Ref. [173]. Here, one approximates $m_{\text{eff}}^2(t)$ by a step function:

$$m_{\text{eff}}^2(t) \approx \begin{cases} m_0^2, & t < 0 \\ m_s^2, & t > 0. \end{cases} \quad (4.28)$$

The initial state fixes m_0^2 . This approximation is quite coarse in that it ignores the intricate early-time behavior of $m_{\text{eff}}^2(t)$ visible in Fig. 4.3. However, it builds in the late-time constancy of $m_{\text{eff}}^2(t)$, a key feature of the infinite N dynamics. Within this approximation, the equations of motion can be solved analytically as the dynamical problem is equivalent to a sudden quench in a free field theory. m_s^2 is a free parameter in this solution. It is fixed by requiring that the self-consistency relation in Eq. (4.23) hold at late times. For further details of the method, see Ref. [173].

Although m_s is numerically *not* equal to the actual late time effective mass, m_f , the two share qualitative features. Specifically, the dimensional dependence of m_f discussed in the previous subsection is reflected by m_s . First, we find that for $d \leq 2$, m_s^2 is always positive for any m_0 . Thus, the final state is always disordered. Second, for $d > 2$, the value of m_s^2 depends on m_0^2 . For deep quenches or “large” m_0 , $m_s > 0$ and the final state is disordered. On decreasing the amplitude of the quench, the value of m_s^2 decreases, until $m_s^2 = 0$. After this point, we find no solutions to the self-consistency relation and the approximation breaks down. This breakdown is indicative of the new physics of coarsening at late times. Note though that coarsening cannot be captured within this approximation as the precise way in which $m_{\text{eff}}^2(t)$ approaches zero is important.

To summarize, the step approximation leads to a disordered state in $d \leq 2$ for any quench and in $d > 2$ for a deep quench. For shallow quenches in $d > 2$, the approximation breaks down, indicating new late-time behavior.

4.5 Scaling and quenches to the critical point

Thus far we have focused on the dimensional dependence of the late time physics upon quenching to the ordered phase. Now we turn to the question of scaling for such quenches due to proximity to the critical point separating the ordered and disordered phases. This aspect of the physics has an interesting dimensional dependence of its own which is the non-equilibrium analog of the variation of equilibrium critical behavior with dimension. We will specifically be interested in the reversion to Gaussian critical behavior in $d \geq 3$. We will focus almost entirely on quenches to the critical point and note at the end the generalization to quenches into the ordered phase.

As before, we prepare the system in the ground state in the disordered phase at some $r_0 > r_c$. The initial conditions are once again as detailed in Eq. (4.24). At $t = 0$, we quench the system to the critical point.

A first observation is that in any dimension the late time state is disordered, i.e. $m_f^2 > 0$ for an initial non-zero m_0 . This is observed in our numerical solutions but it can also be argued, on analytic grounds paralleling our demonstration that coarsening is impossible upon quenching into the ordered phase. For $d < 2$, our previous argument already suffices and for $d > 2$, one can extend it via a consideration of a larger set of momenta at the critical coupling. We note that this result is again consistent with reasoning based on the equilibrium phase diagram—injecting a non-zero energy density at the critical coupling should lead to a finite correlation length. However, this result hides an important difference between $d < 3$ and $d \geq 3$ to which we now turn. This difference is most sharply visible if we consider a scaling limit for sudden quenches, a close cousin of the KZ scaling limit, which makes their universal physics manifest.

Let us first consider $1 < d < 3$ where the critical point is interacting even in the infinite N theory. When the initial state is in the vicinity of this critical point, its correlation length, $1/m_0^{1/z}$, diverges as $(r_0 - r_c)^{-\nu}$, where the critical exponents are $\nu = 1/(d - 1)$, $z = 1$ at infinite N . On the length/time scale $1/m_0$, the equilibrium physics is universal. On the same scale, the dynamics following a sudden quench is also universal in an appropriate scaling limit. This is the limit of $r_0 \rightarrow r_c$ when lengths/times are measured in units of the initial correlation length/time, $1/m_0$. In this limit, the one and two point functions of an operator O have the scaling forms:

$$\langle O(\vec{x}, t) \rangle_{m_0} \sim m_0^\Delta \mathcal{G}_O(t m_0) \quad (4.29)$$

$$\langle O(\vec{x}, t) O(0, 0) \rangle_{m_0} \sim m_0^{2\Delta} \mathcal{G}_{OO}(|\vec{x}| m_0, t m_0), \quad (4.30)$$

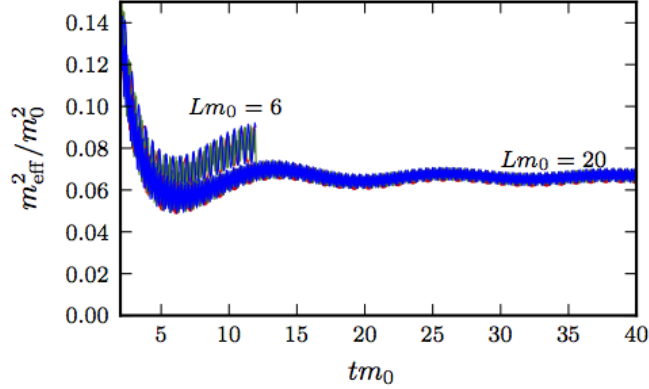


Figure 4.8: Plots of m_{eff}^2/m_0^2 vs tm_0 at different values of Lm_0 in $d = 2$. At each Lm_0 , we show the behavior for three (small) values of m_0 . The scaling collapse provides strong evidence for Eq. (4.31). System parameters: $\Lambda = 1$, $r = r_c$, $\lambda = 3$.

where Δ is the scaling dimension of the operator O and we have used the translational and rotational invariance of the system. The out-of-equilibrium physics in this limit is conjectured to be universal because the quench is very shallow – only the universal low-energy long-wavelength part of the energy spectrum at the critical point is excited for $t > 0$. Those readers familiar with the Kibble-Zurek mechanism will notice that the above scaling limit is very similar to the one in slow ramps. The correlation length and time in the initial state play the roles of the Kibble-Zurek length and time.

The previous computations of universal correlation functions in $d = 1$ are in the scaling limit described above. For example, the two-point correlation functions computed by Calabrese and Cardy[27, 28] using boundary conformal field theory have the scaling form in Eq. (4.30). Finally, the formalism above can be easily generalized to the cases when (a) the dynamic exponent $z \neq 1$, (b) when the system size is finite and (c) when the quench is not exactly to the critical point.

To test the scaling hypothesis, we consider the one-point function, $\langle |\vec{\Phi}|^2(t) \rangle_{m_0}/N$. Equivalently, consider the effective mass squared m_{eff}^2 . Accounting for the finite sys-

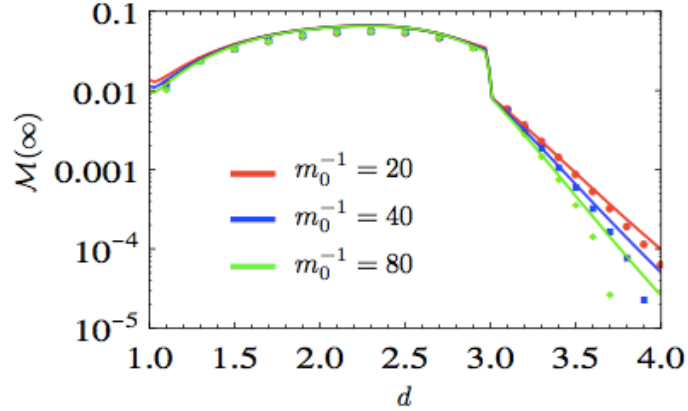


Figure 4.9: $\mathcal{M}(\infty)$ vs spatial dimension d computed for $m_0^{-1} = 20, 40, 80$ with $Lm_0 = 10$. The solid line is $\mathcal{M}(\infty)$ obtained in the step approximation (Sec. 4.4.3) at the same system system sizes and initial conditions. System parameters: $\Lambda = 1$, $r = r_c$, λ is d -dependent and chosen to ensure that the initial state is in the equilibrium scaling region.

tem size L in the numerics, the scaling form of m_{eff}^2 is:

$$m_{\text{eff}}^2(t, L; m_0) \sim m_0^2 \mathcal{M}(t m_0, L m_0). \quad (4.31)$$

We discuss the early and late time behavior of \mathcal{M} below.

By construction in the thermodynamic limit, $\mathcal{M}(0^-) = 1$. At $t = 0^+$, m_{eff}^2 is negative. This reflects the finite correlations in the initial state, unlike the ground state at the critical point. Using the form of $f_k^-(0^-)$ in Eq. (4.23), it is easy to see that:

$$\mathcal{M}(0^+) \sim -m_0^{d-3}. \quad (4.32)$$

Thus, $\mathcal{M}(0^+)$ is negative and divergent in the scaling limit.

The full scaling function can be determined numerically. In Fig. 4.8, we show \mathcal{M} for $Lm_0 = 6, 20$ in $d = 2$. The data collapses for three different values of m_0 at each Lm_0 , providing strong evidence for Eq. (4.31). The negative divergence of \mathcal{M} near

0^+ is not shown in order that the late time behavior be visible. Generically, we find that \mathcal{M} tends to a positive constant at late times. Thus, the late time state is indeed disordered.

In Fig. 4.9, $\mathcal{M}(\infty)$ is plotted as a function of dimension for different values of m_0 at fixed $Lm_0 = 10$. For all $d < 3$, the extrapolation to the thermodynamic limit leads to a positive value of \mathcal{M} as $tm_0 \rightarrow \infty$. The solid line is $\mathcal{M}(\infty)$ in the step approximation discussed in Sec. 4.4.3. In agreement with Eq. (4.31), $\mathcal{M}(\infty)$ is finite in the dynamic scaling limit. The close agreement with the numerical data points appears fortunate rather than principled.

Now consider the case when $d \geq 3$ where the fixed point is Gaussian. If we work directly at the fixed point, we have a free field theory, and the time-dependent mode functions can be calculated exactly for the sudden quench to the critical point (see, for example Ref. [28]). In the language of this article, the computation amounts to ignoring the self-consistency equation for the effective mass and assuming that it is zero at all times. The result is that the correlation functions at late times have a power-law behavior in real space at long distances (light cone effects are irrelevant to this discussion). Now, this is at odds with the observation of a *finite* correlation length in Fig. 4.9 at any *non-zero* m_0 . This discrepancy is resolved if we take proper account of the irrelevant quartic term which is dangerously irrelevant already for the equilibrium behavior, i.e. it cannot be neglected to get proper asymptotic results. The same is true for the non-equilibrium dynamics. This is easy to see in the step approximation. The dependence of the late time (finite) correlation length, ξ_f , on the initial correlation length $1/m_0$ is given by:

$$\xi_f m_0 \sim m_0^{-(d-3)/2} \text{ as } m_0 \rightarrow 0. \quad (4.33)$$

In the marginal $d = 3$ case, ξ_f is only logarithmically greater than m_0 . Thus, if we take the scaling limit keeping distances on the order of $1/m_0$ fixed as described in Ref. [39], we will indeed find Gaussian behavior but this will no longer be a good description of the truly long time asymptotics on the longest time and length scales. As in typical problems with dangerously irrelevant variables, there are now two divergent scales to contend with—a phenomenon likely to be much more common in the non-equilibrium setting as has been noted already with a different example involving string-net coarsening in Ref. [38]. Finally, we note that the dangerous irrelevance of interactions is also germane to quenches into the ordered phase where again a scaling limit can be defined as above. Again, we will find that in $d \geq 3$ Gaussian results hold in the scaling regime, which will exhibit an exponential growth of the local order parameter before being cutoff at the parametrically longer scale by the coarsening physics we described previously.

4.6 Concluding remarks

In our current understanding, as sketched in this paper, the quantum $O(N = \infty)$ vector model appears intermediate between generic systems that exhibit thermalization starting out of equilibrium and integrable systems that do not. It does exhibit stationary behavior at long times following parameter changes but it does not exhibit thermalization. This behavior is consistent with it appearing to have only half the number of conserved quantities appropriate for a fully integrable system. Interestingly, the GGE constructed from the known conserved quantities does *not* describe the late time stationary states which is inconsistent with the GGE conjecture [161]. A definitive resolution to the question of whether the GGE conjecture is false or whether there are additional conserved quantities is desirable. In the absence of the latter the $O(N = \infty)$ vector model would provide an example of a system exhibiting

a large number of emergent conserved quantities at late times. In such a case, all local properties of the system are captured by a modified emergent GGE which includes chemical potentials for the emergent conserved quantities.

Interestingly, the late time states of the $O(N = \infty)$ vector model following quenches exhibit “knowledge” of its equilibrium phase diagram. They exhibit coarsening if and only if the model exhibits a finite temperature ordered phase, which in turn depends on the dimensionality of the system. However, this coarsening process appears to be to a state that is critical. That is, it does not show any signatures of developing long range order on length scales smaller than the coarsening length scale. Elucidating the nature of this critical coarsening and its precise dependence on initial conditions is a fit subject for future work.

We note that the temporal structure of relaxation appears to be quite complicated at large but finite N . The infinite N theory already exhibits finite times scales for the appearance of stationary states in the absence of coarsening and algebraic relaxation in the presence of coarsening. This behavior is initial state dependent. For large N we expect this behavior to give way to genuine thermalization, at least for $d > 1$, on a time scale that is parametrically large in N . How much of this intricate time dependence survives to, say, $N = 3$ is an interesting question.

Finally we note that in $d = 3$ the critical fixed point is Gaussian. In its neighborhood, the scaling limit will be described by the Gaussian theory as we illustrated in this paper for quenches to the critical point. This is potentially amenable to experimental work in cold atomic systems where the $N = 2$ case is the critical theory of the Mott insulator to superfluid transition with particle hole symmetry.

4.A Lack of relaxation to the GGE

In this appendix, we show that the correlations in the late time state of the $O(N)$ model are not reproduced by the appropriate GGE Eq. (4.19). Define a new set of variables linearly related to the mode functions $f_{\vec{k}}$ in Eq. (4.11):

$$g_{\vec{k}} \equiv f_{\vec{k}} \sqrt{\mathcal{N}_{\vec{k}}}. \quad (4.34)$$

We interpret $g_{\vec{k}}$ as the complex coordinate of a 2d classical particle labelled by $\vec{k} > 0$. Next, define the momentum of each particle to be:

$$\pi = \dot{g}^*. \quad (4.35)$$

When absent, the momentum subscript is implied. Then, the condition in Eq. (4.12) implies that the angular momentum of the particle at $\vec{k} > 0$ is given by:

$$l^z \equiv -Im[g(t)\pi(t)] = -\mathcal{N}. \quad (4.36)$$

This classical angular momentum should not be confused with the conserved angular momentum L^z in Eq. (4.17). They are completely unrelated. The above equation implies that l^z is a constant of the motion for the classical system and is set by the value of \mathcal{N} . The dynamics of the classical particles is governed by the Hamiltonian:

$$H_{cl} = \int_{\vec{k}>0} |\pi|^2 + (|\vec{k}|^2 + r)|g|^2 + \frac{\lambda}{4} \left(\int_{\vec{q}>0} |g|^2 \right)^2. \quad (4.37)$$

It is easily checked that the equations of motion derived from H_{cl} reproduce Eq. (4.15,4.16). On solving for the dynamics of the classical particles generated by H_{cl} with fixed angular momentum l^z and the initial conditions derived from Eq. (4.14), we can compute any observable in the $O(N)$ model through Eq. (4.11).

This classical interpretation is useful because it unambiguously identifies the role of the c-number \mathcal{N} in the solution. The radial coordinate of the classical particle, $|g(t)|$, depends on the conserved angular momentum l^z at late times. As the equal time structure factor $S(\vec{k}, t)$ is given by:

$$S(\vec{k}, t) = \frac{|g_{\vec{k}}(t)|^2}{2} \quad (4.38)$$

$$\text{where } \langle \Phi_{\vec{k}} \Phi_{\vec{k}'}^\dagger \rangle = S(\vec{k}, t) (2\pi)^d \delta^d(\vec{k} - \vec{k}'), \quad (4.39)$$

the time-averaged structure factor at late times must depend on $l_{\vec{k}}^z$ as well. The structure factor in the GGE however is independent of this quantity. Thus, the two do not agree and the dynamics in the $O(N)$ model does not thermalize in the generalized sense.

Part II

Entanglement

Chapter 5

Entanglement in the quantum Hall phases

The quantum Hall effect is a centerpiece of modern condensed matter physics. Discovered experimentally in the early 1980s [112, 186] in semiconductor heterostructures, it is the remarkable appearance of gapped quantum liquid phases of electrons confined to two dimensions in a strong perpendicular magnetic field. The classic signature of these phases is shown in Fig. 5.1 (adapted from Refs. [63, 177]). If the electrons behaved classically, then the Hall resistance R_{xy} would increase linearly with the magnetic field B . Instead, R_{xy} exhibits plateaus quantized to one part in 10^8 of the quantum of resistance whenever the longitudinal resistance, R_{xx} , vanishes. There are two kinds of plateaus: ones at inverse integer values and others at rational fractional values. The integer valued plateaus or the integer quantum Hall (IQH) effect can be understood with single-particle quantum mechanics in the presence of disorder [119, 91, 181, 184, 37, 150]. Each gapped IQH phase is characterized by a topological invariant known as the Chern number in the bulk [181], C , and a corresponding collection of C massless chiral Dirac fermions on the boundary. The transverse conductivity σ_{xy} is quantized to C in units of the quantum conductance.

The FQH effect on the other hand, poses more of a puzzle as it would not exist if the electrons did not interact with one another. Further, Landau's theory of symmetry breaking is of no help as the various FQH liquids have the same symmetries. The theory behind the FQH phases developed over the last thirty years [120, 88, 92, 102, 196] required a revolution in our understanding of collective phases in which the topology of the manifold of the electron gas takes a central role [197]. These topological theories predict that the edge is gapless and a universal feature of the phase, while the bulk is gapped and supports excitations with rational fractional quantum numbers and exotic braiding statistics [3, 89]. Fractional charge has now been directly observed in many experiments [53, 166, 200, 124, 193]; whether these excitations have fractional statistics is still being settled [2, 201, 199]. Nevertheless, the particular phases that support non-Abelian excitations, like the Moore-Read state [134] theoretically predicted to describe the $\nu = 5/2$ plateau [198, 203, 138], have been a great source of excitement recently because of their potential as platforms for topological quantum computation [77, 109, 136].

Coincidentally, the idea of a quantum computer or a simulator was put forth by Richard Feynman [69] at about the same time as the discovery of the QH effect (1982). Quantum information theory has developed in parallel and essentially independent of the theory of the QH effect since then. Unlike a classical computer, a quantum computer uses quantum particles to represent information [137]. As a quantum computer operates by the principles of quantum mechanics, it is probabilistic in nature. If we manage to build one, we believe that such a machine will be more powerful than any classical, probabilistic computer. Some of the power of a quantum computer stems from entanglement. When a system is entangled, measurements on distant parts of the system can be much more correlated than is classically allowed [7]. Thus, it becomes possible to teleport quantum bits [8, 18] and break public-key cryptography

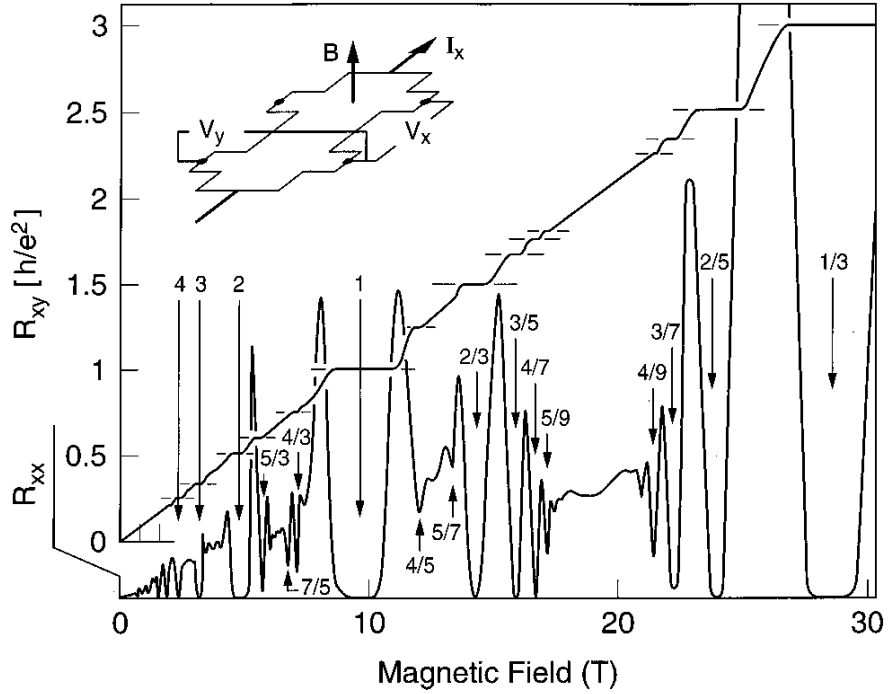


Figure 5.1: Overlay of the Hall resistance $R_{xy} = V_y/I_x$ and the longitudinal magnetoresistance $R_{xx} = V_x/I_x$ vs magnetic field B of a two dimensional electron gas of density $n = 2.33 \times 10^{11} \text{ cm}^{-2}$ at temperature $T = 85 \text{ mK}$. The numbers indicate the filling factor ν , defined as the number of electrons per magnetic flux quantum $\phi_0 = hc/e$. The vanishing of R_{xx} accompanied by the plateaus in R_{xy} at integer and rational fractional values of ν are the hallmarks of the integer and the fractional quantum Hall effect respectively. The inset shows the geometry of the measurement. From Refs. [63, 177].

schemes [170, 80]. Entanglement is thus a resource for quantum computation. Its role in the physics of the QH phases was not appreciated until relatively recently.

In 2006, Kitaev and Preskill [111] and Levin and Wen [121] independently observed that a measure of entanglement known as the entanglement entropy in the FQH ground states contained a universal signature of the order in the phase. Soon after, in 2008, Li and Haldane [123] made a remarkable conjecture. They conjectured that one of the signatures of the FQH liquids – the low energy theory at the edge – was manifest in an organization of the Schmidt values under a real space decomposition that they dubbed the *entanglement spectrum* (ES). The signs were now everywhere.

Entanglement was more than just a resource for quantum computation. Instead, it was perhaps a physical principle underlying collective quantum phases, much like Landau's symmetry breaking paradigm.

In the second part of this dissertation, we present evidence that entanglement indeed deconstructs the physics of FQH phases. We begin with a brief review of the IQH effect, with a focus towards understanding the edge. In this simple setting, we do our first calculation of the real-space entanglement spectrum and demonstrate how it uncovers the physics at the edge. This example will hopefully help the reader build some intuition for the ES that will be invaluable in the more complicated FQH case. We do not review the physics of the FQH phases in this chapter; we introduce the necessary ideas in the introductory and background sections of the two subsequent chapters. In Chapter 6, we offer microscopic evidence for the conjecture by Li and Haldane at a sequence of exactly solvable representatives of FQH phases (the Read-Rezayi sequence). En route, we introduce two entanglement spectra corresponding to two different Schmidt cuts that reveal different facets of the physics of the FQH phases. One is an approximation to the Schmidt cut in real space that probes edge excitations (the orbital ES), while the other is a cut in particle space that probes the bulk excitations (the particle ES). We then provide the first microscopic proof of the bulk-edge correspondence in the ES between these two spectra. Thus, the bulk-edge correspondence in the energy spectrum is reflected in the ES. Finally, in Chapter 7, we investigate the effects of finite system size on the entanglement spectrum.

5.1 The Integer Quantum Hall Effect

An electron with effective mass m^* and charge $-e$ moving on a two-dimensional surface of extent $L_x \times L_y$ under the influence of a uniform magnetic field B is described

by the Hamiltonian:

$$H = \frac{1}{2m^*} \left| \mathbf{p} + \frac{e}{c} \mathbf{A} \right|^2. \quad (5.1)$$

Following Landau, we choose the gauge $\mathbf{A} = Bx\hat{y}$. Assuming periodic boundary conditions in the y direction, the momentum k_y is a good quantum number and H reduces to the Hamiltonian of a one dimensional harmonic oscillator with frequency given by the cyclotron frequency, $\omega_c = \frac{eB}{m^*c}$. As ω_c is independent of k_y , it follows immediately that the energy spectrum is highly degenerate. Each degenerate manifold is called a Landau level and is labeled by n , the occupation of the harmonic oscillator.¹ The degeneracy is given by the total number of flux quanta piercing the system $N_\phi = \frac{BL_xL_y}{2\pi c/e}$, where the denominator $2\pi c/e$ is the flux quantum $\phi_0 = hc/e$ ($\hbar = 1$). Of most interest to us is the lowest Landau level (LLL) $n = 0$, in which the wavefunctions have the form:

$$\psi_{0,k_y}(x, y) = \frac{1}{\sqrt{L_y}} e^{ik_y y} \phi_0(x + k_y l_B^2) \quad (5.2)$$

$$\phi_0(x) = \frac{1}{(\pi l_B^2)^{1/4}} e^{-x^2/2l_B^2} \quad (5.3)$$

where $l_B = \sqrt{\frac{c}{eB}}$ is the magnetic length. Pictorially, the wavefunction is a Gaussian packet of width l_B localized about the *guiding center* $X_{k_y} = -k_y l_B^2$ in the x -direction and has uniform amplitude in the y -direction. The quantization of k_y further implies that the guiding center coordinate is quantized to be an integer multiple of $2\pi l_B^2/L_y$.

On filling the single-particle spectrum described above with N electrons, we obtain the many-body states of an N -electron gas in the presence of a magnetic field. The first observation is that certain *filling factors* $\nu = N/N_\phi$ are special. When ν is an integer, we fill ν Landau levels and obtain a unique, gapped ground state. The gap to

¹We address the issue of boundary conditions in the x -direction shortly.

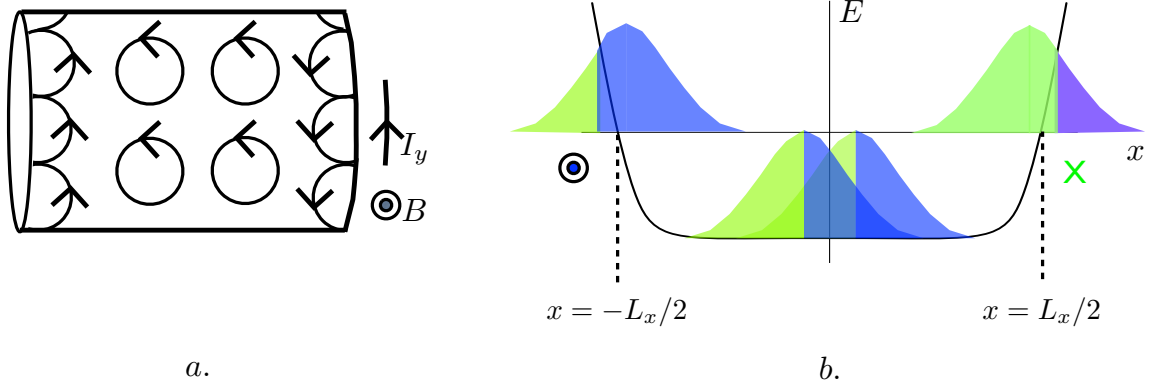


Figure 5.2: a. Classical orbits of electrons moving in a radially outward magnetic field. In the bulk, the orbits are circular. When the electrons cannot complete their circular orbits, they skip along the edge. b. Single particle energy spectrum in a confining potential. There is a level for every value of the guiding center X_{k_y} . Overlay: single-particle wavefunctions centered at their respective guiding center coordinates. Colors indicate the distribution of current density, $\mathbf{j} = j_y \hat{y}$, within a wavefunction. Green represents positive j_y , while blue represents negative j_y . Note the difference in the ratio between green and blue in the bulk and near the edges.

adding a local charge about this state is finite. Thus, at zero temperature, we expect the electron gas to be a featureless incompressible fluid. At first sight, this is a bit disappointing. Do electrons in a magnetic field behave no differently from the trivial band insulator at the same filling?

A closer look at the spatial distribution of charge currents in these states reveals otherwise. The origin of the current imprint is classical. Classical electrons moving in a magnetic field experience a Lorentz force that confines them to the circular orbitals shown in Fig. 5.2a. How is this reflected in the quantum mechanical eigenstates? For simplicity, let us restrict our attention to the lowest Landau level (LLL). The local current density in the wavefunction ψ_{0,k_y} is given by:

$$\mathbf{j}_{k_y} = \frac{-e}{2m} \left(\psi_{0,k_y}^* \mathbf{p} \psi_{0,k_y} - \psi_{0,k_y} \mathbf{p} \psi_{0,k_y}^* + \frac{2e\mathbf{A}}{c} |\psi_{0,k_y}|^2 \right). \quad (5.4)$$

The Landau orbital wavefunctions, Eq. (5.3), have current density:

$$\mathbf{j}_{ky}(\vec{r}) = \hat{y} \frac{-e\omega_c}{\sqrt{\pi}L_y l_B} (x - X_{ky}) \exp\left(-\frac{(x - X_{ky})^2}{l_B^2}\right). \quad (5.5)$$

The current density is uniform in the y -direction, but varies along x . To the left of the guiding center, the current density is positive (green), while to the right, it is negative (blue). See Fig. 5.2b near $x = 0$. This is the manifestation of the classical clockwise currents in the Landau basis². Unfortunately, the current pattern in each Landau orbital is invisible in the many-body ground state at $\nu = 1$. The current density in the $\nu = 1$ state is given by the sum of the current densities in the LLL orbitals and is zero up to exponentially small corrections in the size of the system (assuming as $L_y, L_x \gg l_B$). How do we expose each term in the sum?

5.2 Exposing the current imprint

5.2.1 Physical edge

There are two different ways of exposing the handedness of the current density in each Landau orbital. The first is to create a physical edge. Again, we draw intuition from the classical motion of electrons. When the electrons are confined to a finite region, the classical electrons cannot complete their circular orbits at the boundaries and ‘skip’ along the edges (Fig. 5.2a.) We warn the reader that the analogy between classical and quantum electrons comes with its dangers. It turns out that the net magnetic moment of the classical (spinless) electrons is exactly zero as the moments of the anti-clockwise moving electrons in the bulk and the clockwise skipping electrons on the boundary *exactly* cancel. In contrast, the quantum fluid has a diamagnetic response due to the

²Had we chosen a different basis to parametrize the LLL (the coherent basis), we would have discovered that the current density in each eigenfunction was circulating in the clockwise direction.

oppositely moving edge currents that we discuss below. A beautiful exposition of this physics can be found in Ref. [140].

To create boundaries in the quantum problem, we add a potential $V(x)$ to H that confines the electrons in the x direction. The single particle energy spectrum is the curve in Fig. 5.2b. Near $x = 0$, the potential is a negative constant, and the eigenstates have the form in Eq. (5.3). Near $x = \pm L_x/2$, the eigenfunctions remain approximately Gaussian (like in Eq. (5.3)), but with guiding centers shifted closer to $x = 0$ by an amount proportional to the magnitude of the local electric field. It is easy to check that the eigenfunctions at the edge then carry net current [79] as shown in Fig. 5.2b. What about the ground state of the system with edges? In the ground state, all single particle orbitals with $E < 0$ are occupied. This state has local filling $\nu = 1$. The edges have no effect on the current density in bulk—the current density remains zero. At the boundaries however, there are oppositely moving currents.³ Although the total current carried by the sample is zero, we have identified a distinctive feature of the $\nu = 1$ droplet: the localization of the “in” and “out” currents at different edges.

A physical consequence of the currents at the edges is the IQH effect. Suppose we apply a voltage V_x between the two edges⁴. Then, in steady state, there is a net current I_y in the y direction. It is easy to work out that I_y is proportional to V_x , and that the conductivity σ_{xy} is one (ν in general) in units of the quantum of conductance, $e^2/(2\pi)$.

³The higher Landau levels play a crucial role in the derivation of this result. See for example Ref. [157].

⁴In the clean limit, every eigenfunction in the Landau gauge carries a net current in the y direction when subjected to a uniform electric field in the x direction. Disorder localizes many of these states. See Ref. [79].

5.2.2 Virtual edge

The second way to expose the handedness of the current density in each Landau orbital involves creating a ‘virtual’ edge in the bulk through a Schmidt decomposition and plotting the Schmidt values cleverly. To make this calculation transparent, let us first simplify our description of the bulk. Imagine two semi-infinite IQH liquids: one in the left half plane (L) and the other in the right- half plane (R). Both are infinite in the x direction and of finite extent L_y in the y direction. The physical boundary at $x = 0$ implies that the single particle energy spectrum of the two droplets has the form in Fig. 5.3. The x -value of each level in Fig. 5.3 is its guiding center X_{k_y} . All orbitals up to the Fermi point at zero energy are occupied in the ground state. Excitations about the Fermi point are arbitrarily cheap in the thermodynamic limit $L_y \rightarrow \infty$; thus, the system is gapless. In a low-energy theory, we keep only those states within 2Δ of the boundary in both droplets:

$$H = \sum_{X_{k_y}=-\Delta}^{\Delta} w X_{k_y} [L^\dagger(X_{k_y})L(X_{k_y}) - R^\dagger(X_{k_y})R(X_{k_y})] \quad (5.6)$$

where $L^\dagger(X_{k_y})$ creates an electron in the Landau orbital at $x = X_{k_y}$ in the left droplet and likewise for the right. On the length scale Δ about $x = 0$, we assume that the spectrum in Fig. 5.3 is linear with slope w . Using the relation between the guiding center and y -momentum, $X_k = -kl_B^2$, we arrive at the more familiar Hamiltonian of two uncoupled 1-d wires of free oppositely moving chiral fermions:

$$H = \sum_{k=-\Lambda}^{\Lambda} -vk [L^\dagger(k)L(k) - R^\dagger(k)R(k)] \quad (5.7)$$

where Λ is the momentum cutoff for the low-energy theory and v is the speed of the electron. Note that the motion of electrons along $+\hat{y}$ is equivalent to a current along $-\hat{y}$, so the signs indeed agree with the currents shown in Fig. 5.3.

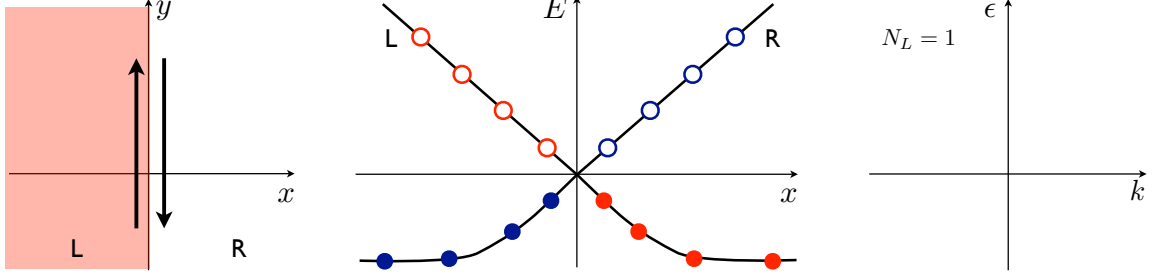


Figure 5.3: Left: Two decoupled semi-infinite IQH droplets, L and R. The arrows indicate the direction of the currents on both edges. Center: Single particle energies vs x . The circles denote single particle levels; their color indicates the nature of the corresponding eigenstate. Eigenstates with weight only in L (R) are colored red (blue). The levels occupied in the many-body ground state are depicted as solid. Right: Entanglement spectrum for a Schmidt cut at $x = 0$ in the $N_L = 1$ sector.

Suppose we now allow the droplets to interact with each other. This couples the edge theories and allows fermions to hop from L to R and vice-versa:

$$H_{int} = -\lambda \sum_k L^\dagger(k)R(k) + R^\dagger(k)L(k) \quad (5.8)$$

The interaction term opens a gap in the single particle spectrum shown in Fig. 5.4. The energies of the two bands are $E_k^\pm = \pm\sqrt{\lambda^2 + (kv)^2}$ with single-particle eigenstates:

$$|k\rangle^\pm = (u_k^\pm L^\dagger(k) + v_k^\pm R^\dagger(k)) |0\rangle \quad (5.9)$$

where $|0\rangle$ is the empty vacuum with no fermions and:

$$u_k^\pm = \frac{1}{\sqrt{1 + \left(\frac{E_k^\pm + vk}{\lambda}\right)^2}} \quad (5.10)$$

$$v_k^\pm = \frac{-(E_k^\pm + vk)}{\lambda\sqrt{1 + \left(\frac{E_k^\pm + vk}{\lambda}\right)^2}}. \quad (5.11)$$

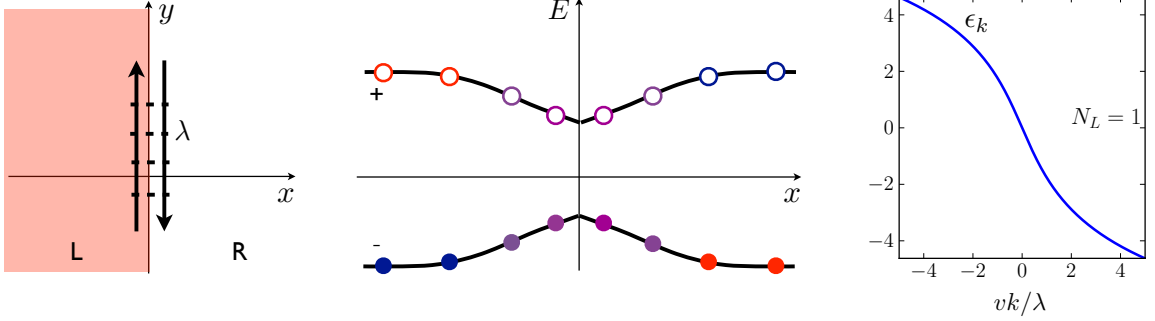


Figure 5.4: Left: Two coupled semi-infinite IQH droplets, L and R. The arrows indicate the direction of the currents on both edges when $\lambda = 0$ (see text). Center: Single particle energy spectrum with two bands. The circles denote single particle levels; their color indicates the nature of the corresponding eigenstate. Eigenstates with weight only in L (R) are colored red (blue). The levels occupied in the many-body ground state are depicted as solid. Right: Entanglement spectrum for a Schmidt cut at $x = 0$ in the $N_L = 1$ sector.

When $k \ll -\lambda/v$, $u_k^- \rightarrow 0$ while $v_k^- \rightarrow 1$. The coupling can be neglected and $|k\rangle^- \approx R^\dagger(k) |0\rangle$. Similarly, for $k \gg \lambda/v$, $|k\rangle^- \approx L^\dagger(k) |0\rangle$. Near $k = 0$, λ is the only energy scale in the system and cannot be neglected. The eigenstates are superpositions of k states on the left and right and the gap is order λ . The many-body ground state obtained by filling the lowest band is clearly gapped and has no net current. Thus, the line $x = 0$ will be no different than any other line in the bulk of an IQH droplet. The information in the energy spectrum about the gapless and chiral nature of the edge is lost.

The entanglement spectrum however has the opposite behavior! It is gapped when $\lambda = 0$, but is gapless when $\lambda \neq 0$. Let us first define the entanglement spectrum [123] in general terms. Any wavefunction of a system composed of two parts, L and R, can be decomposed as:

$$|\psi\rangle = \sum_{LR} C_{LR} |L\rangle |R\rangle \quad (5.12)$$

where $|L\rangle, |R\rangle$ form an orthonormal basis for the L and R subsystems respectively and C is a matrix of complex numbers. The matrix C need not to be diagonal, but

can be diagonalized through a singular value decomposition, $C = U^\dagger D V$. Here U, V are unitary matrices and D is a diagonal matrix of real, positive numbers called the Schmidt values. Substituting in Eq. (5.12):

$$\begin{aligned} |\psi\rangle &= \sum_i D_{ii} \left(\sum_L U_{Li}^\dagger |L\rangle \right) \left(\sum_R V_{iR} |R\rangle \right) \\ &= \sum_i D_{ii} |i\rangle_L |i\rangle_R \end{aligned} \quad (5.13)$$

This is the Schmidt decomposition of the state $|\psi\rangle$. The Schmidt vectors $|i\rangle_L$ and $|i\rangle_R$ form an orthonormal basis in L and R respectively. Finally, we exploit the positivity of the Schmidt values to write,

$$|\psi\rangle = \sum_i e^{-\epsilon_i/2} |i\rangle_L |i\rangle_R \quad (5.14)$$

where the values ϵ_i define the entanglement spectrum (ES).

What is the Schmidt decomposition of the ground state of the two coupled wires?

At any λ , the ground state is:

$$\begin{aligned} |GS\rangle &= \prod_k (u_k^- L^\dagger(k) + v_k^- R^\dagger(k)) |0\rangle \\ &\propto \prod_k \left(\frac{u_k^-}{v_k^-} L^\dagger(k) + R^\dagger(k) \right) |0\rangle \end{aligned} \quad (5.15)$$

where we have dropped a global normalization factor. By expanding the above product, we can bring Eq. (5.15) to the form of Eq. (5.12). The expansion is naturally organized by N_L , the number of fermions in L :

$$|GS\rangle \propto \prod_q R^\dagger(q) |0\rangle + \sum_k \frac{u_k^-}{v_k^-} L^\dagger(k) \prod_{q \neq k} R^\dagger(q) |0\rangle + \dots \quad (5.16)$$

The first term has zero fermions in L, the second has one and so on. As states with different numbers of fermions are orthogonal in L, every Schmidt vector can be labelled by N_L . We say that N_L is a good quantum number for the cut. Let's focus on the sector with one particle in L ($N_L = 1$). As $\langle 0|L(q)L^\dagger(k)|0\rangle \propto \delta_{qk}$, the second term in Eq. (5.16) is already of the Schmidt form Eq. (5.13). Thus, the entanglement spectrum is further labeled by momentum k ,

$$\epsilon_k = -2 \log \left(\frac{u_k^-}{v_k^-} \right) \quad (5.17)$$

dropping a constant shift due to the global normalization. The momentum resolved entanglement spectra are shown in Figs. 5.3 and 5.4. The uncoupled half-droplets ($\lambda = 0$) exhibit gapless energy spectra but infinitely gapped entanglement spectra. At non-zero coupling λ , the two switch character: the energy spectrum develops two bands and a finite gap, but the entanglement spectrum is chiral and gapless⁵. See Fig. 5.4.

The bottom-line of the above analysis is that at a physical edge, the energy spectra are gapless and exhibit chiral propagation, while at a “virtual” edge, the entanglement spectra have these properties. The entanglement spectrum is therefore a bulk property which encodes the physics forced upon the edge by the chiral nature of the Hall state. There is a second type of entanglement spectrum that we have not touched upon in this introduction: the particle ES. We will see that this ES encodes the physics of the bulk of the Hall state and complements the real-space ES discussed above. In the next two chapters, we explore the remarkable connection between the bulk/edge energy spectra and the different ES in greater detail in the context of the more exotic cousins of the IQH phases: the fractional quantum Hall (FQH) phases that occur at fractional fillings ν . These interacting phases are similar

⁵The ES in the $N_R = 1$ sector has the opposite chirality, where N_R is the number of fermions in the right droplet. The energy spectrum of both edges is really the ES in the $N_L = 1$ and $N_R = 1$ sectors.

to the IQH state insofar as they are incompressible electron liquids with gapless chiral edge modes, but detailed properties of the bulk excitations and the associated edge theories are more complicated than the free fermions of the IQH state. For example, the bulk charged excitations can carry fractional quantum numbers and have non-Abelian braiding statistics. Consequently, we will find that the entanglement spectra of virtual edges of FQH states are more interesting than the IQH one.

Chapter 6

Bulk-Edge Correspondence in the Entanglement Spectra

6.1 Introduction

In 2008, Li and Haldane[123] made the remarkable conjecture that the entanglement structure of the ground state wavefunctions of the fractional Quantum Hall (FQH) phases reflects physical properties of the phases.¹ Their work connected two disparate streams of research: the study of QH, or more broadly, topologically ordered phases and quantum information theory. In detail, they constructed the orbital entanglement spectrum (OES), which is an organization of the Schmidt values under a decomposition of the spatially localized orbitals of the lowest Landau level into two parts.² Based on a numerical study, they conjectured that the OES reflects the universal features of the low energy spectrum of the FQH droplet with a physical edge. In this chapter, we provide microscopic evidence for the Li-Haldane conjecture

¹Chapter based on work with M. Hermanns, N. Regnault and B. A. Bernevig [40].

²Heuristically, the Schmidt cut in orbital space is the real-space cut restricted to the lowest Landau level (LLL). The physics requiring Landau level mixing, like the physics at the IQH edge, is invisible in the OES. The OES only probes the ‘interacting’ part of the wavefunction.

by studying the entanglement properties of model wavefunctions (the Read-Rezayi sequence) known to describe a family of FQH phases.

What are the features of the edge of a FQH droplet? Recall that the droplets are gapped in the bulk, and therefore featureless at low energies. The edge is where all the action at low energies is at. In fact, it is responsible for the singular transport signature of the FQH droplets, first observed experimentally three decades ago[186]: the quantization of σ_{xy} . The edge of the FQH droplet is a gapless, chiral, one-dimensional liquid, and is typically described by a universal critical theory like a conformal field theory. The simplest edge theory is that of the integer quantum Hall fluid: a single chiral free fermion (see Chapter 5). A bit more complicated is the edge theory of the Laughlin fluid at $\nu = 1/3$: a chiral boson. The consequence of the universality of the edge theory is that the the low energy spectrum has universal features everywhere in the phase. For example, the counting of the number of energy levels as a function of the total momentum along the edge is the same everywhere in a given FQH phase and is different for different phases with different edge theories. For the IQH/Laughlin phases, this counting is $1, 1, 2, 3, 5, \dots$, while for the Moore-Read phase at $\nu = 5/2$, it is $1, 1, 3, 5, \dots$ ³. Thus, the counting of the low-energy spectrum is a robust signature of a FQH phase. Li and Haldane provided numerical evidence that the counting of the low-lying levels in the OES was also a robust signature of the phase, as it was *equal* to the edge counting. In this chapter, we will *analytically* prove this equality of counting at special points in a family of FQH phases where the ground state is exactly known.

Another interesting feature of the FQH phases is the bulk-edge correspondence. The Laughlin flux threading thought experiment [105, 79] provides some insight into the meaning of this correspondence. Consider the Laughlin fluid on a disk at $\nu = 1/m$ with m odd. Imagine drilling a tiny hole into the fluid and pushing a solenoid through

³The counting depends on where the Schmidt cut is in orbital space; for details, see [123].

it. By varying the current through the solenoid, we may modify the flux piercing the hole. Suppose we slowly increase it from 0 to 2π in units of the flux quantum. A time varying magnetic field induces an electric field in the bulk in the azimuthal direction. This in turn causes a current to flow in the radial direction as $\sigma_{xy} \neq 0$. The reader can easily convince herself that the total charge transported to the edge in this process is $-e/m$. The flux tube in the bulk that binds the charge $+e/m$ is actually the quasi hole, a charged bulk excitation about the FQH vacuum. We have just demonstrated that the process of creating a bulk charged excitation necessarily transports charge to the edge. More formally, there is a connection between the partition function of the bulk (which is a topological field theory) and that of the edge (a conformal field theory). A consequence is the equality of the quasi-degeneracies in the edge and the bulk energy spectra when plotted against suitable quantum numbers. Is there a similar correspondence in the entanglement spectra? We will demonstrate that there is. To wit, we need to first identify the relevant entanglement spectra. The OES is the conjectured analog of the edge energy spectrum; in this chapter, following Ref. [176], we conjecture that a different ES, the particle entanglement spectrum (PES), is the analog of the bulk energy spectrum. In the PES, the Schmidt cut is in particle space. This simulates the presence of quasi-holes in the fluid, much like a cut in orbital space simulates a physical edge. We will show that the counting of the PES matches that of the bulk excitation spectrum, solidifying the connection. We will then show that there is a bulk-edge correspondence in the ES by showing that the PES and the OES have the same counting.

To summarize, we will provide analytic evidence for the Li-Haldane conjecture in a family of microscopic FQH wavefunctions (the Read-Rezayi sequence) in the thermodynamic limit in two ways. First, we prove that the bulk-edge correspondence in energy spectra is reflected in the entanglement spectra. Second, we argue that the PES does count the bulk quasi-hole excitations. Using the bulk-edge correspondence

of the ES, we then have a proof that the OES has the same counting as the edge energy spectrum. In this chapter, for simplicity, we restrict the discussion to the bosonic Read-Rezayi wavefunctions. The generalizations to fermions and the Gaffnian wavefunction are straightforward; we refer the reader to the published article for details[40].

A complementary field theoretic view on the Li-Haldane conjecture is given in Ref. [154]. In this article, the authors imagine that the bulk of a FQH fluid is constructed by turning on a coupling between the edges of two disconnected pieces of the same fluid. They then Schmidt decompose the ground state of the coupled system in terms of the low-energy subspace of each piece, that is, in terms of the degrees of freedom on the edge of each piece, and argue that the Li-Haldane conjecture holds. This approach is very different from the microscopic view of bulk FQH wavefunctions that we take in this chapter. This is also a good place to note that the Li-Haldane conjecture is relatively easy to prove in non-interacting systems, such as the Integer Quantum Hall system and topological insulators[70, 190, 45, 141]. Interacting systems are harder to tackle. Finally, the entanglement spectra of many other systems have also been explored; see Refs. [151, 71, 101, 189, 204, 65, 74, 188, 148, 149, 142, 179, 32, 118, 206, 139, 127, 167].

The chapter is organized as follows: first, we introduce the relevant technical background in Sec. 6.2. This includes a description of the spherical geometry, the Read-Rezayi sequence, clustering and Jack polynomials. We then define the two entanglement spectra, the orbital and the particle, in Sec. 6.3 and discuss their properties. This leads us to our first rigorous result in Sec. 6.4 that the number of non-zero levels in PES is bounded from above by the number of bulk quasi hole excitations. On physical grounds, we then argue that the bound is saturated. In preparation for the second result, we formulate the clustering properties of the model state in the single-particle orbital basis in Sec. 6.5. Sec. 6.6 contains the second result of this

chapter: the outline of the proof for the bulk-edge correspondence in the model wavefunctions. In the same section, we illustrate the ideas of the proof with two examples and identify the parameter range of its validity at finite size. The details of the proof itself are in the appendices.

6.2 Background

6.2.1 Geometry

In the previous chapter, we discussed the Landau problem at integer and fractional filling on the infinite plane. At any finite size (a finite number of particles N), the QH droplet has an edge on the plane. The edge complicates the study of bulk properties like the entanglement spectrum. We therefore move to a geometry with no edge: the surface of a sphere. This technical innovation was introduced by Haldane in 1983 [88]. There are many good textbooks that derive the results stated below carefully: for example, see [103].

Consider a sphere of radius R pierced by a radial and uniform magnetic field with N_ϕ flux quanta in it. The electrons are confined to be on the surface of the sphere. On solving the Landau problem in this geometry in a certain gauge, we find that the single-particle states of each Landau level are eigenstates of \hat{L}_z , the z -component of angular momentum and $|\vec{L}|^2$, the square of the magnitude of the total angular momentum vector [88]. In the Lowest Landau Level (LLL), the degenerate single-particle states belong to a multiplet of angular momentum $L = N_\phi/2$ and consequently, $L_z \in [-N_\phi/2, \dots, N_\phi/2]$. Note that the degeneracy of the LLL is $N_\phi + 1$. Define the spinor coordinates $u = e^{i\phi/2} \cos \theta/2$ and $v = e^{-i\phi/2} \sin \theta/2$, where θ and ϕ are spherical polar coordinates on the sphere. The LLL wavefunction labelled

by L_z is most conveniently written in these coordinates:

$$Y_{L_z}(u, v) = \left[\frac{N_\phi + 1}{4\pi} \begin{pmatrix} N_\phi \\ \frac{N_\phi}{2} - L_z \end{pmatrix} \right]^{1/2} (-1)^{N_\phi/2 - L_z} u^{N_\phi/2 + L_z} v^{N_\phi/2 - L_z} \quad (6.1)$$

The amplitude is uniform in the azimuthal direction and varies only along the θ direction. L_z controls the value of θ at which the $|Y_{L_z}|$ is maximum (θ_{max}): as L_z decreases from $N_\phi/2$ to $-N_\phi/2$, θ_{max} increases from 0 (north pole) to π (south pole). The wavefunctions are polynomially localized in the θ direction about θ_{max} . Compare this to what we found on the infinite plane in the Landau gauge: the LLL wavefunctions were uniform in the y direction, but Gaussian localized about a point in the x -direction determined by k_y .

The parametrization in terms of u and v is redundant as the coordinates are constrained by the relation $|u|^2 + |v|^2 = 1$. To rid ourselves of this redundancy, let us map the surface of the sphere to the infinite plane through a stereographic projection. This defines the complex coordinate: $z = 2Rv/u$. The unnormalized single-particle wavefunctions are then given by:

$$\frac{z^m}{\left(1 + \frac{|z|^2}{4R^2}\right)^{N_\phi/2}}, \quad \text{where } m = \frac{N_\phi}{2} - L_z. \quad (6.2)$$

Above $m = 0, 1 \dots N_\phi$. The factor in the denominator is independent of m . Thus, any wavefunction in the LLL has the form:

$$F(z) \frac{1}{\left(1 + \frac{|z|^2}{4R^2}\right)^{N_\phi/2}} \quad (6.3)$$

where $F(z)$ is a polynomial of z of degree N_ϕ . Similarly, any two-particle wavefunction in the LLL has the form:

$$F(z_1, z_2) \prod_{i=1}^2 \frac{1}{\left(1 + \frac{|z_i|^2}{4R^2}\right)^{N_\phi/2}} \quad (6.4)$$

It is clear that all the information about the wavefunction is in the polynomial F . It is then simpler to not carry the extra factor along by defining single-particle orbitals $|m\rangle$:

$$\langle z|m\rangle = z^m, \quad m = 0, 1 \dots N_\phi \quad (6.5)$$

We refer to these single-particle orbitals as the monomials as z^m is a monomial. From this point on, we use m as the ‘angular momentum’ to label single-particle orbitals in the text. In the figures, we use L_z . The linear relation between the two is $m = \frac{N_\phi}{2} - L_z$. We hope that this dual notation does not confuse the reader.

6.2.2 From one to many

Let the coordinates of N bosons/fermions be z_1, \dots, z_N . As the single-particle basis of particle i is spanned by the monomials of z_i , the many-body basis is spanned by monomials of z_1, \dots, z_N . Consider the many-body state $|\lambda\rangle$ in which the orbitals $\lambda = [\lambda_1, \dots, \lambda_N]$ are occupied. The list λ is sorted in descending order. If the particles were all distinguishable, then the wavefunction of the state in which particle i occupies orbital λ_i is $\prod_{i=1}^N z_i^{\lambda_i}$. When the particles are identical, the wavefunction has to be symmetrized (bosons) or anti-symmetrized (fermions):

$$\langle z_1, \dots, z_N | \lambda \rangle = S[z_1^{\lambda_1} \cdot \dots \cdot z_N^{\lambda_N}] \quad (6.6)$$

where S is the process of symmetrization/anti-symmetrization over all indices i, j . Note that $\lambda_i \neq \lambda_j$ for any $i \neq j$ if the particles are fermions. Any bosonic/fermionic many-body wavefunction is a polynomial of the above symmetrized/anti-symmetrized monomials. Further, a many-body wavefunction of fixed total angular momentum L_z^{tot} is a homogenous polynomial of degree L_z^{tot} . That is, each monomial in such a wavefunction satisfies $\sum_{i=1}^N \lambda_i = L_z^{tot}$.

Every Fock state $|\lambda\rangle$ can be labelled in two ways. We have already introduced the first: the ordered list of occupied orbitals λ . When the degree of the monomial is fixed to be L_z^{tot} , λ is an ordered partition of L_z^{tot} into N parts. We can also label the Fock state by $n(\lambda)$, the occupation number configuration. It is a string of length $N_\phi + 1$ and contains the occupation numbers of the orbitals $m = 0, 1 \dots N_\phi$ in order. For example, if $N_\phi = 2$ and $N = 2$, orbitals 2 and 0 are occupied in the Fock state $|2, 0\rangle$ of the 3 available orbitals. Consequently, $\lambda = [2, 0]$, $n(\lambda) = \{101\}$ and $\langle z_1, z_2 | 2, 0 \rangle = z_1^2 + z_2^2$. Similarly, $\lambda = [1, 1]$, $n(\lambda) = \{020\}$ and $\langle z_1, z_2 | 1, 1 \rangle = z_1 z_2$ for the other Fock state at the same total angular momentum.

6.2.3 The Read-Rezayi sequence

We now briefly discuss the properties of particular many-body wavefunctions whose entanglement properties we will study. The experimentally relevant FQH phases are all composed of fermions. In this chapter, we however work with the bosonic analogs of these phases for simplicity. The proof we present can be extended to the fermionic phases— for details, we refer the reader to the published article [40].

The Read-Rezayi sequence is a family of wavefunctions at filling factors $\nu = k/2$, where k is an integer greater than zero ⁴ [159]. These wavefunctions are the exact ground states of rotationally and translationally invariant Hamiltonians believed to be in the bosonic $\nu = k/2$ FQH phases. The $\nu = k/2$ phases are bonafide FQH phases:

⁴For bosons, ν can exceed one in the LLL. The fermionic analogues are at filling factor $\nu = k/(k+2)$ smaller than one.

the longitudinal conductivity is zero while σ_{xy} is quantized at $\nu e^2/2\pi$. They are gapped in the bulk, but support gapless edge excitations. The gapped quasi-particles carry fractional charge and could have non-Abelian statistics. And remarkably, all this exotic many-body physics is captured by the Hamiltonians of the Read-Rezayi sequence. Our goal in this chapter is to discover all this physics from the entanglement properties of the ground state wavefunction alone. To this end, let us summarize the properties of the Read-Rezayi wavefunctions.

The Read-Rezayi wavefunctions of N bosons are homogenous polynomials of z_1, \dots, z_N . As the wavefunctions live in the LLL, they are holomorphic functions of the z_i . Their defining property is $(k, 2)$ -clustering. Whenever a cluster of $k + 1$ particles is formed at a point in real space (e.g: $z_1 = \dots z_{k+1}$), the wavefunction vanishes. Further, the wavefunction vanishes in a specific way as a particle approaches a cluster of k particles: it vanishes as $\prod_{i>k} (z - z_i)^2$ when $z = z_1 = \dots z_k$. The smallest degree polynomial that has this property is unique; this is why we call it defining. The Hamiltonian that the wavefunction at k is the exact ground state of penalizes $(k + 1)$ clusters [159, 171]. The familiar Laughlin and Moore-Read wavefunctions [120, 134] are a part of this sequence; they occur at $k = 1$ and $k = 2$ respectively.

There is a nice language in terms of partitions and Jack polynomials in which the clustering property of these wavefunctions is explicit. We motivate this below and refer the reader to Refs. [89, 10, 11, 12, 9] for more details.

6.2.4 $(k, 2)$ -admissible configurations

Suppose we had to “guess” the Read-Rezayi wavefunction. How would we proceed? We know that the wavefunction has the following two properties: 1) there need to be k bosons for every two flux quanta ($\nu = k/2$), and 2) it is the ground state of a Hamiltonian that penalizes clusters of more than k bosons in real space. The consequence of the second property in momentum space is that the Hamiltonian

penalizes any configuration with more than k bosons in a single orbital. If a single orbital is filled with $k+1$ bosons, then the probability that the $k+1$ bosons are in the same area Δ is proportional to $(\Delta/2\pi l_B^2)^k$, where l_B is the magnetic length. As this is finite, the energy penalty is finite. 1) further limits the number of bosons in two consecutive orbitals to be k . Thus, we would guess that the occupation configuration with smallest total angular momentum satisfying 1) and 2) is⁵:

$$n(\lambda_0) = \{k0k0k0 \dots k0k\}. \quad (6.7)$$

However, this state cannot be the exact ground state as it is not translationally invariant and the orbitals have finite overlap with one another, making the probability of more than k bosons in a given area finite. Why then is it useful? It turns out that it captures important correlations in the Read-Rezayi wavefunction because the clusters of bosons maximally avoid each other in this configuration. We will sharpen this connection in the next subsection.

A few comments are in order. First, note that $n(\lambda_0)$ is an example of a $(k, 2)$ -admissible configuration. There are no more than k particles in 2 consecutive orbitals in a $(k, 2)$ -admissible configuration. λ_0 is the special unique $(k, 2)$ -admissible configuration with the highest boson density. It is known as the root partition. Second, on repeating the same “guessing” game for the quasi-hole states, the reader will end up writing other $(k, 2)$ -admissible configurations. For example, the quasi-hole state with one extra unit of angular momentum as compared to the ground state would be:

$$\{k0k0k0 \dots k0k-11\}$$

etc.

⁵Another guess is $\{\frac{k}{2}\frac{k}{2} \dots\}$. On the torus, this configuration is permitted. On the sphere however, as the overlap of neighboring orbitals is greater than that between next nearest neighbors, this configuration pays a higher energy cost than Eq. (6.7).

6.2.5 Jack polynomials

A well-known family of symmetric, homogenous polynomials with liquid-like correlations and special clustering properties is the family of Jack polynomials [174, 128, 67]. These polynomials are denoted by J_λ^α and are labelled by a partition λ and a parameter α . Bernevig and Haldane first established a connection between these polynomials and the Read-Rezayi wavefunctions[10]. They showed that the Read-Rezayi ground states and quasi-hole states are all Jack polynomials with $\alpha = -(k + 1)$ and $(k, 2)$ -admissible partitions λ (corresponding to $(k, 2)$ admissible occupation configurations $n(\lambda)$). The $(k, 2)$ -admissibility of the label λ is clearly no accident, but what does it mean?

To understand the meaning of the partition label in the Jack polynomials, we need to define ‘dominance’, ‘squeezing’ and ‘addition’. A partition μ dominates another partition ν ($\mu > \nu$) iff $\sum_{i=0}^r \mu_i \geq \sum_{i=0}^r \nu_i \forall r \in [0, \dots, N]$. An example for μ and ν at $k = 2$ is:

$$n(\mu) = \{202\}$$

$$n(\nu) = \{121\}$$

A set of partitions may always be partially ordered by dominance, indicated by the symbol ‘>’. Squeezing is a two-particle operation that connects $n(\mu)$ to $n(\nu)$. It modifies the orbitals occupied by any two particles in $n(\mu)$ from m_1 and m_2 to m'_1 and m'_2 in $n(\nu)$, such that $m_1 + m_2 = m'_1 + m'_2$ and $m_1 < m'_1 \leq m'_2 < m_2$ if the particles are bosonic or $m_1 < m'_1 < m'_2 < m_2$ if they are fermionic. In the example above, $n(\nu)$ is obtained from $n(\mu)$ by squeezing. Dominance and squeezing are identical concepts: a partition μ dominates a partition ν iff ν can be squeezed from μ by a series of squeezing operations. Finally, the ‘sum’ of two partitions $\mu + \nu$ is defined as the partition with occupation configuration $n(\mu + \nu) = \{n_j(\mu) + n_j(\nu), j = 0, \dots, N_\phi\}$.

Consider the ground state of the Read-Rezayi Hamiltonian: $J_{\lambda_0}^\alpha$. The Jack polynomial cannot be a single monomial like our approximate ground state in Eq. (6.7). Any monomial pays a finite energy cost, while the Jack polynomial is a zero energy state. Thus, it is a linear combination of many monomials. The key property is that the monomials with non-zero weight in $J_{\lambda_0}^\alpha$ all correspond to partitions that are dominated by λ_0 . That is, to improve upon our guess for the ground state in the previous subsection, we need to allow for amplitude on monomials with partitions dominated by λ_0 . In fact, we could imagine systematically improving Eq. (6.7) by including configurations obtained systematically from λ_0 by squeezing. λ_0 thus gives us a good starting point to build the actual ground state wavefunction $J_{\lambda_0}^\alpha$.

The amplitudes of the monomials in $J_{\lambda_0}^\alpha$ are not arbitrary: they are heavily constrained by the clustering property discussed in Sec. 6.2.3. We will derive the linear relations between amplitudes imposed by clustering in Sec. 6.5. Here, we merely state the result that the clustering property *completely* specifies the amplitudes of *all* monomials, given that of λ_0 .

Finally, the Jack polynomials at $\alpha = -(k+1)$ indexed by all the other $(k, 2)$ -admissible root configurations are the quasi-hole wavefunctions. Together, with the ground state, they span the *entire* zero-mode space of the Read-Rezayi Hamiltonian. The quasi-hole wavefunctions are also $(k, 2)$ -clustering polynomials, i.e. they vanish as $\prod_{i>k}(z - z_i)^2$ when $z = z_1 = \dots z_k$. They provide a natural description of the particle entanglement spectrum as we shall see in Sec. 6.4.

6.3 Entanglement Matrices and Spectra

In this section, we define the two kinds of entanglement spectra that are the analogues of the edge and bulk energy excitation spectrum. They are respectively the orbital and the particle entanglement spectrum. We will also define their corresponding

entanglement matrices and give an example of each. We then review some of their properties and set the stage for the first important counting result in this chapter about the particle entanglement spectrum.

6.3.1 The Orbital Entanglement Matrix (OEM)

The FQH model state $|\psi\rangle$ can be written as:

$$|\psi\rangle = \sum_{\lambda} b_{\lambda} |\lambda\rangle \quad (6.8)$$

where b_{λ} is a complex amplitude and $|\lambda\rangle$ is a Fock state. Suppose we divide the single-particle orbitals into two parts, A and B . Let A contain the orbitals with m values from 0 to $l_A - 1$ and B the remaining (l_B orbitals). As the single-particle orbitals are polynomially localized in the $\hat{\theta}$ direction (Eq. (6.1)), this partition in the single-particle momentum space roughly corresponds to an azimuthally symmetric spatial cut.

Consider the Fock state $|\lambda\rangle$. Some of the occupied orbitals in this state belong to A (call this set λ_A) and the remaining belong to B (this set is λ_B). Thus, the above expression is equivalent to:

$$|\psi\rangle = \sum_{\lambda} b_{\lambda_A, \lambda_B} |\lambda_A\rangle |\lambda_B\rangle \quad (6.9)$$

where $b_{\lambda} = b_{\lambda_A, \lambda_B}$. The matrix of coefficients b_{λ_A, λ_B} is the ‘full’ orbital entanglement matrix or the ‘full’ OEM, denoted by \mathbf{C}_f .

Observe that not all entries of \mathbf{C}_f can be non-zero. Take a 2-particle wavefunction with $L_z^{tot} = 2$. We see that b_{λ_A, λ_B} can be non-zero only if $\lambda_{A,B}$ satisfy two relations: 1) As the total number of particles is 2, the number of occupied orbitals in A and B must be exactly 2. 2) As the total angular momentum is 2, the sum of the angular momenta of the occupied orbitals in A and B must equal 2 as well. Thus, \mathbf{C}_f can

have non-zero entries only when the quantum numbers of $|\lambda_A\rangle$ and $|\lambda_B\rangle$ satisfy: 1) $N_A + N_B = N$, and 2) $L_z^A + L_z^B = L_z^{tot}$. In other words, \mathbf{C}_f has a block-diagonal structure labelled by two quantum numbers: the number of particles in A (N_A) and the total angular momentum of the particles in A (L_z^A).

The notation we use henceforth for the block of \mathbf{C}_f with labels N_A, L_z^A is \mathbf{C} . Further, we label the Fock states in A (B) with these labels by $|\mu_i\rangle$ ($|\nu_i\rangle$). Thus,

$$|\psi\rangle = \sum_{N_A, L_z^A} \sum_{i,j} \mathbf{C}_{ij} |\mu_i\rangle |\nu_j\rangle \quad (6.10)$$

An example

Let us consider the bosonic Laughlin wave function of $N = 4$ particles at filling $\nu = 1/2$. The number of flux quanta, N_ϕ is 6 and $L_z^{tot} = 12$. The wave function $|\psi\rangle$ can be expanded in the unnormalized basis as:

$$\begin{aligned} |\psi\rangle &\equiv \sum_{\lambda} b_{\lambda} |\lambda\rangle \\ &= |6, 4, 2, 0\rangle - 2|6, 4, 1, 1\rangle - 2|5, 5, 2, 0\rangle + 4|5, 5, 1, 1\rangle \\ &+ 2|6, 3, 2, 1\rangle - 2|5, 4, 2, 1\rangle + 4|5, 3, 2, 2\rangle + 4|4, 4, 2, 2\rangle \\ &- 2|6, 3, 3, 0\rangle + 2|5, 4, 3, 0\rangle - 6|4, 4, 4, 0\rangle - 4|5, 3, 3, 1\rangle \\ &- 6|6, 2, 2, 2\rangle + 4|4, 4, 3, 1\rangle - 6|4, 3, 3, 2\rangle + 24|3, 3, 3, 3\rangle. \end{aligned} \quad (6.11)$$

We will use this wavefunction several times in the chapter for illustrative purposes.

Let us partition the orbitals into two by picking A to contain the $m = 0, 1, 2$ orbitals. We will construct \mathbf{C} with $N_A = 2$ at different values of L_z^A . The terms in

$|\psi\rangle$ that would contribute to \mathbf{C} at $L_z^A = 2$ are⁶:

$$|2, 0\rangle |6, 4\rangle - 2 |2, 0\rangle |5, 5\rangle - 2 |1, 1\rangle |6, 4\rangle + 4 |1, 1\rangle |5, 5\rangle \quad (6.12)$$

\mathbf{C} is just the arrangement of these coefficients as a matrix:

$$\begin{array}{c} |2, 0\rangle \\ |1, 1\rangle \end{array} \begin{array}{cc} |6, 4\rangle & |5, 5\rangle \\ \left(\begin{array}{cc} 1 & -2 \\ -2 & 4 \end{array} \right), \end{array} \quad (6.13)$$

where we have indicated the states labeling the rows and columns. Note that the rank of this matrix is one. The block \mathbf{C} with $N_A = 2, L_z^A = 3$, also of rank one, is:

$$\begin{array}{c} |2, 1\rangle \end{array} \begin{array}{cc} |6, 3\rangle & |5, 4\rangle \\ \left(\begin{array}{cc} 2 & -2 \end{array} \right) \end{array} \quad (6.14)$$

The block at $N_A = 2, L_z^A = 4$ can be analogously determined. Fig. 6.1 shows the numerically generated OES for the 4 particle Laughlin state in the sphere geometry at $1/2$ filling with $N_A = 2$ and $l_A = 3$. The counting of the entanglement levels in the spectrum equals the ranks of \mathbf{C} at each L_z^A .

Properties

We now discuss some of the general properties of \mathbf{C}_f and \mathbf{C} and introduce the orbital entanglement spectrum (OES).

Any correlation function or observable of interest in A or B can be calculated using \mathbf{C}_f . This is not surprising at all: \mathbf{C}_f is merely a matrix arrangement of all the information in the full wavefunction. Suppose we wish to calculate some 2-point

⁶There is a minimum value of L_z^A for given N_A . This is because all configurations of non-zero weight in the Read-Rezayi wavefunctions are obtained by squeezing the special root partition $k_0 k_0 k_0 \dots$

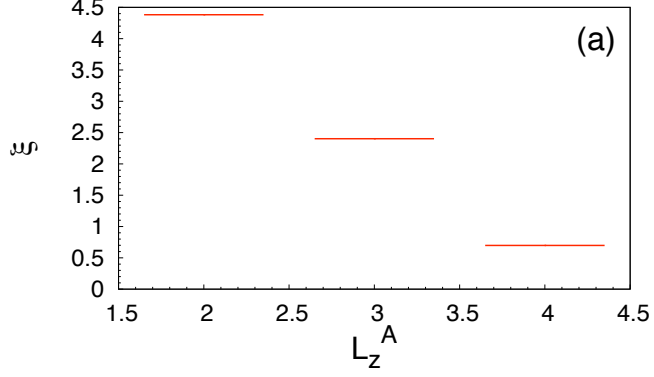


Figure 6.1: Orbital entanglement spectrum of the $\nu = 1/2$ Laughlin state with $N = 4$, $N_A = 2$, and orbital cut after $l_A = 3$ orbitals. The number of non-zero entanglement levels at each angular momentum is equal to the rank of the OEM at that angular momentum.

function in A , $\langle \psi | O(z)O(z') | \psi \rangle$ for $z, z' \in A$. A few steps of algebra using the definition in Eq. (6.9) lead us to the relation:

$$\langle \psi | O(z)O(z') | \psi \rangle = \text{Tr}_A[\mathbf{C}_f \mathbf{C}_f^\dagger O(z)O(z')] \quad (6.15)$$

where Tr_A is the trace over all configurations in A . The combination $\mathbf{C}_f \mathbf{C}_f^\dagger$ is better known as the reduced density matrix of A . It plays the role of the partition function for A . Similarly, the reduced density matrix of B is given by $\mathbf{C}_f^\dagger \mathbf{C}_f$.

The singular value decomposition of \mathbf{C} is given by:

$$\sum_{i,j} \mathbf{C}_{ij} |\mu_i\rangle |\nu_j\rangle = \sum_{i=1}^{\text{rank}(\mathbf{C})} e^{-\xi_i/2} |U_i\rangle |V_i\rangle. \quad (6.16)$$

The kets on the left-hand-side of Eq. (6.16) are defined as in Eq. (6.10). $|U_i\rangle$ and $|V_i\rangle$ are the singular vectors in the Hilbert spaces of A and B restricted to a fixed particle number and z -angular momentum. They are linear combinations of the occupation number basis vectors $|\mu_i\rangle$ and $|\nu_j\rangle$. The ξ_i 's are the 'energies' plotted as a function of L_z^A in the orbital entanglement spectrum (OES) introduced in [123].

The number of finite energies ($\text{rank}(\mathbf{C})$) at each (N_A, L_z^A) is independent of the geometry of the 2-d surface and the symmetrization factors arising due to multiple particles occupying the same orbital. Let \mathbf{C}_f^d and \mathbf{C}_f^s be the full OEMs in the disc and sphere geometry, or in any other two genus 0 geometries. Modifying the geometry of the surface changes the normalization of the single-particle orbitals (the quantum mechanical normalization); thus every b_λ in the expansion of $|\psi\rangle$ in Eq. (6.9) in the disc basis is multiplied by a factor $\mathcal{N}(\lambda) = \prod_{i=1}^N \mathcal{N}(\lambda_i)$ when expanded in the single-particle orbital basis on the sphere. $\mathcal{N}(j)$ is a factor relating the normalization of orbital j on the disc to that on the sphere. The OEM's on the disc and the sphere are thus related as:

$$\begin{aligned} |\psi\rangle &= \sum_{i,j} (\mathbf{C}_f^d)_{ij} |\mu_i^d\rangle |\nu_j^d\rangle \\ &= \sum_{i,j} (\mathbf{C}_f^d)_{ij} \mathcal{N}(\mu_i^d) \mathcal{N}(\nu_j^d) |\mu_i^s\rangle |\nu_j^s\rangle, \end{aligned} \quad (6.17)$$

where the superscripts d and s refer to the disc and sphere geometries, or to any other two genus 0 geometries. \mathbf{C}_f^s is obtained from \mathbf{C}_f^d by multiplying whole rows and columns by normalization factors; thus $\text{rank}(\mathbf{C}_f^s) = \text{rank}(\mathbf{C}_f^d)$. An identical argument shows the rank of \mathbf{C}_f to be independent of the symmetrization factors that arise in the normalization of the *many-body* states constructed from normalized single-particle orbitals. This is the promised justification for working in the unnormalized single-particle basis.

OES of the Read-Rezayi states

We then specialize to the OEM/OES of the $(k, 2)$ -clustering/Read-Rezayi states and introduce the natural number of particles in A and the minimum z -angular momentum in A . We also discuss the empirical numerical observations of the counting of the non-zero entanglement energies of these states.

For a given cut l_A in orbital space, the *maximum* number of particles that can form a $(k, 2)$ -clustering droplet in A is defined to be the natural number of particles $N_{A,nat}$:

$$N_{A,nat} = k \lfloor (l_A + 1)/2 \rfloor, \quad (6.18)$$

where $\lfloor x \rfloor$ is the integer part of x . Physically, $N_{A,nat}/l_A$ is very close to the original filling ν . We may think of the original, homogenous QH fluid as being composed of two droplets in A and B of $N_{A,nat}$ and $N_{B,nat} = N - N_{A,nat}$ particles each, interacting via correlated excitations along their common edge. We would thus expect the OES at $N_{A,nat}$, called the natural spectrum, to be the low-energy sector of the full entanglement energy spectrum and to contain information about the edge theory of the model state. In the thermodynamic limit, the number of finite energies (level counting) of the OES is conjectured to be identical to the counting of the modes of the CFT describing the edge for values $l_A, N_A \rightarrow \infty$ such that $l_A/N_\phi \rightarrow \text{const.}(> 0)$ and $N_A/N_{A,nat} \rightarrow 1$.

As the particles in A avoid each other in the $(k, 2)$ clustering states, they have a minimum total z -angular momentum. This is denoted by $L_{z,min}^A$ and depends only on N_A :

$$L_{z,min}^A = \lfloor N_A/k \rfloor (2N_A - k \lfloor N_A/k \rfloor - k). \quad (6.19)$$

We stress that $L_{z,min}^A$ is the *maximum* value on the x -axis of the *numerically* generated entanglement spectra existing in the literature, due to the different indexing scheme in the text and the figures. For instance, in Fig. 6.2, $L_{z,min}^A$ describes the sector of the OES at $L_z^A = 20$.

For an arbitrary pure bosonic state of N particles, the rank of the OEM \mathbf{C}_f must generically be the smaller of its dimensions. The model states are special because the rank of the OEM block at given (N_A, L_z^A) is in general much smaller than its smaller

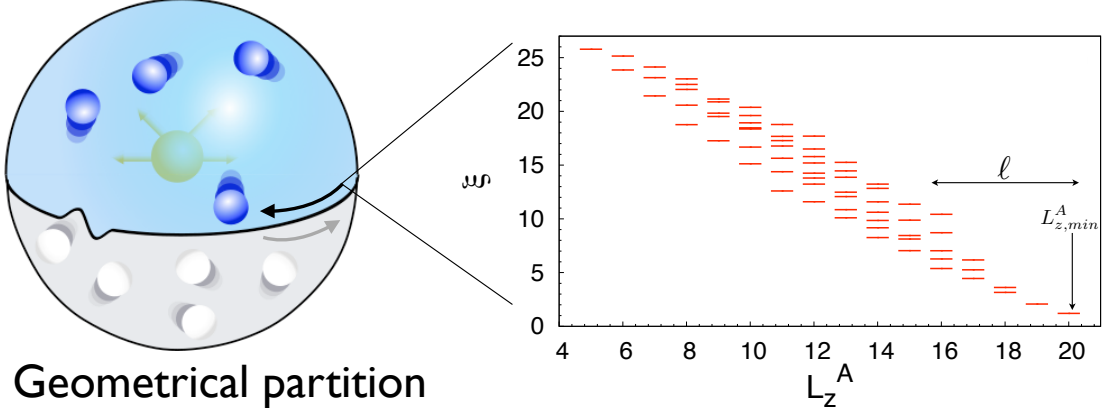


Figure 6.2: Left: Sketch of the partition in orbital space (part B in grey). The tracing procedure creates a virtual edge and the orbital entanglement spectrum (OES) probes the chiral edge mode(s) of part A . Right: OES of the $\nu = 1/2$ Laughlin state of $N = 9$ bosons, with orbital cut $l_A = 8$ and $N_A = 4$. The minimal angular momentum $L_{z,min}^A$ defined in the text is the $L_{z,min}^A = 20$ sector in the plot. The entanglement level counting at $\ell = |L_z^A - L_{z,min}^A| = 0, 1, \dots, 4$ is $(1, 1, 2, 3, 5)$, which is the counting of modes of a $U(1)$ boson in the thermodynamic limit. Finite size effects appear at $L_z^A = 15$.

dimension. The rank of the OEM block at given N_A , as a function of $\ell = |L_z^A - L_{z,min}^A|$ ⁷ is called the counting of the OES. See Fig. 6.2 for the OES of the Laughlin state. For model states, it has been observed from small size numerical calculations that the counting is universal for the first few values of ℓ , [123] *i.e.* independent of N , N_A , and l_A . The universal counting is distinct for each model state, which is why Li and Haldane proposed it as a way to determine the topological order [196] of the FQH states. For instance, for a Laughlin state the universal counting is $\{1, 1, 2, 3, 5, 7, 11, \dots\}$, while for the Moore-Read state it is $\{1, 1, 3, 5, 10, 16, \dots\}$. In the OES of the Laughlin $1/2$ state in Fig. 6.2, the counting is universal for $\ell = 0, \dots, 4$: $\{1, 1, 2, 3, 5, \dots\}$, starting from the right edge of the spectrum. For larger ℓ , finite-size corrections occur. The universal counting is identical to counting the modes of a massless, chiral

⁷We use absolute values to include both the convention in the pictures, where $L_z^A - L_{z,min}^A \leq 0$, and the convention in the text, where $L_z^A - L_{z,min}^A \geq 0$.

boson, which is the conformal field theory describing the edge of the Laughlin FQH states.

6.3.2 The Particle Entanglement Matrix (PEM)

The orbital cut is an approximation to the real-space cut. As evident in Fig. 6.2, the orbital cut probes the correlations across the virtual edge between A and B . Thus, it might be expected to probe properties of a real edge. What about the charged quasi holes in the bulk? Which entanglement spectrum is likely to probe these excitations? The answer to this question is the particle entanglement spectrum (PES). This spectrum was first introduced in Ref. [176] by generalizing ideas in Ref. [94, 207].

One way to create quasi holes in the bulk is to move away from the magic filling $\nu = N/N_\phi = k/2$. On increasing N_ϕ by one flux quantum for fixed N , we would create one charged quasi-hole that binds a flux quantum in the bulk. Another way to arrive at the same physics ($\nu < k/2$) is to decrease the number of particles N . This is the guiding principle behind the particle cut. In the particle cut, we partition the number of particles into groups A and B with N_A and $N_B = N - N_A$ particles. The mathematical definitions will be given below. Physically, it is clear why this is the cut of choice: the configurations in A involve N_A particles in the background of N_ϕ flux quanta, while those in B involve N_B particles in the background of N_ϕ flux quanta. As $N_A, N_B < N$, we might hope that this cut probes the quasi hole excitations of the original fluid.

The particle cut is easiest to understand in the wavefunction language. Consider the model state in the unnormalized real space basis, $\psi(z_1, \dots, z_N) = \sum_\lambda b_\lambda \langle z_1, \dots, z_N | \lambda \rangle$. For simplicity, we choose the particles at positions $\{z_1, \dots, z_{N_A}\}$ as group A and the remaining particles $\{z_{N_A+1}, \dots, z_N\}$ as group B . Without loss of generality, let $N_A \leq N_B$. Each many-body basis state $\langle z_1, \dots, z_N | \lambda \rangle$ can be

decomposed as

$$\langle z_1, \dots, z_N | \lambda \rangle = \sum_{\mu, \nu} \langle z_1, \dots, z_{N_A} | \mu \rangle \cdot \langle z_{N_A+1}, \dots, z_N | \nu \rangle, \quad (6.20)$$

where the sum runs over all possible orbital occupations μ and ν of N_A and N_B particles respectively, such that $\mu + \nu = \lambda$. Unlike the last section, there is no orbital restriction. Then, ψ can be written as:

$$\psi(z_1, \dots, z_N) = \sum_{\lambda} b_{\lambda} \langle z_1, \dots, z_N | \lambda \rangle \quad (6.21)$$

$$= \sum_{\lambda} \sum_{\mu_i + \nu_j = \lambda} (\mathbf{P}_f)_{ij} \langle z_1, \dots, z_{N_A} | \mu_i \rangle \langle z_{N_A+1}, \dots, z_N | \nu_j \rangle, \quad (6.22)$$

where the summation is over all partitions μ_i (ν_j) of N_A (N_B) particles in N_{ϕ} orbitals. The matrix \mathbf{P}_f is the full particle entanglement matrix (PEM). As was the case for the OEM, the matrix elements of the PEM are directly related to the weights of the model wave function by

$$(\mathbf{P}_f)_{ij} = b_{\mu_i + \nu_j}. \quad (6.23)$$

\mathbf{P}_f also has a block-diagonal structure. This is imposed by the fixed total z -angular momentum. $(\mathbf{P}_f)_{ij}$ can be non-zero only if the angular momentum of A (B), L_z^A (L_z^B) satisfy the relation $L_z^A + L_z^B = L_z^{tot}$. We denote the block of \mathbf{P}_f at fixed (L_z^A, N_A) by \mathbf{P} .

An example

We work with the Laughlin wavefunction in Eq. (6.11) in real space to construct the particle entanglement matrices for $N_A = 2$. First, note that every basis state in

Eq. (6.11) is actually a sum of terms in A and B . For example:

$$\begin{aligned} \langle z_1, \dots, z_4 | 6, 4, 1, 1 \rangle &= S[z_1^6 z_2^4 z_3^1 z_4^1] \\ &= S[z_1^6 z_2^4] S[z_3^1 z_4^1] + S[z_1^6 z_2^1] S[z_3^4 z_4^1] + S[z_1^4 z_2^1] S[z_3^6 z_4^1] + S[z_1^1 z_2^1] S[z_3^6 z_4^4] \end{aligned}$$

where S denotes symmetrization. On doing this decomposition for every basis state, we can construct \mathbf{P} at any L_z^A . At the smallest possible angular momentum $L_z^A = L_{z,min}^A = 2$, the PEM and OEM are identical:

$$\begin{array}{c} |2, 0\rangle \\ |1, 1\rangle \end{array} \begin{array}{cc} |6, 4\rangle & |5, 5\rangle \\ \left(\begin{array}{cc} 1 & -2 \\ -2 & 4 \end{array} \right). \end{array} \quad (6.24)$$

The Hilbert space of A at $L_z^A = L_{z,min}^A + 1 = 3$ is spanned by the occupation number states $|3, 0\rangle$ and $|2, 1\rangle$. $|3, 0\rangle$ was not a member of the Hilbert space of A for the orbital cut after $l_A = 3$ orbitals (discussed in the previous section), because the orbital with index 3 belonged to B . The PEM at $L_z^A = 3$ is given by:

$$\begin{array}{c} |3, 0\rangle \\ |2, 1\rangle \end{array} \begin{array}{cc} |6, 3\rangle & |5, 4\rangle \\ \left(\begin{array}{cc} -2 & 2 \\ 2 & -2 \end{array} \right). \end{array} \quad (6.25)$$

Observe that the OEM (6.14) for $N_A = 2, L_z^A = 2$ is a sub-matrix of the PEM. We discuss this connection in the next section.

Fig. 6.1 shows the numerically generated PES for the 4 particle 1/2 Laughlin state for $N_A = 2$. The number of non-zero entanglement energies at L_z^A is equal to be the rank of the corresponding PEM.

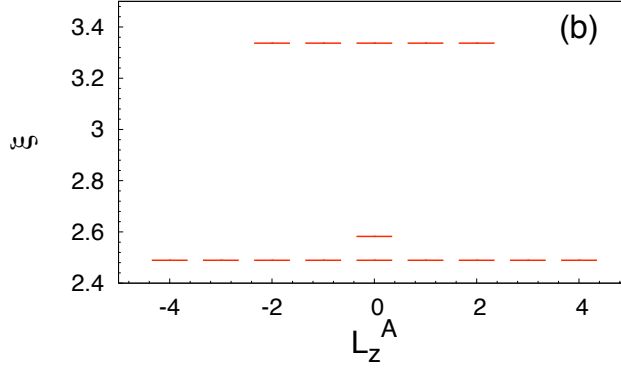


Figure 6.3: Particle entanglement spectrum of the $\nu = 1/2$ Laughlin state with particle cut $N_A = 2$. The entanglement level counting at all angular momenta L_z^A is equal to the rank of the PEM. $L_{z,min}^A$ defined in the text is $L_z^A = 4$ in the plots.

Properties

The properties of the PEM follow by the same arguments as those presented for the OEM. The reduced density matrices of part A and B are given by $\rho_A = \mathbf{P}_f \mathbf{P}_f^\dagger$ and $\rho_B = \mathbf{P}_f^\dagger \mathbf{P}_f$ respectively. They are block-diagonal in L_z^A as well. The singular value decomposition of the PEM by:

$$\sum_{i,j} (\mathbf{P})_{ij} |\mu_i\rangle |\nu_j\rangle = \sum_i e^{-\xi_i/2} |U_i\rangle |V_i\rangle, \quad (6.26)$$

where the singular vectors $|U_i\rangle$ and $|V_i\rangle$ are orthonormal vectors in the Hilbert spaces of A and B restricted to fixed angular momentum. The plot of the ‘energies’ ξ_i vs L_z^A is called the particle entanglement spectrum (PES)[176]. In Fig. 6.4 is an example: the PES of the 9 particle $1/2$ Laughlin state for the particle cut $N_A = 4$. The counting of the PES is defined as the number of non-zero entanglement energies as a function of $\ell = |L_z^A - L_{z,min}^A|$. From numerical calculations, it has been observed[176] that the counting of the PES is identical to the number of quasihole states of the model state with N_A particles in N_ϕ orbitals at all angular momenta L_z^A . In Fig. 6.4 for example, the counting can be checked to be identical to the number of quasihole states of a

Laughlin state with 4 particles in 16 orbitals. A universal result about the relation between the counting of the PES and the number of quasi hole states will be presented in Sec. 6.4. Further, we will find that the counting is universal (independent of N, N_A for the first few values of ℓ).

Two final comments about the PEM are in order. The first is a feature of the spherical geometry, resulting in the flatness of the spectrum in Fig. 6.4. The flatness is reminiscent of a multiplet structure. Indeed, in the spherical geometry, the PEM is labeled by an additional quantum number: the total angular momentum of A , $(\vec{L}^A)^2$. Consequently, the eigenvalues of the block \mathbf{P} with $(\vec{L}^A)^2 = \ell(\ell + 1)$ are $(2\ell + 1)$ -fold degenerate. This multiplet structure does not play any role in our discussions about the counting of the PES.

The second comment is that the PEM at fixed N_A, L_z^A is ‘bigger’ than the corresponding OEM at the same quantum numbers. That is, \mathbf{P} has more rows and columns as compared to \mathbf{C} . It’s easy to see why: the particle cut places has no restriction on which orbitals can be occupied. Therefore, even at fixed L_z^A , there are configurations that contribute to \mathbf{P} in which orbitals with m greater and lesser than l_A are occupied. For the same reason, \mathbf{C} is a sub-matrix of \mathbf{P} . It immediately follows that the counting of the OES is always smaller or equal to that of the PES. The goal of this chapter is to prove their *equality*.

Comparing Figs. 6.2,6.4, we see that the counting of the PES and the OES are the same for the first four values of L_z^A near the left.

6.4 Result I: Counting of the PES

Our first important result is that the number of non-zero levels in the PES at L_z^A is upper bounded by the number of the bulk quasi-hole excitations. We then argue that the lack of further symmetry in the system must imply the bound is saturated.

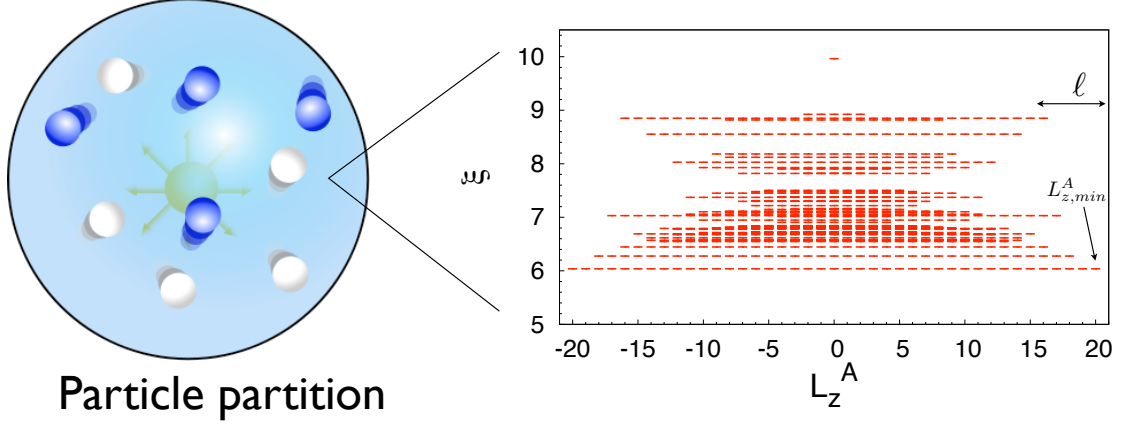


Figure 6.4: Left: Sketch of the partition in particle space. The particles of part B that are traced out are denoted in grey. Right: particle entanglement spectrum (PES) of the $\nu = 1/2$ Laughlin state of $N = 9$ bosons, with particle cut $N_A = 4$. The minimum angular momentum $L_{z,min}^A$ defined in the text is $L_{z,min}^A = 20$ in the plot. The entanglement level counting is identical to the counting of quasiholes in a Laughlin state of 4 particles with total flux $N_\phi = 16$ at all angular momenta L_z^A . For $\ell = |L_z^A - L_{z,min}^A| = 0, 1, \dots, 4$, the counting is universal, *i.e.* independent of N_A : (1, 1, 2, 3, 5).

Recall that the property that defines the k -clustered model state $\psi(z_1, \dots, z_N)$ uniquely is that it is the lowest degree symmetric polynomial that vanishes when $(k + 1)$ particles are at the same position. Similar clustering conditions characterize every ground-state of a pseudopotential Hamiltonian. This vanishing property must persist when we divide the particles into two groups and re-write the model state in Eq. (6.21) as:

$$\psi(z_1, \dots, z_N) = \sum_{L_z^A} \sum_i e^{-\xi_i/2} \langle z_1, \dots, z_{N_A} | U_i \rangle \cdot \langle z_{N_A+1}, \dots, z_N | V_i \rangle, \quad (6.27)$$

using Eq. (6.26) at each L_z^A . If we choose $(k + 1)$ particles in group A , say z_1, \dots, z_{k+1} , to be at the same position z , then the state must vanish at every L_z^A . Further, as the

singular vectors in B form an orthonormal basis:

$$\psi(z, \dots, z, z_{k+2}, \dots, z_N) = 0 \quad (6.28)$$

$$\Rightarrow e^{-\xi_i/2} \langle z, \dots, z, z_{k+2}, \dots, z_{N_A} | U_i \rangle = 0, \forall i, L_z^A. \quad (6.29)$$

A similar relation holds when A and B are interchanged. We conclude that the singular vectors, $\langle z_1, \dots, z_{N_A} | U_i \rangle$ and $\langle z_{N_A+1}, \dots, z_N | V_i \rangle$, must also be clustering polynomials that vanish when $(k+1)$ particles are at the same position. A basis for clustering polynomials is the set of Jack polynomials, $J_{\tilde{\mu}}^{\alpha}$, indexed by $\alpha = -(k+1)$ and the $(k, 2)$ -admissible partition $\tilde{\mu}$ [174, 10, 9]. ψ can therefore be expanded in the Jack basis as:

$$\psi(z_1, \dots, z_N) = \sum_{i,j} (\mathbf{M}_f)_{ij} J_{\tilde{\mu}_i}^{\alpha}(z_1, \dots, z_{N_A}) J_{\tilde{\nu}_j}^{\alpha}(z_{N_A+1}, \dots, z_N), \quad (6.30)$$

where $\tilde{\mu}_i$ and $\tilde{\nu}_j$ denote $(k, 2)$ -admissible partitions of N_A and N_B particles respectively. The matrix \mathbf{M}_f is block-diagonal in angular momentum L_z^A ; let \mathbf{M} refer to the block of \mathbf{M}_f at fixed value of L_z^A . The row and column dimensions of \mathbf{M} are much smaller than those of \mathbf{P} because the $(k, 2)$ -admissible partitions of N_A and N_B form a small subset of the set of all partitions of with fixed L_z^A and L_z^B respectively. Nevertheless, as Eq. (6.27) and (6.30) are equal, \mathbf{M} and \mathbf{P} must have the same rank. As $N_A \leq N_B$, the row dimension of \mathbf{M} is smaller (or equal) than the column dimension and bounds the rank of the PEM block from above at each L_z^A .

Let us reformulate what we have just shown in a more familiar language and argue for the saturation of the bound. The row dimension of \mathbf{M} is given by the number of $(k, 2)$ -admissible configurations of N_A particles in N_{ϕ} orbitals, and thus is equal to the number of distinct bulk quasi-hole excitations of the $(k, 2)$ -clustering model state of N_A particles at angular momentum L_z^A on a sphere pierced by the number of fluxes of the original state [87, 159]. Hence, we find that the rank of the PEM is bounded

by the number of quasihole states for all angular momenta L_z^A . Without further symmetry-induced constraints on the entanglement matrix (we have already used all the symmetries available in the state), we expect this bound to be saturated. In the thermodynamic limit ($N_A, N \rightarrow \infty$ such that $N_A/N > 0$), we therefore argue that the level counting of the entire PES is identical to the number of the bulk quasi-hole excitations. This bound saturation can be proved exactly for the Laughlin states[64].

It is beneficial to identify a set of rows and columns in \mathbf{P} with the same rank as the full matrix. Consider the rows and columns labeled by the $(k, 2)$ -admissible partitions. This sub-matrix of \mathbf{P} is denoted by $\tilde{\mathbf{P}}$ and has the same dimensions as \mathbf{M} . In Appendix 6.A.1, we show that $\tilde{\mathbf{P}}$ and \mathbf{M} have the same rank. $\tilde{\mathbf{P}}$ will play a prominent role in the proof establishing the bulk-edge correspondence in the entanglement spectra.

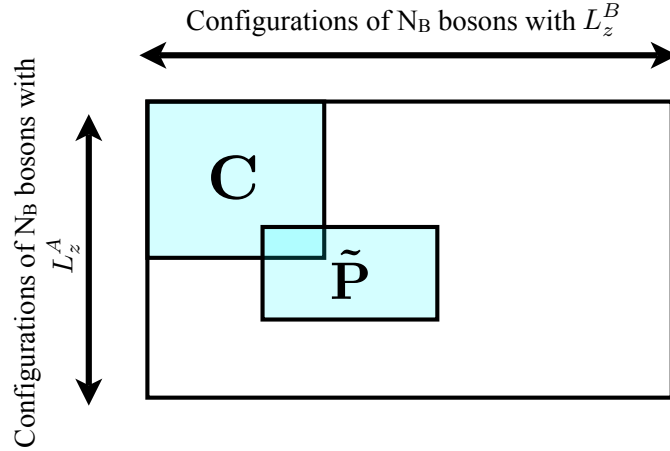


Figure 6.5: A cartoon of the various sub-matrices in the PEM block labeled by the angular momentum L_z^A . The block of the OEM labeled by (N_A, L_z^A) — \mathbf{C} in the figure— is a sub-matrix of the PEM block \mathbf{P} at L_z^A . $\tilde{\mathbf{P}}$ is a sub-matrix of \mathbf{P} containing all rows and columns that are labeled by $(k, 2)$ -admissible partitions of N_A and N_B particles subject to total flux N_ϕ .

6.5 Clustering Constraints

The second result of this chapter is a relation between the counting of the PES and the OES, that is a bulk-edge correspondence in entanglement spectra. To relate the two beasts, we appeal to the defining property of the FQH model states: clustering. Clustering provides constraints on the coefficients of the wavefunctions and consequently, can be used to relate the PEM and the OEM. But first, what are the clustering constraints?

Recall that the Read-Rezayi model wave functions $\psi_{(k,2)}(z_1, z_2 \dots z_N)$ are single Jack polynomials labeled by a root partition λ_0 (Eq. (6.7)), and a parameter $\alpha = -(k+1)$. They satisfy $(k,2)$ -clustering — they are non-zero when a cluster of k particles is at the same point in space $z = z_1 = z_2 = \dots z_k$, but vanish as the second power of the distance between the $(k+1)$ st particle and the cluster as $z_{k+1} \rightarrow z$. The clustering property imposes a rich structure on $\psi_{(k,2)}(z_1, z_2, \dots, z_N)$. All the partitions λ that arise in the expansion of $|\psi\rangle$ in the many-body occupation basis ($|\psi\rangle = \sum_{\lambda} b_{\lambda} |\lambda\rangle$) are dominated by λ_0 . Furthermore, all the coefficients b_{λ} are known up to a multiplicative constant. In the Jacks, this constant is chosen so that $b_{\lambda_0} = 1$. In other words, the clustering property and the requirement to be the densest possible wave function determine $\psi_{(k,2)}(z_1, z_2, \dots, z_N)$ uniquely up to an overall normalization constant. Here, we formulate the conditions imposed by clustering on $\psi_{(k,2)}(z_1, \dots, z_N)$ as linear, homogeneous equations on the coefficients b_{λ} . These are called clustering constraints, and are the main tool to proof the rank equality of the PEM and OEM in Section 6.6.

6.5.1 Derivation

Let us introduce a ‘deletion’ operator d_i for orbital i such that:

$$d_i|\lambda\rangle = \begin{cases} 0 & , i \notin \lambda \\ |\lambda \setminus \{i\}\rangle & , i \in \lambda \end{cases} \quad (6.31)$$

$\lambda \setminus \{i\}$ is the partition with a single occurrence of the orbital i removed from it. The ‘deletion’ operators commute with each other.

We now separate the coordinates of $k + 1$ particles from the rest and rewrite $\psi_{(k,2)}(z_1, z_2, \dots, z_N)$ as:

$$\psi_{(k,2)}(z_1, \dots, z_N) = \sum_{l_1, \dots, l_{k+1}=0}^{N_\phi} \left(\prod_{j=1}^{k+1} z_j^{l_j} \right) \langle z_{k+2}, \dots, z_N | \prod_{j=1}^{k+1} d_{l_j} |\psi\rangle, \quad (6.32)$$

and form a cluster by bringing the k particles with coordinates z_1, \dots, z_k to the same position z . When $z_{k+1} = z$, the LHS vanishes and Eq.(6.32) becomes:

$$0 = \sum_{l_1, \dots, l_{k+1}=0}^{N_\phi} z^{\sum_{j=1}^{k+1} l_j} \langle z_{k+2}, \dots, z_N | \prod_{i=1}^{k+1} d_{l_i} |\psi\rangle. \quad (6.33)$$

The right-hand-side is a polynomial in an arbitrary complex number z , and has to vanish for every power $\beta = \sum_{j=1}^{k+1} l_j$ of z to satisfy the above equation. Thus, the constraints on $|\psi\rangle$ are:

$$\left(\sum_{l_1, \dots, l_k=0}^{N_\phi} d_{\beta - \sum_{j=1}^k l_j} \prod_{j=1}^k d_{l_j} \right) |\psi\rangle = D_\beta |\psi\rangle = 0. \quad (6.34)$$

β is the z -angular momentum of $(k + 1)$ -particles; it ranges from 0 to $N_\phi(k + 1)$. The equation above requires any clustering wave function $|\psi\rangle$ to be simultaneously annihilated by the destruction operators $\{D_i, i = 0 \dots N_\phi(k + 1)\}$.

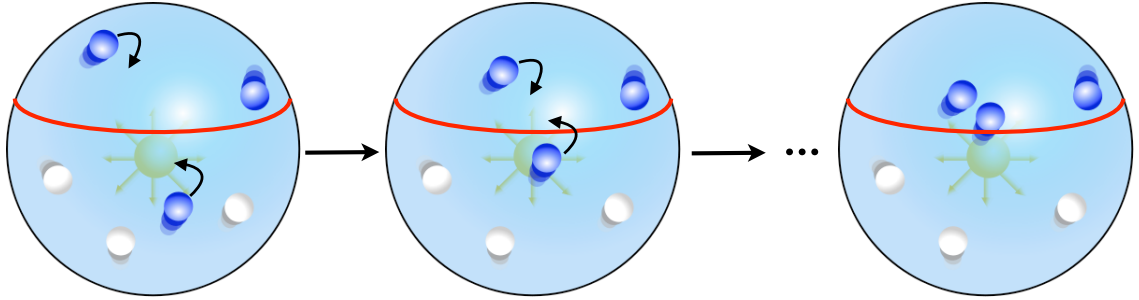


Figure 6.6: The configurations in the PES can be related to those of the OES using the clustering constraints. These constraints reveal the vanishing properties of the FQH state as particles are brought closer together. They relate the long-wavelength properties of the FQH state when two particles are far away from each other to the short-wavelength properties of the state when particles are close together, and hence can be used to ‘drag’ particles from the PES Hilbert space into the more restrictive OES Hilbert space.

6.5.2 Properties

Every value of β in Eq. (6.34) yields, in general, a large number of linear relations between the coefficients of $|\psi\rangle$. Let S_β be the set of all partitions of N particles such that the sum of the z -angular momentum of $(k + 1)$ particles is β . For *every* occupation configuration of $N - (k + 1)$ particles, Eq. (6.34) relates the coefficients of partitions $\lambda \in S_\beta$ in the expansion of $|\psi\rangle$. Examples of such relations are given in Appendix 6.B.

The set of linear, homogeneous equations in Eq.(6.34) are linearly dependent. The dimension of the null-space of the set is *exactly* one for the densest possible wave function, i.e. the vector of coefficients $\{b_\lambda\}$ is uniquely determined up to an overall multiplicative factor. Since the solution to Eq.(6.34) causes ψ to vanish when any cluster of size greater than k is formed in real space, we conclude that the set in Eq.(6.34) includes *all* constraints imposed on $\psi(z_1, \dots, z_N)$ due to clustering.

6.6 Result II: Bulk-edge correspondence in ES

We now have all the ingredients necessary to prove the bulk-edge correspondence in the entanglement spectra. Let us first recap our findings so far. In Sec. 6.4, we constructed the full PEM \mathbf{P}_f for $(k, 2)$ -clustering model states and argued that the PES level counting is equal to the number of quasihole states of the same model state with N_A particles in N_ϕ orbitals. For angular momenta $L_z^A \leq L_{z,min}^A + \lfloor N_A/k \rfloor$, the quasihole state counting is universal, and identical to the counting of modes of the edge CFT.

For given L_z^A , we identified the sub-matrix $\tilde{\mathbf{P}}$ of the PEM block \mathbf{P} , with rows and columns labeled by $(k, 2)$ admissible partitions, which has the same rank as the PEM block \mathbf{P} . The block of the OEM \mathbf{C} at (N_A, L_z^A) is a sub-matrix of the PEM block, thus $\text{rank}(\mathbf{P}) \geq \text{rank}(\mathbf{C})$. In order to show that the ranks are equal, we use the clustering constraints derived in the previous section to express the row/column vectors of \mathbf{P} that constitute $\tilde{\mathbf{P}}$ in terms of those that constitute the OEM block. In the following, we will refer to this as ‘expressing the row/column vectors of $\tilde{\mathbf{P}}$ in terms of the row/column vectors of \mathbf{C} ’. One should always think of the linear relations we derive as linear relations between rows and columns in the bigger matrix \mathbf{P} , which contains both $\tilde{\mathbf{P}}$ and \mathbf{C} . For finite system sizes, we show that the ranks are equal for a certain range of angular momenta, which depends on N_A and l_A (see Eq. (6.38)). This proves that the PES and the OES (at fixed N_A) have the same level counting for a finite range of angular momentum. In the thermodynamic limit, this procedure establishes the equality of the level counting of the *entire* PES and OES when, roughly speaking, $N_A \approx N_{A,nat}$, thus proving a significant part of the Li-Haldane conjecture.

The argument below applies equally well to row and column vectors. To keep the discussion concise, we formulate it using row vectors alone.

6.6.1 Systemizing the constraints

The biggest challenge in relating the row vectors of the PEM to those in the OEM for fixed (N_A, L_z^A) lies in identifying a set of linearly independent equations in the entire set of clustering constraints. To this end, we introduce a few quantities characterizing a partition μ . $n_m(\mu)$ below refers to the occupation number of the m th orbital in partition μ . The orbital cut is after l_A orbitals.

The unit cell— We divide the single-particle orbital space such that the j th unit cell contains the orbitals of z -angular momentum $2j$ and $2j+1$, and $j \in [0, \dots, N_\phi/2]$. As the total number of single-particle orbitals is odd for the bosonic $(k, 2)$ -clustering states, the orbital with angular momentum N_ϕ is its own unit cell with index $N_\phi/2$. Every orbital belongs to exactly one unit cell.

The intact unit cell— The j th unit cell of a partition μ is said to be intact if the occupation numbers of the orbitals with angular momentum $0, \dots, 2j+1$ are identical to those in the root configuration Eq. (6.7), i.e. if $n_i(\mu) = n_i(\lambda_0)$ for $i = 0, \dots, 2j+1$. Clearly, the j th unit cell can only be intact if all unit cells $0, \dots, j-1$ are intact.

The number of intact unit cells in part A— The number of intact unit cells in part A, Δ_μ , is the number of intact unit cells to the left of the orbital cut in $n(\mu)$.

Distance from the cut— If we were to number the orbitals to the right of the cut as $1, 2, \dots$, then the distance from the cut is defined as the sum of the indices of the occupied orbitals to the right of the orbital cut in $n(\mu)$. The distance from the cut, K_μ , is given by:

$$K_\mu = \sum_{m=l_A}^{N_\phi} n_m(\mu)(m - l_A + 1). \quad (6.35)$$

$K(\mu) = 0$ for a partition μ labeling a row of the OEM; for a general partition, it represents the distance in orbital units that all the particles to the right of the cut need to traverse to cross the cut. In Fig. 6.7, we pick as an example a generic partition

μ and identify the number of intact unit cells in A , Δ_μ , and the distance from the cut, K_μ , for two different orbital cuts.

Root configuration of part A— For given N_A and L_z^A there is a unique $(k, 2)$ -admissible (root) configuration $n(\tilde{\mu}_0)$, with the property that $\tilde{\mu}_0$ dominates all the other partitions at angular momentum L_z^A that label rows of the PEM:

$$n(\tilde{\mu}_0) = \{ \underbrace{k0 \dots k0}_{2\lfloor(N_A-1)/k\rfloor} \underbrace{x0 \dots 0}_{\ell-1} 10 \dots 0 \}. \quad (6.36)$$

The value of x is fixed by the total particle number being N_A ($x = (N_A - 1) - k\lfloor(N_A - 1)/k\rfloor$). $\tilde{\mu}_0$ has the maximum (total) number of intact unit cells possible, $\lfloor(N_A - 1)/k\rfloor$.

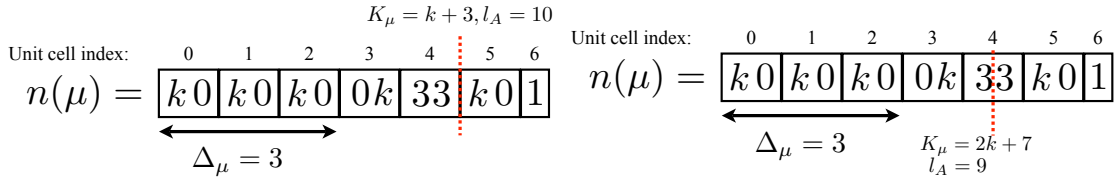


Figure 6.7: The occupation configuration of a generic partition μ with the unit cells, the number of intact unit cells Δ_μ and the distance from cuts after $l_A = 9$ (top) and $l_A = 10$ (bottom) shown. $N_\phi = 12$ here.

6.6.2 The method

Consider $\tilde{\mathbf{P}}$ at L_z^A and the OEM block \mathbf{C} at (N_A, L_z^A) with $L_z^A = L_{z,min}^A + \ell$. We can express all row vectors of $\tilde{\mathbf{P}}$ in terms of row vectors in the OEM block if the root configuration of part A satisfies:

$$\Delta_{\tilde{\mu}_0} \geq K_{\tilde{\mu}_0}. \quad (6.37)$$

For fixed l_A and N_A , relation (6.37) is fulfilled for angular momenta $L_z^A - L_{z,min}^A = 0, \dots, \ell_{max}$ with:

$$\ell_{max} = \begin{cases} \Delta_{\tilde{\mu}_0} - k\bar{\Delta}_{\tilde{\mu}_0}^2 - (2\bar{\Delta}_{\tilde{\mu}_0} + 1)(x + 1) & \text{for } l_A \text{ even, } l_A \leq 2\lfloor(N_A - 1)/k\rfloor \\ \Delta_{\tilde{\mu}_0} - k\bar{\Delta}_{\tilde{\mu}_0}(\bar{\Delta}_{\tilde{\mu}_0} - 1) - 2(x + 1)\bar{\Delta}_{\tilde{\mu}_0} & \text{for } l_A \text{ odd, } l_A \leq 2\lfloor(N_A - 1)/k\rfloor \\ l_A - \Delta_{\tilde{\mu}_0} - 1 & \text{for } l_A > 2\lfloor(N_A - 1)/k\rfloor, \end{cases} \quad (6.38)$$

where we abbreviated the difference of the total number of unit cells and those only in A by $\bar{\Delta}_{\tilde{\mu}_0} = \lfloor(N_A - 1)/k\rfloor - \Delta_{\tilde{\mu}_0}$. Note that $\Delta_{\tilde{\mu}_0} = \min[\lfloor l_A/2\rfloor, \lfloor(N_A - 1)/k\rfloor]$, $\bar{\Delta}_{\tilde{\mu}_0}$, and $x = (N_A - 1) - k\lfloor(N_A - 1)/k\rfloor$ depend only on N_A and l_A . Thus, for all combinations (N_A, l_A) , Eq. (6.38) gives the range of angular momenta $L_z^A = L_{z,min}^A, \dots, L_{z,min}^A + \ell_{max}$ for which all rows of the larger PEM block \mathbf{P} can be expressed as linear combinations of the rows of the OEM block \mathbf{C} only.

For values of $\ell \leq \ell_{max}$, the proof can be broken into two steps —

1. If $\Delta_{\tilde{\mu}_0} \geq K_{\tilde{\mu}_0}$, then $\Delta_{\tilde{\mu}} \geq K_{\tilde{\mu}}$ for all $(k, 2)$ -admissible partitions $\tilde{\mu} < \tilde{\mu}_0$.
2. If $\Delta_{\mu} \geq K_{\mu}$ for a partition μ , then the row vector labeled by μ in \mathbf{P} can be expressed as a linear combination of row vectors in the OEM \mathbf{C} alone.

We prove these statements rigorously in the Appendices 6.C and 6.D. The first step shows that the $\Delta_{\tilde{\mu}} \geq K_{\tilde{\mu}}$ for all partitions $\tilde{\mu}$ labeling rows of \tilde{P} ; the second assures that all these rows can be written as linear combinations of rows in the OEM alone.

To establish the rank equality between the PEM block \mathbf{P} and the OEM block \mathbf{C} with labels (N_A, L_z^A) , we have to express both the rows and the columns of the PEM block in terms of those of the OEM block. An identical argument as shown above can be repeated for the column vectors. Let $\tilde{\nu}_0$ be the $(k, 2)$ -admissible partition that dominates all partitions of L_z^B into N_B parts. For values of ℓ such that $\Delta_{\tilde{\mu}_0} \geq K_{\tilde{\mu}_0}$ and $\Delta_{\tilde{\nu}_0} \geq K_{\tilde{\nu}_0}$, the OEM and PEM have the same counting in finite-size and $\text{rank}(\mathbf{P}) = \text{rank}(\mathbf{C})$.

The heart of the proof lies in the use of the $(k + 1)$ -clustering condition (6.34) at the z -angular momentum of the k particles in the right-most intact unit cell in part A and one particle occupying an orbital to the right of the cut. This relates a *single* row vector belonging to the PEM block with Δ_μ and K_μ to row vectors with $\Delta_{\mu'} = \Delta_\mu - 1$ and $K_{\mu'} \leq K_\mu - 1$. This relation is obtained by using the clustering operator D_β with

$$\beta = 2k(\Delta_\mu - 1) + \mu_1 \quad (6.39)$$

where μ_1 is the angular momentum of the rightmost particle to the right of the orbital cut. The clustering constraints thus allow us to replace a row vector whose partition has distance K_μ with a linear combination of row vectors whose partitions have distances reduced by *at least* one at the cost of using a *single* intact unit cell. If $\Delta_\mu \geq K_\mu$ for a partition μ , then iterating this procedure provides a linear relation between the row vector labeled by partition μ and row vectors with distance zero, i.e. row vectors of the OEM block \mathbf{C} .

To clarify our statements, we consider the special case of the natural spectrum, $N_A = N_{A,nat} = k\lfloor(l_A + 1)/2\rfloor$, for given l_A . It is straightforward to see that $l_A > 2\lfloor(N_A - 1)/k\rfloor$ and $l_B > 2\lfloor(N_B - 1)/k\rfloor$, so for both the rows and columns ℓ_{max} is given by the third line in Eq. (6.38). For the natural spectrum, the number of intact unit cells in part A is $\Delta_{\tilde{\mu}_0} = N_A/k - 1$; for part B it is $\Delta_{\tilde{\nu}_0} = N_B/k - 1$. Consequently, we can express the rows of the PEM block in terms of rows of the OEM block for values $\ell = 0, \dots, l_A - \lfloor(l_A + 1)/2\rfloor = \lfloor l_A/2 \rfloor$, and the columns for $\ell = 0, \dots, \lfloor l_B/2 \rfloor$. Because we chose $l_A \leq l_B$, the bound from B is always larger or equal to that of A . For $\ell = 0, \dots, N_A/k = \lfloor(l_A + 1)/2\rfloor$, we argued that the PES level counting is universal and equal to the counting of modes of the edge CFT. Thus, we find that $\text{rank}(\mathbf{P}) = \text{rank}(\mathbf{C})$ for $L_z^A - L_{z,min}^A = 0, \dots, \lfloor l_A/2 \rfloor$ and both are identical to the

conformal field theory (CFT) mode counting. We can relate this range to the explicit examples given in Figures 6.2 and 6.4, where the OES and PES level counting is indeed identical for $\ell = 0, \dots, \lfloor 8/2 \rfloor = 4$. The range of angular momenta, for which the ranks are equal, grows linearly with system size, when the ratio l_A/N_ϕ is kept constant. Small deviations from the natural number of particles does not change this picture qualitatively. In general, increasing l_A , while keeping N_A fixed, tends to raise ℓ_{max} , while decreasing l_A tends to lower it.

To analyze how the finite size results carry over to the thermodynamic limit, let us fix the ratios N_A/N and l_A/N_ϕ and let $N \rightarrow \infty$. Because in that case N_A and l_A scale with N , the number of intact unit cells in A (B) in $\tilde{\mu}_0$ ($\tilde{\nu}_0$) denoted by $\Delta_{\tilde{\mu}_0}$ ($\Delta_{\tilde{\nu}_0}$) scales with N as well. There are two different scenarios: (I) If $\bar{\Delta}_{\tilde{\mu}_0}$ and/or $\bar{\Delta}_{\tilde{\nu}_0}$ grow faster than \sqrt{N} , then a closer look at Eq. (6.38) shows that $\ell_{max} \rightarrow -\infty$ in the thermodynamic limit, *i.e.* our method is not applicable. (II) If both $\bar{\Delta}_{\tilde{\mu}_0}$ and $\bar{\Delta}_{\tilde{\nu}_0}$ grow slower than \sqrt{N} , then ℓ_{max} grows linear with system size.

As:

$$\bar{\Delta}_{\tilde{\mu}_0} \sim |N_A - N_{A,nat}|, \quad \bar{\Delta}_{\tilde{\nu}_0} \sim |N_B - N_{B,nat}|,$$

$|N_A - N_{A,nat}|$ must grow *slower* than \sqrt{N} . Thus, if we choose N_A (for fixed l_A/N_ϕ) such that in the thermodynamic limit $|N_A - N_{A,nat}|/\sqrt{N} \rightarrow 0$ — or equivalently $N_A/N_{A,nat} \rightarrow 1$ — then Eq. (6.37) is satisfied for all angular momenta and the counting of the *entire* OES and PES is identical. This proves the bulk edge correspondence in the (N_A, l_A) sectors that are most relevant in the thermodynamic limit. In particular, this includes the usual hemisphere cut ($l_A = \lfloor N_\phi/2 \rfloor$) with $N_A = k \cdot \lfloor N/(2k) \rfloor$ particles. For this choice of (N_A, l_A) , the counting of the OES and the PES is identical for angular momenta range $\ell_{max} = N/k - \lfloor N/(2k) \rfloor - 1 \approx N/(2k)$ for finite size systems. Thus, in the thermodynamic limit, $\ell_{max} \rightarrow \infty$, and the counting of the OES and the PES are identical for all angular momenta.

In this section, we outlined the main steps in the proof relating the level counting of the PES and OES; the details of the proof can be found in the appendices. For finite size systems, Eq. (6.38) (and its counterpart for the column vectors) specifies the range of momenta at fixed (N_A, L_z^A) for which the level counting of the PES and OES are equal. For $N_A/N_{A,nat} \rightarrow 1$, when $N \rightarrow \infty$, this range grows linearly with system size. Hence, for this choice of (N_A, l_A) , the entire level counting of the PES and OES are identical in the thermodynamic limit. For Laughlin states one can prove that the counting of the PES is equal to the mode counting of a chiral massless boson, the CFT describing the edge[64]. Thus, the entire natural spectrum simply counts the number of edge excitations in the thermodynamic limit. We argued in Sec. 6.4 that the same is true for the more complicated ($k > 1$) Read-Rezayi model states; the PES counts the number of modes of the CFT describing the edge. Because of the bulk-edge correspondence in the entanglement spectra shown above, we conclude that the OES counting is equal to the number of modes of the edge CFT if we restrict N_A to be the natural number of particles in A , as specified above. This proves a significant part of the Li-Haldane conjecture[123].

6.6.3 Illustrative examples

The proof of the full method is presented in the appendices; here we illustrate the more formal ideas with examples of the general method at work for the $k = 1, 2$ wave functions.

At $k = 1$:

Consider the $\nu = 1/2$ Laughlin state of $N = 7$ bosons with $N_\phi = 12$ and $L_z^{tot} = 42$. Let $l_A = 6$ and the number of particles in A be the natural number $N_A = N_{A,nat} = 3$. We consider the entanglement level counting of the OES and the PES at $L_z^A = L_{z,min} + \ell = L_{z,min} + 3$. We first verify that the conditions, $\Delta_{\tilde{\mu}_0} \geq K_{\tilde{\mu}_0}$ and $\Delta_{\tilde{\nu}_0} \geq K_{\tilde{\nu}_0}$, are satisfied.

The occupation configurations of $\tilde{\mu}_0$ and $\tilde{\nu}_0$ are:

$$\begin{aligned} n(\tilde{\mu}_0) &= \{101000 | 0100000\} & K_{\tilde{\mu}_0} = 2, \Delta_{\tilde{\mu}_0} = 2 \\ n(\tilde{\nu}_0) &= \{000100 | 0010101\} & K_{\tilde{\nu}_0} = 3, \Delta_{\tilde{\nu}_0} = 3 \end{aligned}$$

The cut in orbital space is indicated in the occupation configurations by the ‘|’ symbol. Hence, the method discussed in the previous section should prove the equality of the ranks of the OEM and the PEM at this L_z^A .

The occupation configurations of the $(1, 2)$ -admissible partitions labeling the rows of $\tilde{\mathbf{P}}$ are:

$$\begin{aligned} n(\tilde{\mu}_0) &= \{101000 | 010 \dots 0\} & K_{\tilde{\mu}_0} = 2, \Delta_{\tilde{\mu}_0} = 2 \\ n(\tilde{\mu}_1) &= \{100100 | 100 \dots 0\} & K_{\tilde{\mu}_1} = 1, \Delta_{\tilde{\mu}_1} = 1 \\ n(\tilde{\mu}_2) &= \{010101 | 000 \dots 0\} & K_{\tilde{\mu}_2} = 0, \Delta_{\tilde{\mu}_2} = 0. \end{aligned}$$

$\tilde{\mu}_2$ labels a row that already belongs to the OEM block \mathbf{C} . We now relate the row labeled by the partition $\tilde{\mu}_1$ to rows of the OEM block. In $n(\tilde{\mu}_1)$, only the 0th unit cell is intact and the particle to the right of the cut occupies the orbital with index 6. Following Eq. (6.39) we pick the 2-body clustering constraint at $\beta = 6$ (the sum of the z -angular momenta of the particle in the intact unit cell and the particle to the right of the cut) in Eq. (6.34):

$$(2(d_0d_6 + d_1d_5 + d_2d_4) + d_3d_3)|\psi\rangle = 0 \tag{6.40}$$

For every occupation number configuration of $(N-2)$ bosons with angular momentum $(L_z^{tot} - \beta)$, Eq (6.40) gives one linear relation. The appropriate occupation number

configuration for our purpose is $n([3] + \nu_j)$, as:

$$d_0 d_6 (|\tilde{\mu}_1 + \nu_j\rangle) = |[3] + \nu_j\rangle. \quad (6.41)$$

The partitions ν_j of L_z^B into $N_B = 4$ parts label the columns of the PEM \mathbf{P} . Eq. (6.40) then relates the row indexed by $\tilde{\mu}_1$ to row vectors indexed by following partitions:

$$\begin{aligned} n(\mu_1) &= \{010101 | 000 \dots 0\} & K_{\mu_1} = 0, \Delta_{\mu_1} = 0 \\ n(\mu_2) &= \{001110 | 000 \dots 0\} & K_{\mu_2} = 0, \Delta_{\mu_2} = 0 \\ n(\mu_3) &= \{000300 | 000 \dots 0\} & K_{\mu_3} = 0, \Delta_{\mu_3} = 0. \end{aligned}$$

At every column index j , the explicit relation from Eq. (6.40) is:

$$2(\tilde{\mathbf{P}}_{1j} + \mathbf{P}_{1j} + \mathbf{P}_{2j}) + \mathbf{P}_{3j} = 0, \quad (6.42)$$

where \mathbf{P}_{ij} is the coefficient in \mathbf{P} of the row labeled by μ_i and column labeled by ν_j . We have thus related a row indexed by a partition $\tilde{\mu}_1$ with $K_{\tilde{\mu}_1} = 1$ and $\Delta_{\tilde{\mu}_1} = 1$ to rows indexed by partitions μ_1, μ_2, μ_3 with distance from the cut reduced by 1 and number of intact unit cells in A reduced by 1. These partitions label rows in the OEM in this example. A similar procedure, using the additional clustering constraint at $\beta = 9$, involving the particles in the orbitals of angular momenta 2 and 7, can be used to relate the row of $\tilde{\mathbf{P}}$ indexed by the partition $\tilde{\mu}_0$ to rows in the OEM.

At $k = 2$:

Let us now consider the Moore-Read state with $N = 18$, $N_\phi = 16$, and $L_z^{tot} = 144$ and perform an orbital cut after $l_A = 7$ orbitals. Here, we are interested in relating the rows of the PEM block to the rows of the OEM block for $N_A = 8$ at $L_z^A = L_{z,min}^A + \ell =$

$L_{z,min}^A + 3$. The occupation number configurations of $\tilde{\mu}_0$ and $\tilde{\nu}_0$ are:

$$\begin{aligned} n(\tilde{\mu}_0) &= \{2020201 \mid 00100000\} & K_{\tilde{\mu}_0} = 3, \Delta_{\tilde{\mu}_0} = 3 \\ n(\tilde{\nu}_0) &= \{0000010 \mid 01020202\} & K_{\tilde{\nu}_0} = 2, \Delta_{\tilde{\nu}_0} = 3, \end{aligned}$$

where we indicate the orbital cut by the '|' symbol. Thus, $\Delta_{\tilde{\mu}_0} \geq K_{\tilde{\mu}_0}$ and $\Delta_{\tilde{\nu}_0} \geq K_{\tilde{\nu}_0}$, and we can relate all rows and columns of the PEM to ones in the OEM.

The occupation configurations of the (2, 2)-admissible partitions labeling the rows of $\tilde{\mathbf{P}}$ are given by:

$$\begin{aligned} n(\tilde{\mu}_0) &= \{2020201 \mid 0010 \dots 0\} & K_{\tilde{\mu}_0} = 3, \Delta_{\tilde{\mu}_0} = 3 \\ n(\tilde{\mu}_1) &= \{2020200 \mid 1100 \dots 0\} & K_{\tilde{\mu}_1} = 3, \Delta_{\tilde{\mu}_1} = 3 \\ n(\tilde{\mu}_2) &= \{2020111 \mid 0100 \dots 0\} & K_{\tilde{\mu}_2} = 2, \Delta_{\tilde{\mu}_2} = 2 \\ n(\tilde{\mu}_3) &= \{2020110 \mid 2000 \dots 0\} & K_{\tilde{\mu}_3} = 2, \Delta_{\tilde{\mu}_3} = 2 \\ n(\tilde{\mu}_4) &= \{2011111 \mid 1000 \dots 0\} & K_{\tilde{\mu}_4} = 1, \Delta_{\tilde{\mu}_4} = 1. \end{aligned}$$

The trailing 0's in every occupation configuration indicate that the orbitals with $L_z = 10, \dots, 16$ are unoccupied in the partitions labeling the rows of $\tilde{\mathbf{P}}$. $\Delta_{\tilde{\mu}_i} \geq K_{\tilde{\mu}_i}$ is satisfied for all $i = 0, \dots, 4$, as required in step 1 in Sec. 6.6.2.

We illustrate the use of the 3-body clustering constraints by relating the row labeled by the partition $\tilde{\mu}_3$ to rows labeled by partitions μ_j with distance $K_{\mu_j} = 1$ from the cut. The first unit cell is the rightmost intact unit cell in A in $n(\tilde{\mu}_3)$. Consider the 3-body clustering condition at β equal to the z -angular momentum of the 2 particles in the rightmost intact unit cell and a particle to the right of the cut, i.e. at $\beta = 11 = 2 \times 2 + 7$ (see Eq. (6.39)). It is beneficial to divide the clustering

condition (6.34) into two terms:

$$3 \left(D_{11}^{(1)} + D_{11}^{(2)} \right) |\psi\rangle = 0 \quad (6.43)$$

$$D_{11}^{(1)} = d_2 d_2 d_7 + 2d_2 d_3 d_6 + 2d_2 d_4 d_5 + d_3 d_3 d_5 + d_3 d_4 d_4$$

$$D_{11}^{(2)} = d_0 d_0 d_{11} + 2d_0 d_1 d_{10} + 2d_0 d_2 d_9 + \dots, \quad (6.44)$$

where $D_{11}^{(2)}$ contains all terms involving angular momentum orbitals 0 and/or 1.

The clustering constraints in Eq. (6.43) yield a linear relation between certain coefficients in $|\psi\rangle$, for each occupation number configuration of the remaining $N - 3$ particles. We choose the configurations $n([7, 5, 4, 0, 0] + \nu_j)$, as:

$$|[7, 5, 4, 0, 0] + \nu_j\rangle = d_2 d_2 d_7 (|\tilde{\mu}_3 + \nu_j\rangle), \quad (6.45)$$

where the $|\nu_j\rangle$ label the column vectors of the PEM block. Note that $d_2 d_2 d_7$ is the only term in $D_{11}^{(1)}$ that contains the angular momentum 7 orbital; all other terms have highest angular momentum less or equal 6, and thus smaller distance to the cut. Equivalently we can note that as D_{11}^1 annihilates any configuration with an occupied orbital of z -angular momentum greater than 7, the first term in Eq. (6.43) relates the row labeled by $\tilde{\mu}_3$ only to rows labeled by partitions that are dominated by $\tilde{\mu}_3$:

$$\begin{aligned} n(\mu_1) &= \{2011111 | 1000 \dots 0\} & K_{\mu_1} = 1, \Delta_{\mu_1} = 1 \\ n(\mu_2) &= \{2010220 | 1000 \dots 0\} & K_{\mu_2} = 1, \Delta_{\mu_2} = 1 \\ n(\mu_3) &= \{2002120 | 1000 \dots 0\} & K_{\mu_3} = 1, \Delta_{\mu_3} = 1 \\ n(\mu_4) &= \{2001310 | 1000 \dots 0\} & K_{\mu_4} = 1, \Delta_{\mu_4} = 1. \end{aligned}$$

All the partitions above have one less intact unit cell, and smaller distance $K_{\mu_j} = K_{\tilde{\mu}_3} - 1$ from the cut as compared to $\tilde{\mu}_3$.

The second operator in the clustering condition Eq. (6.43) acts on states with occupation number configurations such as:

$$\begin{aligned}
& \{4000110 \mid 100010 \dots 0\} \\
& \{3100110 \mid 100100 \dots 0\} \\
& \{3010110 \mid 101000 \dots 0\} \\
& \{3001110 \mid 110000 \dots 0\}. \\
& \qquad \qquad \qquad \vdots
\end{aligned}$$

All the above configurations have distance from the cut larger than $K_{\tilde{\mu}_3} = 2$, and *more than 2 particles* in angular momentum orbitals 0 and 1. Hence, they are not dominated by the root partition λ_0 , and have zero weight in the model wave function (the corresponding row in the PEM is identically 0).

Thus, the clustering condition at $\beta = 11$ for the configuration of the remaining particles being $n([7, 5, 4, 0, 0] + \nu_j)$, yields a linear relation between the row labeled by $\tilde{\mu}_3$ and the rows labeled by the partitions μ_1, \dots, μ_4 :

$$\tilde{\mathbf{P}}_{3j} + 2\mathbf{P}_{1j} + 2\mathbf{P}_{2j} + \mathbf{P}_{3j} + \mathbf{P}_{4j} = 0, \tag{6.46}$$

where \mathbf{P}_{ij} is the coefficient in \mathbf{P} in the row labeled by μ_i and column labeled by ν_j . The rows labeled by μ_1, \dots, μ_4 can in turn be related to rows in the OEM by using the clustering constraints at $\beta = 7$.

6.7 Concluding remarks

In this chapter, we have provided a proof that the Li and Haldane natural entanglement spectrum in the thermodynamic limit is bounded from above by the number of levels in the edge energy spectrum. Barring the presence of extra accidental symme-

tries in the system, we argue that the bound should be saturated. In addition, we showed that the two different entanglement spectra we considered— the PES probing the bulk excitations and the OES probing the edge excitations— are related. In fact, they have the same entanglement level counting for a range of angular momenta, specified by Eq. (6.38). The universal counting is different for each model state and provides valuable information about the topological order in the FQH state. When restricting to the natural spectrum, we have proved that in the thermodynamic limit, the level counting of the entire OES and PES are identical. Thus, we established the bulk-edge correspondence in the entanglement spectra. The main tool in proving this are the clustering constraints, which enforce the defining clustering properties of the model states in momentum space. Our method works for both unitary and non-unitary states that are defined as unique highest density zero-modes of Haldane pseudopotential Hamiltonians. In particular, it can be applied to the entire Read-Rezayi series, as well as the Gaffnian state.

6.A Rank of $\tilde{\mathbf{P}}$

6.A.1 $(k, 2)$ -clustering states

The matrices $\tilde{\mathbf{P}}$ and \mathbf{M} were defined in Sec. 6.4 as the particle entanglement matrices with label L_z^A in the $(k, 2)$ -admissible occupation configuration basis and the Jack basis. In Sec. 6.4, we showed that the PEM and \mathbf{M} have the same counting; in this appendix, we show that $\tilde{\mathbf{P}}$ and \mathbf{M} have the same rank. This proves that the counting of the PEM equals the rank of $\tilde{\mathbf{P}}$.

Suppose we are able to show that $\tilde{\mathbf{P}} = \mathbf{DMD}'$, where \mathbf{D}^T and \mathbf{D}' are square triangular matrices with 1's on the diagonal and as such they have nonzero determinant. A theorem in linear algebra states that pre/post multiplying a matrix by one of

triangular form with nonzero determinant leaves its rank unchanged. Thus, we only need to prove that $\tilde{\mathbf{P}} = \mathbf{DMD}'$ to conclude that $\text{rank}(\tilde{\mathbf{P}}) = \text{rank}(\mathbf{M})$.

The row and column dimensions of $\tilde{\mathbf{P}}$ and \mathbf{M} are identical because every $(k, 2)$ -admissible partition μ labels the Jack J_μ^α . We may use partial ordering by dominance to order the $(k, 2)$ -admissible row and column configurations such that if $\tilde{\mu}_k > \tilde{\mu}_i$, then $k \leq i$.

Consider a particular $(k, 2)$ -admissible partition $\tilde{\mu}_i$ ($\tilde{\nu}_j$) labeling the i th row (j th column) of $\tilde{\mathbf{P}}$ and \mathbf{M} . Let the coefficient of $|\tilde{\mu}_i\rangle$ in $|J_{\tilde{\mu}_k}^\alpha\rangle$ be \mathbf{D}_{ik} and the coefficient of $|\tilde{\nu}_j\rangle$ in $|J_{\tilde{\nu}_l}^\alpha\rangle$ be \mathbf{D}'_{lj} . The partial ordering implies that:

$$\mathbf{D}_{ik} = 0 \text{ if } k > i \quad (6.47)$$

$$\mathbf{D}_{ii} = 1 \quad (6.48)$$

$$\mathbf{D}'_{lj} = 0 \text{ if } l > j \quad (6.49)$$

$$\mathbf{D}'_{jj} = 1. \quad (6.50)$$

In other normalizations of Jack polynomials, \mathbf{D}_{ii} is not necessarily one, but is always non-zero. By the definition of a matrix with row-echelon form, \mathbf{D}^T and \mathbf{D}' in row-echelon form. Recall that:

$$\sum_{i,j} \mathbf{M}_{ij} |J_{\tilde{\mu}_i}^\alpha\rangle \otimes |J_{\tilde{\nu}_j}^\alpha\rangle = \sum_{i,j} \mathbf{P}_{ij} |\mu_i\rangle \otimes |\nu_j\rangle \quad (6.51)$$

in every block of the full PEM. $|\mu_i\rangle$ and $|\nu_j\rangle$ are the general occupation-basis states, not just the $(k, 2)$ -admissible configurations. $\tilde{\mathbf{P}}$ is the sub-matrix of \mathbf{P} labeled by $(k, 2)$ -admissible partitions; therefore:

$$\begin{aligned} \tilde{\mathbf{P}}_{ij} &= \sum_{k,l} \mathbf{M}_{kl} \langle \tilde{\mu}_i | J_{\tilde{\mu}_k}^\alpha \rangle \langle \tilde{\nu}_j | J_{\tilde{\nu}_l}^\alpha \rangle \\ \text{i.e. } \tilde{\mathbf{P}}_{ij} &= \sum_{k,l} \mathbf{D}_{ik} \mathbf{M}_{kl} \mathbf{D}'_{lj} \end{aligned} \quad (6.52)$$

$$\Rightarrow \tilde{\mathbf{P}} = \mathbf{DMD}', \quad (6.53)$$

which proves our statement that the rank of the PEM is given by the rank of the matrix of the coefficients indexed by the $(k, 2)$ -admissible partitions.

6.B Two examples of clustering constraints

We write down the explicit relations imposed by the $(k+1)$ -body clustering constraints discussed in Sec. 6.5 on the coefficients of small wave functions at $k = 1, 2$. Let us first consider an example at $k = 1$, i.e. the $1/2$ Laughlin states. The clustering constraints are 2-body:

$$\sum_{i=0}^{\beta} d_{\beta-i} d_i |\psi\rangle = 0, \quad \text{for } \beta = 0, 1, \dots, L_z^{tot}. \quad (6.54)$$

Consider the $N = 3$, $L_z^{tot} = 6$ wave function in the infinite plane geometry in which the number of orbitals is not restricted to $N_\phi + 1 = 5$ as in the case of the sphere. The Hilbert space is spanned by 7 partitions, $\{\lambda_i, i = \dots 7\}$. Their corresponding coefficients in $|\psi\rangle$ are $\{b_i, i = 1 \dots 7\}$:

$$|\psi\rangle = b_1|6, 0, 0\rangle + b_2|5, 1, 0\rangle + b_3|4, 2, 0\rangle + b_4|3, 3, 0\rangle + b_5|4, 1, 1\rangle + b_6|3, 2, 1\rangle + b_7|2, 2, 2\rangle.$$

The relations at $\beta = 0, 1$ respectively are:

$$b_1|6, 0, 0\rangle = 0 \Rightarrow b_1 = 0$$

$$b_2|5, 1, 0\rangle = 0 \Rightarrow b_2 = 0.$$

Thus, the clustering constraints assign zero weight to λ_1 and λ_2 , which are not dominated by the root partition $\lambda_3 = [4, 2, 0]$ ($n(\lambda_3) = \{10101\}$). The values of β from

2 to 6 generate a set of 5 linearly dependent equations that fix 4 out of the 5 remaining coefficients. All the relations obtained are shown in Table 6.1. The solution in terms of the coefficient of the root partition b_3 is $\{b_1, b_2, b_3, b_4, b_5, b_6, b_7\} = \{0, 0, b_3, -2b_3, -2b_3, 2b_3, -6b_3\}$.

Table 6.1: Possible occupation configurations and the clustering constraints for the $N = 3, \nu = 1/2$ Laughlin state at $L_z^{tot} = 6$ on the infinite plane (no restriction to the number of orbitals). On the sphere the first two configurations have zero weight and the last two orbitals are missing as $N_\phi = 4$

Coefficient of m_μ	$n(\mu)$		Constraint
b_1	{2000001}	$\beta = 0:$	$b_1 = 0$
b_2	{1100010}	$\beta = 1:$	$b_2 = 0$
b_3	{1010100}	$\beta = 2:$	$2b_3 + b_5 = 0$
b_4	{1002000}	$\beta = 3:$	$b_4 + b_6 = 0$
b_5	{0200100}	$\beta = 4:$	$2b_6 + 2b_3 + b_7 = 0$
b_6	{0111000}	$\beta = 5:$	$b_5 + b_6 = 0$
b_7	{0030000}	$\beta = 6:$	$2b_3 + b_4 = 0$

The bosonic Moore-Read state is the clustering polynomial at $k = 2$. The clustering constraints involve 3 particles:

$$\sum_{i,j=0}^{\beta} d_{\beta-i-j} d_i d_j |\psi\rangle = 0, \quad \text{for } \beta = 0, 1, \dots, L_z^{tot}. \quad (6.55)$$

Consider the 6-particle wave function with $L_z^{tot} = 12$. Eq. (6.55) for $\beta = 0$ ensures that the weight of the partitions $[4, 4, 4, 0, 0, 0], [5, 4, 3, 0, 0, 0] \dots [12, 0, 0, 0, 0, 0]$ not dominated by $[4, 4, 2, 2, 0, 0]$ is zero in the wave function. The number of such partitions whose coefficients are set to zero at $\beta = 0$ is the number of partitions of 12 into at most 3 parts. Similarly, the constraints at $\beta = 1$ set the weights of the partitions $[4, 4, 3, 1, 0, 0], [5, 4, 2, 1, 0, 0], \dots [11, 1, 0, 0, 0, 0]$ (the number of such partitions is the number of partitions of 11 into at most 3 parts) in the wave function to zero. The linear dependence of the set of constraints in Eq. (6.55) is apparent in the fact that the coefficient of the partition $[7, 4, 1, 0, 0, 0]$ is set to zero by a constraint at $\beta = 0$ and one at $\beta = 1$. The constraints at $\beta = 11, 12$ are also seen to give identical relations to those at $\beta = 0, 1$ for this example. The configurations $[5, 4, 3, 0, 0, 0] \dots [12, 0, 0, 0, 0, 0]$

are only allowed in an infinite plane geometry. On the sphere, they would involve more orbitals than $N_\phi + 1 = 5$ existent ones and would not appear in the Hilbert space of the decomposition of the Moore-Read ground-state. The configurations $[4, 4, 4, 0, 0, 0]$ and $[4, 4, 3, 1, 0, 0]$ appear on the sphere but, due to the same reason as on the infinite plane – that they are not squeezed from the root partition – have zero weight.

The 16 partitions dominated by the root partition $[4, 4, 2, 2, 0, 0]$ and their corresponding coefficients in ψ are shown in the second and first column of Table 6.2 respectively. Let us discuss the 3-body clustering at $\beta = 4$ in more detail:

$$3(d_4d_0d_0 + 2d_3d_1d_0 + d_2d_2d_0 + d_2d_1d_1)|\psi\rangle = 0. \quad (6.56)$$

The four terms in Eq. (6.56) individually are:

$$\begin{aligned} d_4d_0d_0|\psi\rangle &= b_1|4, 2, 2\rangle + b_3|3, 3, 2\rangle \\ d_3d_1d_0|\psi\rangle &= b_6|4, 3, 1\rangle + b_7|4, 2, 2\rangle + b_8|3, 3, 2\rangle \\ d_2d_2d_0|\psi\rangle &= b_1|4, 4, 0\rangle + b_7|4, 3, 1\rangle + b_{12}|4, 2, 2\rangle \\ &\quad + b_{11}|3, 3, 2\rangle \\ d_2d_1d_1|\psi\rangle &= b_2|4, 4, 0\rangle + b_9|4, 3, 1\rangle + b_{10}|4, 2, 2\rangle \\ &\quad + b_{14}|3, 3, 2\rangle. \end{aligned} \quad (6.57)$$

The right-hand-side of each of the four terms above is a linear combination of different occupation configurations of 3 bosons with total angular momentum $L_z^{tot} - \beta = 8$. Since different occupation configuration states are orthogonal to each other, Eq. (6.56) can only be satisfied if the coefficient in front of every non-interacting many-body state is zero. Thus, we obtain four constraints on the coefficients from each of the

four occupation configurations in Eq. (6.57):

$$\begin{aligned}
|4, 2, 2\rangle : b_1 + 2b_7 + b_{12} + b_{10} &= 0 \\
|3, 3, 2\rangle : b_3 + 2b_8 + b_{11} + b_{14} &= 0 \\
|4, 3, 1\rangle : 2b_6 + b_7 + b_9 &= 0 \\
|4, 4, 0\rangle : b_1 + b_2 &= 0.
\end{aligned} \tag{6.58}$$

The last relation also arises from the clustering constraint at $\beta = 2$.

All the relations imposed by the clustering constraints at $\beta = 2, \dots, 6$ are shown in Table 6.2. Although not obvious, in this case as in the previous, the dimension of the null space of Eq. (6.55) is 1. This can be analytically proved by realizing that the Moore-Read state is the densest unique ground-state of a Haldane pseudopotential Hamiltonian which can be written in terms of the clustering operators

Table 6.2: Possible occupation configurations and the clustering constraints for the $N = 6$ Moore-Read state at $L_z^{tot} = 12$

	$n(\mu)$	Constraint
b_1	{20202}	$\beta = 2:$ $b_1 + b_2 = 0$ $b_3 + b_6 = 0$
b_2	{12102}	
b_3	{20121}	$\beta = 3:$ $3b_3 + 6b_7 + b_9 = 0$ $3b_4 + 6b_8 + b_{13} = 0$ $6b_2 + b_5 = 0$
b_4	{20040}	
b_5	{04002}	
b_6	{12021}	$\beta = 4:$ $b_1 + 2b_7 + b_{10} + b_{12} = 0$ $b_3 + 2b_8 + b_{11} + b_{14} = 0$ $2b_6 + b_7 + b_9 = 0$
b_7	{11211}	
b_8	{11130}	
b_9	{03111}	$\beta = 5:$ $2b_2 + 2b_7 + b_9 + b_{10} = 0$ $2b_7 + 2b_{11} + b_{14} + b_{15} = 0$ $2b_6 + 2b_8 + b_{13} + b_{14} = 0$ $2b_3 + b_6 + b_7 = 0$
b_{10}	{02301}	
b_{11}	{10320}	
b_{12}	{10401}	$\beta = 6:$ $6b_1 + 3b_2 + 6b_7 + 3b_3 + b_{12} = 0$ $6b_2 + 3b_5 + 6b_9 + 3b_6 + b_{10} = 0$ $6b_3 + 3b_6 + 6b_8 + 3b_4 + b_{11} = 0$ $6b_7 + 3b_9 + 6b_{14} + 3b_8 + b_{15} = 0$ $6b_{12} + 3b_{10} + 6b_{15} + 3b_{11} + b_{16} = 0$
b_{13}	{03030}	
b_{14}	{02220}	
b_{15}	{01410}	
b_{16}	{00600}	

6.C Proof of step 1 Sec. 6.6.2

We now prove the statement in step 1 of Section 6.6.2— $K_{\tilde{\mu}_0} \leq \Delta_{\tilde{\mu}_0}$ implies that $K_{\tilde{\mu}} \leq \Delta_{\tilde{\mu}}$ for all $(k, 2)$ -admissible partitions $\tilde{\mu}$ that are dominated by $\tilde{\mu}_0$. We defined $\tilde{\mu}_0$ to be the partition that dominates all other $(k, 2)$ -admissible partitions at given N_A, L_z^A , (Eq. (6.36)):

$$n(\tilde{\mu}_0) = \underbrace{k0 \dots k0}_{2\lfloor(N_A-1)/k\rfloor} \underbrace{x0 \dots 01}_{\ell} 0 \dots 0, \quad (6.59)$$

where $0 \leq x < k$ is fixed by the total particle number being N_A . We are given that $\Delta_{\tilde{\mu}_0} \geq K_{\tilde{\mu}_0}$.

The main idea how to prove this statement is to reduce the distance from the cut by squeezing particles across the cut. Squeezing with the particle just left to the cut— at angular momentum $(l_A - 1)$ — cannot reduce the distance, but squeezing with any other particle to the left of the cut does. Let us in the following only consider squeezing operations from orbitals with index $m_1 \geq l_A$ and $m_2 < l_A - 1$ to orbitals with index $m'_1 = m_1 - 1$ and $m'_2 = m_2 + 1$. Starting from a $(k, 2)$ -admissible partition, there are two choices to reduce the distance to the cut by one and still retain $(k, 2)$ -admissibility: either one squeezes with a particle of the rightmost unit cell, which reduces the number of unit cells by one, or one squeezes with a particle that is not in an intact unit cell. The latter may retain $(k, 2)$ -admissibility, depending on the occupation configuration of the remaining particles, and does not change the number of intact unit cells. All $(k, 2)$ -admissible configurations $\tilde{\mu}' < \tilde{\mu}_0$ can be obtained from $\tilde{\mu}_0$ by such a series of squeezings. As $K_{\tilde{\mu}_0} \leq \Delta_{\tilde{\mu}_0}$, they obey $K_{\tilde{\mu}'} \leq \Delta_{\tilde{\mu}'}$. Let us make this argument more rigorous in the following paragraphs.

The case when $K_{\tilde{\mu}_0} = 0$ is trivial. All $(k, 2)$ -admissible partitions have distance from the cut 0 and at least 0 intact unit cells; therefore $K_{\tilde{\mu}} \leq \Delta_{\tilde{\mu}}$ for all $(k, 2)$ -admissible partitions $\tilde{\mu}$.

In order to prove the required statement for $K_{\tilde{\mu}_0} > 0$, we consider all $(k, 2)$ -admissible partitions $\tilde{\mu} < \tilde{\mu}_0$ at given, but arbitrary $K_{\tilde{\mu}} < K_{\tilde{\mu}_0}$. Let us construct the partition μ (not necessarily $(k, 2)$ -admissible) at the given distance $K_{\tilde{\mu}} = K_{\mu} > 0$ that is dominated by all the $(k, 2)$ -admissible partitions. This partition can always be obtained by first reducing the distance to the cut $K_{\tilde{\mu}_0} - K_{\tilde{\mu}}$ times, by squeezing each time with a particle from the rightmost intact unit cell, and afterwards squeezing all the particles at angular momenta $\geq (l_A - 1)$ to their maximally dense configuration. The latter operation does not change the distance from the cut. Assume that the orbital to the left of the cut is unoccupied, i.e. $n_{l_A-1}(\tilde{\mu}_0) = 0$. If the number of particles to the right of the cut in $\tilde{\mu}_0$, $N_r(\tilde{\mu}_0)$, is equal to one then the occupation number configuration of μ is given by:

$$n(\mu) = \underbrace{k0 \dots k0}_{2\Delta_{\mu}} \underbrace{(k-1)1 \dots (k-1)1}_{2(\Delta_{\tilde{\mu}_0} - \Delta_{\mu})} \underbrace{x0 \dots 0}_{l_A - 2\Delta_{\tilde{\mu}_0}} | \underbrace{0 \dots 01}_{K_{\mu}}, \quad (6.60)$$

where we denote the orbital cut by ‘|’ in the occupation configuration. For $N_r(\tilde{\mu}_0) > 1$, $n(\mu)$ is:

$$n(\mu) = \underbrace{k0 \dots k0}_{2\Delta_{\mu}} \underbrace{(k-1)1 \dots (k-1)1(k-1)0}_{2(\Delta_{\tilde{\mu}_0} - \Delta_{\mu})} | X \dots X, \quad (6.61)$$

where the sequence $X \dots X$ denotes the occupation configuration of $(N_r(\tilde{\mu}_0) + 1)$ particles at distance K_{μ} that is maximally squeezed.

The configurations in Eq. (6.60) and (6.61) are such that the particles on the left of the cut form the densest possible $(k, 2)$ -admissible configuration, *ie.* squeezing any two particles on the left of the cut yields a configurations that is not $(k, 2)$ -admissible. As the particles to the right are in their most squeezed configuration, we conclude that any $(k, 2)$ -admissible partition with distance to the cut K_{μ} dominates μ .

As compared to $n(\tilde{\mu}_0)$, the z -angular momentum of the particles to the left of the cut in $n(\mu)$ is increased by $\Delta_{\tilde{\mu}_0} - \Delta_\mu$, while that of the particles to the right of the cut is reduced by $K_{\tilde{\mu}_0} - K_{\tilde{\mu}}$. Since $n(\mu)$ has the same total z -angular momentum as $n(\tilde{\mu}_0)$:

$$\begin{aligned}\Delta_{\tilde{\mu}_0} - \Delta_\mu &= K_{\tilde{\mu}_0} - K_\mu \\ \Delta_{\tilde{\mu}_0} \geq K_{\tilde{\mu}_0} &\Rightarrow \Delta_\mu \geq K_\mu.\end{aligned}$$

As every $(k, 2)$ -admissible partition $\tilde{\mu}$ with distance $K_{\tilde{\mu}} = K_\mu$ that dominates μ has *at least* Δ_μ intact unit cells:

$$\Delta_{\tilde{\mu}} \geq \Delta_\mu, \quad K_{\tilde{\mu}} = K_\mu \quad \Rightarrow \quad \Delta_{\tilde{\mu}} \geq K_{\tilde{\mu}} \quad (6.62)$$

at every distance from the cut.

The argument for $n_{l_A-1}(\tilde{\mu}_0) \neq 0$ is identical to the one described above. The only difference lies in the form of $n(\mu)$:

$$n(\mu) = \underbrace{k0 \dots k0}_{2\Delta_\mu} \underbrace{(k-1)1 \dots (k-1)10}_{2(\Delta_{\tilde{\mu}_0} - \Delta_\mu)} | X \dots X, \quad (6.63)$$

where the sequence $X \dots X$ is the maximally squeezed configuration of $x+1$ particles (for $N_r(\tilde{\mu}_0) = 1$) respectively $k + N_r(\tilde{\mu}_0)$ (for $N_r(\tilde{\mu}_0) > 1$) at distance K_μ .

6.D Proof of step 2 in Sec. 6.6.2

6.D.1 Effect of dominance on the distance from the cut

We show that dominance, *i.e.* $\mu > \mu'$ implies that the distance to the cut $K_\mu \geq K_{\mu'}$, or that squeezing cannot increase the distance from the cut. The property of dominance

is defined by:

$$\mu > \mu' \Rightarrow \sum_{i=1}^n \mu_i \geq \sum_{i=1}^n \mu'_i \quad (6.64)$$

for all $n \leq N$. Recall that $\mu_i \geq \mu_j$ for $i < j$, where μ_i and μ_j are the components of the partition μ . Let us denote the number of particles to the right of the cut for any partition μ by $N_r(\mu)$. The distance from the cut K_μ can then be rewritten as:

$$\begin{aligned} K_\mu &= \sum_{m=l_A}^{N_\phi} n_m(\mu)(m - l_A + 1) \\ &= \sum_{i=1}^{N_r(\mu)} (\mu_i - l_A + 1). \end{aligned} \quad (6.65)$$

When comparing the total distances for two partitions, μ and μ' , there are three possibilities, $N_r(\mu) = N_r(\mu')$, $N_r(\mu) > N_r(\mu')$ and $N_r(\mu) < N_r(\mu')$. We will discuss them in that order:

- $N_r(\mu) = N_r(\mu')$:

$$\begin{aligned} \mu > \mu' &\Rightarrow \sum_{i=1}^{N_r(\mu)} \mu_i \geq \sum_{i=1}^{N_r(\mu)} \mu'_i \\ &\Rightarrow \underbrace{\sum_{i=1}^{N_r(\mu)} (\mu_i - l_A + 1)}_{=K_\mu} \geq \underbrace{\sum_{i=1}^{N_r(\mu)} (\mu'_i - l_A + 1)}_{=K_{\mu'}} \end{aligned} \quad (6.66)$$

Thus, $K_\mu \geq K_{\mu'}$.

- $N_r(\mu) > N_r(\mu')$:

$$\mu > \mu' \Rightarrow \sum_{i=1}^{N_r(\mu')} \mu_i \geq \sum_{i=1}^{N_r(\mu')} \mu'_i$$

$$\Rightarrow \sum_{i=1}^{N_r(\mu')} (\mu_i - l_A + 1) \geq \underbrace{\sum_{i=1}^{N_r(\mu')} (\mu'_i - l_A + 1)}_{=K_{\mu'}}. \quad (6.67)$$

As $\mu_i \geq l_A$ for all particles to the right of the cut, $K_\mu = \sum_{i=1}^{N_r(\mu)} (\mu_i - l_A + 1) > \sum_{i=1}^{N_r(\mu')} (\mu_i - l_A + 1)$. This shows that $K_\mu > K_{\mu'}$.

- $N_r(\mu) < N_r(\mu')$:

$$\begin{aligned} \mu > \mu' &\Rightarrow \sum_{i=1}^{N_r(\mu')} \mu_i \geq \sum_{i=1}^{N_r(\mu')} \mu'_i \\ &\Rightarrow \underbrace{\sum_{i=1}^{N_r(\mu)} (\mu_i - l_A + 1)}_{=K_\mu} + \underbrace{\sum_{i=N_r(\mu)+1}^{N_r(\mu')} (\mu_i - l_A + 1)}_{\leq 0} \\ &\geq \sum_{i=1}^{N_r(\mu')} (\mu'_i - l_A + 1) = K_{\mu'}. \end{aligned} \quad (6.68)$$

The second term must be ≤ 0 , as the particles to the left of the cut have angular momentum $\mu_i < l_A$. It is strictly negative if at least one of the μ_i for $N_r(\mu) < i \leq N_r(\mu')$ is smaller than $(l_A - 1)$.

Thus, $K_\mu \geq K_{\mu'}$ for every μ' that is dominated by μ .

6.D.2 Effect of clustering constraints

We show that the $(k + 1)$ -body clustering constraints presented in the body of the paper (Eq. (6.34)) relate partitions μ with $\Delta_\mu > 0$ intact unit cells and distance $K_\mu > 0$ from the cut to partitions μ' with number of intact unit cells given by $\Delta_\mu - 1$ and distance from the cut by $K_{\mu'} < K_\mu$.

Let us consider an arbitrary partition μ with Δ_μ intact unit cells ($2\Delta_\mu$ orbitals) and distance K_μ :

$$n(\mu) = \{ \underbrace{k0 \dots k0}_{2\Delta_\mu} \underbrace{x \dots x}_{l_A - 2\Delta_\mu} \mid \underbrace{x \dots x}_{\leq K_\mu} 0 \dots 0 \}, \quad (6.69)$$

where we placed the orbital cut after l_A orbitals. In order to keep the discussion general, we denote an arbitrary occupation number configuration by the sequence $x \dots x$.⁸ For the orbitals to the right of the cut (with angular momentum $\geq l_A$) two examples of such configurations with distance from the cut, K_μ , are:

$$\begin{aligned} & \{ \underbrace{k0 \dots k0}_{2\Delta_\mu} \underbrace{x \dots x}_{l_A - 2\Delta_\mu} \mid \underbrace{0 \dots 0}_{K_\mu - 1} 10 \dots 0 \} \\ & \{ \underbrace{k0 \dots k0}_{2\Delta_\mu} \underbrace{x \dots x}_{l_A - 2\Delta_\mu} \mid K_\mu 0 \dots 0 \}. \end{aligned} \quad (6.70)$$

Let us now analyze the clustering condition that involve the k particles of the $(\Delta_\mu - 1)$ -th unit cell and the rightmost particle to the right of the cut in the partition μ (6.69). Remember that we chose to number the intact unit cells starting from 0. We choose $\beta = 2k(\Delta_\mu - 1) + \mu_1$ for the clustering operator (6.34) and require the remaining $N_A - (k + 1)$ particles to occupy the same orbitals as in $n(\mu)$. For instance, for the configuration in the first line of (6.70), we choose $\beta = 2k(\Delta_\mu - 1) + (l_A - 1 + K_\mu)$ and require the remaining $N_A - (k + 1)$ particle to have the occupation configuration:

$$\{ \underbrace{k0 \dots k0}_{2\Delta_\mu - 2} \underbrace{00 x \dots x}_{l_A - 2\Delta_\mu} \mid 0 \dots 0 \}. \quad (6.71)$$

⁸The actual occupation number configuration is not generally known or important to the proof.

While for the second line we choose $\beta = 2k(\Delta_\mu - 1) + l_A$ and the occupation number configuration of the remaining $N_A - (k + 1)$ particles to be:

$$\{\underbrace{k0 \dots k0}_{2\Delta_\mu - 2} \underbrace{00x \dots x}_{l_A - 2\Delta_\mu} | (K_\mu - 1)0 \dots 0\}. \quad (6.72)$$

In particular, the occupation configurations of the remaining particles have $\Delta_\mu - 1$ intact unit cells.

The clustering condition relates μ only to partitions that are dominated by a partition μ' of the form ⁹:

$$n(\mu') = \{\underbrace{k0 \dots k0}_{2\Delta_\mu - 2} (k - 1)1 \underbrace{x \dots x}_{l_A - 2\Delta_\mu} | \tilde{x} \dots \tilde{x}0 \dots 0\} \quad (6.73)$$

where $\tilde{x} \dots \tilde{x}$ is used to indicate an occupation number configuration where the right-most particle to the right of the cut is moved to the left by one orbital. The distance from the cut is reduced by one: $K_{\mu'} = K_\mu - 1$. For our examples in Eq. (6.70), the dominating partition is given by:

$$n(\mu') = \{\underbrace{k0 \dots k0}_{2\Delta_\mu - 2} (k - 1)1 \underbrace{x \dots x}_{l_A - 2\Delta_\mu} | \underbrace{0 \dots 0}_{K_\mu - 2} 10 \dots 0\} \quad (6.74)$$

for the configuration of the first line of Eq. (6.70), and:

$$n(\mu') = \{\underbrace{k0 \dots k0}_{2\Delta_\mu - 2} (k - 1)1 \underbrace{x \dots x}_{l_A - 2\Delta_\mu} | (K_\mu - 1)0 \dots 0\} \quad (6.75)$$

for the configuration in the second line of Eq. (6.70).

Using the results from Appendix 6.D.1, we conclude that all partitions $\mu' \neq \mu$ involved in the clustering condition have $\Delta_{\mu'} = \Delta_\mu - 1$ intact unit cells and distance

⁹Any other configuration has zero weight in the model wave function, since it is not dominated by the root partition (6.7)

from the cut $K_{\mu'} \leq K_{\mu} - 1$. The $(k+1)$ -body clustering condition yields one constraint on the rows labeled by all the involved partitions. Thus we have shown that the row labeled by μ can be written as a linear combination of the rows labeled by partitions μ' with $K_{\mu'} < K_{\mu}$ and one less intact unit cell.

6.D.3 Relating PEM rows to OEM rows

Let us assemble the results of the previous appendices to prove the following statement: any PEM row labeled by a partition μ with $K_{\mu} \leq \Delta_{\mu}$ is linearly dependent on rows labeled by partitions $\hat{\mu}_j$ with $K_{\hat{\mu}_j} = 0$. The latter are partitions that label the rows of the OEM. We prove this statement by induction, starting with a row partition μ with $K_{\mu} = 1$ and $\Delta_{\mu} \geq 1$. Such a row partition is necessarily of the form:

$$\{\underbrace{k0 \dots k0}_{2\Delta_{\mu}} \underbrace{x \dots x}_{l_A - 2\Delta_{\mu}} | 10 \dots 0\}. \quad (6.76)$$

Using the $(k, 2)$ clustering constraint for $\beta = 2k(\Delta_{\mu} - 1) + l_A$ and fixing the occupation configuration of the remaining $N - (k + 1)$ particles to be:

$$\{\underbrace{k0 \dots k0}_{2\Delta_{\mu} - 2} \underbrace{00x \dots x}_{l_A - 2\Delta_{\mu}} | 0 \dots 0\} \quad (6.77)$$

the row partition (6.76) can be related to rows labeled by $\hat{\mu}_j$, which satisfying $K_{\hat{\mu}_j} = 0$. This result is independent on Δ_{μ} as long as $\Delta_{\mu} \geq 1$.

For the induction hypothesis let us now assume that all row partitions λ_j with $K_{\lambda_j} \leq K_{\lambda}$ (for given $K_{\lambda} > 1$) and $\Delta_{\lambda_j} \geq K_{\lambda_j}$ can be written as linear combinations of rows labeled by partitions $\hat{\mu}_j$ with $K_{\hat{\mu}_j} = 0$.

Now consider a row partition μ with $K_{\mu} = K_{\lambda} + 1$ and $K_{\mu} \leq \Delta_{\mu}$. In Appendix 6.D.2 we have showed that a clustering condition involving any of the particles to the right of the cut and the k particles of the rightmost intact unit cell (to the left of

the OEM cut) relates this partition to partitions μ' with $K_{\mu'} < K_{\mu}$ and $\Delta_{\mu'} = \Delta_{\mu} - 1$. This implies that the row partition μ is a linear combination of the row partitions λ_j . Using the induction hypothesis yields that all partitions μ with distance to the cut $K_{\mu} \leq K_{\lambda} + 1$ fulfilling $K_{\mu} \leq \Delta_{\mu}$ can be written as linear combinations of rows of the OEM. This shows that any row partition μ fulfilling $K_{\mu} \leq \Delta_{\mu}$ can be written as a linear combination of rows labeled by partitions $\hat{\mu}_j$ that have distance to the cut $K_{\hat{\mu}_j} = 0$. These are the partitions that label the rows of the OEM.

Chapter 7

Haldane Statistics in the Finite Size Entanglement Spectra of $1/m$ FQH States

7.1 Introduction

For the Laughlin family of wavefunctions at filling $\nu = 1/m$, two numbers characterize the edge theory¹. The first is the central charge, which is one for the whole family. The physical meaning ascribed to this number is that it is the number of fields on the edge. In the IQH phases, for example, it is just the number of current carrying channels on the edge and equals ν . The central charge alone determines the counting of the many-body energy spectrum, and by Chapter 6, the counting of the orbital entanglement spectrum in the thermodynamic limit. The second number characterizing the edge theory of the Laughlin fluid is the boson compactification radius. Physically, this number determines the quantization of the charge carried by the excitations on the edge, e/m . This fractional charge of an electron has been observed in shot noise

¹Chapter based on work with M. Hermanns, N. Regnault and B. A. Bernevig [96].

experiments [166, 53, 42]. The energy spectrum alone is agnostic about this number in the thermodynamic limit. However, when the edge has a finite length, the counting differs from the thermodynamic one in a distinctive way for each m . Is counting of the OES at finite-size also distinctive? Can the value of m be extracted from it? In this chapter, we will answer these questions in the affirmative by conjecturing and numerically checking a counting principle for the finite-size OES of Laughlin states.

There is a second practical motivation to understand the finite-size counting of entanglement spectra. The power of the entanglement spectrum lies in its ability to numerically diagnose the topological order of *any* given wavefunction. The procedure is as follows: compute the OES of the wavefunction of interest, for example, the exact ground state of the Hamiltonian with Coulomb interaction at filling ν . Compare the counting of the low-lying levels of the OES to the known counting of the energy spectra of different edge theories. When you find a match, conclude that the given wavefunction is in the FQH phase with that edge theory. Li and Haldane’s conjecture[123] implies that this procedure is perfect in the thermodynamic limit. However, at computationally accessible system sizes, “low-lying” is hard to define. The universal part of the spectrum strongly mixes with the spurious levels higher in the OES of the Coulomb ground state, making it hard to separate. Using a flat-band procedure called the conformal limit, the non-universal part of the Coulomb spectrum can be completely separated from a low-lying part with the *same* counting as the finite-size OES of the model FQH state at the same filling by a *full* entanglement gap[180]. This also suggests a counting principle behind the finite-size level counting of the model states.

The counting principle that we conjecture is intimately related to the counting of the Hilbert space of the quasiholes of the Laughlin fluid. The Laughlin quasiholes are anyons with $1/m$ self-statistics [3]. That is, when one quasiparticle is adiabatically taken around the other, the wavefunction of the system picks up an Aharonov-Bohm

phase of $\exp(\pm 2\pi i/m)$.² Haldane [89] provided an alternate definition of statistics as the change in the dimension of the single particle Hilbert space on the addition of one particle. Thus, the Pauli exclusion principle implies the minus sign on the interchange of two fermions. Turning this definition on its head, Haldane showed that the statistics of the Laughlin quasiholes follows from a generalized Pauli exclusion principle for these particles. It turns out that configurations with no more than one particle in m consecutive orbitals counts the Hilbert space of particles with self-statistics $1/m$. As the counting of excitations of a Laughlin droplet about the edge are in one-to-one correspondence with the counting of quasiholes in the bulk, the Hilbert space dimension of the quasiholes and their statistics naturally enters our story of the finite-size counting of the OES.

In this chapter, we conjecture a counting principle for the finite-size spectra of Laughlin $\nu = 1/m$ states for any $m \in \mathbb{Z}^+$ (fermionic or bosonic). When the system is cut in orbital space, the number of non-zero Schmidt values as a function of the angular momentum of subsystem A exhibits Haldane exclusion statistics [89] of a boson of compactification radius \sqrt{m} quantized in a box of finite orbital length. The conjecture predicts the observed counting of the *full* entanglement spectrum of the $m = 2, 3$ states and most of the counting of the spectra of the $m > 3$ states. The existence of such a counting principle lends meaning to the OES at finite size and suggests a new interpretation of the entanglement gap in the Coulomb spectrum, known to be non-zero in the thermodynamic limit from numerical studies [180], as protecting the Haldane statistics of the phase.

As promised, our counting principle shows that the finite-size OES resolves the central charge of the edge theory, as well as the compactification radius \sqrt{m} or the fractional charge at the edge e/m , previously determined by intricate scaling arguments [175, 29]. The finite-size OES thus determines *all* the quantum numbers of the

²The statistical phase is defined only up to a sign.

$1/m$ Laughlin states, and thereby— as long as the entanglement gap is finite— all the topological properties of the Coulomb state at the same filling.

The organization of the chapter is as follows: we first review the effects of finite size on the counting of the edge energy spectrum of the Laughlin droplet in Sec. 7.2. We then state the conjecture for the counting of the corresponding finite-size OES in Sec. 7.3, illustrate the principle with an example and provide numerical evidence in support of the conjecture. Finally, in Sec. 7.4, we demonstrate that the conjecture predicts the correct finite-size counting of the OES away from the model state.

7.2 Effects of a finite bulk on the edge excitation spectrum

The intimate connection between the OES and the edge excitation spectrum suggests that the understanding of the finite-size effects in the latter transfers to the former. Let us therefore investigate the effects of finite size in the energy spectrum in the simplest case of $m = 1$, that is, the integer quantum Hall (IQH) droplet. Recall that in Chapter 5, following Ref. [91], we presented the energy spectrum of the IQH droplet with two edges in the Landau gauge in Fig. 5.2. For the reader's convenience, we reproduce the lowest Landau level in Fig. 7.1(a). The Fermi energy is set at zero and the bulk filling is one. At the right edge of the droplet, a wave packet above the Fermi level has positive group velocity and moves into the plane, while on the left edge, the wave packet does the opposite. Again, this is the origin of the chirality at the edge. What are the excitations above the ground state? They involve creating electron-hole pairs about each of the Fermi points. For small momentum/energies above the ground state (black arrows), the excitations are localized at the two edges. Thus, the counting of the number of levels in the excitation spectrum is the same as the counting of the excitation spectrum of two non-interacting one-dimensional wires of opposite

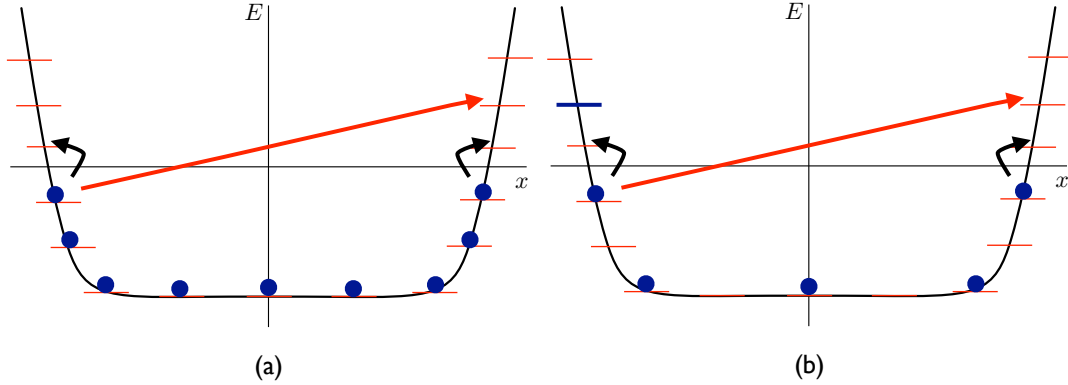


Figure 7.1: The single particle energy spectrum of the (a) $\nu = 1$, and (b) $\nu = 1/2$ droplet (see text for interpretation) with edges (also see Fig. 5.2). The blue dots indicate occupied orbitals in the ground state. The ground state has two Fermi points and the allowed particle-hole excitations above it are indicated by the arrows. For small momenta above the ground state (black arrows), the excitations are localized at the two edges and the degeneracy is the same as in the thermodynamic limit. For large momenta above the ground state (red arrow), the two edges interact and the number of excitations is reduced.

chirality. Nothing changes as we take the thermodynamic limit at this stage. The situation is different at large momenta/energy. At large momenta, the hole excitations of the two edges are the same excitation. In contrast, in the thermodynamic limit, the hole excitations of the two edges are always distinguishable. Thus, the number of excitations at finite size is smaller than that in the thermodynamic limit. For a given system size, the entire finite-size spectrum is easy to construct and the deviations from the thermodynamic limit counting can be analytically determined at each momentum.

Thus, at least for the IQH phase with non-interacting spinless electrons, we understand exactly how finite-size effects appear in the excitation spectrum. What bearing does this knowledge have on the $m > 1$ Laughlin phases? There is a simple heuristic picture arising from work by Haldane [89] that generalizes the IQH counting for $m > 1$. The key insight is that for the purposes of counting of excitations, we can work with free electrons even at $\nu = 1/m$, if we impose that the allowed occupation configurations are $(1, m)$ -admissible. A configuration is $(1, m)$ admissible if there is

no more than one electron in m consecutive orbitals. In Fig. 7.1(b) is shown the configuration corresponding to the ground state for $m = 2$, that is, the densest possible $(1, m)$ admissible configuration. We emphasize that the occupation configuration in Fig. 7.1(b) is merely a caricature of the correlations in the actual Laughlin state and is not to be literally interpreted as the many-body wavefunction. As we discussed in Sec. 6.2.5, the $(1, m)$ admissible configurations label wavefunctions with liquid-like correlations given by Jack polynomials [10]. To count the number of excitations of the $\nu = 1/m$ liquid at momentum δk above the ground state, all we have to do is to count the number of $(1, m)$ admissible configurations at that momentum. These are our allowed ‘particle-hole’ excitations. For example, some excitations about Fig. 7.1(b) are counted by:

$$\begin{aligned}
 \delta k = 0 : & \quad 0010101010100 \\
 \delta k = 1 : & \quad 0010101010010 \\
 & \quad \quad \quad \underline{0010101001100} \\
 \delta k = 2 : & \quad 0010101010001 \\
 & \quad \quad \quad 0010101001010 \\
 & \quad \quad \quad \underline{0010011010010} \\
 & \quad \quad \quad \vdots
 \end{aligned}$$

The first orbital in all configurations above is denoted by the thick blue line in (b). The crossed out configurations are not $(1, 2)$ -admissible. The list is not complete even at $\delta k = 0, 1, 2$ as we have only listed configurations with excitations about the right edge. For example, at $\delta k = 0$, a $(1, 2)$ -admissible configuration that should be counted is:

$$0100101010010$$

To connect to the $m = 1$ case discussed above, note that $(1, 1)$ admissible configurations are just valid fermionic configurations. Thus, counting the number of particle hole excitations at some momentum is equivalent to the number of $(1, 1)$ admissible configurations at that momentum. Following the argument that we presented for $m = 1$, we see that the counting of excitations will be reduced at sufficiently high momenta/energy. The precise analytical formula that quantifies this reduction will be presented for the OES in the next section.

To summarize, we have presented a cartoon of the effect of the finite size of the bulk on the edge excitation spectrum in the $1/m$ Laughlin states (Fig. 7.1). At sufficiently high momentum/energy above the ground state, the number of excitations is smaller than that in the thermodynamic limit.

7.3 Effects of a finite bulk on the OES

Let us now investigate the effects of the finite bulk on the OES. For a description of the geometry, the definition and properties of the OES and the special properties of the Laughlin model states, we refer the reader to Sections 6.2.1-6.3. Any undefined symbols below refer to the same quantities as in Chapter 6. Briefly, we perform the orbital cut after l_A orbitals. A is assumed to be the smaller sub-system $l_A \leq l_B$. The block of the orbital entanglement matrix (OEM) at fixed number of particles in A (N_A) z -angular momentum in A , L_z^A is denoted by C .

We define $\Delta L_z = L_{z,max}^A - L_z^A$, where $L_{z,max}^A = mN_A(N - N_A)/2$ is the z -angular momentum of the configuration where the particles in A are maximally close to the North pole. In the thermodynamic limit ($l_A \rightarrow \infty$ before $N_A \rightarrow \infty$), the number of levels in the OES for any m grows as $(1, 1, 2, 3, 5, 7, 11 \dots)$ for $\Delta L_z = 0, 1, 2 \dots$, matching the number of excitations of a chiral $U(1)$ boson at each ΔL_z . Corrections to this counting occur because of the finite number of particles or orbitals in A . The

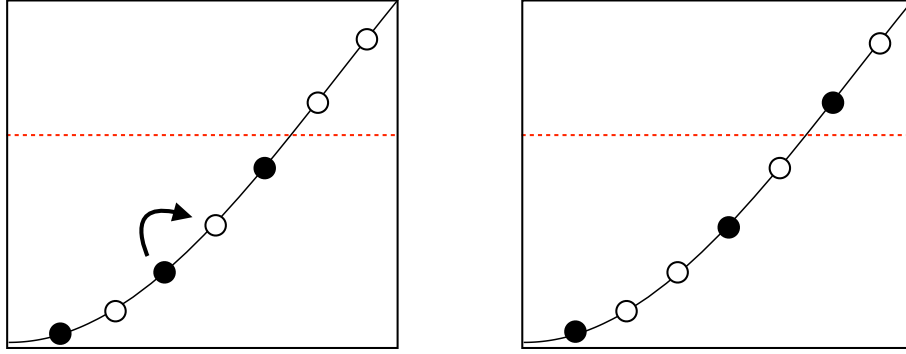


Figure 7.2: Schematic indicating the excitations above the $\nu = 1/2$ ground state that count the number of levels in the OES with $N_A = 3$ in $l_{enl} = 7$ orbitals. Haldane statistics implies that each occupied orbital ‘blocks’ its two neighboring orbitals. Thus, only the excited state in the right box contributes to the level counting of the OES at $\Delta L_z = 1$, while the configuration arising out of the transition (arrow) in the left box does not.

OES counting for a finite N_A as $l_A \rightarrow \infty$ is different from the above $U(1)$ counting, but remains the same for all $1/m$ Laughlin states. Dependence of the OES counting on m arises only when l_A is also finite.

Let us assume for the moment that B is infinite, i.e. $l_B, N_B \rightarrow \infty$. We argue that the level counting of the OES exhibits Haldane exclusion statistics by identifying all the configurations in A with a set of $(1, m)$ -admissible configurations with the same quantum numbers. The latter obey the generalized Pauli principle that there is no more than one particle in m consecutive orbitals corresponding to the statistical interaction $g = m$ [89]. Observe that the orbital cut at l_A imposes a ‘hard-wall’ potential on the subsystem A ; it forbids the occupation of any orbital with $L_z \geq l_A$. For values of l_A and ΔL_z such that none of the configurations in A probe this wall, the $(1, m)$ -admissible configurations count the number of levels in the OES [40]. For all other values, we conjecture that the $(1, m)$ -admissible configurations of N_A particles continue to count the levels in the OES, if we move the hard wall and increase the orbital size of A to $l_{enl} > l_A$. A schematic view of this counting principle is shown in Fig. 7.2. To determine l_{enl} , we use the fact that there is exactly one level in the OES at the minimal possible angular momentum, $L_{z,min}^A$. This is because there is

only one allowed configuration in $A - \{0 \dots 0N_A | \dots\}$ for bosonic Laughlin states and $\{0 \dots 01 \dots 1 | \dots\}$ for the fermionic ones, where ‘|’ denotes the orbital cut. We therefore fix l_{enl} such that there is *exactly one* $(1, m)$ -admissible partition at angular momentum $L_{z,min}^A$ and none at smaller angular momenta: $l_{enl} = l_A + m(N_A - 1)/2$ (bosons) and $l_{enl} = l_A + (m - 1)(N_A - 1)/2$ (fermions).

In a numerically accessible system, both A and B are of finite size. The arguments in the previous paragraph then apply to both subsystems. We thus conjecture an upper bound $\mathcal{N}_s(l_A, N_A, \Delta L_z)$ to the level counting of the OES at given N_A , l_A , and ΔL_z , taking both subsystems into account:

$$\mathcal{N}_s(l_A, N_A, \Delta L_z) = \min[\mathcal{N}(l_A, N_A, \Delta L_z), \mathcal{N}(l_B, N_B, \Delta L_z)], \quad (7.1)$$

where $\mathcal{N}(l_a, N_a, \Delta L_z)$ for $a = A, B$ is the number of $(1, m)$ -admissible states of N_a particles in $l_{enl,a} = l_a + m(N_a - 1)/2$ (bosons) or $l_{enl,a} = l_a + (m - 1)(N_a - 1)/2$ (fermions) orbitals at angular momentum ΔL_z . It is defined by the generating function:

$$\sum_{\Delta L_z=0}^{N_a \cdot N_a^h} \mathcal{N}(l_a, N_a, \Delta L_z) q^{\Delta L_z} = \frac{(q)_{N_a + N_a^h}}{(q)_{N_a} (q)_{N_a^h}}, \quad (7.2)$$

with $(q)_n = \prod_{i=1}^n (1 - q^i)$ and $N_a^h = l_{enl,a} - m(N_a - 1) - 1$. $\mathcal{N}(l_a, N_a, \Delta L_z)$ is a well-known quantity; it is the number of linearly independent Laughlin states of N_a particles with N_a^h added flux quanta at angular momentum ΔL_z [158]. For nearly all values of N_A , l_A , and ΔL_z , the bound is saturated and the observed counting is given by $\mathcal{N}_s(l_A, N_A, \Delta L_z)$. Specifically, Eq. (7.1) predicts the correct level counting for the *entire* OES for $m = 2, 3$, and for *most* (N_A, l_A) sectors of the $m > 3$ states.

For given (N_A, l_A) , Eq. (7.1) predicts the observed counting of the full spectrum if $\mathcal{N}_s(l_A, N_A, \Delta L_z)$ simplifies to $\mathcal{N}(l_A, N_A, \Delta L_z)$ for *all* ΔL_z (or alternatively if it simplifies to $\mathcal{N}(l_B, N_B, \Delta L_z)$ for all ΔL_z). In other words, Eq. (7.1) holds exactly when the corrections to the thermodynamic counting are only due to the finite-size

of a single subsystem. For the bosonic states, a necessary and sufficient condition for this is (i) $N_B \geq \min(N_A, N_A^h)$. For fermionic states, an additional condition (ii) $l_A - N_A \leq (m - 1)(N - 1)/2$ has to be imposed as a consequence of the Pauli exclusion statistics of the fermions in part B . For $m = 2, 3$, restricting the orbital cut to $l_A \leq N_\phi/2$ ensures that these conditions are satisfied. For $m > 3$, both conditions can always be satisfied by choosing the system size to be sufficiently large.

When $N_B < \min(N_A, N_A^h)$ ((i) does not hold), $\mathcal{N}_s(l_A, N_A, \Delta L_z)$ simplifies to $\mathcal{N}(l_B, N_B, \Delta L_z)$ at small ΔL_z and to $\mathcal{N}(l_A, N_A, \Delta L_z)$ at large ΔL_z . If (ii) is not satisfied, the situation is reversed—the level counting at small ΔL_z is equal to $\mathcal{N}(l_A, N_A, \Delta L_z)$, while the number of levels at large ΔL_z is equal to $\mathcal{N}(l_B, N_B, \Delta L_z)$. At both ends of the spectrum, the level counting of the OES is equal to $\mathcal{N}_s(l_A, N_A, \Delta L_z)$. In fact, Eq. (7.1) is the observed level counting everywhere except possibly at a few values around ΔL_z^0 , when $\mathcal{N}(l_A, N_A, \Delta L_z^0) \approx \mathcal{N}(l_B, N_B, \Delta L_z^0)$. Near ΔL_z^0 , the counting is dependent on the finite sizes of A and B and Eq. (7.1) is only an upper bound. We have tested our conjecture for all possible orbital cuts at all numerically accessible system sizes, i.e up to $N = (16, 15, 11, 11, 9, 9, 7, 7)$ particles for $m = (2, 3, \dots, 9)$.

7.3.1 An example

Let us illustrate Eq. (7.1), the counting principle behind the finite-size OES counting of the $1/m$ Laughlin states, with a simple example at $N = 8$, $m = 2$. Consider the sectors of the OES at $l_A = 5$, $N_A = 3$. As $l_A \leq l_B$, condition (i) is satisfied and we need only consider subsystem A . We fix $l_{enl,A}$ so that the single occupation number configuration at $L_{z,min}^A$, $\{00003 | \dots\}$, is identified with exactly one (1, 2)-admissible configuration at the same angular momentum:

$$000 \overleftarrow{0} 3 | \overrightarrow{0} 0 \leftrightarrow 00 \overleftarrow{0} 111 | \overrightarrow{0} \leftrightarrow 0010101 |. \quad (7.3)$$

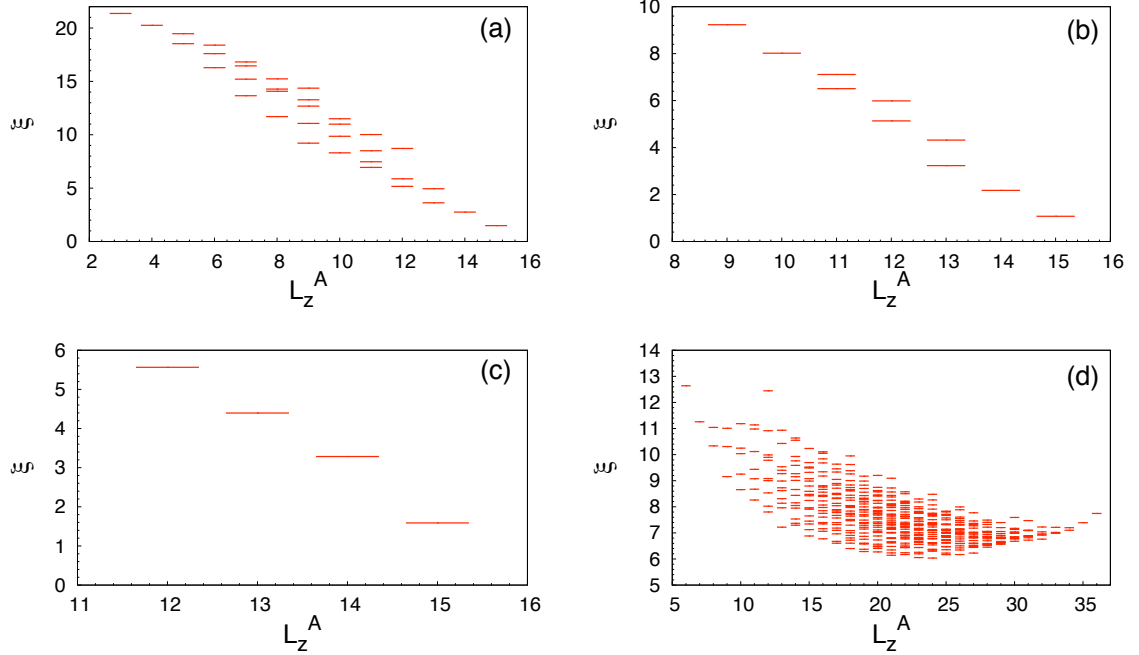


Figure 7.3: OES of the bosonic $m = 2$ Laughlin state for $N = 8$ and (a) $N_A = 3$, $l_A = 7$, (b) $N_A = 3$, $l_A = 5$, (c) $N_A = 3$, $l_A = 4$ and OES of the $m = 2$ state with $N = 12$ and (d) $N_A = 6$ and $l_A = 11$ in the conformal limit. The counting of plots (a), (b) and (c) should be compared to the number of $(1, 2)$ -admissible configurations listed in Table 7.1 at each ΔL_z . In all cases, the full counting is predicted exactly by $\mathcal{N}(l_A, N_A, \Delta L_z)$, defined by Eq. (7.2).

where the hard wall is indicated by ‘|’. The arrows indicate angular-momentum conserving operations that result in a $(1, 2)$ -admissible configuration. Pushing the hard wall further to the right allows for $(1, 2)$ -admissible configurations at angular momenta lower than $L_{z, \min}^A$. Thus, $l_{enl, A} = l_A + 2 = 7$. The conjectured counting of the OES is therefore $\mathcal{N}_s(l_A, N_A, \Delta L_z) = \mathcal{N}(5, 3, \Delta L_z)$. The middle column of Table 7.1 lists the possible $(1, 2)$ -admissible configurations of 3 particles in $l_{enl, A} = 7$ orbitals at every ΔL_z . The resulting counting, $(1, 1, 2, 2, 2, 1, 1)$, is identical to the counting of the numerically generated OES, Fig. 7.3(b). We also list some of the $(1, 2)$ -admissible partitions of $N_A = 3$ particles for orbital cuts $l_A = 7, 4$ ($l_{enl, A} = 9, 6$), in the first and third column respectively. Their number is identical to the numerically observed level counting shown in Fig. 7.3(a) and (c).

$l_A = 7,$	$N_A = 3$	$l_A = 5,$	$N_A = 3$	$l_A = 4,$	$N_A = 3$
$\Delta L_z = 0:$	101010000	$\Delta L_z = 0:$	1010100	$\Delta L_z = 0:$	101010
$\Delta L_z = 1:$	101001000	$\Delta L_z = 1:$	1010010	$\Delta L_z = 1:$	101001
$\Delta L_z = 2:$	101000100	$\Delta L_z = 2:$	1010001	$\Delta L_z = 2:$	100101
	100101000		1001010	$\Delta L_z = 3:$	010101
$\Delta L_z = 3:$	101000010	$\Delta L_z = 3:$	1001001		
	100100100		0101010		
	010101000	$\Delta L_z = 4:$	1000101		
$\Delta L_z = 4:$	101000001		0101001		
	100100010	$\Delta L_z = 5:$	0100101		
	100010100	$\Delta L_z = 6:$	0010101		
	010100100				
	...				

Table 7.1: Examples of the finite-size counting of the $m = 2$ Laughlin state. The number of $(1, 2)$ -admissible partitions in $l_A + 2$ orbitals at each ΔL_z equals the number of levels in the OES for the cut with N_A particles in l_A orbitals in Fig. 7.3.

A few general remarks about the OES counting of the model FQH states are in order. For a generic state, one expects the rank of the OEM to be equal to the smaller of its dimensions. What makes the model FQH states special is the factorially many linear dependencies in their OEMs that keep the rank finite even in the thermodynamic limit. The finite-size counting conjectured in this article is expected to be hard to prove in general, although the level counting at both high and low angular momenta L_z^A can be analytically determined. The generic $U(1)$ level counting in the OES of N_A particles at angular momenta $\Delta L_z = 0, 1, \dots, N_A^h$ has been rigorously shown for certain orbital cuts [40]. At $L_{z,min}^A, L_{z,min}^A + 1, \dots, L_{z,min}^A + N_A^h$, the rank of the OEM is the Hilbert space dimension of part A . For instance, in the $m = 2$ Laughlin state with $N_A = 3, l_A = 5$, there is only one level in the OES at $L_{z,min}^A$ and $L_{z,min}^A + 1$ corresponding to the configurations $\{00003 | \dots\}$ and $\{00012 | \dots\}$ of A . For values of $L_z^A > L_{z,min}^A + 2$, the OEM rank is less than the Hilbert space dimension of A , indicative of the nontrivial structure of the OEM.

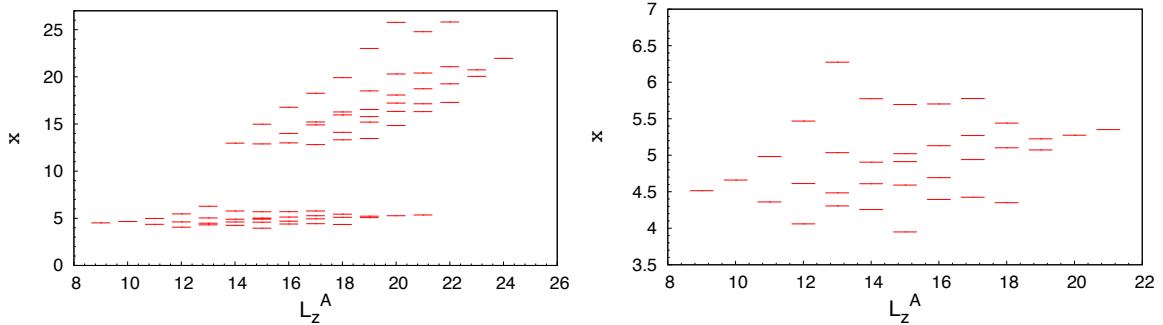


Figure 7.4: Coulomb entanglement spectrum of $N = 8$ bosons at filling $1/2$ in the sector $l_A = 7$, $N_A = 3$ in the conformal limit. Left: The full entanglement spectrum with a clear entanglement gap. Right: The low-‘energy’ part of the conformal entanglement spectrum. The level counting is identical to the Laughlin entanglement spectrum in Fig. 7.3(a).

7.4 Away from the model state

It is worthwhile to demonstrate the role of our conjecture for the Laughlin states in the OES counting of Coulomb states at the same filling. Fig. 7.4 shows the entanglement spectrum for the bosonic Coulomb state of $N = 8$ particles at filling fraction $\nu = 1/2$ in the sector $l_A = 7$, $N_A = 3$ in the conformal limit. The low-‘energy’ part— shown in the right figure— is separated from the levels higher in the spectrum by a gap at all L_z^A . In contrast to the entanglement entropy calculations that rely on scaling arguments, we can determine all the quantum numbers of the edge theory of the state using the conjectured counting of the model OES at a *single* system size and a *single* orbital cut. For instance, the level counting at high L_z^A in Fig. 7.4 is $(1, 1, 2, 3, 5)$ for $\Delta L_z = 0, \dots, 4$, identical to the counting of 3 particles in any Laughlin state, $\mathcal{N}(l_A, 3, \Delta L_z)$, as $l_A \rightarrow \infty$. From Eq. (7.2), we observe that the *first* discrepancy from the counting at $l_A \rightarrow \infty$ is at $\Delta L_z = N_A^h + 1$. In Fig. 7.4, this occurs at $\Delta L_z = 5$, which fixes $N_A^h = 4$. Inserting this value into the expression for N_A^h , we find that $m = 2(l_A - 1 - N_A^h)/(N_A - 1) = 2$. As the ΔL_z of the first finite-size correction is the only information required, this analysis works equally well for the cases where the conjecture only provides an upper bound to the counting.

7.5 Concluding remarks

In this chapter, we explored the effect of the finite size of the system on the edge excitation spectrum and the orbital entanglement spectrum. In both cases, we found that the counting of the spectrum is reduced at large momentum above the ground state. We showed that the physics leading to the reduced counting in both spectra is related to the counting of the number of $(1, m)$ -admissible configurations in a box of finite size. This led us to conjecture that the counting of the finite-size OES of the $\nu = 1/m$ Laughlin states exhibits Haldane exclusion statistics of a boson with compactification radius \sqrt{m} in a box of known orbital length. We supported our claim with extensive numerical evidence at many different system sizes. Our conjecture shows that the OES determines all the quantum numbers of the Laughlin state edge theory—its central charge through the thermodynamic limit counting, and the compactification radius or quasi hole charge through the finite-size counting. It suggests that the entanglement gap in the Coulomb spectrum protects the Haldane statistics of the phase in the thermodynamic limit and thus provides us with a new way of extracting the boson compactification radius for any state with a finite gap.

A natural direction for future research is understanding the counting of the non-abelian states, which is complicated by more quantum numbers. More generally, we can ask if all the quantum numbers of any chiral edge theory can be determined from the entanglement spectrum alone. It would also be interesting to extend the analysis in this article to two orbital cuts [29] on the torus [118, 126] or the sphere. The resulting OES is expected to be the combination of the finite-size spectra of the two edges if they are non-interacting.

Bibliography

- [1] O. Aharony, S. S. Gubser, J. Maldacena, H. Ooguri, and Y. Oz. Large N field theories, string theory and gravity. *Physics Reports*, 323(3-4):183 – 386, 2000.
- [2] S. An, P. Jiang, H. Choi, W. Kang, S. H. Simon, L. N. Pfeiffer, K. W. West, and K. W. Baldwin. Braiding of Abelian and Non-Abelian Anyons in the Fractional Quantum Hall Effect. *ArXiv e-prints*, Dec. 2011, e-print arXiv:1112.3400.
- [3] D. Arovas, J. R. Schrieffer, and F. Wilczek. Fractional statistics and the quantum hall effect. *Phys. Rev. Lett.*, 53(7):722–723, Aug 1984.
- [4] T. Barthel and U. Schollwöck. Dephasing and the steady state in quantum many-particle systems. *Phys. Rev. Lett.*, 100:100601, Mar 2008.
- [5] D. Basko, I. Aleiner, and B. Altshuler. Metal–insulator transition in a weakly interacting many-electron system with localized single-particle states. *Annals of Physics*, 321(5):1126 – 1205, 2006.
- [6] C. Bauerle, Y. M. Bunkov, S. N. Fisher, H. Godfrin, and G. R. Pickett. Laboratory simulation of cosmic string formation in the early universe using superfluid ^3He . *Nature*, 382(6589):332–334, 07 1996.
- [7] J. S. Bell. *Speakable and Unspeakable in Quantum Mechanics*. Cambridge University Press, Cambridge, UK, 1987.
- [8] C. H. Bennett, G. Brassard, C. Crépeau, R. Jozsa, A. Peres, and W. K. Wootters. Teleporting an unknown quantum state via dual classical and einstein-podolsky-rosen channels. *Phys. Rev. Lett.*, 70:1895–1899, Mar 1993.
- [9] B. A. Bernevig and F. D. M. Haldane. Generalized clustering conditions of jack polynomials at negative jack parameter α . *Phys. Rev. B*, 77(18):184502, 2008.
- [10] B. A. Bernevig and F. D. M. Haldane. Model fractional quantum hall states and jack polynomials. *Phys. Rev. Lett.*, 100(24):246802, Jun 2008.
- [11] B. A. Bernevig and F. D. M. Haldane. Properties of non-abelian fractional quantum hall states at filling $\nu = k/r$. *Phys. Rev. Lett.*, 101(24):246806, Dec 2008.

- [12] B. A. Bernevig and F. D. M. Haldane. Clustering properties and model wave functions for non-abelian fractional quantum hall quasielectrons. *Phys. Rev. Lett.*, 102:066802, Feb 2009.
- [13] L. M. Bettencourt and C. Wetterich. Time evolution of correlation functions in non-equilibrium field theories. *Physics Letters B*, 430(1-2):140 – 150, 1998.
- [14] G. Biroli, L. F. Cugliandolo, and A. Sicilia. Kibble-Zurek mechanism and infinitely slow annealing through critical points. *Phys. Rev. E*, 81(5):050101, May 2010.
- [15] N. D. Birrell and P. C. W. Davies. *Quantum Fields in Curved Space*. Cambridge University Press, 1982.
- [16] I. Bloch, J. Dalibard, and W. Zwerger. Many-body physics with ultracold gases. *Rev. Mod. Phys.*, 80:885–964, Jul 2008.
- [17] P. Bonderson. *Non-Abelian Anyons and Interferometry*. PhD thesis, Caltech, 2007.
- [18] D. Bouwmeester, J.-W. Pan, K. Mattle, M. Eibl, H. Weinfurter, and A. Zeilinger. Experimental quantum teleportation. *Nature*, 390(6660):575–579, 12 1997.
- [19] M. J. Bowick, L. Chandar, E. A. Schiff, and A. M. Srivastava. The cosmological kibble mechanism in the laboratory: String formation in liquid crystals. *Science*, 263(5149):943–945, 02 1994.
- [20] D. Boyanovsky, H. J. de Vega, R. Holman, and J. Salgado. Nonequilibrium bose-einstein condensates, dynamical scaling, and symmetric evolution in the large n ϕ^4 theory. *Phys. Rev. D*, 59:125009, May 1999.
- [21] D. Boyanovsky, H. J. de Vega, R. Holman, and J. F. J. Salgado. Analytic and numerical study of preheating dynamics. *Phys. Rev. D*, 54:7570–7598, Dec 1996.
- [22] A. J. Bray. Theory of phase-ordering kinetics. *Advances in Physics*, 43(3):357 – 459, 1994.
- [23] P. Breitenlohner and D. Z. Freedman. Stability in Gauged Extended Supergravity. *Ann. Phys.*, 144:249, 1982.
- [24] F. Burnell and S. H. Simon. Space-time geometry of topological phases. *Annals of Physics*, 325(11):2550 – 2593, 2010.
- [25] F. J. Burnell, S. H. Simon, and J. K. Slingerland. Condensation of achiral simple currents in topological lattice models: Hamiltonian study of topological symmetry breaking. *Phys. Rev. B*, 84:125434, Sep 2011.

- [26] F. J. Burnell, S. H. Simon, and J. K. Slingerland. Phase transitions in topological lattice models via topological symmetry breaking. *New Journal of Physics*, 14(1):015004, 2012.
- [27] P. Calabrese and J. Cardy. Time dependence of correlation functions following a quantum quench. *Phys. Rev. Lett.*, 96:136801, Apr 2006.
- [28] P. Calabrese and J. Cardy. Quantum quenches in extended systems. *Journal of Statistical Mechanics: Theory and Experiment*, 2007(06):P06008, 2007.
- [29] P. Calabrese, J. Cardy, and E. Tonni. Entanglement entropy of two disjoint intervals in conformal field theory. *Journal of Statistical Mechanics: Theory and Experiment*, 2009(11):P11001, 2009.
- [30] P. Calabrese, F. H. L. Essler, and M. Fagotti. Quantum quench in the transverse-field ising chain. *Phys. Rev. Lett.*, 106:227203, Jun 2011.
- [31] P. Calabrese and A. Gambassi. Ageing properties of critical systems. *Journal of Physics A: Mathematical and General*, 38(18):R133, 2005.
- [32] P. Calabrese and A. Lefevre. Entanglement spectrum in one-dimensional systems. *Phys. Rev. A*, 78(3):032329, Sep 2008.
- [33] S. Casado, W. González-Viñas, and H. Mancini. Testing the kibble-zurek mechanism in rayleigh-bénard convection. *Phys. Rev. E*, 74(4):047101, Oct 2006.
- [34] C. Castelnovo, R. Moessner, and S. Sondhi. Spin ice, fractionalization, and topological order. *Annual Review of Condensed Matter Physics*, 3(1):35–55, 2012.
- [35] C. Castelnovo, R. Moessner, and S. L. Sondhi. Thermal quenches in spin ice. *Phys. Rev. Lett.*, 104:107201, Mar 2010.
- [36] M. A. Cazalilla. Effect of suddenly turning on interactions in the luttinger model. *Phys. Rev. Lett.*, 97:156403, Oct 2006.
- [37] J. T. Chalker and P. D. Coddington. Percolation, quantum tunnelling and the integer hall effect. *Journal of Physics C: Solid State Physics*, 21(14):2665, 1988.
- [38] A. Chandran, F. J. Burnell, V. Khemani, and S. L. Sondhi. Kibble-Zurek scaling and string-net coarsening in topologically ordered systems. *Journal of Physics: Condensed Matter*, 2013. To appear.
- [39] A. Chandran, A. Erez, S. S. Gubser, and S. L. Sondhi. Kibble-Zurek problem: Universality and the scaling limit. *Phys. Rev. B*, 86:064304, Aug 2012.
- [40] A. Chandran, M. Hermanns, N. Regnault, and B. A. Bernevig. Bulk-edge correspondence in entanglement spectra. *Phys. Rev. B*, 84:205136, Nov 2011.

- [41] A. Chandran, A. Nanduri, S. S. Gubser, and S. L. Sondhi. On equilibration and coarsening in the quantum $O(N)$ model at infinite N . Apr. 2013, e-print arXiv:1304.2402.
- [42] A. M. Chang. Chiral luttinger liquids at the fractional quantum hall edge. *Rev. Mod. Phys.*, 75(4):1449–1505, Nov 2003.
- [43] D. Chen, M. White, C. Borries, and B. DeMarco. Quantum quench of an atomic mott insulator. *Phys. Rev. Lett.*, 106(23):235304, Jun 2011.
- [44] I. Chuang, R. Durrer, N. Turok, and B. Yurke. Cosmology in the laboratory: Defect dynamics in liquid crystals. *Science*, 251(4999):1336–1342, 1991.
- [45] M.-C. Chung and I. Peschel. Density-matrix spectra of solvable fermionic systems. *Phys. Rev. B*, 64(6):064412, Jul 2001.
- [46] F. Cooper, S. Habib, Y. Kluger, and E. Mottola. Nonequilibrium dynamics of symmetry breaking in $\lambda\phi^4$ theory. *Phys. Rev. D*, 55:6471–6503, May 1997.
- [47] M. Cramer, C. M. Dawson, J. Eisert, and T. J. Osborne. Exact relaxation in a class of nonequilibrium quantum lattice systems. *Phys. Rev. Lett.*, 100:030602, Jan 2008.
- [48] M. Cramer and J. Eisert. A quantum central limit theorem for non-equilibrium systems: exact local relaxation of correlated states. *New Journal of Physics*, 12(5):055020, 2010.
- [49] C. M. A. Dantas, I. A. Pedrosa, and B. Baseia. Harmonic oscillator with time-dependent mass and frequency and a perturbative potential. *Phys. Rev. A*, 45:1320–1324, Feb 1992.
- [50] S. Das and K. Sengupta. Non-equilibrium dynamics of $o(n)$ nonlinear sigma models: a large- n approach. *Journal of High Energy Physics*, 2012:1–17, 2012.
- [51] C. De Grandi, V. Gritsev, and A. Polkovnikov. Quench dynamics near a quantum critical point. *Phys. Rev. B*, 81:012303, Jan 2010.
- [52] C. De Grandi, A. Polkovnikov, and A. W. Sandvik. Universal nonequilibrium quantum dynamics in imaginary time. *Phys. Rev. B*, 84:224303, Dec 2011.
- [53] R. de Picciotto, M. Reznikov, M. Heiblum, V. Umansky, G. Bunin, and D. Mahalu. Direct observation of a fractional charge. *Nature*, 389(6647):162–164, 09 1997.
- [54] W. DeGottardi, D. Sen, and S. Vishveshwara. Topological phases, majorana modes and quench dynamics in a spin ladder system. *New Journal of Physics*, 13(6):065028, 2011.
- [55] Deng, S., Ortiz, G., and Viola, L. Dynamical non-ergodic scaling in continuous finite-order quantum phase transitions. *EPL*, 84(6):67008, 2008.

- [56] P. Di Francesco, P. Mathieu, and D. Senechal. *Conformal Field Theory*. Springer, corrected edition, Jan. 1999.
- [57] U. Divakaran, A. Dutta, and D. Sen. Quenching along a gapless line: A different exponent for defect density. *Phys. Rev. B*, 78:144301, Oct 2008.
- [58] U. Divakaran, V. Mukherjee, A. Dutta, and D. Sen. Defect production due to quenching through a multicritical point. *Journal of Statistical Mechanics: Theory and Experiment*, 2009(02):P02007, 2009.
- [59] S. Ducci, P. L. Ramazza, W. González-Viñas, and F. T. Arecchi. Order parameter fragmentation after a symmetry-breaking transition. *Phys. Rev. Lett.*, 83(25):5210–5213, Dec 1999.
- [60] S. Dusuel, M. Kamfor, R. Orús, K. P. Schmidt, and J. Vidal. Robustness of a perturbed topological phase. *Phys. Rev. Lett.*, 106:107203, Mar 2011.
- [61] J. Dziarmaga. Dynamics of a quantum phase transition: Exact solution of the quantum ising model. *Phys. Rev. Lett.*, 95(24):245701, Dec 2005.
- [62] J. Dziarmaga. Dynamics of a quantum phase transition and relaxation to a steady state. *Advances in Physics*, 59(6):1063–1189, 2010.
- [63] J. P. Eisenstein and H. L. Stormer. The fractional quantum hall effect. *Science*, 248(4962):1510–1516, 1990.
- [64] B. Estienne. *private communication*, 2010.
- [65] M. Fagotti, P. Calabrese, and J. E. Moore. Entanglement spectrum of random-singlet quantum critical points. *Phys. Rev. B*, 83:045110, Jan 2011.
- [66] M. Fagotti and F. H. L. Essler. Reduced Density Matrix after a Quantum Quench. 2013, e-print arXiv:1302.6944.
- [67] B. Feigin, M. Jimbo, T. Miwa, and E. Mukhin. A differential ideal of symmetric polynomials spanned by jack polynomials at $r = -(r=1)/(k+1)$. *International Mathematics Research Notices*, 2002(23):1223–1237, 2002.
- [68] A. M. Ferrenberg and D. P. Landau. Critical behavior of the three-dimensional ising model: A high-resolution monte carlo study. *Phys. Rev. B*, 44:5081–5091, Sep 1991.
- [69] R. Feynman. Simulating physics with computers. *International Journal of Theoretical Physics*, 21(6-7):467–488, 1982.
- [70] L. Fidkowski. Entanglement spectrum of topological insulators and superconductors. *Phys. Rev. Lett.*, 104(13):130502, 2010.

- [71] L. Fidkowski, T. S. Jackson, and I. Klich. Model characterization of gapless edge modes of topological insulators using intermediate brillouin-zone functions. *Phys. Rev. Lett.*, 107:036601, Jul 2011.
- [72] M. Fisher. Scaling, universality and renormalization group theory. In F. Hahne, editor, *Critical Phenomena*, volume 186 of *Lecture Notes in Physics*, pages 1–139. Springer Berlin / Heidelberg, 1983.
- [73] E. Fradkin and S. H. Shenker. Phase diagrams of lattice gauge theories with higgs fields. *Phys. Rev. D*, 19:3682–3697, Jun 1979.
- [74] F. Franchini, A. Its, V. Korepin, and L. Takhtajan. Spectrum of the density matrix of a large block of spins of the xy model in one dimension. *Quantum Information Processing*, 10(3):325–341, 2011.
- [75] K. Fredenhagen and M. Marcu. Confinement criterion for qcd with dynamical quarks. *Phys. Rev. Lett.*, 56:223–224, Jan 1986.
- [76] K. Fredenhagen and M. Marcu. Dual interpretation of order parameters for lattice gauge theories with matter fields. *Nuclear Physics B - Proceedings Supplements*, 4(0):352 – 357, 1988.
- [77] M. H. Freedman. P/np, and the quantum fieldcomputer. *Proceedings of the National Academy of Sciences*, 95(1):98–101, 1998.
- [78] C. Gils, S. Trebst, A. Kitaev, A. W. W. Ludwig, M. Troyer, and Z. Wang. Topology-driven quantum phase transitions in time-reversal-invariant anyonic quantum liquids. *Nature Physics*, 5:834, 2009.
- [79] S. M. Girvin. *Les Houches - Ecole d’Ete de Physique Theorique*, volume 69, pages 53–175. Springer Berlin Heidelberg, 1999.
- [80] N. Gisin, G. Ribordy, W. Tittel, and H. Zbinden. Quantum cryptography. *Rev. Mod. Phys.*, 74:145–195, Mar 2002.
- [81] R. J. Glauber. Time-dependent statistics of the ising model. *Journal of Mathematical Physics*, 4(2):294–307, 1963.
- [82] N. Goldenfeld. *Lectures on Phase Transitions and the Renormalization Group*. Addison-Wesley, Advanced Book Program, Reading, Mass., 1992.
- [83] M. Grady. Infinite set of conserved charges in the ising model. *Phys. Rev. D*, 25:1103–1113, Feb 1982.
- [84] K. Gregor, D. A. Huse, R. Moessner, and S. L. Sondhi. Diagnosing deconfinement and topological order. *New Journal of Physics*, 13(2):025009, 2011.
- [85] M. Greiner, O. Mandel, T. Esslinger, T. W. Hansch, and I. Bloch. Quantum phase transition from a superfluid to a mott insulator in a gas of ultracold atoms. *Nature*, 415(6867):39–44, 01 2002.

- [86] M. Greiner, O. Mandel, T. W. Hansch, and I. Bloch. Collapse and revival of the matter wave field of a bose-einstein condensate. *Nature*, 419(6902):51–54, 09 2002.
- [87] V. Gurarie and E. Rezayi. Parafermion statistics and quasihole excitations for the generalizations of the paired quantum hall states. *Phys. Rev. B*, 61(8):5473–5482, 2000.
- [88] F. D. M. Haldane. Fractional quantization of the hall effect: A hierarchy of incompressible quantum fluid states. *Phys. Rev. Lett.*, 51(7):605–608, Aug 1983.
- [89] F. D. M. Haldane. “fractional statistics” in arbitrary dimensions: A generalization of the pauli principle. *Phys. Rev. Lett.*, 67(8):937–940, Aug 1991.
- [90] B. I. Halperin. *Physics of Defects*. Proceedings of the Les Houches Summer Institute. North Holland, Amsterdam, 1981.
- [91] B. I. Halperin. Quantized hall conductance, current-carrying edge states, and the existence of extended states in a two-dimensional disordered potential. *Phys. Rev. B*, 25:2185–2190, Feb 1982.
- [92] B. I. Halperin. Statistics of quasiparticles and the hierarchy of fractional quantized hall states. *Phys. Rev. Lett.*, 52:1583–1586, Apr 1984.
- [93] T. Hansson, V. Oganesyan, and S. Sondhi. Superconductors are topologically ordered. *Annals of Physics*, 313(2):497 – 538, 2004.
- [94] M. Haque, O. Zozulya, and K. Schoutens. Entanglement entropy in fermionic laughlin states. *Phys. Rev. Lett.*, 98(6):060401, Feb 2007.
- [95] P. C. Hendry, N. S. Lawson, R. A. M. Lee, P. V. E. McClintock, and C. D. H. Williams. Generation of defects in superfluid 4He as an analogue of the formation of cosmic strings. *Nature*, 368(6469):315–317, 03 1994.
- [96] M. Hermanns, A. Chandran, N. Regnault, and B. A. Bernevig. Haldane statistics in the finite-size entanglement spectra of $1/m$ fractional quantum hall states. *Phys. Rev. B*, 84:121309, Sep 2011.
- [97] M. Hindmarsh and A. Rajantie. Defect formation and local gauge invariance. *Phys. Rev. Lett.*, 85:4660–4663, Nov 2000.
- [98] D. Hochberg, C. Molina-París, J. Pérez-Mercader, and M. Visser. Effective action for stochastic partial differential equations. *Phys. Rev. E*, 60(6):6343–6360, Dec 1999.
- [99] P. C. Hohenberg and B. I. Halperin. Theory of dynamic critical phenomena. *Rev. Mod. Phys.*, 49:435–479, Jul 1977.
- [100] Y. Hu, S. D. Stirling, and Y.-S. Wu. Ground-state degeneracy in the levin-wen model for topological phases. *Phys. Rev. B*, 85:075107, Feb 2012.

- [101] T. L. Hughes, E. Prodan, and B. A. Bernevig. Inversion-symmetric topological insulators. *Phys. Rev. B*, 83:245132, Jun 2011.
- [102] J. K. Jain. Composite-fermion approach for the fractional quantum hall effect. *Phys. Rev. Lett.*, 63(2):199–202, Jul 1989.
- [103] J. K. Jain. *Composite Fermions*. Cambridge University Press, 2007.
- [104] H. K. Janssen, B. Schaub, and B. Schmittmann. New universal short-time scaling behaviour of critical relaxation processes. *Zeitschrift für Physik B Condensed Matter*, 73:539–549, 1989.
- [105] A. Karlhede, S. A. Kivelson, and S. L. Sondhi. Quantum hall effect: The article. In V. J. Emery, editor, *Correlated electron systems: Proceedings of the 9th Jerusalem Winter School, Jerusalem, Israel*, volume 92, 1993.
- [106] T. W. B. Kibble. Topology of cosmic domains and strings. *Journal of Physics A: Mathematical and General*, 9(8):1387, 1976.
- [107] T. Kinoshita, T. Wenger, and D. S. Weiss. A quantum newton’s cradle. *Nature*, 440(7086):900–903, 04 2006.
- [108] J. G. Kissner. *Ordering kinetics of systems far from equilibrium*. PhD thesis, University of Manchester, 1992.
- [109] A. Kitaev. Fault-tolerant quantum computation by anyons. *Annals of Physics*, 303(1):2 – 30, 2003.
- [110] A. Kitaev and C. R. Laumann. *Exact Methods in Low-dimensional Statistical Physics and Quantum Computing: Lecture Notes of the Les Houches Summer School: Volume 89, July 2008: Lecture Notes of the Les Houches Summer School: Volume 89, July 2008*, volume 89, chapter Topological phases and quantum computation. OUP Oxford, 2008.
- [111] A. Kitaev and J. Preskill. Topological entanglement entropy. *Phys. Rev. Lett.*, 96(11):110404, Mar 2006.
- [112] K. v. Klitzing, G. Dorda, and M. Pepper. New method for high-accuracy determination of the fine-structure constant based on quantized hall resistance. *Phys. Rev. Lett.*, 45:494–497, Aug 1980.
- [113] Y. Kluger, E. Mottola, and J. M. Eisenberg. Quantum vlasov equation and its markov limit. *Phys. Rev. D*, 58(12):125015, Nov. 1998.
- [114] J. Kockelkoren and H. Chaté. Comment on “Deterministic equations of motion and phase ordering dynamics”. *Phys. Rev. E*, 65:058101, May 2002.
- [115] J. Kockelkoren and H. Chaté. Late stages of coarsening in model c. *Physica D: Nonlinear Phenomena*, 168-169:80 – 92, 2002.

- [116] J. B. Kogut. An introduction to lattice gauge theory and spin systems. *Rev. Mod. Phys.*, 51:659–713, Oct 1979.
- [117] M. Kolodrubetz, B. K. Clark, and D. A. Huse. Nonequilibrium dynamic critical scaling of the quantum ising chain. *Phys. Rev. Lett.*, 109:015701, Jul 2012.
- [118] A. M. Läuchli, E. J. Bergholtz, J. Suorsa, and M. Haque. Disentangling entanglement spectra of fractional quantum hall states on torus geometries. *Phys. Rev. Lett.*, 104(15):156404, 2010.
- [119] R. B. Laughlin. Quantized hall conductivity in two dimensions. *Phys. Rev. B*, 23:5632–5633, May 1981.
- [120] R. B. Laughlin. Anomalous quantum hall effect: An incompressible quantum fluid with fractionally charged excitations. *Phys. Rev. Lett.*, 50:1395–1398, May 1983.
- [121] M. Levin and X.-G. Wen. Detecting topological order in a ground state wave function. *Phys. Rev. Lett.*, 96(11):110405, Mar 2006.
- [122] M. A. Levin and X.-G. Wen. String-net condensation: A physical mechanism for topological phases. *Phys. Rev. B*, 71:045110, Jan 2005.
- [123] H. Li and F. D. M. Haldane. Entanglement spectrum as a generalization of entanglement entropy: Identification of topological order in non-abelian fractional quantum hall effect states. *Phys. Rev. Lett.*, 101(1):010504, Jul 2008.
- [124] P. V. Lin, F. E. Camino, and V. J. Goldman. Superperiods in interference of $e/3$ laughlin quasiparticles encircling filling $2/5$ fractional quantum hall island. *Phys. Rev. B*, 80(23):235301, Dec 2009.
- [125] F. Liu and G. F. Mazenko. Defect-defect correlation in the dynamics of first-order phase transitions. *Phys. Rev. B*, 46:5963–5971, Sep 1992.
- [126] Z. Liu, E. J. Bergholtz, H. Fan, and A. M. Läuchli. Edge-mode combinations in the entanglement spectra of non-abelian fractional quantum hall states on the torus. *Phys. Rev. B*, 85:045119, Jan 2012.
- [127] Z. Liu, H.-L. Guo, V. Vedral, and H. Fan. Entanglement spectrum: Identification of the transition from vortex-liquid to vortex-lattice state in a weakly interacting rotating bose-einstein condensate. *Phys. Rev. A*, 83:013620, Jan 2011.
- [128] I. G. MacDonald. *Symmetric Functions and Hall Polynomials*. Oxford University Press, New York, 2nd edition, 1995.
- [129] A. Maniv, E. Polturak, and G. Koren. Observation of magnetic flux generated spontaneously during a rapid quench of superconducting films. *Phys. Rev. Lett.*, 91(19):197001, Nov 2003.

- [130] P. C. Martin, E. D. Siggia, and H. A. Rose. Statistical dynamics of classical systems. *Phys. Rev. A*, 8(1):423–437, Jul 1973.
- [131] M. S. Miguel, J. D. Gunton, G. Dee, and P. S. Sahni. Theory of spinodal decomposition in relaxational tricritical models. *Phys. Rev. B*, 23:2334–2345, Mar 1981.
- [132] A. Mitra and T. Giamarchi. Thermalization and dissipation in out-of-equilibrium quantum systems: A perturbative renormalization group approach. *Phys. Rev. B*, 85:075117, Feb 2012.
- [133] R. Monaco, J. Mygind, M. Aaroe, R. J. Rivers, and V. P. Koshelets. Zurek-kibble mechanism for the spontaneous vortex formation in Nb-Al/al_{ox}/Nb josephson tunnel junctions: New theory and experiment. *Phys. Rev. Lett.*, 96:180604, May 2006.
- [134] G. Moore and N. Read. Nonabelions in the fractional quantum hall effect. *Nuclear Physics B*, 360:362 – 396, 1991.
- [135] M. Moshe and J. Zinn-Justin. Quantum field theory in the large n limit: a review. *Physics Reports*, 385(3-6):69 – 228, 2003.
- [136] C. Nayak, S. H. Simon, A. Stern, M. Freedman, and S. Das Sarma. Non-abelian anyons and topological quantum computation. *Rev. Mod. Phys.*, 80(3):1083–1159, Sep 2008.
- [137] M. A. Nielsen and I. Chuang. *Quantum Computation and Quantum Information*. Cambridge University Press, Cambridge, UK, 2000.
- [138] W. Pan, J.-S. Xia, V. Shvarts, D. E. Adams, H. L. Stormer, D. C. Tsui, L. N. Pfeiffer, K. W. Baldwin, and K. W. West. Exact quantization of the even-denominator fractional quantum hall state at $\nu = 5/2$ landau level filling factor. *Phys. Rev. Lett.*, 83:3530–3533, Oct 1999.
- [139] Z. Papić, B. A. Bernevig, and N. Regnault. Topological entanglement in abelian and non-abelian excitation eigenstates. *Phys. Rev. Lett.*, 106:056801, Feb 2011.
- [140] R. Peierls. *Surprises in theoretical physics*. Princeton University Press, 1979.
- [141] I. Peschel. On the reduced density matrix for a chain of free electrons. *Journal of Statistical Mechanics: Theory and Experiment*, 2004(06):P06004, 2004.
- [142] D. Poilblanc. Entanglement spectra of quantum heisenberg ladders. *Phys. Rev. Lett.*, 105(7):077202, 2010.
- [143] A. Polkovnikov. Universal adiabatic dynamics in the vicinity of a quantum critical point. *Phys. Rev. B*, 72:161201, Oct 2005.
- [144] A. Polkovnikov. Microscopic expression for heat in the adiabatic basis. *Phys. Rev. Lett.*, 101:220402, Nov 2008.

- [145] A. Polkovnikov. Microscopic diagonal entropy and its connection to basic thermodynamic relations. *Annals of Physics*, 326(2):486 – 499, 2011.
- [146] A. Polkovnikov and V. Gritsev. Breakdown of the adiabatic limit in low-dimensional gapless systems. *Nat Phys*, 4(6):477–481, 06 2008.
- [147] A. Polkovnikov, K. Sengupta, A. Silva, and M. Vengalattore. *Colloquium* : Nonequilibrium dynamics of closed interacting quantum systems. *Rev. Mod. Phys.*, 83:863–883, Aug 2011.
- [148] F. Pollmann and J. E. Moore. Entanglement spectra of critical and near-critical systems in one dimension. *New Journal of Physics*, 12(2):025006, 2010.
- [149] F. Pollmann, A. M. Turner, E. Berg, and M. Oshikawa. Entanglement spectrum of a topological phase in one dimension. *Phys. Rev. B*, 81:064439, Feb 2010.
- [150] R. E. Prange and S. M. Girvin. *The Quantum Hall Effect*. Springer New York, 2nd edition, 1990.
- [151] E. Prodan, T. L. Hughes, and B. A. Bernevig. Entanglement spectrum of a disordered topological chern insulator. *Phys. Rev. Lett.*, 105(11):115501, Sep 2010.
- [152] T. Prosen. A new class of completely integrable quantum spin chains. *Journal of Physics A: Mathematical and General*, 31(21):L397, 1998.
- [153] K. Pyka, J. Keller, H. L. Partner, R. Nigmatullin, T. Burgermeister, D.-M. Meier, K. Kuhlmann, A. Retzker, M. B. Plenio, W. H. Zurek, A. del Campo, and T. E. Mehlstäubler. Symmetry Breaking and Topological Defect Formation in Ion Coulomb Crystals. *ArXiv e-prints*, Nov. 2012, e-print arXiv:1211.7005.
- [154] X.-L. Qi, H. Katsura, and A. W. W. Ludwig. General relationship between the entanglement spectrum and the edge state spectrum of topological quantum states. *Phys. Rev. Lett.*, 108:196402, May 2012.
- [155] A. Rahmani and C. Chamon. Exact results on the quench dynamics of the entanglement entropy in the toric code. *Phys. Rev. B*, 82:134303, Oct 2010.
- [156] A. Rajantie. Formation of topological defects in gauge field theories. *International Journal of Modern Physics A*, 17(01):1–43, 2002.
- [157] R. Rajaraman and S. L. Sondhi. Landau level mixing and solenoidal terms in lowest landau level currents. *Modern Physics Letters B*, 08(17):1065–1073, 1994.
- [158] N. Read and E. Rezayi. Quasiholes and fermionic zero modes of paired fractional quantum hall states: The mechanism for non-abelian statistics. *Phys. Rev. B*, 54(23):16864–16887, 1996.

- [159] N. Read and E. Rezayi. Beyond paired quantum hall states: Parafermions and incompressible states in the first excited landau level. *Phys. Rev. B*, 59:8084–8092, Mar 1999.
- [160] M. Rigol. Breakdown of thermalization in finite one-dimensional systems. *Phys. Rev. Lett.*, 103:100403, Sep 2009.
- [161] M. Rigol, V. Dunjko, V. Yurovsky, and M. Olshanii. Relaxation in a completely integrable many-body quantum system: An *Ab Initio* study of the dynamics of the highly excited states of 1d lattice hard-core bosons. *Phys. Rev. Lett.*, 98:050405, Feb 2007.
- [162] V. M. H. Ruutu, V. B. Eltsov, A. J. Gill, T. W. B. Kibble, M. Krusius, Y. G. Makhlin, B. Placais, G. E. Volovik, and W. Xu. Vortex formation in neutron-irradiated superfluid ^3He as an analogue of cosmological defect formation. *Nature*, 382(6589):334–336, 07 1996.
- [163] J. Sabbatini, W. H. Zurek, and M. J. Davis. Causality and defect formation in the dynamics of an engineered quantum phase transition in a coupled binary bose-einstein condensate. *New Journal of Physics*, 14(9):095030, 2012.
- [164] S. Sachdev. *Quantum Phase Transitions*. Cambridge University Press, Cambridge, UK, 1999.
- [165] L. E. Sadler, J. M. Higbie, S. R. Leslie, M. Vengalattore, and D. M. Stamper-Kurn. Spontaneous symmetry breaking in a quenched ferromagnetic spinor bose-einstein condensate. *Nature*, 443(7109):312–315, 09 2006.
- [166] L. Saminadayar, D. C. Glattli, Y. Jin, and B. Etienne. Observation of the $e/3$ fractionally charged Laughlin quasiparticle. *Phys. Rev. Lett.*, 79:2526–2529, Sep 1997.
- [167] J. Schliemann. Entanglement spectrum and entanglement thermodynamics of quantum hall bilayers at $\nu = 1$. *Phys. Rev. B*, 83:115322, Mar 2011.
- [168] B. Sciolla and G. Biroli. Quantum quenches, dynamical transitions and off-equilibrium quantum criticality. *ArXiv e-prints*, Nov. 2012, e-print arXiv:1211.2572.
- [169] D. Sen, K. Sengupta, and S. Mondal. Defect production in nonlinear quench across a quantum critical point. *Phys. Rev. Lett.*, 101:016806, Jul 2008.
- [170] P. Shor. Polynomial-time algorithms for prime factorization and discrete logarithms on a quantum computer. *SIAM Review*, 41(2):303–332, 1999.
- [171] S. H. Simon, E. H. Rezayi, and N. R. Cooper. Pseudopotentials for multiparticle interactions in the quantum hall regime. *Phys. Rev. B*, 75(19):195306, 2007.

- [172] S. L. Sondhi, S. M. Girvin, J. P. Carini, and D. Shahar. Continuous quantum phase transitions. *Rev. Mod. Phys.*, 69(1):315–333, Jan 1997.
- [173] S. Sotiriadis and J. Cardy. Quantum quench in interacting field theory: A self-consistent approximation. *Phys. Rev. B*, 81(13):134305, Apr. 2010, e-print arXiv:1002.0167.
- [174] R. Stanley. Some combinatorial properties of jack symmetric functions. *Adv. Math.*, 77:76, 1989.
- [175] J.-M. Stéphan, S. Furukawa, G. Misguich, and V. Pasquier. Shannon and entanglement entropies of one- and two-dimensional critical wave functions. *Phys. Rev. B*, 80(18):184421, 2009.
- [176] A. Sterdyniak, N. Regnault, and B. A. Bernevig. Extracting excitations from model state entanglement. *Phys. Rev. Lett.*, 106:100405, Mar 2011.
- [177] H. L. Stormer, D. C. Tsui, and A. C. Gossard. The fractional quantum hall effect. *Rev. Mod. Phys.*, 71:S298–S305, Mar 1999.
- [178] A. Strominger. The dS/CFT correspondence. *JHEP*, 10:034, 2001.
- [179] R. Thomale, D. P. Arovas, and B. A. Bernevig. Nonlocal order in gapless systems: Entanglement spectrum in spin chains. *Phys. Rev. Lett.*, 105(11):116805, 2010.
- [180] R. Thomale, A. Sterdyniak, N. Regnault, and B. A. Bernevig. Entanglement gap and a new principle of adiabatic continuity. *Phys. Rev. Lett.*, 104(18):180502, 2010.
- [181] D. J. Thouless, M. Kohmoto, M. P. Nightingale, and M. den Nijs. Quantized hall conductance in a two-dimensional periodic potential. *Phys. Rev. Lett.*, 49:405–408, Aug 1982.
- [182] S. Trebst, P. Werner, M. Troyer, K. Shtengel, and C. Nayak. Breakdown of a topological phase: Quantum phase transition in a loop gas model with tension. *Phys. Rev. Lett.*, 98:070602, Feb 2007.
- [183] S. Trotzky, Y.-A. Chen, A. Flesch, I. P. McCulloch, U. Schollwöck, J. Eisert, and I. Bloch. Probing the relaxation towards equilibrium in an isolated strongly correlated one-dimensional bose gas. *Nat Phys*, 8(4):325–330, 04 2012.
- [184] S. A. Trugman. Localization, percolation, and the quantum hall effect. *Phys. Rev. B*, 27(12):7539–7546, Jun 1983.
- [185] D. I. Tsomokos, A. Hamma, W. Zhang, S. Haas, and R. Fazio. Topological order following a quantum quench. *Phys. Rev. A*, 80:060302, Dec 2009.

- [186] D. C. Tsui, H. L. Stormer, and A. C. Gossard. Two-dimensional magneto-transport in the extreme quantum limit. *Phys. Rev. Lett.*, 48:1559–1562, May 1982.
- [187] I. S. Tupitsyn, A. Kitaev, N. V. Prokof'ev, and P. C. E. Stamp. Topological multicritical point in the phase diagram of the toric code model and three-dimensional lattice gauge higgs model. *Phys. Rev. B*, 82:085114, Aug 2010.
- [188] A. M. Turner, F. Pollmann, and E. Berg. Topological phases of one-dimensional fermions: An entanglement point of view. *Phys. Rev. B*, 83:075102, Feb 2011.
- [189] A. M. Turner, Y. Zhang, R. S. K. Mong, and A. Vishwanath. Quantized response and topology of magnetic insulators with inversion symmetry. *Phys. Rev. B*, 85:165120, Apr 2012.
- [190] A. M. Turner, Y. Zhang, and A. Vishwanath. Entanglement and inversion symmetry in topological insulators. *Phys. Rev. B*, 82(24):241102, 2010.
- [191] M. Uhlmann, R. Schützhold, and U. R. Fischer. $o(n)$ symmetry-breaking quantum quench: Topological defects versus quasiparticles. *Phys. Rev. D*, 81:025017, Jan 2010.
- [192] S. Ulm, J. Roßnagel, G. Jacob, C. Degünther, S. T. Dawkins, U. G. Poschinger, R. Nigmatullin, A. Retzker, M. B. Plenio, F. Schmidt-Kaler, and K. Singer. Observation of the Kibble-Zurek scaling law for defect formation in ion crystals. *ArXiv e-prints*, Feb. 2013, e-print arXiv:1302.5343.
- [193] V. Venkatachalam, A. Yacoby, L. Pfeiffer, and K. West. Local charge of the $[n\text{gr}] = 5/2$ fractional quantum hall state. *Nature*, 469(7329):185–188, 01 2011.
- [194] J. Vidal, S. Dusuel, and K. P. Schmidt. Low-energy effective theory of the toric code model in a parallel magnetic field. *Phys. Rev. B*, 79:033109, Jan 2009.
- [195] F. J. Wegner. Duality in generalized ising models and phase transitions without local order parameters. *Journal of Mathematical Physics*, 12(10):2259–2272, 1971.
- [196] X.-G. Wen. Topological orders and edge excitations in fractional quantum hall states. *Advances in Physics*, 44(5):405 – 473, 1995.
- [197] X. G. Wen and Q. Niu. Ground-state degeneracy of the fractional quantum hall states in the presence of a random potential and on high-genus riemann surfaces. *Phys. Rev. B*, 41(13):9377–9396, May 1990.
- [198] R. Willett, J. P. Eisenstein, H. L. Störmer, D. C. Tsui, A. C. Gossard, and J. H. English. Observation of an even-denominator quantum number in the fractional quantum hall effect. *Phys. Rev. Lett.*, 59:1776–1779, Oct 1987.

- [199] R. L. Willett, C. Nayak, K. Shtengel, L. N. Pfeiffer, and K. W. West. Magnetic field-tuned Aharonov-Bohm oscillations and evidence for non-Abelian anyons at $\nu=5/2$. *ArXiv e-prints*, Jan. 2013, e-print arXiv:1301.2639.
- [200] R. L. Willett, L. N. Pfeiffer, and K. W. West. Measurement of filling factor $5/2$ quasiparticle interference with observation of charge $e/4$ and $e/2$ period oscillations. *Proceedings of the National Academy of Sciences*, 106(22):8853–8858, 2009.
- [201] R. L. Willett, L. N. Pfeiffer, K. W. West, and M. Manfra. Aharonov-Bohm effect and coherence length of charge $e/4$ quasiparticles at $5/2$ filling factor measured in multiple small Fabry-Perot interferometers. *ArXiv e-prints*, Jan. 2013, e-print arXiv:1301.2594.
- [202] E. Witten. Multi-trace operators, boundary conditions, and ads/cft correspondence. *ArXiv High Energy Physics - Theory e-prints*, Dec 2001, e-print arXiv:arXiv:hep-th/0112258.
- [203] J. S. Xia, W. Pan, C. L. Vicente, E. D. Adams, N. S. Sullivan, H. L. Stormer, D. C. Tsui, L. N. Pfeiffer, K. W. Baldwin, and K. W. West. Electron correlation in the second Landau level: A competition between many nearly degenerate quantum phases. *Phys. Rev. Lett.*, 93:176809, Oct 2004.
- [204] H. Yao and X.-L. Qi. Entanglement entropy and entanglement spectrum of the Kitaev model. *Phys. Rev. Lett.*, 105(8):080501, 2010.
- [205] B. Zheng. Deterministic equations of motion and phase ordering dynamics. *Phys. Rev. E*, 61:153–156, Jan 2000.
- [206] O. S. Zozulya, M. Haque, and N. Regnault. Entanglement signatures of quantum Hall phase transitions. *Phys. Rev. B*, 79(4):045409, 2009.
- [207] O. S. Zozulya, M. Haque, and K. Schoutens. Particle partitioning entanglement in itinerant many-particle systems. *Physical Review A*, 78:042326, 2008.
- [208] W. H. Zurek. Cosmological experiments in superfluid helium? *Nature*, 317(6037):505–508, Oct. 1985.
- [209] W. H. Zurek. Cosmological experiments in condensed matter systems. *Physics Reports*, 276(4):177 – 221, 1996.
- [210] W. H. Zurek, U. Dorner, and P. Zoller. Dynamics of a quantum phase transition. *Phys. Rev. Lett.*, 95:105701, Sep 2005.